2016

Effects of gas atmosphere on reduction of quartz and its reaction with silicon carbide for silicon production

Xiang Li
University of Wollongong, xl450@uowmail.edu.au

UNIVERSITY OF WOLLONGONG

EFFECTS OF GAS ATMOSPHERE ON REDUCTION OF QUARTZ AND ITS REACTION WITH SILICON CARBIDE FOR SILICON PRODUCTION

A thesis submitted to the University of Wollongong as fulfilment for the degree of

Doctor of Philosophy

from

University of Wollongong

by

Xiang Li

School of Mechanical, Materials and Mechatronic Engineering

University of Wollongong, Australia

2016

ACKNOWLEDGEMENTS

The completion of this PhD project has been possible thanks to the important contribution of many people. First of all I would like to thank my supervisors, Dr Guangqing Zhang, Professor Oleg Ostrovski and Professor Brian Monaghan, who provided continuous support, guidance, and encouragement throughout the whole project on both the research and personal levels. Your patience with my slowness and mistake is very much appreciated.

I am very grateful for the financial support of ELKEM AS, and Mr Ragnar Tronstad and Dr Astrid Storesund for ICP-OES analysis at ELKEM.

I wish to express my gratitude to Dr Kai Tang and Dr Sarina Bao for their perfect combination of theoretical and technical support during my visiting at SINTEF. Thanks for your warm welcome.

The technical assistance at UOW and UNSW has been invaluable and I would like to thank Dr Raymond Longbottom, Dr Neslihan Dogan, Dr Xing Xing and Mr. Greg Tillman for equipment maintence and training, Mr Andrew Acobie and Mr Stuart Rodd for building equipment, Mr Nick Mackie for XRD analysis, Mr Mitchell Nancarrow for SEM analysis, Dr Gilberto Casillas for TEM analysis and Dr Sarah Kelloway for LECO analysis.

I would also like to thank my friends: Dr Hazem L. George, Dr Iis Aisyah, Mr Dalin Cai, Dr Zhongwei Wang, Mr Hamed Abdeyazdan, Dr Lei Zhang, Mr Zhe Wang, Miss Ay Ching Hee, Miss Jingxiu Wang, Miss Jianjian Lin for the wonderful time we spent together.

Furthermore, I would like to thank all my family members for their mental support and constant encouragement throughout the whole course of my PhD study.

This project was made possible by funding from the Australian Research Council's Linkage Projects funding scheme (Project No. LP100100866). University of Wollongong is also acknowledged for providing a Vice Chancellor's Special Scholarship and an International Postgraduate Tuition Award (IPTA).

ABSTRACT

Wider use of solar energy is impeded by high cost of solar-grade silicon used in photovoltaics. Carbothermal synthesis of silicon carbide (SiC) followed by further reacting with quartz is a novel and economical approach for production of solar-grade silicon. The aim of the project was to investigate carbothermal reduction of quartz to SiC and production of silicon from quartz and SiC in different gas atmosphere, and establish reaction mechanism. The concentrations of CO, CO_2 and CH_4 in the off gas during reaction were measured online using an infrared gas analyzer. The samples after reduction were characterized by XRD, LECO analyser, SEM and TEM. The major findings of this project are as follows:

Carbothermal reduction of quartz to SiC in argon and hydrogen gas

The quartz was crushed to < 70 μm, uniformly mixed with graphite and pressed into pellets. Reduction was studied in isothermal and temperature programmed reduction experiments in a fix bed reactor in argon, hydrogen and argon–hydrogen gas mixtures. The carbothermal reduction of quartz in hydrogen was faster than in argon. Formation of silicon carbide started at 1300 °C in argon, and 1200 °C in hydrogen. Synthesis of silicon carbide in hydrogen was close to completion in 270 minutes at 1400 °C, 140 minutes at 1500 °C, and 70 minutes at 1600 °C. Faster carbothermal reduction rate in hydrogen was attributed to the involvement of hydrogen in the reduction reactions by directly reducing silica and/or indirectly, by reacting with graphite to form methane as an intermediate reductant.

In the reduction process in hydrogen, the reaction between methane and SiO resulted to growth of SiC whiskers on the surface and inside the pellet by vapour-liquid-solid

(VLS) mechanism under catalytic effect of iron at 1400–1600 °C. The whiskers had prism structure with diameter 100–800 nm and length up to tens of microns.

Carbothermal reduction of quartz to SiC in methane–hydrogen–argon gas mixture

Synthesis of SiC by carbothermal reduction of quartz in a methane–hydrogen–argon gas mixture was investigated in a laboratory fixed-bed reactor in the temperature range of 1300 to 1550 °C. A mixture of quartz-graphite powders with C/SiO_2 molar ratio of 2 was pressed into pellets and used for reduction experiments. The reduction was completed within 2 hours under the conditions of T $\geqslant$1500 °C, methane content 0.5 to 2 vol % and hydrogen content $\geqslant$ 70 vol %. Methane partially substituted carbon as a reductant in the SiC synthesis and enhanced the reduction kinetics significantly. An increase in the methane content above 2 vol % caused excessive carbon deposition which had a detrimental effect on the reaction rate. Hydrogen content in the gas mixture above 70 vol % suppressed the cracking of methane. Hydrogen was also directly involved in reduction of quartz to SiO.

Reduction in methane–hydrogen–argon gas mixture resulted in growth of two types of SiC whisker; one was formed by VLS mechanism at 1200–1600 °C, the other type of whiskers was synthesized at 1400–1600 °C by vapour-solid (VS) mechanism, and exhibited cylinder structure and high aspect ratio.

Reduction of quartz to silicon monoxide

The reduction of quartz was studied isothermally in a fluidized bed reactor with continuously flowing methane–hydrogen gas mixture in the temperature range 1350–1500 °C. The CO content in the off-gas was measured online using an infrared gas analyzer. The main phases of the reduced samples identified by XRD analysis were

quartz and cristobalite. Significant weight loss in the reduction process indicated that the reduction products were SiO and CO. Reduction of SiO_2 to SiO by methane starts with adsorption and dissociation of CH_4 on the silica surface. The high carbon activity in the CH_4–H_2 gas mixture provided a strongly reducing condition. At 1350 °C, the reduction was very slow. The rate and extent of reduction increased with increasing temperature to 1450 °C. A further increase in temperature to 1500 °C resulted in a decrease in the rate and extent of reduction. An increase in the gas flow rate from 0.4 to 0.8 NL/min and increase in the methane content in the CH_4–H_2 gas mixture from 0 to 5 vol pct favored the reduction. Methane content in the gas mixture should be maintained below 5 vol pct in order to suppress methane cracking.

Study of gas atmosphere in silicon production

The formation of silicon by reaction between quartz and SiC has been studied in the temperature range of 1600–1900 °C in argon and hydrogen atmospheres. The reaction process was monitored by an infrared gas analyser, and the reaction products were characterised by LECO, XRD and SEM. Quartz–SiC reactions with SiO_2/SiC molar ratio of 1:1 and 1:2 were studied in a fixed bed reactor in a graphite furnace. The production of silicon from quartz and SiC was strongly affected by temperature, SiO_2/SiC molar ratio and gas atmosphere. The yield of silicon in the reaction at 1900 °C in argon from samples with SiO_2/SiC molar ratios of 1:1 and 1:2 reached 32.7 % and 44.5 % respectively. SiO_2–SiC reaction at 1900 °C in hydrogen with the SiO_2/SiC molar ratio of 1:2 resulted in the silicon yield of 66.7 %. Higher silicon yield in hydrogen was attributed to the involvement of hydrogen in the direct reduction of silica to SiO.

DECLARATION ON PUBLICATIONS

This thesis includes the following chapters that have been published or in the process of publication.

Chapter 2: Xiang Li, Guangqing Zhang, Kai Tang, Oleg Ostrovski, Ragnar Tronstad, "*Carbothermal Reduction of Quartz in Different Gas Atmospheres*". **Metallurgical and Materials Transactions B**, 2015, vol. 46, pp. 1343–1352.

Contributions

Xiang Li: experimental work, understanding of the experimental results, developing of the method, paper writing;

Guangqing Zhang: defining of the experimental setting, discussion of the experimental results, paper revision;

Kai Tang: discussion of the experimental results, paper revision;

Oleg Ostrovski: discussion of the experimental results, paper revision;

Ragnar Tronstad: discussion of the experimental results, paper revision.

Chapter 3: Xiang Li, Guangqing Zhang, Kai Tang, Oleg Ostrovski, Ragnar Tronstad, "*Carbothermal Reduction of Quartz in Methane–Hydrogen–Argon Gas Mixture*". **Metallurgical and Materials Transactions B**, 2015, vol. 46, pp. 2384–2393.

Contributions

Xiang Li: experimental work, understanding of the experimental results, developing of the method, paper writing;

Guangqing Zhang: defining of the experimental setting, discussion of the experimental results, paper revision;

Kai Tang: discussion of the experimental results, paper revision;
Oleg Ostrovski: discussion of the experimental results, paper revision;
Ragnar Tronstad: discussion of the experimental results, paper revision.

Chapter 4: Xiang Li, Guangqing Zhang, Ragnar Tronstad, Oleg Ostrovski, "*Synthesis of SiC whiskers by VLS and VS process*". **Ceramics International,** 2016, vol. 42, pp. 5668–5676.

Contributions
Xiang Li: experimental work, understanding of the experimental results, developing of the method, paper writing;
Guangqing Zhang: defining of the experimental setting, discussion of the experimental results, paper revision;
Ragnar Tronstad: discussion of the experimental results, paper revision;
Oleg Ostrovski: discussion of the experimental results, paper revision.

Chapter 5: Xiang Li, Guangqing Zhang, Ragnar Tronstad, Oleg Ostrovski, "*Reduction of Quartz to Silicon Monoxide by Methane–hydrogen Mixtures*". **Metallurgical and Materials Transactions B,** 2016, press online, DOI 10.1007/s11663-016-0670-5

Contributions
Xiang Li: experimental work, understanding of the experimental results, developing of the method, paper writing;
Guangqing Zhang: defining of the experimental setting, discussion of the experimental results, paper revision;
Ragnar Tronstad: discussion of the experimental results, paper revision;

Oleg Ostrovski: discussion of the experimental results, paper revision.

Chapter 6: Xiang Li, Guangqing Zhang, Oleg Ostrovski, Ragnar Tronstad, "*Effect of Gas Atmosphere on the Silicon Formation*". **Journal of Materials Science**, 2016, vol. 51, pp. 876–884.

Contributions

Xiang Li: experimental work, understanding of the experimental results, developing of the method, paper writing;

Guangqing Zhang: defining of the experimental setting, discussion of the experimental results, paper revision;

Oleg Ostrovski: discussion of the experimental results, paper revision;

Ragnar Tronstad: discussion of the experimental results, paper revision.

Xiang Li	Dr. Guangqing Zhang
April 2016	April 2016
PhD Candidate	Principal Supervisor

TABLE OF CONTENTS

LIST OF FIGURES

Chapter 1:

Chapter 2:

Chapter 3:

Chapter 4:

Chapter 5:

Chapter 6:

LIST OF TABLES

Chapter 1:

Chapter 2:

Chapter 3:

Chapter 5:

Chapter 6:

CHAPTER 1

GENERAL INTRODUCTION

1.1 Introduction

Conventional energy resources, such as petroleum, natural gas, coal etc., are becoming scarcer and their production is becoming more expensive as the proved reserves are unable to meet the energy demand for rapid economic growth of developing countries. As shown in Figure 1, a worldwide shortage of fossil energy sources is expected in the future. Many efforts are aimed to develop renewable energy sources such as hydroelectric power, wind power, solar power, marine energy, bioenergy and geothermal energy to reduce the dependence on fossil energy use and to minimize environmental pollution and to positively impact the environment in many ways [1].

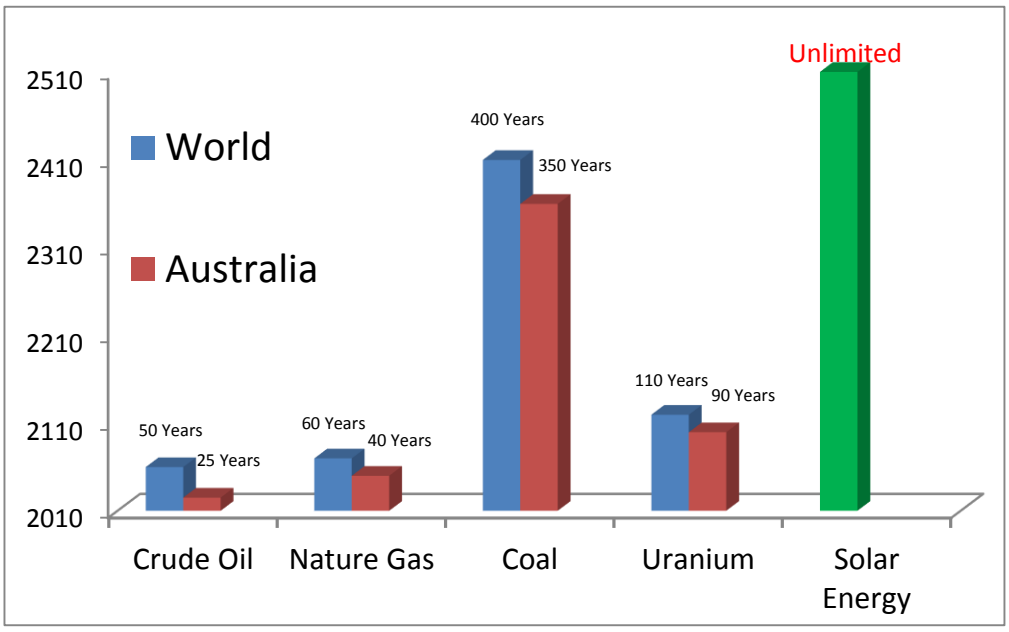

Fig. 1 Forecast of energy reserves [1].

Our planet receives approximately 2.9×10^{14} kWh of solar power a day, which is about

25 times as much as yearly energy consumption [2]. This indicates that the earth receives more solar energy in an hour than the total energy consumed by humans in an entire year. Solar energy alone has the potential capacity to meet the planet's entire energy needs in the future. In the past 20 years, the photovoltaic (PV) industry has grown by an average 30% per annum. Australia doubled its cumulative installed solar PV capacity in two years from 2011 to 2013 (Figure 2) [3].

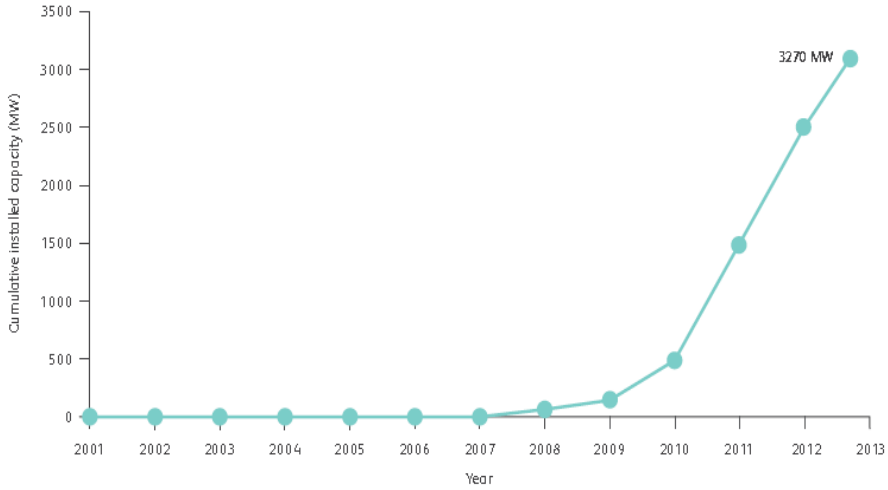

Fig. 2 Cumulative installed solar PV capacity in Australia [3].

The majority of solar cells are made of high purity silicon SoG-Si (solar grade silicon) which requires impurity level below ~1 ppm (99.9999 %, 6N) [4]. A cost and energy breakdown of a PV module and system are given in Figure 3. It can be seen that the solar silicon occupies about half of the cost of the solar cell module. Furthermore, module cost contributes about 55 % of the system cost, bringing the cost of the silicon in the final cost to 25–30 %. In addition, the energy required for solar silicon production occupies 59 % of the total system energy consumption. This leads to the conclusion that the most efficient avenue for the reduction of PV electricity price is in the silicon refining process [5]. Currently the best PV electricity price (in the sunniest locations) is approaching 25 cents/kWh, which is approximately 5 times higher than coal-fired electricity [6]. The PV electricity survives today only receiving government subsidy.

The greatest limitations for silicon based photovoltaic systems are the purity (especially for boron and phosphorus) and price of the solar silicon [7].

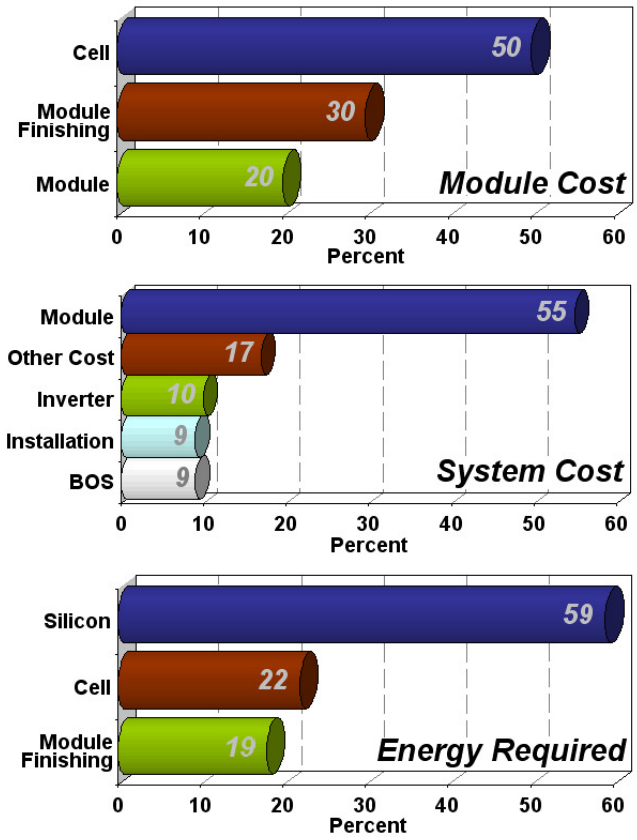

Fig. 3 Cost and energy breakdown for solar modules and system [8].

Traditional methods for production of SoG-Si are based on refining or further processing of metallurgical silicon (Siemens, NEDO and other [9–15]). The Siemens process converts silicon to silanes using HCl. After redistribution and distillation of the silanes, they are decomposed to pure polysilicon by chemical vapor deposition. Modifications to the Siemens process aim to reduce the energy consumption and increase silicon yield. In metallurgical routes, metallurgical grade silicon (MG-Si) is purified in its elemental form. It avoids formation and handling of toxic and potentially explosive chlorosilane compounds. In 2004, New Energy and Industrial Technology Development Organization (NEDO) and Kawasaki Steel Corporation in Japan developed a process involving electron beam melting in vacuum for phosphorus

removal, plasma treatment for boron removal and two directional solidification steps. In general, the production of SoG-Si by traditional methods is complex and expensive operation.

The most econonmically feasible way to produce MG-Si is still by carbothermal reduction of quartz in an electric submerged arc furnace at a high temperature of 1800–2100 °C. Solid carbon such as charcoal, coal and coke is used as reduction agent in the silicon process to release the silicon from quartz. The low carbon activity of traditional solid carbon caused a high temperature to need for reduction. More seriously, significant inpurities entered to silicon are derived from carbon materials.

This project is a part of the efforts to develop a new technology for production of SoG-Si by carbothermal reduction using natural gas as reduction agent or part of reduction agent. High carbon activity of the reducing gas is the key to achieve high rates and extents of reduction of metal oxides by natrual gas. Quartz will be converted to silicon carbide (SiC) in methane-containing gas atmosphere occurs in the solid state at temperature ≤ 1600 °C; SiC will further react with quartz to form silicon at temperature ≤ 1900 °C. The reduction of quartz at lower temperatures with potential advantages over conventional reduction of quartz from molten slags. Natural gas contains a low level of metallic impurities (totally, <1 ppmw) and phosphorus (<0.5 ppmw) [16]. Silicon produced from high purity quartz using natural gas will contain low concentrations of impurities, which will significantly cut the purification cost in solar silicon production.

Solar silicon production proposed in this project is based on the usage of high purity raw materials and efficient removal of impurities during carbothermal reaction. However, limited by experimental facilities and time, the behaviour of impurities in the reduction process was beyond the scope of this PhD project. The behaviour of impurities will be studied in the follow-up research.

It should be mentioned that the thermodynamics of the reactions involved in production of silicon is well documented [17], however, their mechanisms need further study and understanding. The thesis investigates the effects of gas atmosphere, including hydrogen and methane, on the formation of silicon carbide and elemental silicon. Data obtained in the experimental study of conversion of quartz to SiC were used for further understanding of reaction mechanisms.

This PhD thesis is prepared in the format of a series (5) publications following the University of Wollongong suggested thesis structure. Chapter 1 consists of a brief introduction of the research project, the literature review and experiment section. The literature review in section 1.2 includes the general introduction of silicon and SiC production, an overview of thermodynamics and process kinetics, as well as the behavior of impurities. The experiment section 1.3 presents the experimental setups and procedures for SiC and silicon synthesis in different experimental series. Furthermore, the sample characterization and data analysis method are presented.

Chapter 2–6 presents the main contribution to the thesis in the form of five papers. By the time of submitting this final version, the five papers have been published or accepted to publish by international journals. The PhD candidate of this thesis is the first author of all the papers.

Chapter 2 investigates the carbothermal reduction of a quartz ore to SiC in different gas atmospheres. The reduction conditions and mechanisms of SiC synthesis in argon and hydrogen are established in this Chapter.

Chapter 3 presents an investigation of synthesis of SiC by the carbothermal reduction of quartz in methane-containing gas. Methane is demonstrated to substitute partial reductant graphite and enhance the reduction rate. It is also shown that the methane content is limited and high hydrogen content in the gas is necessary to suppress thermal

decomposition of methane and carbon deposition in the high temperature reduction process.

During the carbothermal reduction of quartz in hrdrogen and methane-containing gas, a part of synthesised SiC appeared in the form of whiskers. Chapter 4 discusses the effects of gas atmosphere and temperature on the structure and morphologies of SiC and the growth mechanisms of the whiskers.

To better understand the role of methane in the carbothermal reduction process, Chapter 5 studies the reaction rate and kinectic of reduction of quartz to SiO by the CH_4–H_2 gas mixture.

As proposed in the project, synthesised SiC will further react with SiO_2 to form high purity silicon. Chapter 6 presents some preliminary results on the reaction of quartz and SiC for silicon production in different gas atmosphere, to establish fundamental understanding of the reaction and provide evidence for improving silicon production technology.

Finally, the main conclusions are summarized in Chapter 7 together with suggestions for further development.

1.2 Literature Review

1.2.1 Silicon Production and Refining

The production of the solar grade silicon (SoG-Si) goes through two stages: the manufacture of metallurgical grade silicon (MG-Si) by carbothermal reduction of silica, and further refining of MG-Si to obtain SoG-Si.

1.2.1.1 Production of MG-Si

MG-Si is produced industrially by the reaction of silica with carbon in an electric arc furnace. The purity of MG-Si is about 98.5~99.9 % Si [18]. The overall reduction reaction is:

$$SiO_2 + 2\ C = Si\ (l) + 2\ CO\ (g) \qquad (1)$$

Schematic of silicon production is shown in Figure 4**.** The silicon plant consists of the submerged electric arc furnace (SAF), the raw materials silos, the energy recovery system, the gas cleaning system and the metal handing system. The core of the plant is the SAF, which is charged with quartz ore lumps and carbonaceous materials. Three electrodes submerged into the charge supply a three-phase current that passes through the content of the furnace. The current heats the charge to about 2000 °C in the hottest part. At this temperature the quartz is reduced to liquid silicon. The silicon is tapped from the furnace through a taphole at the bottom and refined by slag treatment or gas purging. After refining, the liquid silicon is allowed to cool in a suitable mould and then crushed to the specified size. The consumption of electric energy is 11–13 MWh per metric ton of silicon metal [17].

A furnace is thus typically divided into high and low temperature zones which are also denoted as the inner and outer reactions zones, respectively. A stoichiometric model

developed by Schei and Halvorsen [19] summarises the main chemical reactions and material flows in the process as shown in Figure 5.

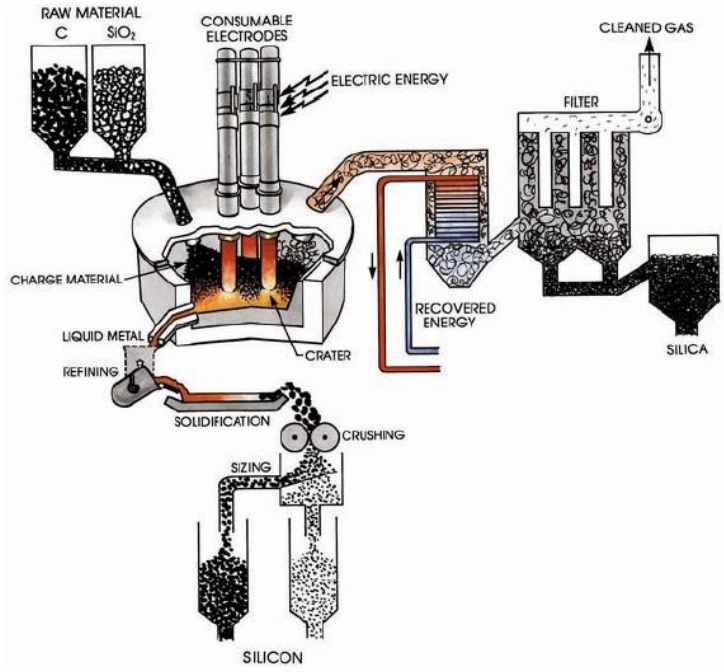

Fig. 4 Schematic of a modern MG-silicon plant [17].

1) Outer reaction zone

The main reactions in the outer reaction zone are:

$$SiO\ (g) + 2\ C = SiC + CO\ (g) \quad (2)$$

$$2\ SiO\ (g) = Si\ (l) + SiO_2 \quad (3)$$

$$SiO_2 + 3C = SiC + 2\ CO\ (g) \quad (4)$$

Figure 6 presents the equilibrium relations of the main reactions in the Si-O-C system and the stable phases at different temperature and partial pressure of SiO gas.

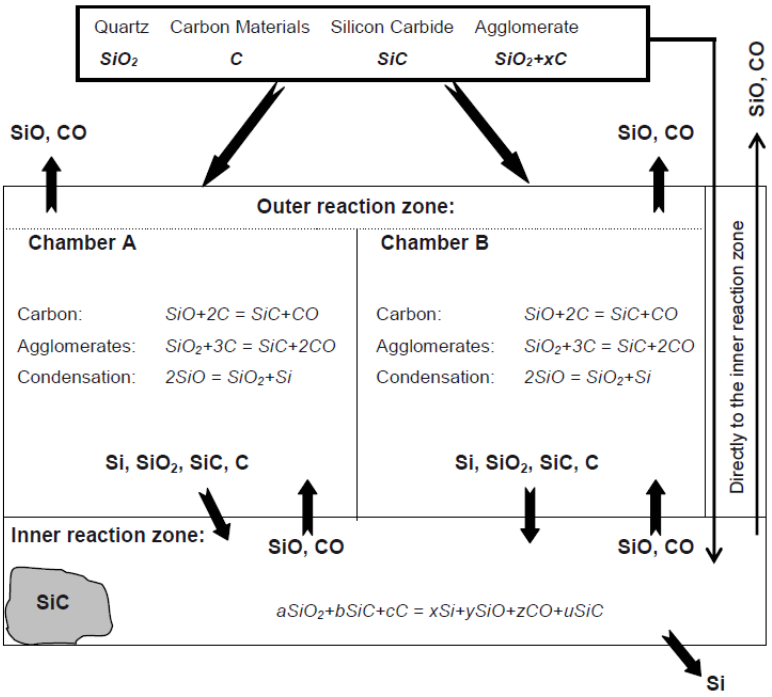

Fig. 5 The stoichiometric model illustrating chemical reactions in the inner and outer reaction zones as well as materials flow [17].

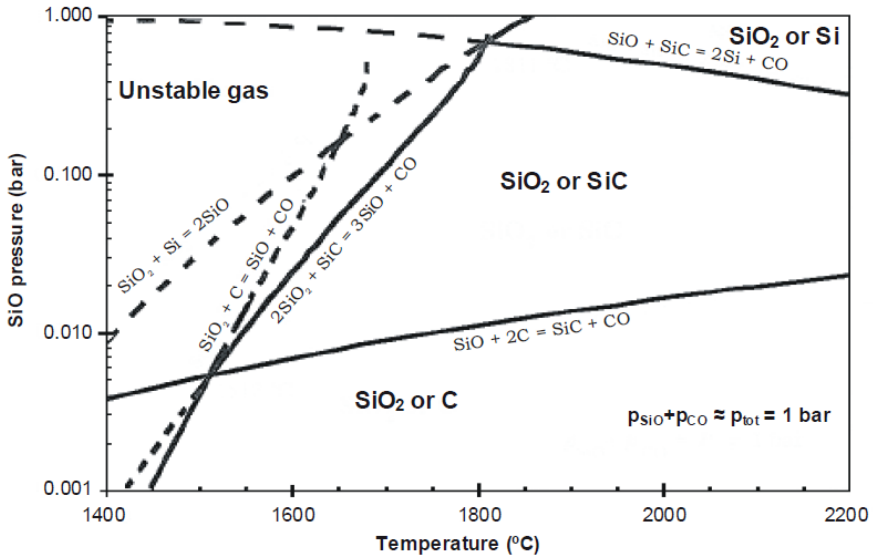

Fig. 6 SiO partial pressure in the SiO–CO gas phase (total pressure 1 atm) in equilibrium with the condensed phase combinations C–SiC, SiO_2–C, SiO_2–SiC, SiC–Si and SiO_2–Si. Gas compositions corresponding to points above the condensation reactions are unstable. Broken lines indicate that the gas composition is in an unstable area [17].

The bulk of the SiO gas generated in the inner reaction zone is recovered by reaction with carbonaceous reduction materials according to Reaction (2). This is the most important reaction in the outer reaction zone as SiC is an intermediate product in the process which is essential for the silicon producing reactions in the inner reaction zone.

2) Inner reaction zone

The silicon producing reactions take place at higher temperatures. The intermediate product, SiC, produced in the outer reaction zone reacts with SiO_2 in the inner reaction zone. Filsinger *et al.* [20] presented the following reactions to be of importance in this zone:

$$2\ SiO_2 + SiC = 3\ SiO\ (g) + CO\ (g) \quad (5)$$

$$SiO_2 + Si\ (l) = 2\ SiO\ (g) \quad (6)$$

$$SiC + SiO\ (g) = 2\ Si\ (l) + CO\ (g) \quad (7)$$

From the above reactions, the importance of generation of SiC in the outer reaction zone is obvious as this compound is necessary for production of liquid silicon as expressed by Reaction (7).

The SiO generating reactions in the inner reaction zone are highly endothermic; the reaction enthalpy for Reaction (5) is $\Delta H_{1500°C}$ = 1416.3 KJ, and for Reaction (6) $\Delta H_{1500°C}$ = 625.0 KJ. These reactions consumed most of the heat generated by electricity. They are believed to be the slowest of the proposed reactions and are not limited by the chemical equilibrium [17].

1.2.1.2 Production of SoG-Si

1) Chemical routes – conventional processes

Substantial efforts have been made in recent years in developing technologies for solar

silicon production. Three large commercial routes are described below:

- Siemens Process. The first step of the process is the synthesis of trichlorosilane with low boiling point (31.8 °C) via the reaction of $SiCl_4$ and H_2 with comminuted metallurgical-grade silicon [21, 22]:

$$Si\,(s) + 3\,SiCl_4\,(g) + 2\,H_2\,(g) = 4\,HSiCl_3\,(g) \quad (8)$$

The obtained trichlorosilane is purified by fractional distillation. The second step is decomposition of $HSiCl_3$ with high purity hydrogen in a deposition reactor at about 1100 °C, followed by the rectification of the intermediate and final products. The main reactions are [23]:

$$H_2\,(g) + HSiCl_3\,(g) = Si\,(s) + 3\,HCl\,(g) \quad (9)$$

$$2\,HSiCl_3\,(g) = SiH_2Cl_2\,(g) + SiCl_4\,(s) \quad (10)$$

$$SiH_2Cl_2\,(g) = Si\,(s) + 2\,HCl\,(g) \quad (11)$$

$$HCl\,(g) + HSiCl_3\,(g) = SiCl_4\,(s) + H_2\,(g) \quad (12)$$

- Union Carbide Process. This process is similar to the Siemens Process, except using monosilane (SiH_4) rather than $HSiCl_3$. Union Carbide Process, having a lower process temperature in comparison to Siemens Process, and almost 100 % decomposition of SiH_4, has gained a significant market share. The main reactions are [24]:

$$3\,SiCl_4\,(s) + 2\,H_2\,(g) + Si\,(s) = 4\,SiHCl_3\,(g) \quad (9)$$

$$2\,SiHCl_3\,(g) = SiH_2Cl_2\,(g) + SiCl_4\,(g) \quad (13)$$

$$3\,SiH_2Cl_2\,(g) = SiH_4\,(g) + 2\,SiHCl_3\,(g) \quad (14)$$

$$SiH_4\,(g) = 2\,H_2\,(g) + Si\,(s) \quad (15)$$

- Ethyl Corporation Process. Silane (SiH_4) gas is produced from silicon fluoride by reaction with sodium aluminium hydride ($NaAlH_4$) or lithium aluminium hydride ($LiAlH_4$). The silicon fluoride is cheap as a waste by-product of the fertilizer industry. Silane is decomposed in a fluidized bed reactor to silicon and hydrogen, the main reactions are [25, 26]:

$$2\ H_2\ (g) + M\ (s) + Al\ (s) = MAlH_4\ (s),\ M \text{ being Na or Li} \quad (16)$$

$$SiF_4\ (g) + AlMH_4 = SiH_4\ (g) + AlMF_4 \quad (17)$$

$$SiH_4\ (g) = 2\ H_2\ (g) + Si\ (s) \quad (15)$$

All mentioned chemical processes for production of pure silicon are energy intensive, involve toxic chemicals and have a relatively low capacity. The cost for SoG-Si is US $ 25–45/kg [27, 28].

2) Metallurgical routes

The most common techniques for MG-Si refining are acid leaching [29, 30], alloying [31, 32], unidirectional solidification (UDS) [33], vacuum refining [37–39], reactive gas blowing [34] and slagging [35, 36].

Purification of MG-Si to SoG-Si by metallurgical techniques is considered to be the most cost efficient for removing metal impurities; however, boron and phosphorous are not removed. In the NEDO purification process, phosphorus is removed from molten metallurgical silicon by electron beam melting under vacuum, then silicon is subjected to the first UDS, plasma melting to remove boron and carbon using a reactive gas such as H_2–H_2O vapour mixture, second UDS, then crushing and cleaning [30]. Refining of MG-Si to SoG-Si is a complex and expensive process. It was estimated that the cost of SoG-Si produced by refining of MG-Si is US$ 20–60 /kg depending on the purity of metallurgical silicon [38].

In Elkem process, liquid silicon produced in SAF is transferred to a slag furnace, where boron is removed by a liquid-liquid extraction process with alkali metal silicate as the extractant. Subsequent crushing and acid leaching process is used to remove phosphorus and other impurities. The final step is unidirectional solidification to further reduce the levels of phosphorus and other metallic impurities [40, 41].

1.2.1.3 Towards direct reduction of silica to obtain SoG-Si

Gribov and Zinov'ev [39] compared the concentrations of typical impurities in MG-Si and SoG-Si, as presented in Table 1. The carbothermal reduction of SiO_2 can, in principle, be used to produce not only metallurgical-grade but also high-purity silicon. This possibility was first investigated by Dosaj *et al.* [42] with the aim of producing a low-cost solar-grade silicon (estimated cost no higher than US $10/kg). They reduced quartz sand by purified carbon materials (coal, carbon black, or oil coke) in an arc furnace. However, the impurity concentrations in the resultant silicon were above the level of solar grade silicon, and therefore, further purification was needed. The general requirements for the optimal carbothermal reduction process are as follows [43, 44]:

a. The use of low-cost pure silica raw materials;
b. High-purity carbon reductants;
c. Insignificant contamination of silicon in the course of reduction and smelting.

1) Silica

The commercial quartzite or quartz sand commonly used in the preparation of metallurgical-grade silicon contains high levels of impurities, including boron and phosphorus. To obtain solar-grade silicon, pure natural quartzite (99.9+ % SiO_2) with low boron and phosphorus concentrations are required. Such quartzite has been found in Russia, China and other countries [45].

Table 1. Impurities contents of MG-Si and SoG-Si [39].

Impurity	Impurity mass fraction/10^{-6}			Segregation coefficient
	Metallurgical-grade		Solar-grade	
	98 %–99 %	99.50 %		
Al	1000–4000	50–600	<0.1	2.0×10^{-3}
Fe	1500–6000	100–1200	<0.1	8.0×10^{-6}
Ca	250–2200	100–300	<1	$1.3\times10^{-4} – 5.2\times10^{-4}$*
Mg	100–400	50–70	<1	3.2×10^{-6}
Mn	100–400	50–100	<<1	1.3×10^{-5}
Cr	30–300	20–50	<<1	1.1×10^{-5}
Ti	30–300	10–50	<<1	2.0×10^{-6}
V	50–250	<10	<<1	4.0×10^{-6}
Zr	20–40	<10	<<1	1.6×10^{-8}
Cu	20–40	<10	<1	4.0×10^{-4}
B	10–50	10–15	0.1–1.5	0.8
P	20–42	10–20	0.1–1	0.35
C	1000–3000	50–100	0.5–5	0.05

The purity of quartzite can be improved by conventional processes: crushing, sieving, and washing. The total impurity content of the resulting quartz concentrate is about 100 ppm. An even purer material (high grade quartz) can be obtained by chemically refining comminuted quartz or glass prepared by melting SiO_2 with fluxes [46, 47]. This step is rather expensive and affects the total manufacturing cost.

Recently, a refining process for high-purity amorphous silica from biogenic diatomaceous earth was proposed by Bessho et al. [48]. The process consists of extraction, precipitation, and acid leaching for silica refining, as shown in Figure 7. The boron content of refined silica was less than 5 ppmw, while phosphorous content was below the detection limit of ICP-AES technique. The reduction experiment suggested

that the produced silica amorphous silica powder was reduced to silicon more easily than quartz above 1800 °C, which was attributed to the higher specific surface area of refined amorphous silica [49]. The resultant silicon obtained by carbothermal reduction of high purity amorphous silica contained ~100 ppm carbon [50].

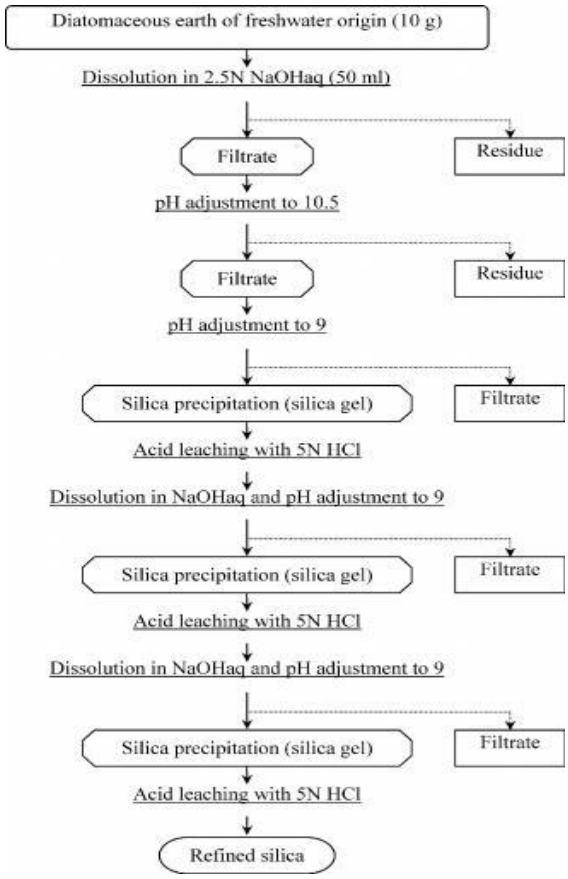

Fig. 7 Process chart to produce amorphous silica from diatomaceous earth [49].

2) Reductant

The reductants reported in the literature include petroleum coke, charcoal, graphite, and carbon black (various grades and combinations). The best results were obtained with carbon black produced by the cracking of methane or propane [39], which had good reducing ability and high purity (Table 2). Silicon produced using high-purity quartzite and carbon black in the carbothermal reduction has the highest purity [50].

Table 2. Purity of raw materials and silicon prepared by carbothermal reduction using high-purity silica and carbon black [39].

Material	Impurity content, ppm					
	B	P	Al	Ti	Fe	C
High-purity SiO_2	<0.05	<0.2	0.8	0.5	0.5	–
Carbon black granules	<0.1	0.6	<0.1	<0.1	1.8	–
As-reduced silicon (before refining)	0.1	1	1.4	3.5	11.7	>1000
Solar-grade silicon (after refining)	0.1–0.2	<0.05	<0.01	<0.05	<0.01	0.2–1.2

A simulation also pointed out that CH_4 was an efficient reducing agent based on follow reaction [51]:

$$CH_4\ (g) = C\ (s) + 2H_2\ (g) \tag{18}$$

Due to the easy purification of CH_4, it stands in the advantage status compared with conventional reducing agent—coal or coke, which gives rise to some impurities [52].

3) Carbothermal reduction process

In optimizing the carbothermal reduction process in SAF, contamination of silicon with refractory materials and graphite electrodes should be taken into account. The level of Si contamination in the course of reduction also depends on the reactor design [50, 53]. The purity of the graphite electrodes must be no worse than that of the raw materials. The bottom of the furnace, where the silicon melt accumulates, may be lined with spectral-grade graphite. The other parts, including the outlet gutter, should also be fabricated from spectral-grade graphite or from less pure graphite coated with CVD SiC. To reduce contamination, molten silicon must be constantly poured off into high-purity silica crucibles.

Promising results in the carbothermal reduction and smelting of silicon from quartz

materials have been obtained by the Direct Arc Reactor. The purity of silicon obtained in this reactor was 99.99+ % [54]. Aratani et al. [50, 54] suggested a two-stage carbothermal reduction/smelting process using a shaft arc furnace with a distinct temperature difference in the zones where SiO, SiC, and Si are formed. In the first zone, highly active SiC is synthesized under optimal conditions in quartz or graphite crucibles, while smelting of metallurgical silicon is performed in the second zone.

Silicon of solar-grade quality can be obtained using the plasma-assisted refinement of metallurgical silicon with respect to impurities (especially carbon and boron) [55, 56]. Such technology was implemented in the pilot plant by the Solsilc Development Co. (Netherlands); the first experimental commercial batch with a volume of about 100 tons was installed at the end of 2007 [57]. The silicon production was separated into two steps (Figure 8), the first producing SiC in a rotary plasma furnace [58], and the second obtaining Si from SiC and silica in an electric arc furnace.

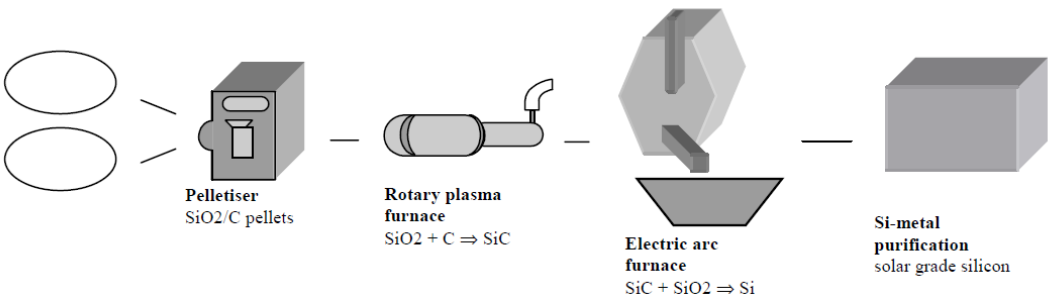

Fig. 8 Schematic Solsilc process of production of SoG-Si [57].

Demin et al. [59] considered the possibility of reduction of quartzite with hydrogen and a mixture of hydrogen with hydrocarbons at temperatures higher than 2500 ^{o}C. Reduction in gaseous mixtures occurred at a lower temperature than in the case where pure hydrogen was used. However, carbon formed when hydrocarbons were used in the gas mixture can contaminate the final product. By varying the composition of the gas mixture (C/H) and temperature, optimal conditions for production of pure silicon can be

found. Reduction of SiO_2 proceeded in two stages: SiO_2 was first reduced to gaseous SiO which was reduced further to silicon. The high volatility of SiO makes possible to separate it from a number of impurities with a much lower volatility. If very pure reducer (hydrogen) is used for reduction of SiO, the obtained silicon will have purity higher than that of starting SiO_2 [11].

In order to obtain silicon monoxide from silicon dioxide, carbon black and metallurgical silicon were used in addition to gaseous reductants [60, 61]. In order to increase the SiO output during reaction, the process was conducted at high temperatures (as high as 2000 ºC) or in an electric-arc plasma. The obtained gaseous silicon monoxide can be deposited at temperatures lower than 800 °C in a special chamber with a filter for collection of SiO. The condensate is represented by loose powder with yellow-brown color and very low apparent density. If SiO powder is used as an intermediate product for obtaining pure silicon, this powder is again transformed into the gaseous phase (at a temperature higher than 1300 °C) and reduced to silicon. Carbon, silicon carbide, hydrogen, and hydrogen–hydrocarbon mixtures [11, 62] can be used as reductants for silicon monoxide production. Reduction of SiO occurs at 1700–1900 °C. The main reactions when hydrogen is used for reduction of SiO are:

$$SiO_2 + C = SiO\ (g) + CO\ (g) \quad (19)$$

$$SiO_2 + Si\ (l) = 2\ SiO\ (g) \quad (6)$$

$$SiO\ (g) + H_2\ (g) = Si\ (l) + H_2O\ (g) \quad (20)$$

Ma et al. [63] reported a similar 5N SoG-Si production method from SiO. The difference was that they generated silicon and silica via disproportionation Reaction (3), followed by separation of silica by heating liquefaction or HF etching, with UDS as a final step.

These reports signify that the processes performed stage-by-stage under optimal

conditions for each stage (including separate reactors for each stage) are quite promising for implementation in the large-scale SG-Si production.

1.2.2 Production of Silicon Carbide

SiC is an important ceramic material which has various applications. It has features such as high thermal conductivity, hardness second to diamond, high melting point, high chemical inertness and oxidation resistance. These features make SiC a perfect candidate for cutting material, refractory material and high-temperature semiconductor [64, 65]. In this project, silicon carbide is synthesized and studied as the intermediate for solar silicon production.

SiC is commercially produced primarily by carbothermal reduction of quartz using carbonaceous materials (petroleum coke, anthracite coal, bituminous coal and carbon black) at temperatures above 2000 °C [66]. Other methods include direct carbonization of elemental Si [67, 68], chemical vapour deposition (CVD) from silane [69, 70] and sol–gel method [71]. These methods have their own strengths and weaknesses. SiC powder made by sol-gel method and CVD has high purity. However the cost of production is high, and raw materials involve toxic chemicals. Carbothermal reduction process is simple and cheap, while it leaves a large amount of unreacted silica and high level of impurities [66]. Currently, carbothermal reduction is the primary method for the synthesis of SiC.

1.2.2.1 Acheson process

The Acheson process is the most common process for the industrial production of SiC, which was established as early as 1892 [72]. The product, with grain dimension and quality changing in broad ranges, is often impure with a relatively high oxygen content. It finds applications mostly as an abrasive, while the preparation of high performance SiC ceramics requires added purification steps and ball milling.

The Acheson electric resistance furnace can have different geometries, but it is usually composed of a central core of graphite and coke that works as an electrical heater, as shown in Figure 9. The reaction mixture, typically SiO_2 and petroleum coke, is filled around the core. The walls of the furnace comprise of bricks loosely laid together to allow gases produced in the reaction to escape. Hence the walls are removable and the reaction is not usually sealed from air. The temperature cycles can vary, however the temperature of the central core reaches a maximum temperatures of ca. 2700 °C and is then lowered and maintained for about 30 hours at ca. 2000 °C. Subsequently, the furnace is allowed to cool and the produced SiC is removed, purified and graded according to size. The best quality samples are found near the core where the temperature is higher [73].

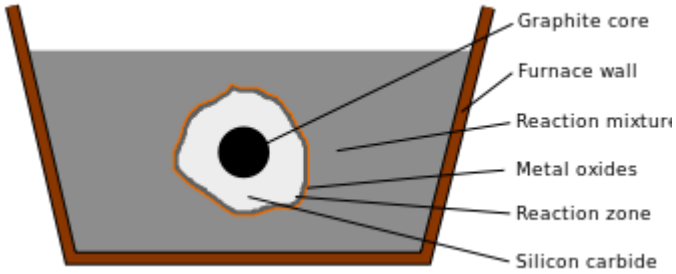

Fig. 9 Cross-section of an Acheson furnace [73].

All SiC is initially formed as small crystals of the cubic beta form. β-SiC can be formed at temperatures as low as 525 °C [74]. In Acheson furnaces, however, the reaction takes place at temperatures above 1527 °C. The transformation of relatively pure β-SiC to the alpha crystalline form (α-SiC) occurs at temperatures above 1900 °C [66].

The SiO_2 source for SiC manufacture can be sand, quartzite or crystalline rock quartz. Only the purest quartz can be used for production of high purity SiC. The most common carbon source is petroleum coke, the final residue from crude oil refining. Porosity agents are traditionally incorporated into SiC furnace mixes to make them permeable to the escaping of CO. Sawdust, bagasse and rice hulls are commonly used. Liquid

adhesives such as lignin sulfonates have also been successfully used to prevent settling of mixes and the consequent decrease in open porosity [73].

1.2.2.2 Lely process

In 1955, Lely developed a method that was considered to have a major advantage over the Acheson process. In the Lely method, SiC lumps are filled between two concentric graphite tubes (Figure 10). After proper packing the inner tube is carefully withdrawn leaving a porous SiC layer inside the outer graphite tube called the crucible. The furnace is then heated to approximately 2500 °C in an Argon environment at atmospheric pressure. The SiC powder near the crucible wall sublimes and decomposes because of a higher temperature in this region. Since the temperature at the inner surface of the charge is slightly lower, SiC crystals start nucleating at the inner surface of the porous SiC cylinder. High purity crystals can be obtained using better grade SiC charge and Ar gas. However, the Lely method is not suitable for industrial production due to the low yield (~ 3 %) [72].

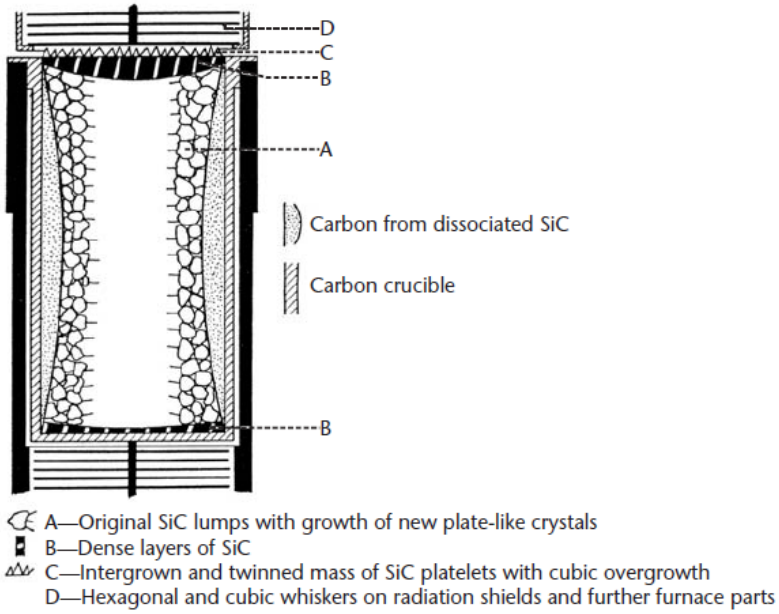

Fig. 10 Cross-section of a Lely furnace [72].

1.2.2.3 Fluidized bed reactor processes

Fluidized bed reactors have been investigated for the carbothermal synthesis of non-oxide ceramic powders, such as SiC, Si_3N_4 and AlN. Since conventional carbothermal reduction processes involve the highly endothermic reaction, it is critical that energy is provided efficiently to the reaction zone and that the reactants are in intimate contact throughout the process. Processes in fluidized bed reactors are generally not heat transfer limited.

A continuous fluidized bed version of the Acheson process for manufacturing SiC has been commercialized by Superior Graphite Company [75, 76]. Silica sand and petroleum coke are continuously introduced as free flowing granular solids into a closed vessel. An insert gas, such as N_2, or a recycled product gas stream containing CO, is used to fluidize the solid reactants. An electrical potential is applied between the vessel and a centrally positioned electrode (Figure 11(a) and (b)) or between electrodes in direct contact with the particles to heat the contents of the fluidized bed to a temperature of 1900 °C to 2000 °C. In one mode of operation, in production of coarse SiC, a product is discharged below the fluidized bed, while in production of fine SiC, it is removed above the bed.

O'Connor and McRae [77] developed a fluidized bed process for SiC synthesis (Figure 12) in which the energy required to drive the endothermic reaction is supplied by radiation from an exothermic combustion reaction in the upper part of the bed. Carbon and Si-containing compound are reacted in the lower fluidized bed with product removal from the middle discharge zone. Methane, added to the fluidizing gas stream, cracks to hydrogen and carbon in the lower fluidized bed. The carbon reacts with volatile Si-containing compounds to SiC while the hydrogen is combusted in the upper part of the bed with added oxygen.

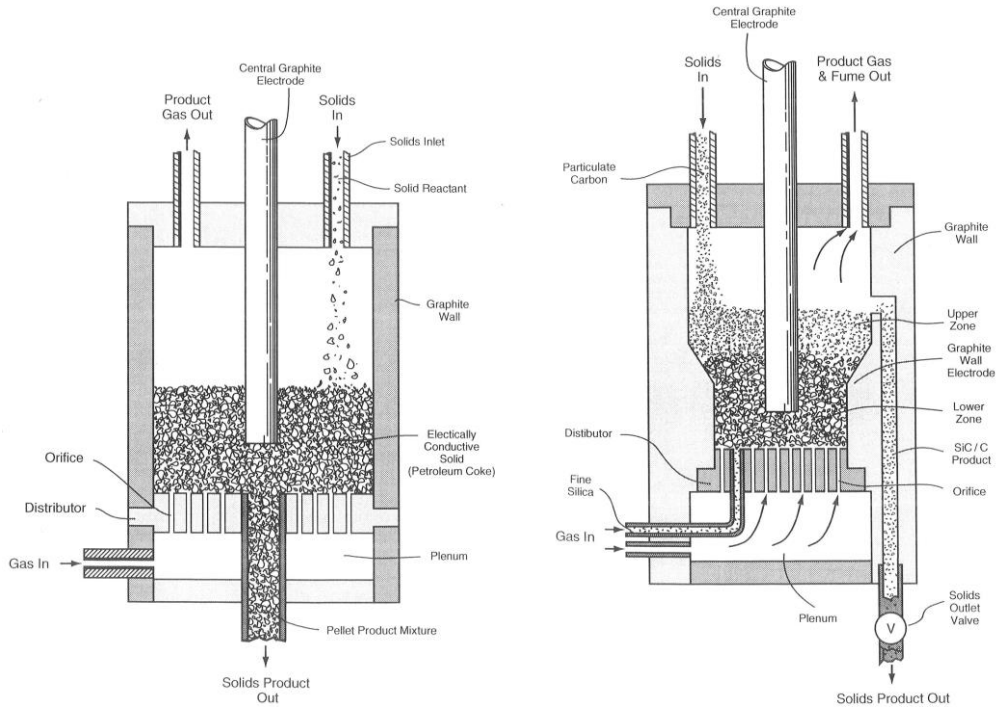

(a) (b)

Fig. 11 Electrothermal fluidized bed: (a) below bed product discharge; (b) above bed product discharge [75].

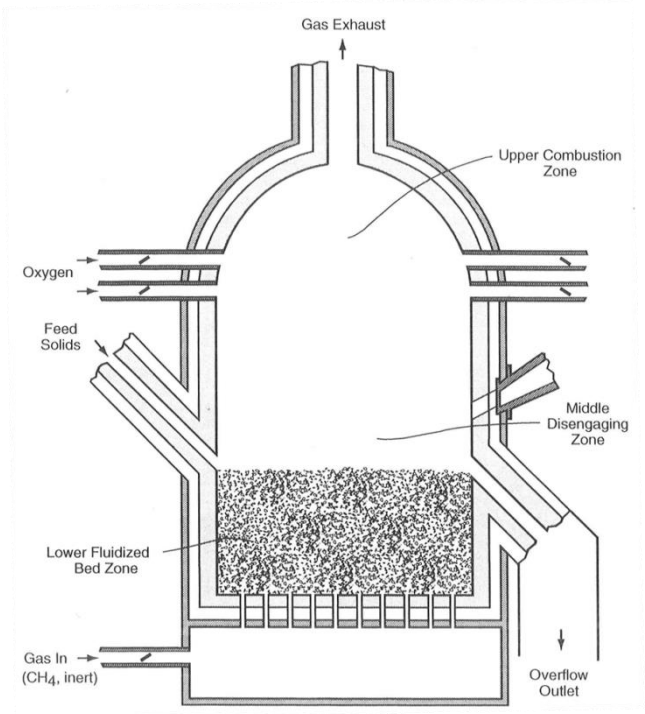

Fig. 12 Fluidized bed process heated by combustion of gaseous reaction products for synthesizing SiC [77].

Robb [78] describes a batch fluidized bed process developed by General Electric Company for the manufacture of WC and Mo_2C. A carbothermal nitridation process for the synthesis of AlN was developed by Carborundum [79]. Alusuisse-Lonza Service Ltd. [80] investigated a fluidized bed process for the carbothermal nitridation synthesis of Si_3N_4.

Fluidized beds have advantages for processes which involve gas-solid reactions, including reactions which generate CO. On the other hand, the agitation of the solids in fluidized beds may promote the separation of the solid reactants.

1.2.3 Factors Affecting Carbothermal Reduction of Silica

1.2.3.1 Temperature

Carbothermal reduction of silica is very sensitive to the reaction temperature. Figure 13 shows the change of equilibrium composition of a system starting with 1 mole of SiO_2 and 2 moles of C (stoichiometric ratio for the Si synthesis) with temperature at 1 atm (calculated using HSC software). It can be noticed that the reactions occur mainly in two temperature ranges: 1510 to 1760 °C and above 2220 °C. At 1510–1760 °C, silica is converted to solid SiC and gaseous SiO; above 2220 °C, SiC and SiO further react to form elementary silicon. In a laboratory or industrial process, CO is continuously removed from the reaction zone, therefore reactions occur under conditions different from those used in calculations of equilibrium phases in Figure 13.

At temperatures between 1200 and 1400 °C, the rate of release of SiO and the rate of formation of SiC are sufficiently low [81]. This is consistent with Zhang and Cannon [82] who reported formation of a significant amount of SiO when the reaction temperature was greater than 1400 °C. Hirasawa and Tada [83] reported a two-stage reduction process for silicon production. It was found that silicon yield was higher at 2000 °C than at 1950 °C. The reduction of SiO_2 to SiO(g) by Reaction (4) was the

reaction rate controlling step.

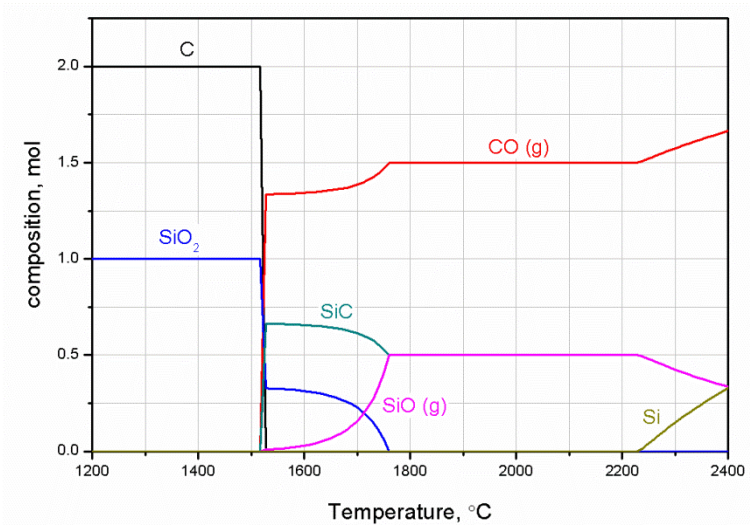

Fig. 13 Equilibrium composition of a system starting with 1 mol of SiO_2 and 2 mol of C (HSC modelling).

Poch and Dietzel [84] investigated the reaction between SiO_2 and SiC in argon atmosphere, in the temperature range of 1480–2000 °C with SiO_2/SiC molar ratio of 2.5. The reaction rate was found to be rather low at temperatures below 1550 °C but increased rapidly with increasing temperature. Below 1790 °C the final weight loss measured in the reaction agreed with the stoichiometry of Reaction (4). Above 1790 °C there was an additional weight loss of about 5 %., which was attributed to the silicon evaporation.

The overall reaction for the manufacture of SiC from silica and carbon is:

$$SiO_2\,(s) + 3C\,(s) = SiC\,(s) + 2CO\,(g) \qquad (4)$$

$$\Delta G^\circ = 598.18 - 0.3278\,T \quad (kJ)$$

The standard Gibbs free energy of the above reaction decreases with increasing temperature and becomes zero at 1525 °C. However, the reaction can take place at

lower temperatures when the CO partial pressure is lower than atmospheric pressure. There is strong evidence that SiC is synthesized through the gaseous intermediate silicon monoxide (SiO) with the following reactions being most important [85]:

$$C\,(s) + SiO_2\,(s) = SiO\,(g) + CO\,(g) \quad (21)$$

$$SiO_2\,(s) + CO\,(g) = SiO\,(g) + CO_2\,(g) \quad (22)$$

$$C\,(s) + CO_2\,(g) = 2CO\,(g) \quad (23)$$

$$SiO\,(g) + 2C\,(s) = SiC\,(s) + CO\,(g) \quad (2)$$

SiO(g) is initially formed at the contact points of the silica and carbon according to Reaction (21). The gas-solid route through Reactions (22) and (23) is the one which makes Reaction (2) possible once the silica and carbon at contact points are consumed [86]. The standard Gibbs free energy changes for Reactions (4), (21), (22), (23) and (2) are plotted in Figure 14.

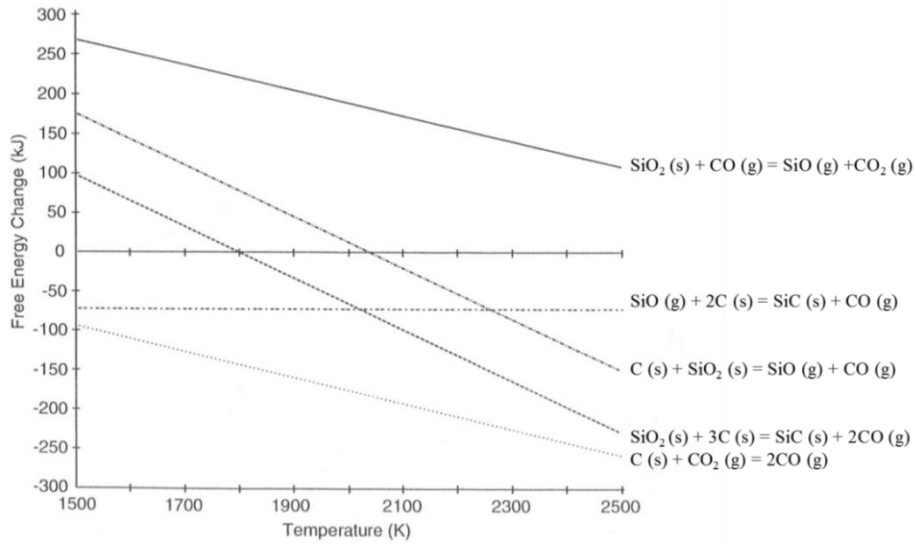

Fig. 14 Standard Gibbs free energy changes for SiC synthesis reactions [87].

A schematic of this mechanistic model for synthesis according to Reactions (21), (22), (23) and (2) is shown in Figure 15. The synthesis of SiC (Reacion (4)) is characterized by an irreversible phase boundary controlled reaction of spherical carbon particles for

which the thickness of the reaction zone is small compared with the dimensions of the particle [87], as described by Equation (24):

$$k = \frac{1-(1-X)^{\frac{1}{3}}}{t} = \frac{27.4}{d}\exp(\frac{-383000}{R_g T}) \quad (24)$$

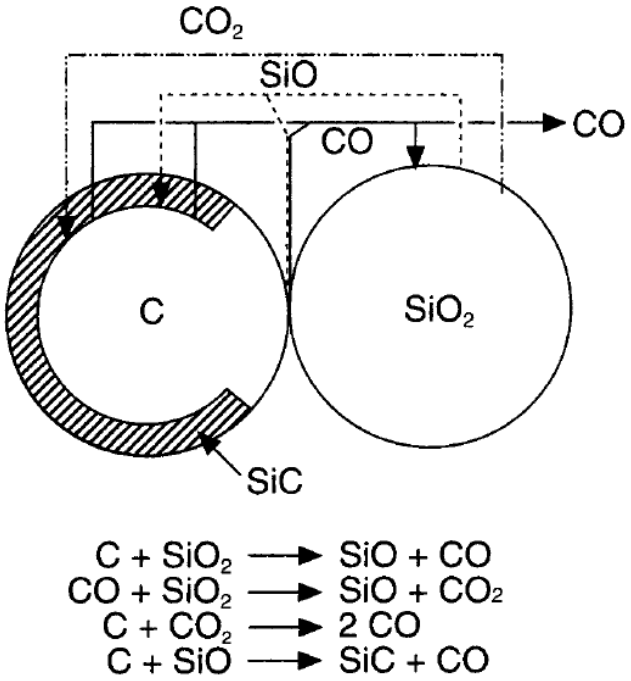

Fig. 15 Schematic of SiC synthesis reaction mechanism [87].

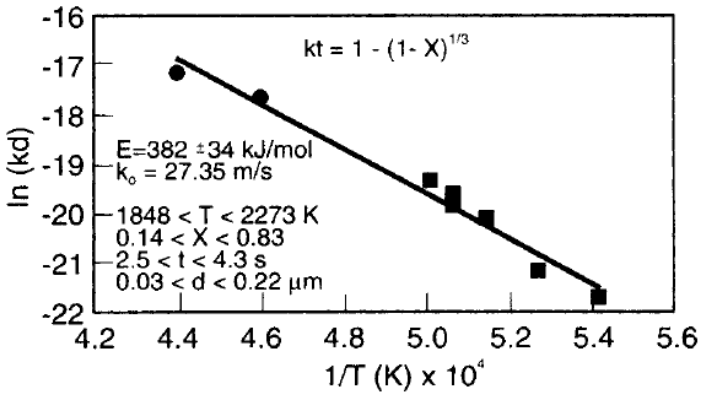

Fig. 16 Reaction kinetics (Reaction (4)) for contracting volume model with phase boundary control [87].

The fit of this model to experimental data for different carbon particle sizes and its

range of applicability are shown in Figure 16.

A broad range of activation energies ($251 < E_a < 552$ kJ/mol) for Reaction (4) has been reported by numerous investigators for the synthesis of SiC by carbothermal reduction of SiO_2 (Table 3). This is most likely due to the broad range of rate equation forms.

Table 3. Reaction rate constant and activation energy for SiC synthesis by carbothermal reduction.

Reference	Carbon		T(K)	k (S^{-1})	E (kJ/mol)
	Source	d (μm)			
Blumenthal, Santy and Burns (1966) [91]	Carbon black	0.017	1573	1.0E-03	287
			1673	5.7E-03	
			1773	1.5E-02	
Khalafalla and Haas (1972) [92]	Graphite	-	1673	1.4E-03	322
			1698	1.7E-03	
			1723	1.9E-03	
			1788	2.8E-03	
Klinger, Strauss and Komarek (1966) [88]	Graphite	<44	1818	3.2E-07	510
			1863	4.5E-07	
			1913	1.7E-06	
			1943	2.3E-06	
			1983	4.5E-06	
			2038	1.4E-05	
Kuzenestova, Dmitrenko and Kokurin (1980) [93]	Carbon black	0.187	1773	1.7E-02	251
			1873	5.8E-02	
			1973	7.6E-02	
			2073	2.1E-01	
	Carbon black	0.385	1773	7.8E-03	288
			1873	2.8E-02	
			1973	6.2E-02	
			2073	1.3E-01	
	Coke	0.198	1773	9.2E-03	299
			1873	3.1E-02	
			1973	6.2E-02	
			2073	1.6E-01	

Table 3. (Continued) Reaction rate constant and activation energy for SiC synthesis by carbothermal reduction.

Reference	Carbon		T(K)	k (S^{-1})	E (kJ/mol)
	Source	d (μm)			
Lee and Cutler (1975) [94]	Charcoal	70	1623	5.0E-04	544
			1643	1.0E-03	
			1673	1.5E-03	
			1703	3.9E-03	
			1713	4.0E-03	
Ono and Kurachi (1991) [89]	Pyrolyzed polymer	-	1795	3.2E-03	391
			1813	3.5E-03	
			1821	5.5E-03	
			1881	1.2E-02	
			1962	2.7E-02	
Shimoo, Sugimoto and Okamura (1990) [90]	Pyrolyzed polymer	-	1773	1.5E-02	352
			1873	2.7E-02	
			1973	4.5E-02	
Viscomi and Himmel (1978) [95]	Coke breeze	-	1673	1.1E-02	552
			1723	1.4E-02	
			1773	2.5E-02	
Weimei et al. (1993) [87]	Carbon black	0.030	1848	1.2E-02	382
			1898	2.0E-02	
			1948	6.2E-02	
			1973	8.9E-02	
			1998	1.2E-01	
		0.218	2173	9.2E-02	
			2273	1.5E-01	
Johnson et al. (2002) [96]	Carbon black	0.030	2073	2.5E-01	340
			2173	6.2E-01	
			2473	6.1	
			2573	11.6	
		0.213	2073	3.5E-02	
			2173	8.7E-02	
			2473	8.6E-01	
			2573	1.64	

1.2.3.2 Starting materials

According to the overall reactions for silicon (Reaction (1)) and SiC (Reaction (4))

production, stoichiometric molar ratio of C/SiO_2 is 2 and 3, respectively; however, for the complete conversion of silica, carbon should be taken in excess. Excess carbon ensures sufficient particle contact between SiO_2 and C [97] and improves SiO generation [98].

Carbon source has a substantial influence on the product SiC morphology and rate of reaction [73] with the product SiC crystallites resembling the starting carbon crystallites prior to grain growth. SiC crystallites sinter and grow with increasing temperature and reaction time. Finer carbon crystallites react faster than larger ones. In a study of the effects of silica particle size and milling time on the synthesis of silicon carbide nanoparticles by carbothermal reduction, Moshtaghioun et al. [99] found that the particle size of silica and milling time were important parameters determining the rate of carbothermal reduction and size and morphology of SiC particles produced. The SiC nanoparticles were between 5 and 25 nm when nano silica was used, and in the range of 20–70 nm when micro silica was used.

Dal Martello *et al.* [100] investigated silicon production from quartz and SiC using pellets of quartz-SiC powder and quartz lumps. More SiO was produced and almost no quartz was left when pellets of a SiO_2–SiC mixture were used as charge materials in the case of SiO_2/SiC molar ratio of 1:1. In comparison, a higher silicon yield was achieved with quartz lumps because of less loss of SiO.

1.2.3.3 Gas atmosphere

Previous works [101–105] have demonstrated that the gas atmosphere can change the reaction mechanisms of various carbothermal reduction reactions and the reaction kinetics. Data obtained by Terayama and Ikeda [106] for the carbothermal reduction of MnO showed that MnO is reduced much faster in helium than in argon. Similar results were obtained by Yastreboff et al. [107] in reduction of MnO, manganese ore, and ferromanganese slag. Ostrovski et al. [104] studied the carbothermal solid state

reduction of manganese, titanium and aluminum oxides in argon, helium and hydrogen. The difference in helium and in argon was attributed to different diffusion coefficients of gaseous reactants and products, which are much higher in helium than in argon. When carbothermal reduction took place in hydrogen, it was involved in the reduction process by reducing oxides to suboxides and by formation of methane as an intermediate reductant.

However, the effect of gas atmosphere on the carbothermal reduction of silica has been studied to a lesser extent. The SiC formation will stop when the CO partial pressure in Reaction (4) reaches the equilibrium value. CO has to diffuse out of the reactant mixture for further reaction to take place.

Results of previous studies have shown that H_2 can enhance the reduction kinetics, of which the mechanism is still not clear [108, 109]. In the thermodynamic analysis of carbothermal formation of SiC and elemental Si using methane, Lee et al. [51] demonstrated that methane decomposes completely at temperatures above 1250 °C. In a practical process, a thermodynamic equilibrium is not reached, so inclusion of highly reactive methane in a high temperature reaction system can improve the reaction kinetics as demonstrated by reduction of other metal oxides. However, no experimental investigations have been reported in literature on the direct reduction of SiO_2 to SiC by methane containing gas.

1.2.3.4 Catalyst

Several research works have confirmed that some transition metals act as catalysts in the SiC formation [99, 110–112]. Addition of catalyst allowed the growth of SiC to take place at lower temperatures with an increase in the reaction rate of the carbothermal reduction process. For example, Fe and Co enhances SiO formation without agglomeration of reactants, such that SiC formation can proceed to near completion, resulting in high yield of SiC. Mn, Cu and Ni have a positive effect on SiO formation

and agglomeration (or sintering) of the reactants simultaneously. Addition of Al and B affects the crystal growth rate and the dominant crystal structure of the products.

At a higher temperature (1600 °C or higher), the reaction between SiO and CO favoured whisker formation [113, 114]. Transition metals (especially Fe, Co, Ni) have been shown to act as catalysts in the gas–gas reaction to form whisker via VLS (vapor–liquid–solid) mechanism of formation [113]. Initially, the catalyst was in contact with substrate as the temperature was raised to the melting points of transition metals. The liquid globule absorbed Si and C from SiO and CO vapour until it became supersaturated. Nucleation of SiC occurred at the interface with the substrate and continued solution of gas species into the liquid catalyst ball allowed the whiskers to grow as additional SiC precipitated.

Besides metallic catalysts, boron compounds were reported to have catalytic effects on the reaction product [116]. SiC reduced from boric acid (H_3BO_3) treated rice husk had better crystallinity with higher yield and purity. During heating, H_3BO_3 decomposed to HBO_2 and then to B_2O_3 liquid phase that was miscible with SiO_2 thoroughly. The liquid phase helped the migration of SiO_2 particles through the rice husk, increasing the contact of SiO_2 with C and allowing the reaction to take place more effectively [117].

1.2.4 Behavior of Impurities in the High Temperature Synthesis of Silicon

The behavior of different elements in silicon production depends on several factors:

a. The temperature in the furnace.
b. Relative stability of the elements and their compounds.
c. The volatility of the elements and their compounds.
d. The solubility of the elements in the liquid silicon.
e. Type of raw materials.

Mass flow of materials in production of silicon is schematically shown in Figure 17.

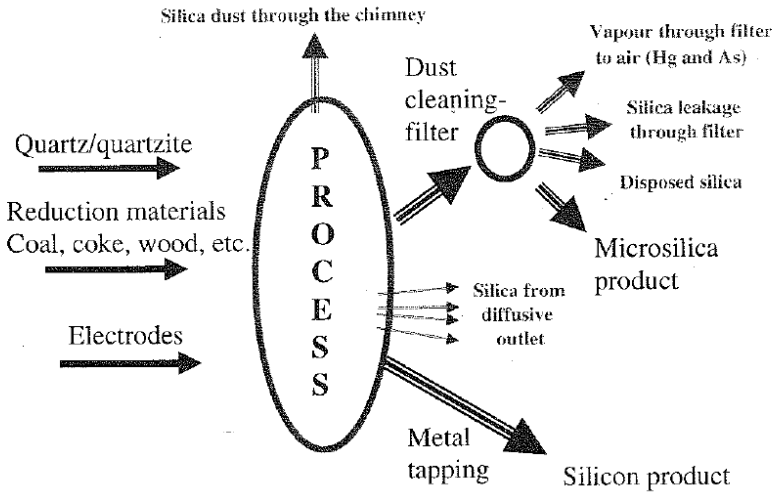

Fig. 17 The main mass flows in the silicon production process [115].

The Ellingham diagram in Figure 18 shows the standard Gibbs free energies of formation of oxides per mole of oxygen reacted. Oxides above the Si/SiO_2 equilibrium line can be reduced to their metal state at a given temperature at partial pressures of oxygen higher than needed for the reduction of SiO_2 to Si. Other metal oxides which require a lower oxygen potential than SiO_2 to be reduced to metal are assumed to remain as oxides up to the melting point to silica [25]. It should be mentioned that the Ellingham diagram represents conditions for the reduction of pure oxides to pure metals while impurities in production of silicon exist in the form of compounds or oxide and metal solutions.

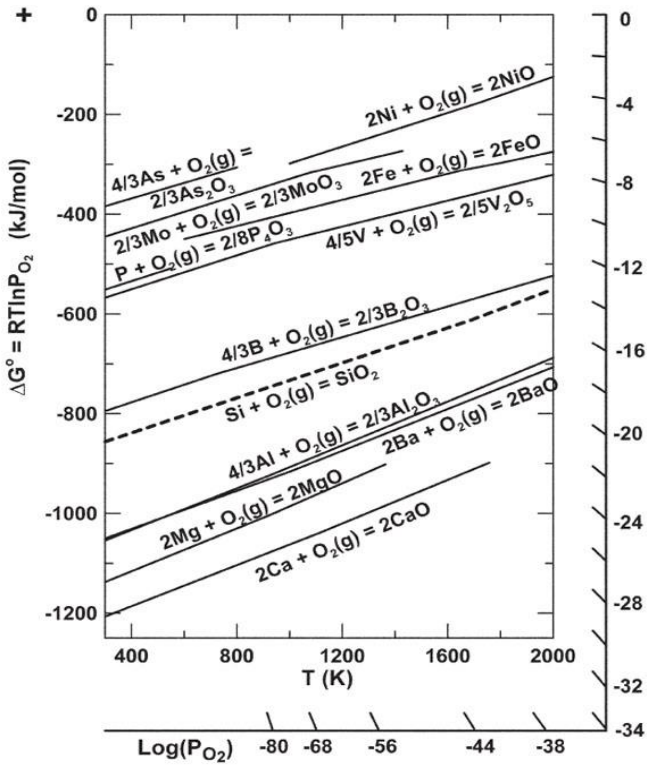

Fig. 18 Ellingham diagram for oxides [25].

Myrhaug and Tveit [115] developed a simplified model to predict the behavior of the trace elements in the silicon production process based on the boiling temperatures of these elements, as shown in Figure 19(a). The critical temperature is the highest temperature in the reaction zone of an arc furnace, set to 2000 °C in this model. The elements with boiling points higher than this temperature, such as boron, were expected to remain in the liquid silicon. The other critical temperature of 1300 °C is the temperature at the top of charged materials. The elements with boiling points lower than it, such as phosphorus, were expected to follow the SiO and CO in the off-gas. Elements with boiling points between 1300 °C and 2000 °C were expected to distribute among liquid metal, slag, and SiO and CO in the off-gas, and condense together with the SiO_2-particles. Figure 19(b) shows that this model describes the behavior of most of the elements, with the most serious disagreement involving phosphorus. The model predicts that all phosphorus should be volatilized, and in fact 75 % of the phosphorus leaves in silicon.

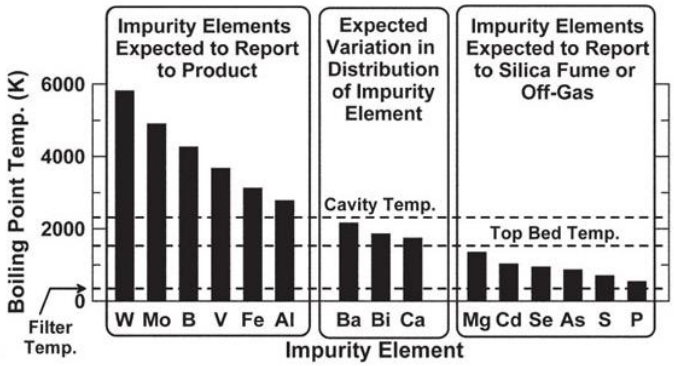

(a)

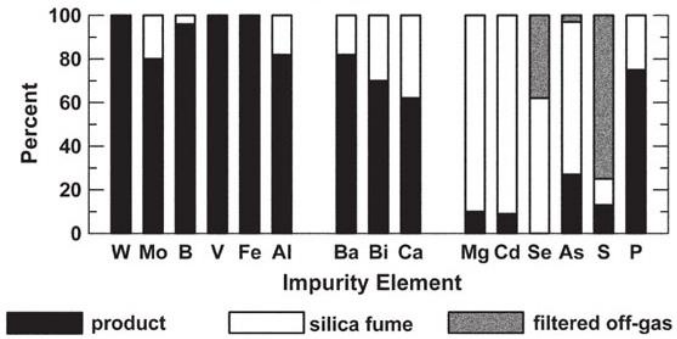

(b)

Fig. 19 Boiling temperatures (a) and distribution (b) in different outlets of the trace elements [115].

In the production of SoG-Si, removal of phosphorous and boron is most challenging and expensive task. Their behavior is reviewed below.

1.2.4.1 Phosphorus

MG-Si usually contains about 40 ppm phosphorus of which 45 % comes from quartz, 45 % from carbon and the other 10 % from the electrode. P_4O_6 boils at 176 °C while P_2 boils at 280 °C, which means that phosphorus should have left the furnace in the off gas, as described in Figure 19(a). However, raw materials also contain iron oxides. Both iron and phosphorus, being reduced to elements, form a stable compound FeP [118]. FeP is estimated to have a boiling temperature of 3200–3300 °C [119]. Much of P enters the silicon metal, as shown in Figure 19(b).

Under reducing conditions, phosphate is reduced to form P_2 vapor. Formation of phosphorus hydrides such as PH_3 also helps removal of P [120]. It has been demonstrated experimentally that phosphorus in MG-Si is removed by vaporization during vacuum melting [121, 122]. Miki *et al.* [123] have determined the thermodynamics of this process, which is described by Reactions (25) and (26).

$$\frac{1}{2}\ P_2\ (g) = P\ (1\ \%\ in\ Si(l)) \quad (25)$$

$$\Delta G° = -139.12 + 0.043\ T \quad (kJ)$$

$$P\ (g) = P\ (1\ \%\ in\ Si(l)) \quad (26)$$

$$\Delta G° = -387.02 + 0.103\ T \quad (kJ)$$

At low concentrations of phosphorus where its Henrian activity coefficient is unity, the relationship between the phosphorous concentration in silicon and the equilibrium partial pressure of monoatomic phosphorus is given as follows:

$$\frac{[\%P]}{P_P} = \exp\left(\frac{-\Delta G^0_{Reaction\ 26}}{RT}\right) \quad (27)$$

Figure 20 shows the calculated concentration of phosphorus dissolved in silicon at 1550 °C for monoatomic and diatomic phosphorous vapour.

Zheng *et al.* [124] analysed the possibility of removing phosphorus from MG-Si by a vacuum treatment. In the vacuum treatment of silicon to remove phosphorus, silicon is also vapourised. Results of their analyses, as presented in Figure 21, show how the yield of silicon is related to the attained phosphorous concentration with an initial phosphorus content of 13.3 ppmw, and phosphorous removal is achieved at the highest efficiency in the temperature range of 1550–1700 °C.

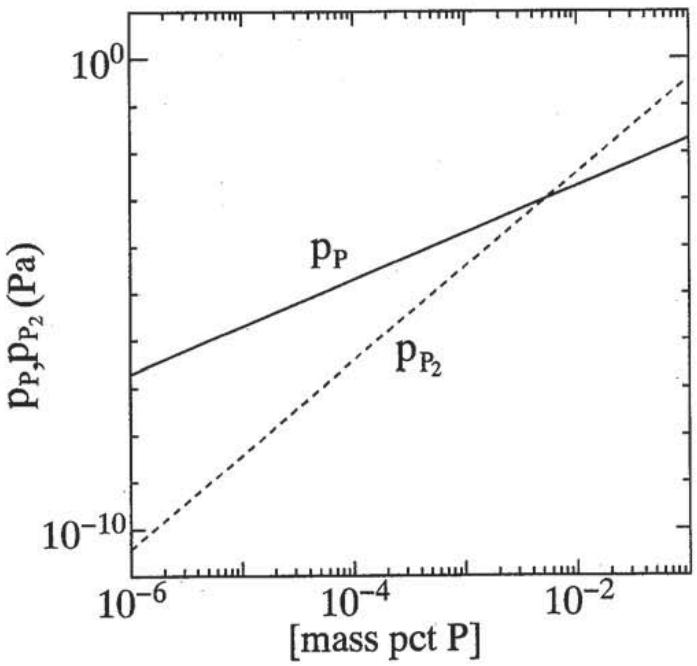

Fig. 20 Relationship between equilibrium partial pressures of P and P_2 (Pa), and phosphorus concentration in silicon at 1550 °C [123].

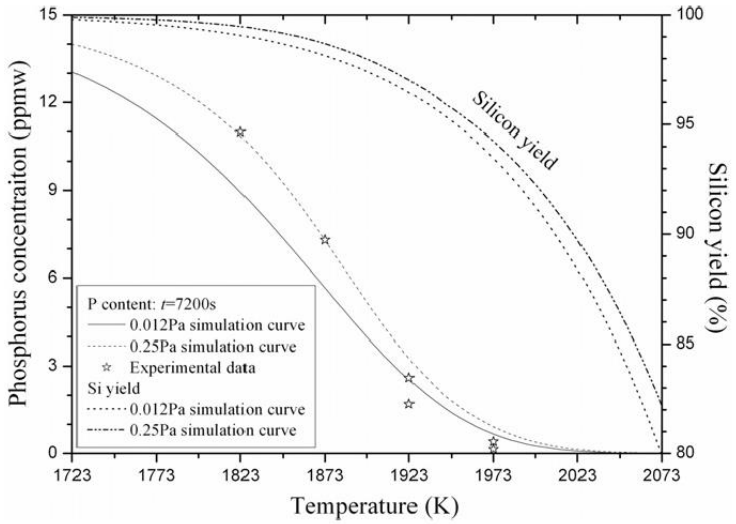

Fig. 21 Relationship between the yield of silicon and attained phosphorus concentration during vacuum treatment [124].

1.2.4.2 Boron

The boron content in silicon is directly linked to the impurity level in quartz and reducing materials. Materials free of boron are crucial for obtaining pure MG-Si. In the reduction conditions of an arc furnace, B_2O_3 may be converted into different compounds, including:

$$B_2O_3\,(l) = B_2O_3\,(g) \quad (28)$$

$$B_2O_3\,(l) + C = B_2O_2\,(g) + CO\,(g) \quad (29)$$

$$2B_2O_3\,(l) + 7C = B_4C + 6CO\,(g) \quad (30)$$

Reaction (30) has been proven to dominate [125], which leads to contamination of silicon with boron in the carbothermal reduction of silica. Boron can be removed by introduction of H_2 or H_2O, in accordance with the following reaction [126–129]:

$$B_2O_3\,(l) + C + H_2\,(g) = 2\,BHO\,(g) + CO\,(g) \quad (31)$$

Figure 22 shows the equilibrium partial pressures of various boron species in the arc furnace at different temperatures, calculated using data from NIST-JANAF Thermochemical Tables. When a CO pressure is 10 kPa, BHO partial pressure can reach up to 1.2 kPa at 1400 ^{o}C, which is reasonably high to effectively remove B from raw materials.

Ikeda *et al.* [122, 130] used an argon arc plasma remelting furnace to remove impurities in MG-Si under 60 KPa. The apparent rate constant of boron removal increased with increasing water vapour content, which was 3.8×10^{-3} s^{-1} at 1.24 vol % H_2O. Silicon yield was about 94 % after 60 minutes reduction. Boron content dropped to below 1 ppm within 15 minutes.

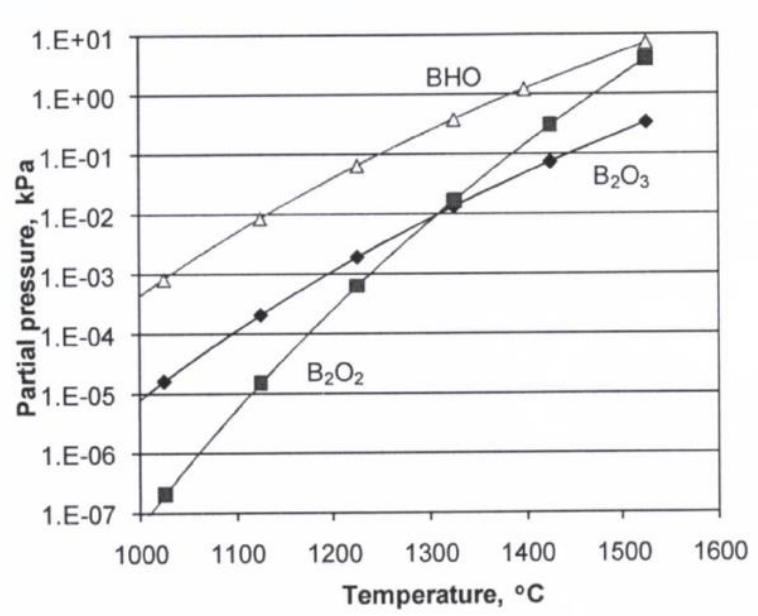

Fig. 22 Equilibrium partial pressure of B_2O_3, B_2O_2, and BHO. P_{CO} =10 kPa.

1.2.5 Project's Objectives

From the literature review above, it appears that direct carbothermal reduction of silica to produce SoG-Si is a reasonable route. Although in any case, final refining is needed, the carbothermal process can be upgraded further to improve silicon purity in order to reduce operational and manufacturing costs of SoG-Si.

Although investigations of carbothermal synthesis of silicon carbide and elemental silicon have been conducted for decades, there are deficiencies and inconsistencies in the literature. Particularly, the effect of gas atmosphere was rarely covered. The mechanism of silicon carbide formation needs further understanding. The value in use of natural gas in silicon production was incompletely underdtood.

The final aim of this project is to develop a new technology for production of high purity silicon. Quartz will be converted to SiC using natural gas as reduction agent or partially replacing solid carbon (which can also be produced by natural gas). SiC will be processed further by reacting with quartz to form silicon. This study will focus on the

effects of operational parameters on the carbothermal synthesis of silicon carbide and elemental silicon, and the mechanisms of their formation.

The project will study:

1) Mechanism of production of SiC by carbothermal reduction of quartz in hydrogen containing gases.
2) Reduction of quartz to SiC by methane containing gases in a fixed bed reactor.
3) Reduction of quartz to SiO in fluidized bed reactor, and the kinetics of reaction between methane and quartz.
4) Mechanism of production of silicon in different gas atmospheres.

1.3 Experimental

1.3.1 Materials

1.3.1.1 Quartz powder

Quartz used in this study was provided by Elkem AS (Oslo, Norway) in the form of lumps. Quartz powder was obtained by crushing quartz lumps to different particle size ranges in a 6 inch agate pulveriser in a Rocklabs ring mill. The crushing service was provided by Commonwealth Scientific and Industrial Research Organization (CSIRO, Melbourne, Australia). The agate was made of grey silica so that contamination to the quartz sample was minimized.

The size of quartz powder used in experiments described in Chapters 2, 3, 4, and 6 was less than 70 μm. The size ranges of quartz powder considered in Chapter 5 were 53~100 μm, 100~140 μm and 140~200 μm.

The impurity contents of quartz lumps were provided by the supplier, as shown in Table 4.

Table 4. Impurity contents in quartz lumps, mg/kg.

B	P	Fe	Al	Ca	Ti	Mn	Mg
0.5	1.0	33.0	219.0	26.0	7.9	1.9	27.0

1.3.1.2 Quartz sphere

The quartz spheres used in Chapter 5 were made from commercially available fused quartz glass (Guolun Quartz Products Co. Ltd., Lianyungang, China). The diameter of spheres used in the experiments was approximately 15.90 mm. All quartz spheres were made with a circular hole (0.6 mm diameter).

1.3.1.3 Graphite powder

The graphite powder was of purity ≥ 99.99 %, supplied by Sigma-Aldrich Chemical Company, Inc. (St. Louis, U.S.A.). The graphite was synthetic with particle size less than 45 μm.

1.3.1.4 Silicon carbide powder

The α-SiC powder used in Chapter 6 was supplied by Pacific Rundum Co., Ltd. (Toyama, Japan), which was synthetic with particle size range of 50–200 μm. The impurity contents were provided by the supplier, as shown in Table 5.

Table 5. Impurity contents in α-SiC powder, mg/kg.

Fe	Ni	Ca	Al	P	B	Na	K	Ti	V	Zr	N
5.0	0.8	0.5	14.0	1.0	<0.1	0.4	<1	3.5	0.7	0.4	123

1.3.1.5 Gases

Argon, hydrogen and methane were supplied by Coregas Pty. Ltd. (Unanderra, Australia) as compressed gases in gas cylinders. The gases used in the experiments were of 99.999 % purity with typical impurities of H_2O (< 3ppm), O_2 (< 2ppm), and total hydrocarbon (< 0.5 ppm). The argon–hydrogen gas mixtures were formed by mixing individual gases, controlled by mass flow controllers.

1.3.2 Carbothermal Reduction of Quartz to SiC

1.3.2.1 Experimental setup

Experimental setup used in the carbothermal synthesis of silicon carbide, includes (1) fixed bed reactor and vertical tube furnace, (2) gas system and (3) off gas composition analysis.

1) Fixed bed reactor and furnace

Reduction of quartz in different gas atmospheres was carried out in a fixed bed reactor heated in a vertical tube furnace (Model GSL-1600, Zhengzhou Kejing Electric & Trade CO. Ltd., Zhengzhou, China). The furnace configuration is presented in Table 6.

Table 6. Vertical tube electric furnace configuration.

Model	GSL-1600
Maximum operation temperature	1650 °C
Temperature controller	YUDIAN AI-208
Heating elements	Kanthal Super 1800-$MoSi_2$ resistance
Furnace tube	High purity recrystallised alumina
Tube internal diameter	50 mm
Tube external diameter	60 mm
Tube length	1000 mm
Thermocouples	Type B: Pt 30% -Rh / Pt 13 % -Rh

A temperature profile for GSL-1600 furnace was established to determine the position and length of the stable hot zone, as presented in Figure 23. The thermal profile was measured using a type B thermocouple installed in the reactor. The reactor was progressively inserted into the middle of furnace tube with increments of 5 cm. A period of 10 minutes was allowed for thermal stabilisation and the temperature was recorded at given position of the reactor in the furnace.

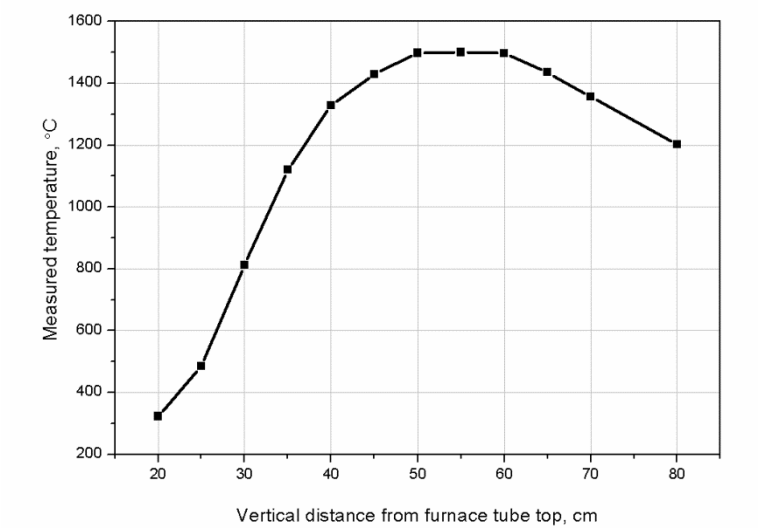

Fig. 23 Temperature profile for GSL-1600 vertical tube furnace used in the carbothermal reduction experiments. Furnace set temperature was 1542 °C.

The sample temperature inside the reactor was calibrated against set temperature of the furnace using a type B thermocouple. The reactor was placed into the hot zone of the furnace and the furnace was heated to different temperatures. At each point, the furnace was left for 30 minutes to stabilise thermally, and the thermocouple reading was recorded. GSL-1600 vertical tube furnace produced a linear response in the sample temperature to the set point temperature, as presented in Figure 24.

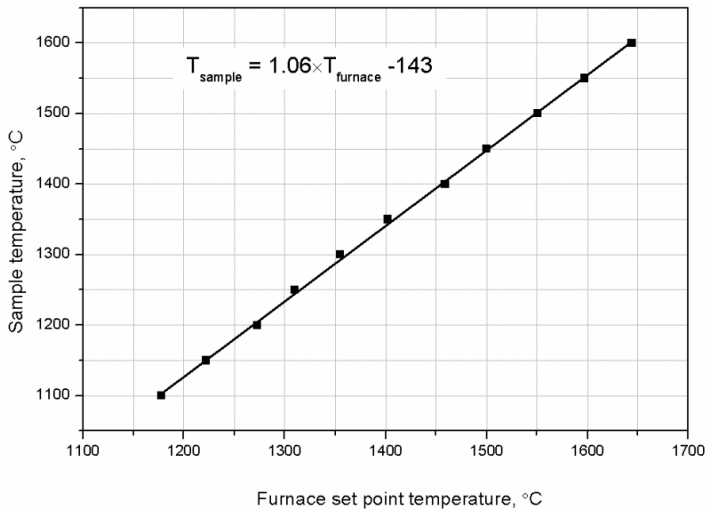

Fig. 24 Sample temperature response to the set point temperature for GSL-1600 vertical tube furnace.

The schematic of the fixed bed reactor is presented in Figure 25. A sample pellet was loaded in the inner recrystallized alumina tube. The pellet was supported by an alumina plug, which was fixed by an alumina pin via holes drilled at the bottom of inner tube. Sample temperature during reaction was measured by type B thermocouple, which was protected against reaction gas atmosphere by an alumina thermocouple sheath.

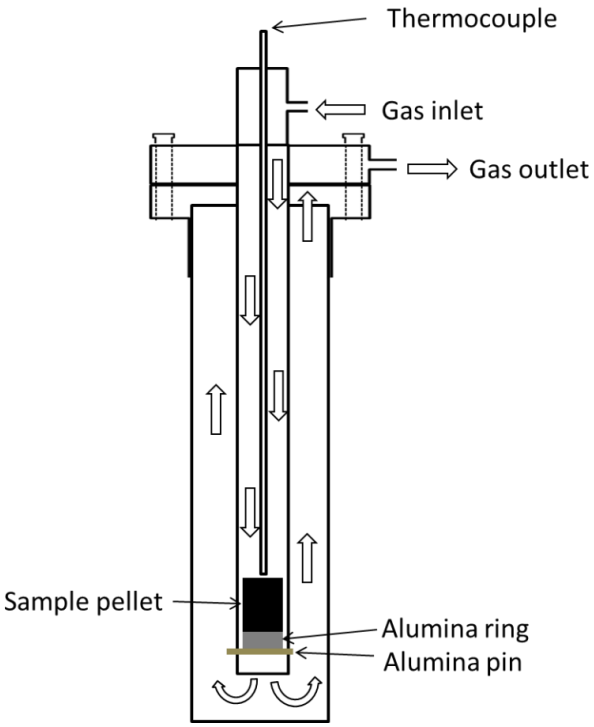

Fig. 25 Schematic of the fixed bed reactor.

The inner tube with a sample pellet was inserted into the outside recrystallized alumina sheath with the inner diameter of 19 mm. The inner tube, outside tube and the thermocouple sheath were fixed by special metal fittings and sealed with O-rings. Reaction gas was introduced into the reaction system from the top of inner tube, flowed through a pellet sample and plug, and then left the reactor from the gap between the outside tube and inner tube. After assembling the reactor with a sample pellet, the reactor was inserted into the hot zone of the furnace to heat up to target temperature.

2) Gas system

The flow rate of gas was controlled by individual mass flow controllers. Three mass flow controllers (Model DFC26S, AALBORG Instruments and Controls, Inc., Orangeburg, U.S.A.) regulated the gas flow rates of argon, hydrogen and methane. The composition of a gas mixture was achieved by precisely controlling the flow rate of each gas. The mass flow controllers were remotely operated by computer with software supplied by the manufacturer.

3) Off gas composition analysis system

During reduction experiments, the off gas composition was continuously monitored by an infrared gas analyzer (Advanced optima AO2020, ABB Ltd., Ladenburg, Germany) connected with a computer. The gas concentrations were recorded every 5 seconds. The upper limits of CO and CO_2 to be accurately detected are 30,000 ppm and 3,000 ppm, respectively. Concentrations of CH_4 can be detected in two different ranges, 0–3,000 ppm and 0–100,000 ppm. The gas flow rate passing through the analyser can be changed in the range of 20 to 100 L/hour.

1.3.2.2 Experimental procedure

The carbothermal reduction of quartz to silicon carbide was studied in isothermal reduction experiments and temperature programmed reduction experiments.

1) Pellet preparation

Weighed quartz powder and synthetic graphite powder were mixed with distilled water (80 wt % of solid mixture) in a plastic jar with zirconia milling balls. The mixture had a C/SiO_2 molar ratio of 2 or 3.6.The plastic jar containing mixture was rolled on a rolling machine (Model 2B, Inversion Machine Ltd., Alberta, Canada) for 8 hours to ensure a homogeneous composition. Then water was removed by heating the mixture at 120 °C for 48 hours. The dried mixture was rolled on the rolling machine for a few minutes to

separate milling balls with loose powder. Weighed mixture was packed into a cylindrical stainless steel die of 8 mm diameter, and pressed into pellets approximately 1 g each by a uniaxial hydraulic press (Enerpac 10 Tonne, Enerpac, Wisconsin, U.S.A.). The pressing was carried out at a load of 20 KN for 2 minutes.

2) Isothermal reduction

The reactor was loaded with a sample pellet and assembled at room temperature, then was purged using the gas mixture for reaction atmosphere control at a flow rate of 1 NL/min for 10 minutes. The reactor was heated to a desired temperature by inserting the reactor into the furnace preheated to an experimental temperature. Reaction was stopped after certain duration by raising the reactor above the furnace hot zone and cooling down. The gas was kept continuously flowing until the temperature of a sample became below 100 °C to avoid oxidation. The reactor was inserted or removed from furnace hot zone with several intervals to avoid thermal shock which causes cracking of the reactor tube. Finally, the reactor was disassembled and the sample was taken from the inner tube for weighing and characterization.

3) Temperature programmed reduction

The procedure of temperature programmed reduction experiments was basically the same as in the isothermal reduction experiments. The reactor was loaded in the hot zone position and heated with the furnace from 300 °C to 1600 °C with ramping rate of 3 °C /min. When the temperature reached 1600 °C, the reactor was lifted up from the furnace hot zone to stop the reaction. After reduction, the reduced pellets were weighed and analyzed.

1.3.3 Reduction of Quartz to SiO

1.3.3.1 Experimental setup

1) Cold model of fluidized bed reactor

The fluidization of quartz particles was first verified using a cold model fluidization reactor made of Perspex material. The structure and dimensions of the cold model are shown in Figure 26. It consists of two zones, fluidization zone and settling zone, with inner diameter of 20 mm and 40 mm, respectively. Particles form a fluidized bed in the fluidization zone. The settling zone has an enlarged intersection where quartz particles brought into by gases settle and return to the fluidized bed zone. An NPT type connector with a filter was installed at the bottom of the fluidized bed which played a role of gas distributor.

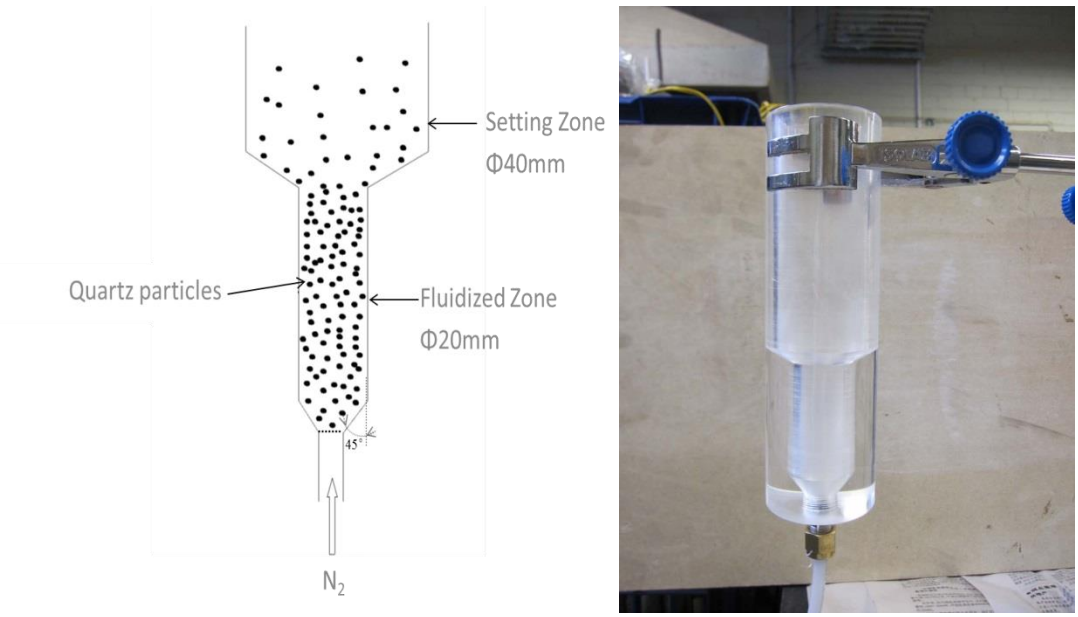

(a) **(b)**

Fig. 26 Schematic (a) and picture (b) of the cold model of the fluidized bed reactor.

2) Fluidized bed reactor and vertical tube furnace

Figure 27 presents the schematic of the fluidized bed reactor used for reduction of quartz by methane containing gas. The vertical tube furnace was the same as described in Section 1.3.2.1.

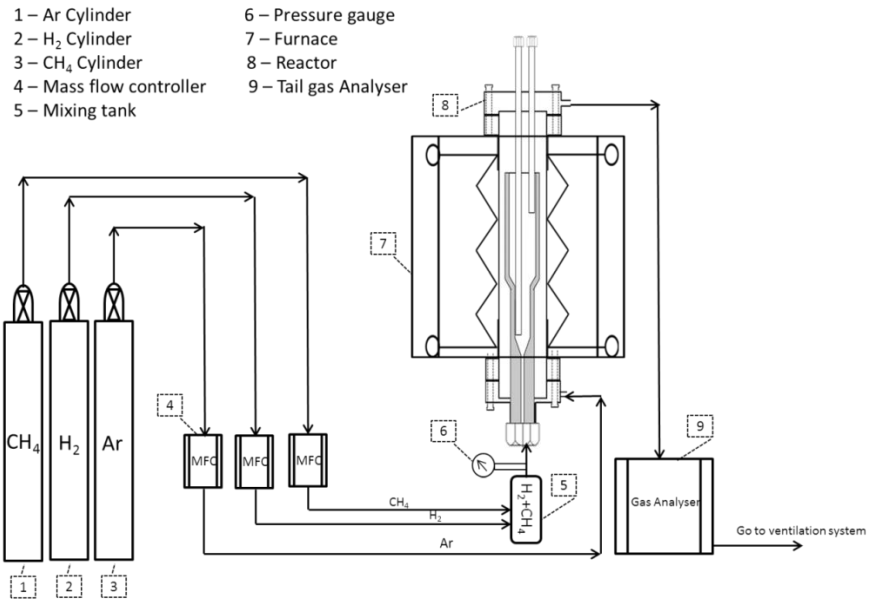

Fig. 27 Schematic flowsheet of the experimental set up for reduction of quartz by methane containing gas.

The schematic of fluidized bed reactor is presented in Figure 28. The fluidized bed high-temperature reactor was manufactured from graphite and protected by an alumina outside tube of 50 mm ID. The diameter of fluidization zone is 20 mm, and the diameter of settling zone is 40 mm. Argon was introduced between the alumina tube and graphite reactor to remove air and avoid forming a dead volume which could hold reaction products. A type B thermocouple protected by alumina sheath was inserted into the fluidization zone to measure temperature before introducing quartz powder, then removed from the fluidization zone to avoid disturbing the fluidization of quartz particles during reaction.

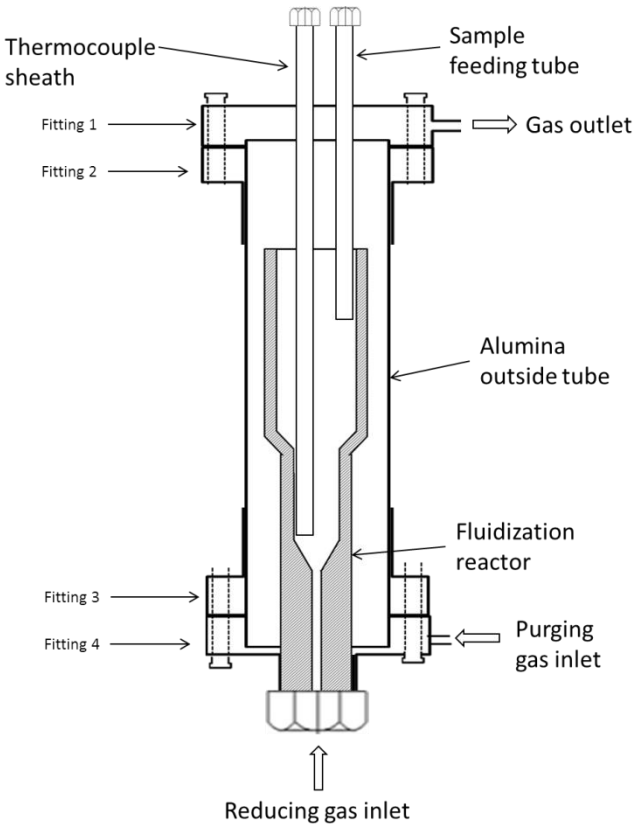

Fig. 28 Schematic of the fluidized bed reactor setup.

The reaction system also included a sample feeding tube which allowed direct addition of the quartz particles into the reactor when the furnace was heated to the desired temperature and a stable reacting gas stream was established.

3) Fixed bed reactor

The rate of formation of SiO by the reaction of methane with quartz was measured in a fixed bed reactor, which was installed in the graphite tube furnace (Model 1000-2560-FP20, GT Advanced Technologies, Santa Rosa, U.S.A.), as shown in Figure 29. The furnace configuration is presented in Table 7. The quartz sphere was suspended by a tungsten wire with 0.5 mm diameter from the top into the hot zone of the reactor tube. The tube was made from high-purity graphite, with 26 mm internal diameter and 550 mm length. A purified methane–hydrogen gas mixture was passed through the tube, from top to bottom.

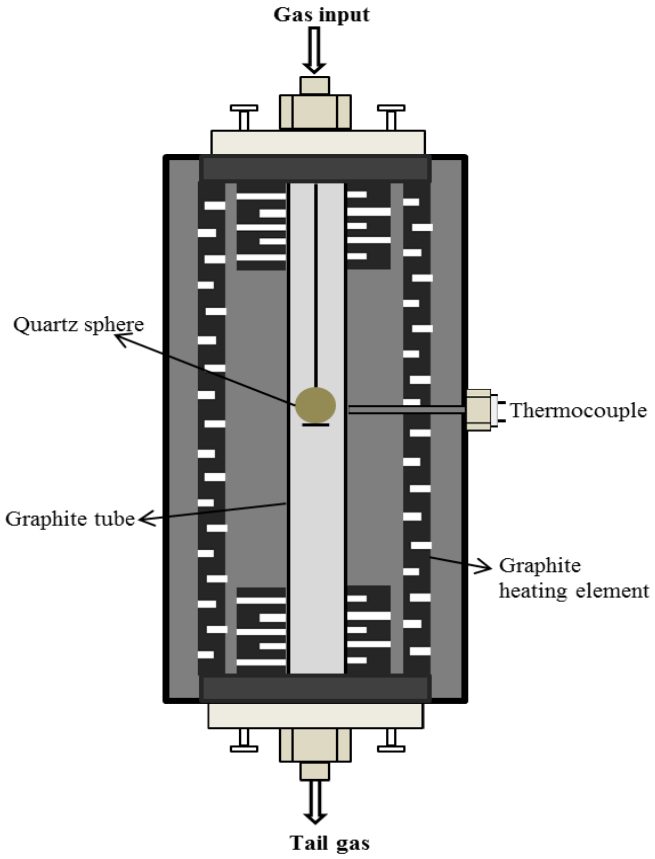

Fig. 29 Schematic of the fixed bed reactor installed in the graphite tube furnace.

Table 7. Graphite tube furnace configuration.

Model	1000-2560-FP20
Maximum operation temperature	2500 °C
Temperature controller	Eurotherm 2404
Heating elements	D04521008-001 graphite resistance
Furnace tube	Graphite tube
Tube internal diameter	26 mm
Tube external diameter	34 mm
Tube length	550 mm
Thermocouples	Type C: Tungsten/rhodium alloy

1.3.3.2 Experimental procedure

1) Cold model of the fluidized bed reactor

1 gram of quartz powder with a particle size of 53~100 μm, 100~140 μm or 140~200 μm was packed in the cold model fluidization reactor. A nitrogen stream with different flow rates was introduced from the bottom of the reactor. The change in the quartz bed was recorded by a video camera (D5100, Nikon Corporation, Tokyo, Japan).

2) Reduction of quartz to SiO in the fluidized bed reactor

The reactor system was first assembled, purged with argon, and heated to a desired temperature. Then the methane–hydrogen gas mixture was introduced into the reactor, and 2 g of quartz was added into the fluidizing zone of the reactor via a sample feeding tube with the assistance of a purging argon gas. After certain reduction duration, the furnace was cooled, and the reactor disassembled, then the sample was taken for characterization. During the entire heating process, a certain flow rate of argon was introduced between the graphite reactor and outside alumina tube. The total inlet gas flow rate was maintained at 1.00 NL/min. The outlet gas composition was continuously monitored by an infrared gas analyzer (Advanced optima AO2020, ABB, Ladenburg, Germany) connected with a computer.

3) Reduction of quartz to SiO in the fixed bed reactor

The furnace was first evacuated to a residual pressure less than 1×10^{-2} atm, and subsequently filled with argon (99.999 vol %) to 1 atm. Then the furnace was heated to 400 °C at 10 °C/min and kept constant for 20 minutes. Evacuation and refilling with argon process was repeated twice at 400 °C, in order to remove adsorbed moisture, CO_2 and O_2 from graphite parts of the furnace. The furnace was heated to the target temperature at 20 °C/min. Then methane–hydrogen gas mixture was introduced into the reactor. The outlet gas composition was monitored and recorded by AO2020 gas

analyzer. Reaction was stopped after certain duration by closing reaction gas inlet and lowering the temperature at 20 °C/min. After reaction, the reduced sample was weighed and analyzed.

1.3.4 Synthesis of Silicon from Quartz and SiC

Production of silicon from silicon carbide and quartz (Chapter 6) was performed in a fixed bed reactor under gas atmosphere of argon and hydrogen.

1.3.4.1 Experimental setup

Production of silicon in different gas atmospheres was studied in a laboratory graphite tube furnace (Model 1000-2560-FP20, GT Advanced Technologies, Santa Rosa, U.S.A.). The schematic of the fixed bed reactor is presented in Figure 30. A silicon carbide crucible containing sample powder was loaded in the inner graphite tube. The crucible was supported by a graphite tube with diameter of 20 mm in the hot zone of the furnace. Sample temperature during reaction was measured by a type C thermocouple which was protected against reaction gas atmosphere by a tungsten alloy thermocouple sheath.

The graphite tube end outside the furnace was connected to the gas inlet tube and outlet tube. The graphite tube and the thermocouple were fixed by special metal fitting and sealed with O-rings. Reaction gas was introduced into the reaction system from the top of the graphite tube, reached sample crucible, and then left the reactor from the bottom of the graphite tube.

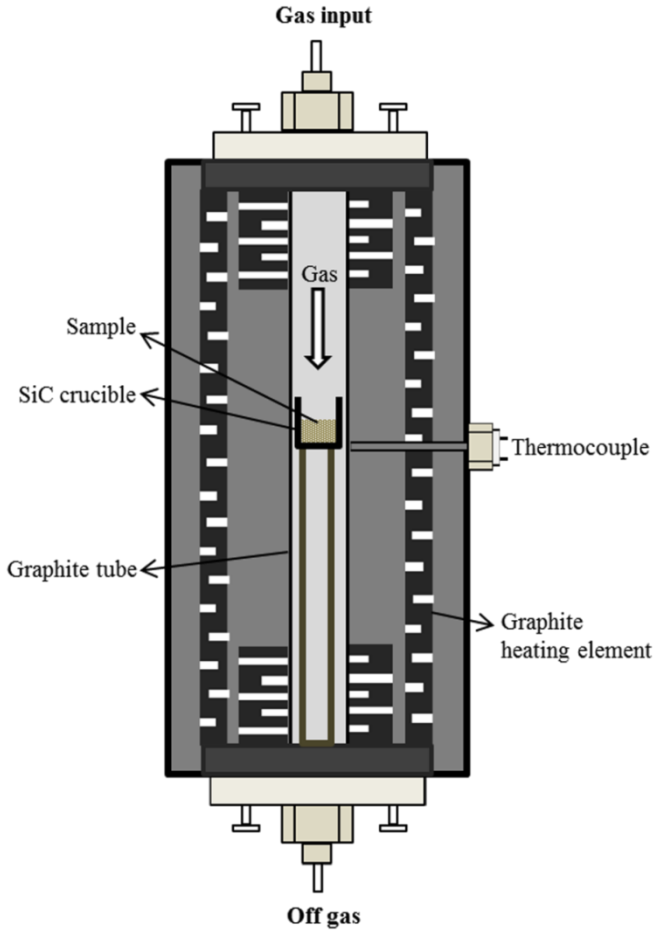

Fig. 30 Schematic of a high-temperature graphite tube furnace.

During reduction experiments, the off gas composition was continuously monitored by an infrared CO/CO_2 analyzer (ULTRAMAT 23, Siemens AG, Munich, Germany) connected with a computer. The gas composition was recorded every 1 second. Maximum concentration of CO_2 which can be accurately detected is 20 vol %. Concentrations of CO can be measured in two different ranges, 0–2.50 vol % and 0–100 vol %. The gas flow rate is in the range of 50 to 120 L/hour.

1.3.4.2 Experimental procedure

1) Sample preparation

Weighed quartz powder and silicon carbide powder were mixed with distilled water (80 wt % of solid mixture) in a plastic jar with zirconia milling balls. The mixture had a

SiC/SiO_2 molar ratio of 1 or 2. The plastic jar containing a mixture was rolled on a rolling machine (Model 2B, Inversion Machine Ltd., Alberta, Canada) for 8 hours to ensure a homogeneous composition. Then water was removed by heating the mixture at 393 K (120 °C) for 48 hours. The dried mixture was rolled on the rolling machine for a few minutes to separate milling balls with loose powder.

2) Silicon synthesis

A typical temperature profile of reaction at 1800 °C for 20 minutes was presented in **Figure 31**. The furnace was first evacuated to less than 1×10^{-2} atm, and subsequently filled with 99.999 wt % pure argon to 1 atm. Then the furnace was heated to 400 °C at 10 °C/min and kept constant for 20 minutes. Evacuation and refilling with argon process was repeated twice at 400 °C, in order to remove any adsorbed moisture, CO_2 and O_2 from graphite parts of the furnace. The mixture was heated to the target temperature at 40 °C/min. Reaction was stopped after certain duration by lowering the temperature rapidly while keeping gas flowing. After reaction, the mixture was weighed and analyzed.

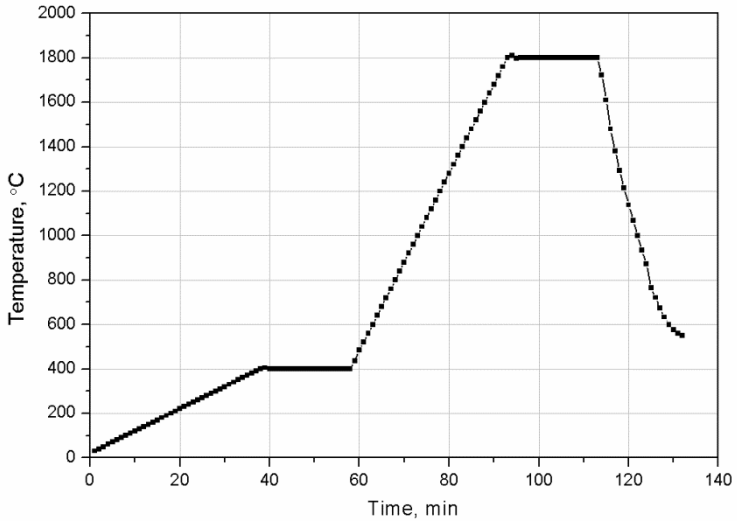

Fig. 31 Temperature profile of a reduction experiment at 1800 °C.

1.3.5 Sample Characterization

The phase compositions of samples were determined by powder X-ray diffraction (XRD) analysis. The morphologies of the samples were investigated by field-emission scanning electron microscopy (FESEM) and transmission electron microscopy (TEM). The content of oxygen in samples was tested by LECO oxygen analysis. The free carbon in the sample after reduction was determined by a Carbon/Sulfur Determinator. The impurity concentrations in samples were analyzed by inductively coupled plasma optical emission spectrometry (ICP-OES).

1.3.5.1 X-ray diffraction analysis

The original mixture and reduced samples were analyzed by an X-ray diffractometer (MMA, GBC Scientific Equipment, Braeside, Australia). The fine powder of a sample after grinding was scanned from 20 ° to 70 ° at a speed of 2 °/min and step size 0.02° with CuK radiation generated at 35 kV and 28.6 mA.

1.3.5.2 Scanning electron microscopy

SEM images were recorded by field-emission scanning electron microscopy (FESEM, JCM-6000 and JSM-7001F, JEOL, Tokyo, Japan) operated at 15 KV. Both equipped with an energy-dispersive X-ray spectrometer (EDS), were also used to characterize the chemical composition of the samples. The samples were coated with gold before SEM observation to obtain good conductivity.

1.3.5.3 Transmission electron microscopy

TEM images and selected area diffraction patterns (SADE) were recorded on a JEM 2011 electron microscope (JEOL, Tokyo, Japan) operated at 200 KV. The specimen was prepared by mixing sample powder with ethanol and dispersed by an ultrasonic generator. Then the liquid suspension was dropped on a copper grid.

1.3.5.4 LECO oxygen analysis

The oxygen content of the reduced samples was determined by a LECO Nitrogen/Oxygen Determinator (TC-436 DR, St. Joseph, USA). A weighed sample was loaded into a tin crucible in a nickel basket. A graphite crucible was placed between two electrodes. High current passed through this crucible heating it up to temperatures above 3100 °C. After an outgassing procedure the nickel basket containing a sample was dropped into the graphite crucible from a loading head purged by helium. At the high temperature, oxygen from the sample combined with carbon of the crucible to form carbon monoxide (CO) and carbon dioxide (CO_2) which were detected by infrared detectors. The instrument was calibrated using standard samples with appropriate oxygen contents.

1.3.5.5 Free carbon analysis

The contents of free carbon in reacted samples were determined by a Carbon/Sulfur Determinator (CS-2000, ELTRA Elemental Analyzers, Haan, Germany). A weighed sample was placed into a ceramic crucible. The system was closed and purged with oxygen. The crucible was heated in a resistance furnace with fixed temperature 940°C in oxygen atmosphere. Free carbon from the sample reacted with oxygen to form CO and CO_2 which were analysed by infrared detectors. At this low temperature, carbon in the form of SiC does not react with oxygen. The instrument was calibrated using standard samples with appropriate carbon contents.

1.3.6 Data Analysis

1.3.6.1 Thermodynamic equilibrium calculation

Thermodynamic equilibrium calculation was performed using HSC Chemistry 6.1 software (Outokumpu Research Oy, Pori, Finland).

1.3.6.2 Calculation of the extent of reduction of quartz (Chapters 2, 3)

The extent of reduction was defined as a fraction of oxygen in quartz removed in the course of reduction. Oxygen was removed in the form of CO, CO_2 and SiO. The main oxygen-containing product was CO, as CO_2 was converted to CO by the Boudouard reaction. Using the CO and CO_2 concentrations in the off gas, the extent of reduction was calculated using Equation (32).

$$X' = \frac{1}{n_{O-i}} \int_0^t \frac{F}{22.4}\left(C_{V-CO} + 2 \times C_{V-CO_2}\right)dt \quad (32)$$

where X' = the conversion of silica based on CO/CO_2, %;

C_{V-CO} = volume concentration of CO, vol %;

C_{V-CO_2} = volume concentration of CO_2, vol %;

F = gas flow rate, L/min;

22.4 = the volume for 1 mol ideal gas under standard condition, L/mol;

n_{O-i} = initial content of oxygen in starting mixture, mol;

t = reaction time, min.

More accurate value of X was obtained by the calibration according to the residual oxygen content in the reacted sample derived from the LECO oxygen analysis. The conversion of SiO_2 was obtained using Equation (33).

$$X = \frac{1}{n_{O-i}} \left(n_{O-i} - n_{O-LECO}\right) \quad (33)$$

where X = the conversion of silica at the end of reaction, %;

n_{O-LECO} = final content of oxygen in reacted sample, mol.

Plots of the extent of reduction X versus the reaction time t were obtained by normalizing the final extent of reduction from on-line gas analysis (Equation (32)) to

the values determined using LECO analyzer.

1.3.6.3 Calculation of yield of SiC (Chapter 3)

Assuming that reduced samples consisted of SiC, SiO_2 and free carbon, the yield of SiC (percentage of silicon in an original sample converted to SiC), was calculated using the following equation:

$$Y_{SiC} = \frac{100m}{40 \times n_{Si}} \times \left(1 - C_{C-free} - \frac{60}{32} C_{O-LECO}\right) \quad (34)$$

where Y_{SiC} = yield of SiC, %;

n_{Si} = initial content of SiO_2 in pellet before reduction, mol;

m = weight of pellet after reduction, g;

C_{C-free} = mass concentration of free carbon in pellet after reduction, %;

C_{O-LECO} = mass concentration of oxygen in pellet after reduction, %.

1.3.6.4 Calculation of loss of silicon as SiO in synthesis of SiC (Chapter 3)

During reduction, the part of SiO generated blown out from pellet was defined as loss of silicon as SiO and calculated by Equation (35).

$$Y_{SiO} = \frac{1}{n_{Si}}\left[n_{Si}(100 - Y_{SiC}) - \frac{100m}{32} C_{O-LECO}\right] \quad (35)$$

where Y_{SiO} = loss of silicon as SiO, %.

1.3.6.5 Calculation of yield of Si (Chapter 6)

Assuming that reduced samples consisted of SiC, SiO_2 and silicon metal, the yield of Si, (mole percentage of elemental silicon in an original sample converted to silicon metal), was calculated using the following equation:

$$Y_{Si} = \frac{1}{28 n_{Si}} m \left(100 - \frac{40}{12} C_{C-LECO} - \frac{60}{32} C_{O-LECO}\right) \quad (36)$$

where Y_{Si} = yield of Si, %;

n_{Si} = initial content of elemental silicon in mixture before reduction, mol;

m = weight of mixture after reduction, g;

C_{C-LECO} = mass concentration of total carbon in mixture after reduction, %;

C_{O-LECO} = mass concentration of mixture in mixture after reduction, %.

1.3.6.6 Calculation of loss of silicon as SiO in synthesis of Si (Chapter 6)

During reduction, the part of generated SiO blown out from the pellet was defined as loss of silicon as SiO and calculated by Equation (37).

$$Y_{SiO} = \frac{100}{n_{Si}} \left[n_{Si} \left(1 - \frac{Y_{Si}}{100}\right) - m \frac{C_{O-LECO}}{32} - m \frac{C_{C-LECO}}{12} \right] \quad (37)$$

where Y_{SiO} = loss of silicon as SiO, %.

References

1. Jacobson M. Z.: *Review of solutions to global warming, air pollution and energy security.* Energy & Environmental Science, 2009, vol. 2, pp. 48–173.
2. Lewis N. S., Crabtree G., Nozik A. J., Wasielewski M. R. and Alivisatos A. P.: *Basic Research Needs for Solar Energy Utilization*. U.S. Department of Energy, Washington DC, 2005, pp. 13.
3. *Clean Energy Australia Report 2013*. Clean Energy Council, 2013. https://www.cleanenergycouncil.org.au/policy-advocacy/reports.html.
4. Ranjan S., Balaji S., Panella R. A. and Ydstie B. E.: *Silicon solar cell production.* Computers & Chemical Engineering, 2011, vol. 35, pp. 1439–1453.
5. Tao M.: *Inorganic Photovoltaic Solar Cells Silicon and Beyond*. The Electrochemical Society Interface, 2008, vol. 17, pp. 30–35.
6. *Solar Module Price Highlights.* http://www.solarbuzz.com, accessed on 8 June 2014.
7. Koot E.: *The global, independent solar energy platform*. The Solar Future Conference, 2009, Munich, Germany, pp. 351–355.
8. Mitrašinović A.: *Photo-catalytic properties of silicon and its future in photovoltaic applications.* Renewable and Sustainable Energy Reviews, 2011, 15, pp. 3603–3607.
9. Gloeckner R., Odden J. O., Halvorsen G., Tronstad R., and de-Wild Scholten M. J.: *Environmental life cycle assessment of the elkem solar metallurgical process route to solar grade silicon with focus on energy consumption and greenhouse gas emissions*. Silicon for the Chemical and Solar Industry IX, 2008, Oslo, Norway, pp. 235–241.
10. Yuge N., Abe M., Hanazawa K., Baba H., Nakamura N., Kato Y., Sakaguchi Y., Hiwasa S. and Aratani F.: *Purification of metallurgical-grade silicon up to solar grade*. Progress in Photovoltaics: Research and Applications, 2001, vol. 9, pp. 203−209.
11. Gribov B. G. and Zinov'ev K. V.: *New Technologies for Production of Polycrystalline Silicon for Solar Power Engineering*. Semiconductors, 2008, vol. 42, pp. 1475–1479.

12. Braga A. F. B., Moreira S. P., Zampieri P. R., Bacchin J. M. G., and Mei P. R.: *New processes for the production of solar-grade polycrystalline silicon: A review*. Solar Energy Materials & Solar Cells, 2008, vol. 92, pp. 418–424.
13. Yasuda K., Morita K., Okabe T. H.: *Processes for Production of Solar-Grade Silicon Using Hydrogen Reduction and/or Thermal Decomposition*. Energy Technology, 2014, vol. 2, pp. 141–154.
14. Luo T., Lv G., Ma W., Wei K., Yang X., Li S.: *Numerical and experimental study of vacuum directional solidification purification process for SoG-Si in metallurgical route*. Journal of Crystal Growth, 2013, vol. 384, pp. 122–128.
15. Tronstad R.: *A sustainable product for the solar cells using Si-Sn solvent*. Silicon for the Chemical and Solar Industry XI, Bergen-Ulvik, Norway, 2012, pp. 197–206.
16. Wang D., Deng M., Liu Y., Liu Y., Li X., and Lu, R.: *Discovery of the Metal Trace Elements in Natural Gas and Its Ecological Environment Significance.* Earth Science Frontiers, 2008, vol. 15, pp. 124–132.
17. Schei A., Tuset J. and Tveit H.: *Production of High Silicon Alloys.* Tapir forlag, Trondheim, Norway, 1998, pp. 13–72.
18. Schei A., Rong H. and Forwald A. G.: *Impurity distribution in silicon*. Silicon for the Chemical Industry I, 1992, Trondheim, Norway, pp. 11–23.
19. Schei A. and Halvorsen S. H.: *A stoichiometric model of the ferrosilicon process*. Proceedings from the Kjetil Motzfeldt Symposium, Institute of Inorganic Chemistry, 1991, NTH, Trondheim, Norway, pp. 41–56.
20. Filsinger D. H. and Bourrie D. B.: *Silica to Silicon: Key Carbothermic Reactions and Kinetics*. Journal of the American Ceramic Society, 1990, vol. 73, pp. 1726–1732.
21. Hunt L.: *Silicon precursors: Their manufacture and properties.* Handbook of semiconductor silicon technology, William Andrew Publishing, New York, 1990, pp. 1–32.
22. Ceccaroli B. and Lohne O.: *Solar Grade Silicon Feedstock.* Handbook of Photovoltaic Science and Engineering. John Wiley & Sons, New York, 2003, pp.

153–204.

23. Pizzini S.: *Towards solar grade silicon: Challenges and benefits for low cost photovoltaics*. Solar Energy Materials and Solar Cells, 2010, vol. 94, pp. 1528–1533.
24. Liehr M., Greenlief C. M., Kasi S. R. and Offenberg M.: *Kinetics of silicon epitaxy using SiH_4 in a rapid thermal chemical vapor deposition reactor*. Applied Physics Letters, 1990, vol. 56, pp. 629–631.
25. Ciftja A., Engh T. A. and Tangstad M.: *Refining and Recycling of Silicon: A Review*, Annual Report Department of Materials Science and Engineering, NTNU Trondheim, 2008, pp. 1–40.
26. Rogers L. C.: *Polysilicon Preparation;* Handbook of semiconductor silicon technology. Noyes Publications, New Jersey, 1990, pp. 33–69.
27. RSI presentation: www.Rsi-silicon.com/RSIMGTRRES Feb 181009.ppt., accessed on 10 May 2009.
28. Pizzini S., Acciarri M. and Binetti S.: *From Electronic Grade to Solar Grade Silicon: Chances and Challenges in Photovoltaics*. Physica Status Solidi (a), 2005, vol. 202, pp. 2928–2942.
29. Bathey B. and Cretella M.: *Solar-Grade Silicon*. Journal of Materials Science, 1982, vol. 17, pp. 3077–3096.
30. Juneja J. and Mukherjee T.: *A study of the purification of metallurgical grade silicon*. Hydrometallurgy, 1986, vol. 16, pp. 69–75.
31. Yoshikawa T., Arimura K. and Morita K.: *Boron Removal by Titanium Addition in Solidification Refining of Silicon with Si-Al Melt*. Metallurgical and Materials Transactions B: Process Metallurgy and Materials Processing Science, 2005, vol. 36B, pp. 837–842.
32. Bracht H.: *Copper Related Diffusion Phenomena in Germanium and Silicon*. Materials Science in Semiconductor Processing, 2004, vol. 7, pp. 113–124.
33. Morita K. and Miki T.: *Thermodynamics of solar-grade-silicon refining*. Intermetallics, 2003, vol. 11, pp. 1111–1117.

34. Dai Y., Ma W., Yang B., Wu J., Wang F., Liu D., Xu B., Xie K., Zhou Y., Yao Y., *et al.*: *Direct oxidation refining purification method for industrial silicon melt*. CN Patent, 101481112A, 2009.
35. Pizzini S.: *Bulk solar grade silicon: how chemistry and physics play to get a benevolent microstructured material*. Applied Physics A: Materials Science & Processing, 2009, vol. 96, pp. 171–188.
36. Gu X., Yu X. and Yang D.: *Low-cost solar grade silicon purification process with Al-Si system using a powder metallurgy technique*. Separation and Purification Technology, 2011, vol. 77, pp. 33–39.
37. Zheng S. S., Chen C. and Luo X. T.: *Research progress in phosphorus removal by metallurgical refining*. Materials Review, 2009, vol. 23, pp. 11−14.
38. Imahori H., Kang S., Hayashi H., Haruta M., Kurata H., Isoda S., Canton S. E., Infahsaeng Y., Kathiravan A., Pascher T., Chábera P., Yartsev A. P. and Sundström V.: *Photoinduced Charge Carrier Dynamics of Zn−Porphyrin−TiO_2 Electrodes: The Key Role of Charge Recombination for Solar Cell Performance*. The Journal of Physical Chemistry A, 2011, vol. 115, pp. 3679–3690.
39. Gribov B. G. and Zinovev K. V.: *Preparation of high-purity silicon for solar cells*. Inorganic Materials, 2003, vol. 39, pp. 653−662.
40. Peter K., Enebakk E., Friestad K., Tronstad R. and Dethloff C.: *Investigation of multicrystalline silicon solar cells from solar grade silicon feedstock.* 20th European Photovoltaic Solar Energy Conference, Barcelona, Spain, 2005, pp. 615−618.
41. Vedde J. and Tronstad R.: *PV-FZ—A cost effective route to high efficiency solar cell*. 21th European Photovoltaic Solar Energy Conference, Dresden, Germany, 2006, pp. 976−977.
42. Dosaj V. D., Hunt L. P. and Schei A.: *High-Purity Silicon for Solar Cells Applications*. JOM., 1978, vol. 30, pp. 8–13.
43. Nashelskii A. Ya. and Pulner E. O.: *State-of-the-Art Technology of Silicon for Solar Energy Conversion*. Vysokochist. Veshchestva, 1996, pp. 102–112.
44. Gribov B. G.: *Does Russia Need Intrinsic Silicon*. Elektronika, 2001, pp. 5–7.

45. Tynyshtykbaev K. B., Igibaev K. T., Suleev D. K. and Babich B. P.: *Direct carbothermal receiving of solar grade silicon*. Materials Science and Engineering: B, 2006, vol. 134, pp. 296–302.

46. Vodopyanov A. G. and Kozhevnikov G. N., *Commercial-Scale Production of Improved-Purity Silicon.* Tsvetn. Met., 1998, pp. 86–89.

47. Yoshiyagawa M., Ishizaki M. and Kawahara T.: *Production of SOG-Si by Carbothermic Reduction of High Purity Silica*. ISES Solar World Congress: Clean and Safe Energy Forever, Parkville, 1989, pp. 40–45.

48. Bessho M., Fukunaka Y., Kusuda H. and Nishiyama T.: *High-Grade Silica Refined from Diatomaceous Earth for Solar-Grade Silicon Production.* Energy & Fuels, 2003, vol. 23, pp. 4160–4165.

49. Bessho M., Y Fukunaka., Oishi T., Nishiyama T. and Kusuda H.: *Carbothermic Reduction of Amorphous Silica Refined from Diatomaceous Earth*. Metallurgical and Materials Transactions B: Process Metallurgy and Materials Processing Science, 2012, vol. 41B, pp. 350–358.

50. Aratani F., Sakaguchi Y., Yuge N., Ishizaki M. and Kawahara T.: *Production of Solar Grade Silicon by Carbothermic Reduction of High Purity Silica*. Bulletin of the Japan Institute of Metals, 1991, vol. 30, pp. 433–435.

51. Lee H. C., Dhage S., Akhtar M. S, Kwak D. H., Lee W. J., Kim C. Y. and Yang O. B.: *A simulation study on the direct carbothermal reduction of SiO_2 for Si metal*. Current Applied Physics, 2010, vol. 10, pp. S218–S221.

52. Jacobson N. S., Lee K. N. and Fox D. S.: *Reactions of Silicon Carbide and Silicon (IV) Oxide at Elevated Temperatures*. Journal of the American Ceramic Society, 1992, vol. 75, pp. 1603–1611.

53. Barthey B. R. and Gretell M. C.: *Solar Grade Silicon*. Journal of Materials Science, 1982, vol. 17, pp. 3077–3096.

54. Sakaguchi Y., Ishizaki M., Kawahara T., Fukai M., Yoshiyagwa M. and Aratani F.: *Production of High Purity Silicon by Carbothermic Reduction of Silica Using AC-arc Furnace with Heated Shaft*. ISIJ International, 1992, vol. 32, pp. 643–649.

55. Abdyukhanov I. M.: *Development of basic technology of high purity silicon metal for the surface power*. Rossiiskii Khimicheskii Zhurnal, 2001, vol. 45, pp. 107–111.
56. Geerling L. J., Wyers G. P., Jensen R., Raaness O., Wærnes A. N., Santen S., Reinink A., Wiersma B., *Solar-grade silicon by a direct route based on carbothermic reduction of silica: requirements and production technology.* 12th NREL Workshop on Crystalline Silicon Solar Cells, Materials and Processes, 2002, pp. 2–5.
57. Nygaard L.: *The Solsilc process (ppt)*. Energiseminar, Amsterdam, 2008. www.fesil.com.
58. Raaness O., Jensen R., Løvsland A. A.: *Plasma Rotary Furnace*. Norwegian Patent, 970735, 1997.
59. Demin V. N., Titov A. A., Vashchenko S. P. and Kuznetsov F. A.: *Method of producing silicon.* Conference "Silicon-2004", Irkutsk, Russia, 2004, pp. 19–24.
60. Funahashi T., Ueda K., Uchimura R. and Oguchi M.: *Method and apparatus for producing pulverous SiO powder*. JP Patent, 62027318, 1990.
61. Prokhorov A. M., Petrov G. N., Kaluzhskii N. A., et al.: *Waste-free multistage production of multi- and monocrystalline silicon from quartz*. RU Patent, 2173738, 1999.
62. Afanas'ev V. D., Gorokhov A. D., Gribov B. G., et al.: *Method for preparation of high-purity silicon*. RU Patent, 2367600, 2006.
63. Ma W., Dai Y., Yang B., Liu D., Lu D., Wei K., Mei X., Wu J., Wang J., Xu B.: *Method for preparing high purity silicon for use in solar cell from carbon reductant and silica mineral, waste optical fiber or/and waste quartz*. CN Patent, 101372334 A, 2009.
64. Järrendahl K. and Davis R.: *Material Properties and Characterization of SiC*. Semiconductors & Semimetals, 1998, vol. 52, pp. 1–20.
65. Chiew Y. L. and Cheong K. Y.: *A review on the synthesis of SiC from plant-based biomasses.* Materials Science and Engineering: B, 2011, vol. 176, pp. 951–964.
66. Gupta G. S., Vasanth Kumar P., Rudolph V. R. and Gupta M.: *Heat-transfer model*

for the acheson process. Metallurgical and Materials Transactions A, 2001, vol. 32, pp. 1301–1308.

67. Zollfrank C.: *Microstructure and phase morphology of wood derived biomorphous SiSiC-ceramics*. Journal of the European Ceramic Society, 2004, vol. 24, pp. 495–506.
68. Ermekova Z. S., Mansurov Z. A. and Mukasyan A. S.: *Influence of precursor morphology on the microstructure of silicon carbide nanopowder produced by combustion syntheses*. Ceramics International, 2010, vol. 36, pp. 2297–2305.
69. Halamka M., Kavecky S., Docekal B., Madejova J. and Sajgalik P.: *Synthesis of high purity Si_3N_4 and SiC powders by CVD method*. Ceramics-Silikáty, 2003, vol. 47, pp. 88–93.
70. Suzuki M., Maniette Y., Nakata Y. and Okutani T.: *Comparison of the SiH_4–C_2H_4 and SiH_2Cl_2–C_2H_4 systems during the synthesis of silicon carbide ultrafine particles by laser-induced gas-phase reaction*. Ceramics International, 1993, vol. 19, pp. 407–413.
71. Narisawa M., Okabe Y., Iguchi M. and Okamura K.: *Synthesis of ultrafine SiC powders from carbon-silica hybridized precursors with carbothermic reduction*. Journal of Sol-Gel Science and Technology, 1998, vol. 12, pp. 143–152.
72. Saddow S. E., Agarwal A.: *Advances in Silicon Carbide Processing and Applications*. Artech House Publishers, London, 2004, pp. 4–8.
73. Weimer A. W.: *Carbide, Nitride and Boride Materials Synthesis and Processing*. Chapman & Hall, London, 1997, pp. 115–130.
74. Baumann H. N.: *The relationship of alpha and beta silicon carbide*. Journal of The Electrochemical Society, 1952, vol. 99, pp. 109–114.
75. Goldberger W. M.: *Method for the Continuous Production of Carbides*. US Patent, 4543240, 1985.
76. Goldberger W. M.: *Method of making ultra-microcrystallite silicon carbide product*. US Patent, 4435444, 1984.
77. O'Connor T. L. and McRae W. A.: *Fluidized bed process for the preparation of*

colloidal silicon carbide. US Patent, 3368871, 1969.

78. Robb W. L.: *Process for production carbides*. US patent, 3077385, 1963.
79. Kim J. J., Venkateswaran V. and Kujawa R.: *Apparatus for the continuous production of high purity, ultra-fine, aluminium nitride powder by the carbo-nitridization of alumina*. US Patent, 5108713, 1992.
80. Dijen F. K. Van: *The design of a circulating fluid bed reactor for the carbothermal synthesis of silicon nitride*. Journal of the European Ceramic Society, 1994, vol. 14, pp. 397–401.
81. Krishnarao R. V., Godkhindi M. M. and Chakraborty M.: *Maximisation of SiC whisker yield during the pyrolysis of burnt rice husks*. Journal of Materials Science, 1992, vol. 27, pp. 1227–1230.
82. Zhang S. and Cannon W.: *Preparation of Silicon Nitride from Silica*. Journal of the American Ceramic Society, 1984, vol. 67, pp. 691–695.
83. Tada M. and Hirasawa M.: *A Two-stage Reduction Process for silicon production*. High Temperature Materials and Processes, 2000, vol. 19, pp. 281–297.
84. Poch W. and Dietzel A.: *Bildung von Siliziumcarbid aus Siliziumoxid und Kohlenstoff*. Berichte der Deutschen Keramischen Gesellschaft, 1962, vol. 39: pp. 413–426.
85. Lee J. G., Miller P. D., and Cutler I. B.: *Reactiviity of solids*. Plenum Press, New York, 1976, pp. 707–712.
86. Kevorkijan V., Komac M. and Kolar D.: *Low temperature synthesis of sinterable SiC powders by carbothermal reduction of colloidal SiO_2*. Journal of Materials Science, 1992, vol. 27, pp. 2705–2712.
87. Weimer A. W., Nilsen K. J., Cochran G. A. and Roach R. P.: *Kinetics of Carbothermal Reduction Synthesis of Beta Silicon Carbide Reactors*. AIChE Journal, 2004, vol. 39, pp. 493–503.
88. Klinger N., Strauss E. L. and Komarek K. L.: *Reactions between silica and graphite*. Journal of the American Ceramic Society, 1966, vol. 49, pp. 369–375.
89. Ono K. and Kurachi Y.: *kinetic atudies on beta-SiC formation from homogeneous*

precursors. Journal of Materials Science, 1991, vol. 26, pp. 388–392.

90. Shimoo T., Sugimoto M. and Okamura K.: *Synthesis of silicon carbide powders from organosilicon polymers*. Powder metallurgy, 1990, vol. 37, pp. 1132–1137.
91. Blumenthal J. L., Santy M. J. and Burns E. A.: *Kinetic studies of high-temperature carbon-silica reactions in charred silica-reinforced phenolic resins.* AIAA Journal, 1966, vol. 4, pp. 1053–1057.
92. Khalafalla S. E. and Haas L. A.: *Kinetics of carbothermal reduction of quartz under vacuum*. Journal of the American Ceramic Society, 1972, vol. 55, pp. 414–417.
93. Kuzenestova V. L., Dmitrenko V. A. and Kokurin A. D.: *Kinetics of formation of silicon carbide*. Proceedings of Mendeleev Chemical Society, 1980, vol. 25, pp. 118–119.
94. Lee J. G. and Cutler I. B.: *Formation of silicon carbide from rice hulls*. Ceramic Bulletin, 1975, vol. 54, pp. 195–198.
95. Viscomi F. and Himmel L.: *Kinetic and mechanistic study on the formation of silicon carbide from silica flour and coke breeze*. JOM, 1978, vol. 30, pp. 21–24.
96. Johnson J. A., Hrenya C. M. and Weimer A. W.: *Intrinsic Reaction and Self-Diffusion Kinetics for Silicon Carbide Synthesis by Rapid Carbothermal Reduction*. Journal of the American Ceramic Society, 2002, vol. 85, pp. 2273–2280.
97. Durham S. J. P., Shanker K., Drew R. A. L.: *Carbothermal Synthesis of Silicon Nitride: Effect of Reaction Conditions*. Journal of American Ceramic Society, 1991, vol. 74, pp. 31–38.
98. Komeya K. and Inoue H.: *Synthesis of the Alpha Form of Silicon Nitride from Silica*. Journal of Materials Science, 1975, vol. 10, pp. 1243–1246.
99. Moshtaghioun B. M., Monshi A., Abbasi M. H., and Karimzadeh F.: *A study on the effects of silica particle size and milling time on synthesis of silicon carbide nanoparticles by carbothermic reduction*. International Journal of Refractory Metals and Hard Materials, 2011, vol. 29, pp. 645–650.
100. Dal Martello E., Tranell G., Gaal S., Raaness O. S., Tang K. and Arnberg L.: *Study of Pellets and Lumps as Raw Materials in Silicon Production from Quartz and*

Silicon Carbide. Metallurgical and Materials Transactions B, 2011, vol. 42: pp. 939–950.

101. Kononov R., Ostrovski O. and Ganguly S.: *Carbothermal reduction of manganese oxide in different gas atmosphere*. Metallurgical and Materials Transactions B, 2008, vol. 39, pp. 662–668.
102. Dewan M. A. R., Zhang G. and Ostrovski O.: *Carbothermal reduction of ilmenite concentrates and synthetic rutile in different gas atmospheres*. Institutions of Mining and Metallurgy Transactions. Section C: Mineral Processing and Extractive Metallurgy, 2011, vol. 120, pp. 111–117.
103. Fruehan R. J. and Carkin G.: *Mechanism and rate of reaction of Al_2O, Al, and CO vapors with carbon*. Metallurgical and Materials Transactions B, 2004, vol. 35: pp. 617–623.
104. Ostrovski O., Zhang G., Kononov R., Dewan M. A. R. and Li J.: *Carbothermal Solid State Reduction of Stable Metal Oxides*. Steel Research International, 2011, vol. 81, pp. 841–846.
105. Wan X., Zhang G., Ostrovski O. and Aral H.: *Carbothermal reduction of silica in nitrogen and nitrogen-hydrogen mixture.* Proceedings of the Thirteenth International Ferroalloys Congress, 2013, Karaganda, Kazakhstan, pp. 739–748.
106. Terayama K., and Ikeda M.: *Study on Reduction of MnO with Carbon by Effluent Gas Analysis Method.* Transactions of the Japan Institute of Metals, 1985, vol. 26, pp. 108–114.
107. Yastreboff M., Ostrovski O., and Ganguly S.: *Effect of Gas Composition on the Carbothermic Reduction of Manganese Oxide*. ISIJ International, 2003, vol. 43, pp. 161–165.
108. Eick B. M. and Youngblood J. P.: *Carbothermal reduction of metal-oxide powders by synthetic pitch to carbide and nitride ceramics*. Journal of Materials Science, 2009, vol. 44, pp. 1159–1171.
109. Belmonte T., Bonnetain L. and Ginoux J. L.: *Gas flow nature influence on silicon carbide whiskers synthesis in fixed bed*. Vacuum, 1996, vol. 47, pp. 291–295.

110. Lin Y. J. and Chuang C. M.: *The effects of transition metals on carbothermal synthesis of b-SiC powder*. Ceramics International, 2007, vol. 33, pp. 779–784.

111. Narciso-Romeroa F. J., Rodrıguez-Reinosoa F. and Dıez M. A.: *Influence of the carbon material on the synthesis of silicon carbide*. Carbon, 1999, vol. 37, pp. 1771–1778.

112. Sujirote K. and Leangsuwan P.: *Silicon carbide formation from pretreated rice husks*. Journal of Materials Science, 2003, vol. 38, pp. 4739–4744.

113. Silva P. C. and Figueiredo J. L.: *Production of SiC and Si3N4 whiskers in C+SiO2 solid mixtures.* Materials Chemistry and Physics, 2001, vol. 72, pp. 326–331.

114. Koc R. and Cattamanchi S. V.: *Synthesis of beta silicon carbide powders using carbon coated fumed silica*. Journal of Material Science, 1998, vol. 33, pp. 2537–2549.

115. Myrhaug E. H. and Tveit H.: *Material Balances of Trace Elements in the Ferrosilicon and Silicon Processes*. Electric Furnace Conference Proceedings, 2000, vol. 58, pp. 591–604.

116. Raman V., Parashar V. K. and Bahl O. P.: *Influence of boric acid on the synthesis of silicon carbide whiskers from rice husks and polyacrylonitrile*. Journal of Materials Science Letters, 1997, vol. 16, pp. 1252–1254.

117. čerović LJ. S., Milonjić S. K. and Bibić N. M.: *Influence of boric acid concentration on silicon carbide morphology*. Journal of Materials Science Letters, 1995, vol. 14, pp. 1052–1054.

118. Lynch D. C.: *Physical Chemistry of Silicon Production: Phosphorus in the Arc*. Proceedings of the Silicon for the Chemical Industry VII, Trondheim, Norway, 2004, pp. 17–33.

119. Ueda S., Morita K. and Sano N.: *Thermodynamics of phosphorus in molten Si-Fe and Si-Mn alloys*. Metallurgical and Materials Transactions B, 1997, vol. 28, pp. 1151–1155.

120. Jung E. J., Moon B. M., Min D. J.: *Quantitative evaluation for effective removal of phosphorus for SoG-Si*. Solar Energy Materials & Solar Cells, 2011, vol. 95, pp.

1779–1784.

121. Suzuki K., Sakaguchi K., Nakagiri T. and Sano N.: *Gaseous Removal of Phosphorus and Boron from Molten Silicon*. Journal of the Japan Institute of Metals and Materials, 1990, vol. 54, pp. 161–167.
122. Ikeda T. and Maeda M.: *Elimination of boron in molten silicon by reactive rotating plasma arc melting*. Materials Transactions, 1996, vol. 37, pp. 983–987.
123. Miki T., Morita K. and Sano N.: *Thermodynamics of Phosphorous in Molten Silicon*. Metallurgical and Materials Transactions B, 1996, vol. 27, pp. 937–941.
124. Zheng S. S., Engh T. A., Tangstad M., Luo X. T.: *Separation of Phosphorus from silicon by induction vacuum refining*. Separation and Purification Technology, 2011, vol. 82, pp. 128–137.
125. Lynch D.: *Winning the Global Race for Solar Silicon*. JOM, 2009, vol. 61, pp. 41–48.
126. Theuerer H. C.: *Removal of Boron from Silicon by Hydrogen Water Vapor Treatment*. JOM, 1956, vol. 8, pp. 1316–1319.
127. Lynch D. C.: *Thermodynamics for the Silicon Industry: A Look at Advancements in the Last Decade*. Proceedings of the Silicon for the Chemical Industry VI, Trondheim, Norway, 2002, pp. 73–93.
128. Wu J. J., Ma W. H., Yang B., Dai Y. N. and Morita K.: *Boron removal from metallurgical grade silicon by oxidizing refining*. Transactions of Nonferrous Metals Society of China, 2009, vol. 19, pp. 463–467.
129. Nordstrand E. F. and Tangstad M.: *Removal of Boron from Silicon by Moist Hydrogen Gas*. Metallurgical and Materials Transactions B, 2012, vol. 43, pp. 814–822.
130. Ikeda T. and Maeda M.: *Purification of metallurgical silicon for solar-grade silicon by electron beam button melting*. ISIJ International, 1992, vol. 32, pp. 635–642.

CHAPTER 2

CARBOTHERMAL REDUCTION OF QUARTZ IN DIFFERENT GAS ATMOSPHERE

Carbothermal Reduction of Quartz in Different Gas Atmosphere

Xiang Li[1], Guangqing Zhang[1], Kai Tang[2], Oleg Ostrovski[3], Ragnar Tronstad[4]

[1]School of Mechanical, Materials and Mechatronic Engineering, University of Wollongong, Wollongong, NSW 2522, Australia

[2]SINTEF Materials and Chemistry, N-7465 Trondheim, Norway

[3]School of Materials Science and Engineering, University of New South Wales, Sydney, NSW 2052, Australia

[4]Elkem AS, Hoffsveien 65B, 0377 Oslo, Norway

Abstract

This article examines the influence of gas atmosphere on the synthesis of silicon carbide by carbothermal reduction of quartz. The quartz was crushed to <70 μm, uniformly mixed with graphite and pressed into pellets. Reduction was studied in isothermal and temperature-programmed reduction experiments in a tube reactor in argon, hydrogen and Ar–H_2 gas mixtures. The concentrations of CO, CO_2, and CH_4 in the off gas were measured online using an infrared gas analyzer. The samples after reduction were characterized by X-ray diffraction, scanning electron microscope, and LECO analyzer. The carbothermal reduction of quartz in hydrogen was faster than in argon. Formation of silicon carbide started at 1573 K (1300 °C) in argon, and 1473 K (1200 °C) in hydrogen. Synthesis of silicon carbide in hydrogen was close to completion in 270 minutes at 1673 K (1400 °C), 140 minutes at 1773 K (1500 °C), and 70 minutes at 1873 K (1600 °C). Faster carbothermal reduction rate in hydrogen was attributed to the involvement of hydrogen in the reduction reactions by directly reducing silica and/or indirectly, by reacting with graphite to form methane as an intermediate reductant.

I. Introduction

Silicon carbide (SiC) is an important ceramic material which has diverse industrial applications. It has exclusive properties such as high hardness and strength, chemical and thermal stability, high melting point, oxidation resistance, high erosion resistance, and other. These qualities make SiC a perfect candidate for high power, high temperature electronic devices as well as abrasion and cutting applications [1, 2].

SiC is commercially produced primarily by carbothermal reduction of quartz using carbonaceous materials (petroleum coke, anthracite coal, bituminous coal, and carbon black) at temperatures above 2273 K (2000 °C) [3]. Other methods include direct carbonization of elemental Si [4], chemical vapour deposition (CVD) from silane [5, 6] and sol–gel method [7]. These methods have their advantages and disadvantages. For example, the SiC powder made by CVD and sol–gel method has high purity and narrow particle size distribution. But the reactants are unstable and toxic, and the production cost is high. Direct carbonization method is simple and cheap, but it leaves a significant amount of unreacted silicon and high level of impurities [5]. Currently, carbothermal reduction is the prevailing method for the synthesis of SiC powder.

Carbothermal reduction is the primary chemical process practiced commercially for the synthesis of many ceramic materials, including SiC. The overall reduction reaction can be written as

$$SiO_2\,(s) + 3C\,(s) = SiC\,(s) + 2CO\,(g) \qquad (1)$$

$$\Delta G^\circ = 598.18 - 0.3278\,T\ (kJ)$$

The Gibbs free energy change with temperature of Reaction [1] and other reactions in this paper was calculated using HSC Chemistry 6.1 in the range of 1273 K to 2273 K (1000 °C to 2000 °C) [8, 9]. The standard Gibbs free energy of the above reaction

decreases with increasing temperature and becomes zero at 1798 K (1525 °C). However, the reaction can take place at lower temperatures when the CO partial pressure is significantly lower than atmospheric pressure. It is generally accepted that SiC is synthesized through intermediate silicon monoxide (SiO) [10]:

$$C\,(s) + SiO_2\,(s) = SiO\,(g) + CO\,(g) \quad (2)$$

$$\Delta G^\circ = 668.07 - 0.3288\,T\ (kJ)$$

$$SiO\,(g) + 2C\,(s) = SiC\,(s) + CO\,(g) \quad (3)$$

$$\Delta G^\circ = -78.89 + 0.0010\,T\ (kJ)$$

The standard Gibbs free energy of Reaction [3] is negative in the examined temperature range, therefore the overall reaction of SiC formation is defined by the reaction of SiO formation. It is well established that the kinetics of carbothermal reduction of SiO_2 is affected by temperature [11, 12], molar SiO_2/C ratio [13], carbon and SiO_2 particle size [14, 15], and initial bulk density [13, 16]. The effect of gas atmosphere on the carbothermal reduction of silica has been studied to a lesser extent. The SiC formation will stop when the CO partial pressure in Reaction [1] reaches the equilibrium value. CO has to diffuse out of the reactant mixture for further reaction to take place.

Recent work demonstrated that the gas atmosphere has a strong effect on the kinetics of the carbothermal reductions of manganese oxides [17–20], titania [21, 22] and alumina [23, 24]. Data obtained by Terayama and Ikeda [20] for the carbothermal reduction of MnO showed that MnO is reduced much faster in helium than in argon. Similar results were obtained by Yastreboff et al. [19] in reduction of MnO, manganese ore, and ferromanganese slag. Ostrovski et al. [24] studied the carbothermal solid state reduction of manganese, titanium and aluminum oxides in argon, helium and hydrogen. The difference in helium and in argon was attributed to different diffusion coefficients of gaseous reactants and products, which are much higher in helium than in argon. When

carbothermal reduction took place in hydrogen, it was involved in the reduction process by reducing oxides to suboxides and by formation of methane as an intermediate reductant.

The strong response of the reduction rate to the change of gas atmosphere provides an insight into the reaction mechanism.

This study investigated the carbothermal reduction of quartz in argon and hydrogen containing gas. The aim of this article was to establish the effects of temperature and gas composition on the extent, rate, and mechanisms of carbothermal reduction of quartz.

II. Experimental

Quartz powder (particle size <70 μm) was obtained by crushing quartz lumps in a 6 in. agate pulversiver in a Rocklabs ring mill. The agate was made of gray silica so that contamination to the quartz sample was minimized. Quartz powder and synthetic graphite (<45 μm, Sigma-Aldrich Co. Ltd, Germany) were mixed with distilled water (80 wt pct of solid mixture) in a plastic jar with zirconia balls for 8 hours. The quartz–graphite mixture had a C/SiO_2 molar ratio of 3.6. Water was removed by heating the mixture at 393 K (120 °C) for 48 hours. Then the mixture was pressed into pellets in a uniaxial hydraulic press by applying 20 KN of load for 2 minutes. The pellets with a mass of approximately 1 g were 8 mm in diameter and about 14 mm in height.

Reduction of quartz by graphite in argon, hydrogen, and $Ar–H_2$ gas mixtures was studied in a laboratory fixed bed reactor heated in an electric vertical tube furnace. The schematic of the fixed bed reactor is presented in Figure 1. A pellet was loaded at the bottom of the inner reactor tube at room temperature, and then heated to a desired temperature by inserting the reactor into the furnace preheated to a designated temperature for isothermal reduction experiments. Reaction was stopped after certain

duration by raising the reactor above the furnace hot zone and cooling down. A typical temperature profile of isothermal reduction at 1773 K (1500 °C) was presented in Figure 2. While in temperature-programmed reduction experiments, the reactor was loaded in hot zone first and heated with furnace from 573 K to 1873 K (300 °C to 1600 °C) at 3 K/min. The gases used in the investigation were of 99.999 pct purity. The total gas flow rate was maintained at 1.0 NL/min at 1 atm. After reduction, the reduced pellets were weighed and analyzed.

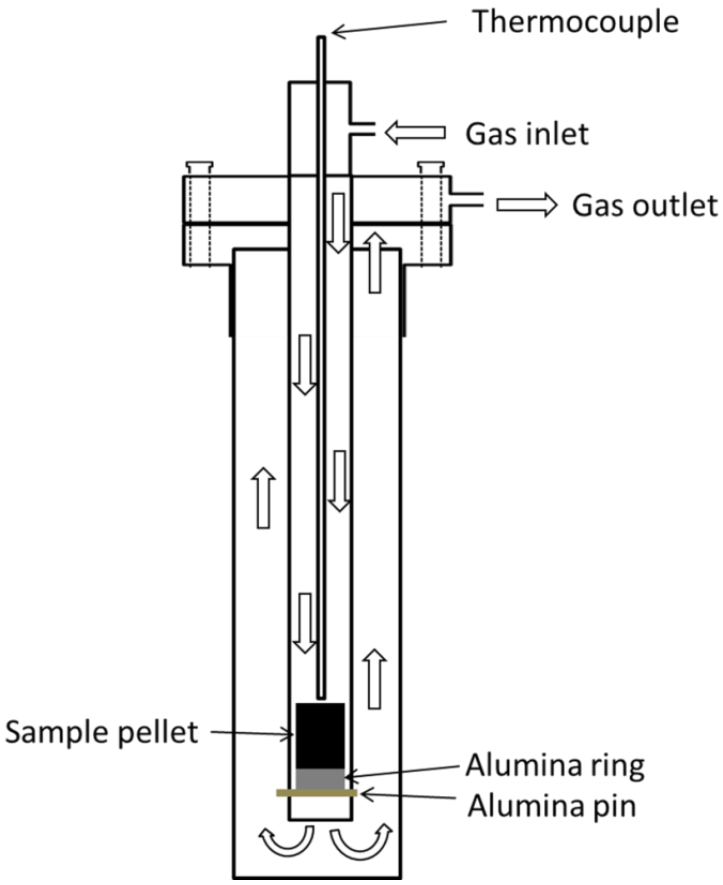

Fig. 1 Schematic of the fixed bed reactor.

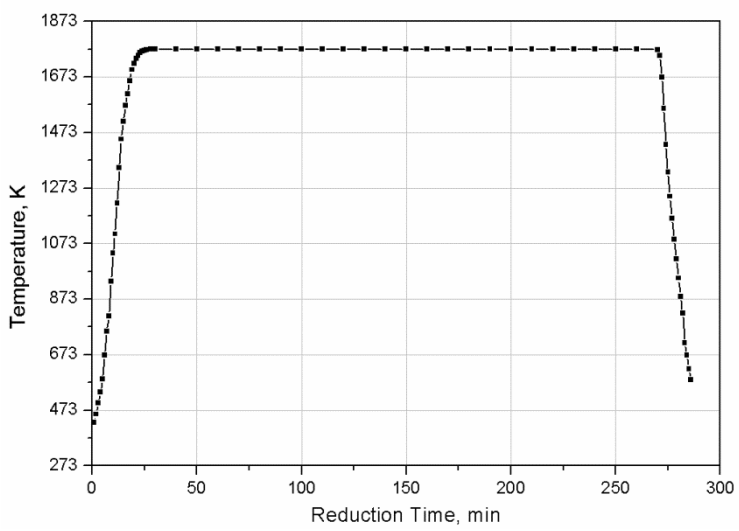

Fig. 2 Temperature profile of an isothermal reduction experiment at 1773 K (1500 °C).

During reduction experiments, the outlet gas composition was continuously monitored by an infrared $CO/CO_2/CH_4$ analyzer (Advanced optima AO2020, ABB, Ladenburg, Germany) connected with a computer. The gas concentrations were recorded every 5 seconds.

The original mixture and reduced samples were analyzed by X-ray diffraction (XRD, MMA, GBC Scientific Equipment, Braeside, Australia). The fine powder of a sample after grinding was scanned at a speed of 0.02 deg/s and step size 0.02 deg with CuK radiation generated at 35 kV and 28.6 mA. The morphologies of the samples were investigated by field-emission scanning electron microscopy (FESEM, JCM-6000 and JSM-7001F, JEOL, Tokyo, Japan) operated at 15 kV.

The oxygen content in the reduced samples was determined by LECO TC-436 DR Nitrogen/Oxygen Determinator. A graphite crucible containing a sample was placed between two electrodes. High current passing through this crucible generated heat which heated the sample up to 3373 K (3100 °C). After an outgassing procedure the sample was dropped into the crucible from a helium purged loading head. The oxygen released from the sample combined with the carbon of the crucible to form CO and CO_2 of which the contents were measured by infrared detectors.

The extent of reduction was defined as a fraction of oxygen in quartz removed in the course of reduction. Oxygen was removed in the form of CO, CO_2, and SiO. The main oxygen-containing product was CO, as CO_2 was converted to CO by the Boudouard reaction, and SiO reacted with graphite forming SiC. Using the CO and CO_2 concentrations in the off gas, the extent of reduction was calculated using Eq. (4).

$$X' = \frac{1}{n_{O-i}} \int_0^t \frac{GFR}{22.4} \left(C_{V-CO} + 2 \times C_{V-CO_2}\right) dt \quad (4)$$

where X' is the conversion of silica based on CO and CO_2 concentrations, pct at time t; C_{V-CO} is the concentration of CO and C_{V-CO_2} the concentration of CO_2, vol pct; GFR is the gas flow rate, NL/min; n_{O-i} is the initial content of oxygen in quartz, mol; and t is the reaction time, min.

More accurate extent of reduction was obtained using residual oxygen content in a reacted sample determined by LECO oxygen analysis. The conversion of SiO_2 can be obtained using Eq. (5).

$$X = \frac{1}{n_{O-i}} \left(n_{O-i} - n_{O-LECO}\right) \quad (5)$$

where X is the conversion of silica at the end of reduction, pct; n_{O-LECO} is the content of oxygen in the reacted sample, mol.

Plots of the extent of reduction X versus the reaction time t were obtained by normalizing the final extent of reduction from on-line gas analysis (Eq. (4)) to the values determined using LECO analyzer. The error of measured oxygen content by LECO analysis depends on the residual oxygen content in the reduced sample. For a sample with extent of reduction 90 pct, the error was about 0.1 pct, which gives an error in the extent of reduction 0.3 pct. Including other errors such as in weighing and gas

flow rate, the overall error of the final extent of reduction is estimated to be less than 1 pct.

Thermodynamic equilibrium calculations were performed with Outokumpu HSC Chemistry software (Version 6.1, Outokumpu Research Oy, Pori, Finland).

III. Results

A Temperature-programmed reduction

Temperature-programmed reduction experiments were studied in the temperature range from 573 K to 1873 K (300 °C to 1600 °C), with ramping rate of 3 K/min. The extent of reduction of quartz in different gas atmospheres *vs* temperatures is presented in Figure 3. Reduction rate in pure argon was low at temperatures below 1773 K (1500 °C). The extent of reduction was below 30.0 pct at 1773 K (1500 °C); it increased to 89.0 pct when the temperature was increased to 1873 K (1600 °C). Addition of 10 vol pct hydrogen to argon significantly increased the reduction rate. The reduction of quartz was close to completion at 1873 K (1600 °C). Further increasing hydrogen content in the Ar–H_2 gas mixture to 100 vol pct accelerated the reduction; the increase in the reduction rate was particularly strong when the hydrogen content was increased from 60 to 100 vol pct.

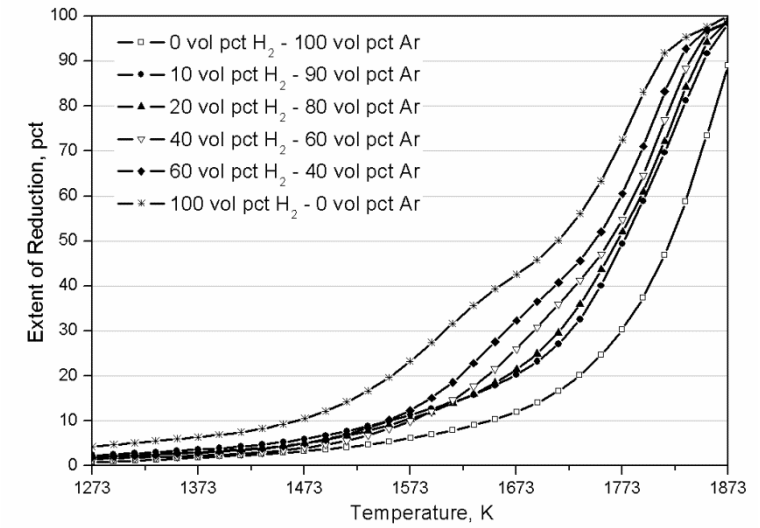

Fig. 3 Effect of hydrogen content in the Ar–H_2 gas mixtures on the extent of reduction of quartz in the temperature-programmed reduction experiments from 573 K (300 °C) to 1873 K (1600 °C). The ramping rate was at 3 K/min.

To identify the changes of phase composition during the carbothermal reduction of quartz, the temperature programmed reduction peocesses ended at different temperatures, then the obtained samples were analyzed by XRD. Figure 4 presents the XRD patterns of the samples in argon. In a sample heated to 1473 K (1200 °C), the only phases identified were quartz and graphite as in the original mixture. A weak peak of β-SiC was observed in the XRD spectrum of a sample heated to 1573 K (1300 °C), at $2\theta = 35.66^{o}$ (d = 2.516 **Å**). Cristobalite was identified in samples heated to 1773 K and 1873 K (1500 °C and 1600 °C), as a result of the transformation of quartz to cristobalite which took place above 1743 K (1470 °C) [25]. When the temperature increased to 1873 K (1600 °C), the amount of β-SiC significantly increased, with graphite and a small amount of cristobalite as residual reactants.

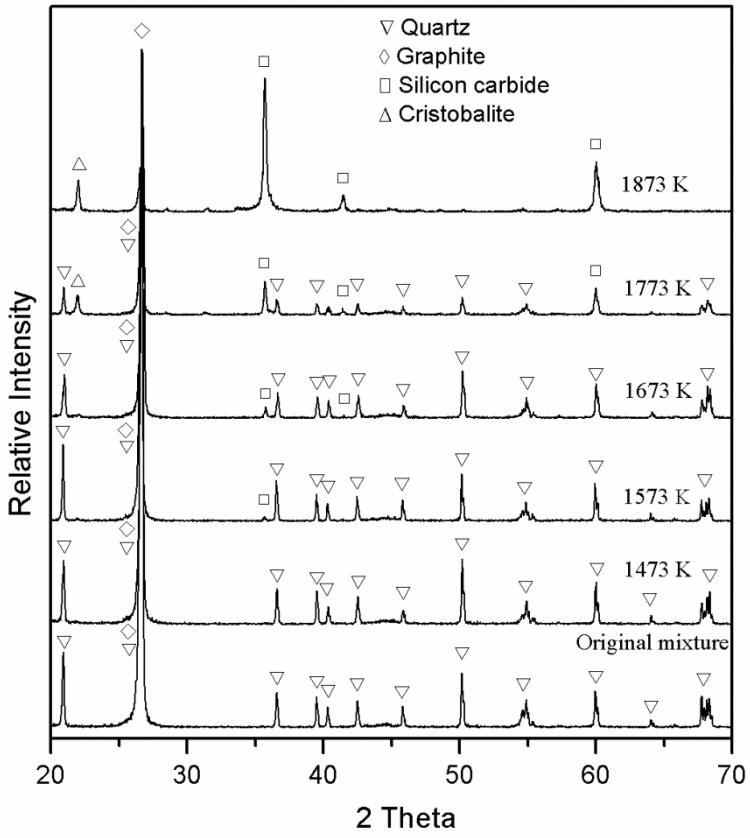

Fig. 4 XRD patterns of samples in the progress of temperature-programmed reduction in pure argon. The ramping rate was 3 K /min.

Figure 5 presents the XRD patterns of the samples heated to different temperatures in hydrogen. There was no visible change up to 1373 K (1100 °C). When the temperature was increased to 1473 K (1200 °C), a small amount of β-SiC was identified. With the increase of temperature, the peak intensity of β-SiC in the reduced sample became stronger, corresponding to the decrease of quartz peaks intensities. In the sample subjected to reduction until 1873 K (1600 °C), only β-SiC was present besides a small amount of residual graphite. In the sample reduced in hydrogen, no cristobalite phase was detected by the XRD analysis. These results indicate that carbothermal reduction in hydrogen was faster than in argon; it can be suggested that the rate of quartz reduction was faster than its transformation to crystobalite.

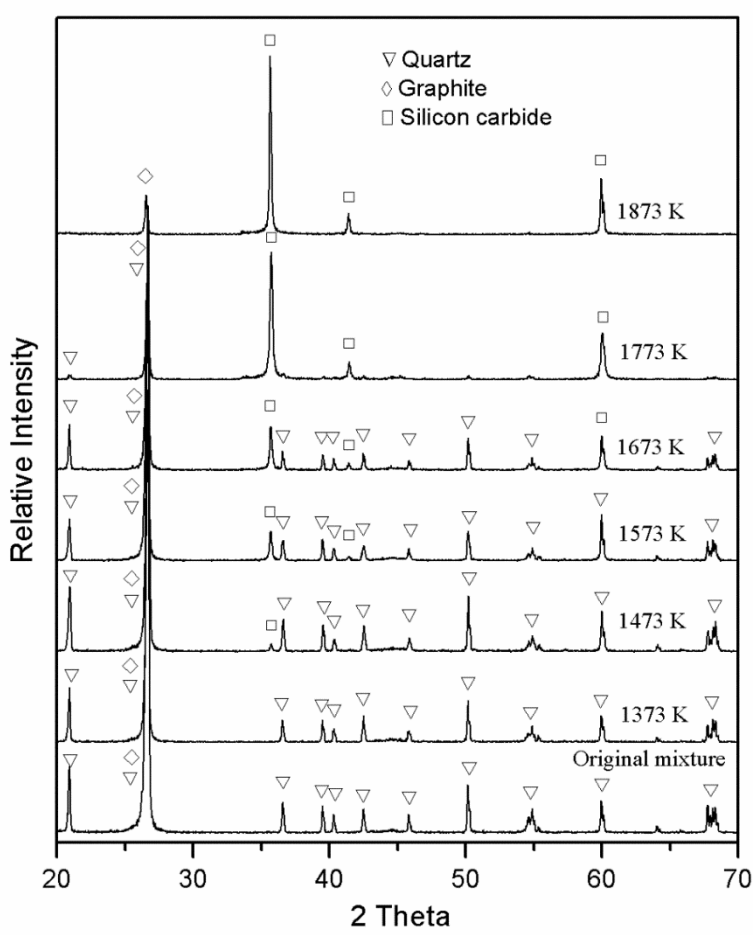

Fig. 5 XRD patterns of samples in the progress of temperature programmed reduction in pure hydrogen. The ramping rate was 3 K/min.

B. Isothermal Reduction

The extent of reduction *vs* time at different temperatures in argon in isothermal experiments is presented in Figure 6. Figure 7 shows the XRD spectra of the samples reduced at different temperatures for 270 minutes. Carbothermal reduction of quartz in argon was very slow below 1673 K (1400 °C). After reduction at 1473 K (1200 °C), only a small amount of SiC was detected with the extent of reduction of 7.8 pct. The extent of reduction increased to 12.6 and 27.7 pct at 1573 K and 1673 K (1300 °C and 1400 °C), respectively. Increasing temperature to 1773 K (1500 °C) resulted in a significant increase of the reduction rate, and the extent of reduction reached 85.9 pct. SiC became the predominant compound in the reduction product, with a small amount

of cristobalite detected. The reduction rate was further enhanced at 1873 K (1600 °C), where the formation of SiC was close to completion in about 75 minutes, with an extent of reduction of 99.3 pct as determined from oxygen analysis in the reduced sample using LECO analyser.

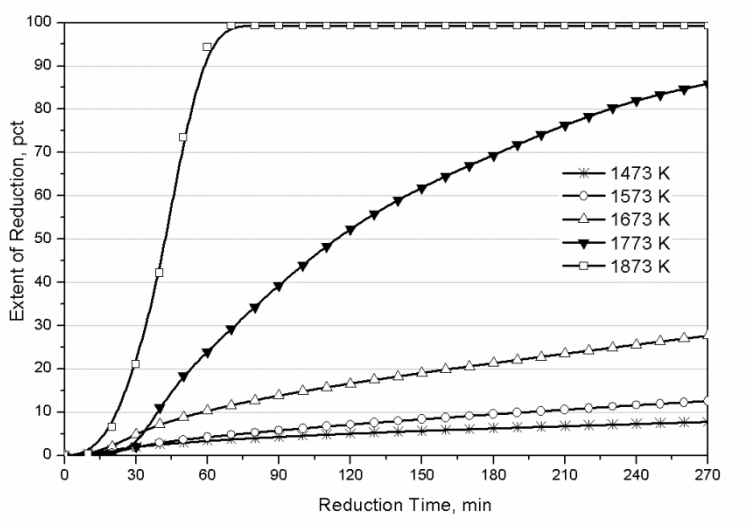

Fig. 6 Effect of temperature on the extent of reduction of quartz in argon.

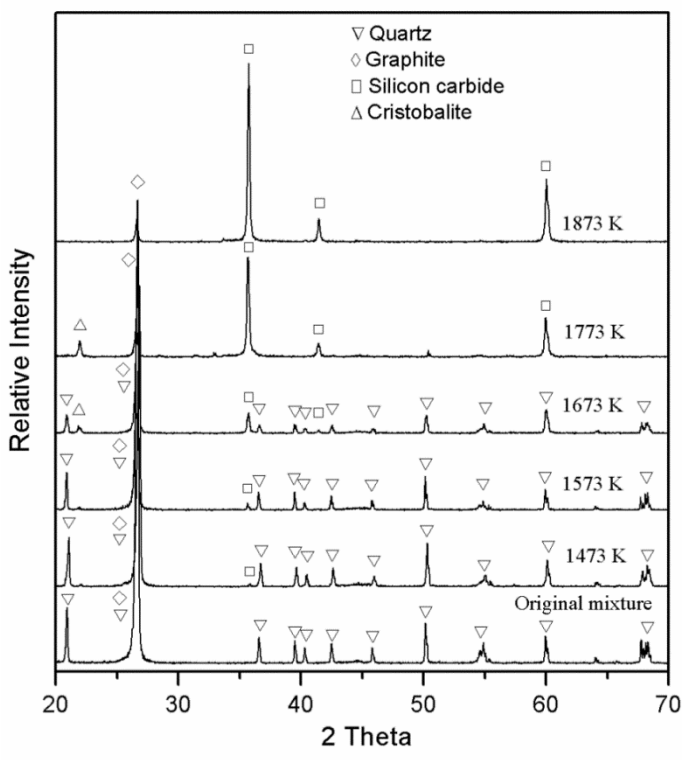

Fig. 7 XRD patterns of samples reduced at different temperatures in argon for 270 minutes.

The extent of reduction *vs* time at different temperatures in hydrogen is shown in Figure 8. The XRD patterns of the samples after 270 minutes' reduction are presented in Figure 9. The carbothermal reduction in hydrogen was significantly faster than in argon at 1473 K to 1773 K (1200 °C to 1500 °C). The extent of reduction at 1473 K (1200 °C) after 270 minutes reached 36.0 pct, which is higher than that reached at 1673 K (1400 °C) in argon. Further increasing temperature to 1673 K (1400 °C) enhanced SiC formation; silica was undetectable in the sample reduced for 270 minutes, when the extent of reduction reached 98.5 pct. In the experiment at 1773 K (1500 °C), the extent of reduction raised to 99.1 pct in 140 minutes. The reduction was almost complete (99.6 pct) in 70 minutes at 1873 K (1600 °C). Graphite peaks in the XRD spectrum of the sample reduced at 1873 K (1600 °C) were undetectable by XRD. The difference of reduction rate between in argon and in hydrogen at 1873 K (1600 °C) was relatively small. At this high temperature, the rate of reduction was controlled by mass transfer instead of intrinsic kinetics, which was less sensitive to the gas atmosphere.

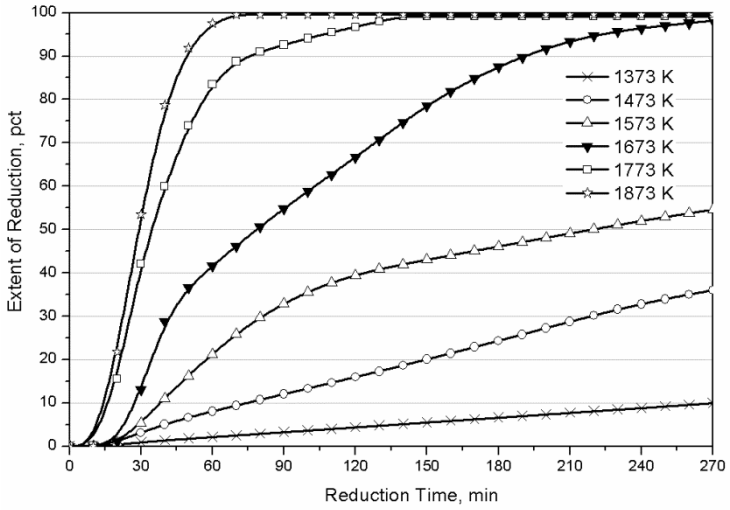

Fig. 8 Effect of temperature on the extent of reduction of quartz in hydrogen.

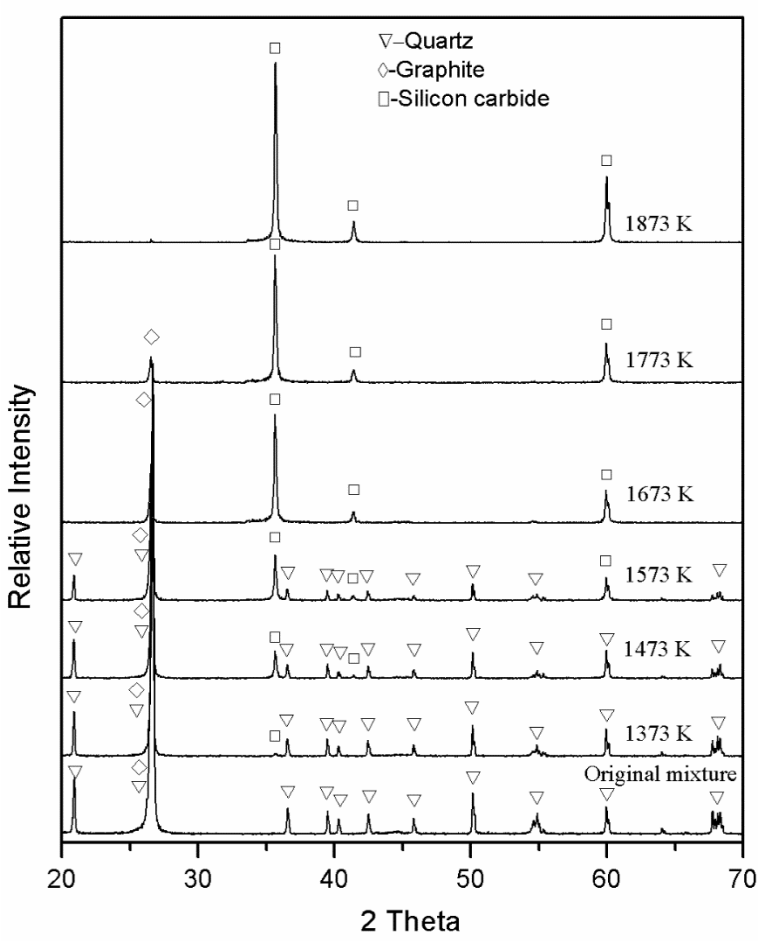

Fig. 9 XRD patterns of samples reduced at different temperatures in hydrogen for 270 minutes.

The effect of hydrogen content in the Ar–H_2 gas mixtures on the carbothermal reduction of quartz was studied at 1673 K (1400 °C). The reduction curves are presented in Figure 10. The extent of reduction in pure argon was only 27.7 pct after reduction for 270 minutes. The addition of 10 vol pct hydrogen to argon increased the reaction rate significantly. The final extent of reduction increased to 67.7 pct. Further increasing of hydrogen content continuously accelerated the reduction rate.

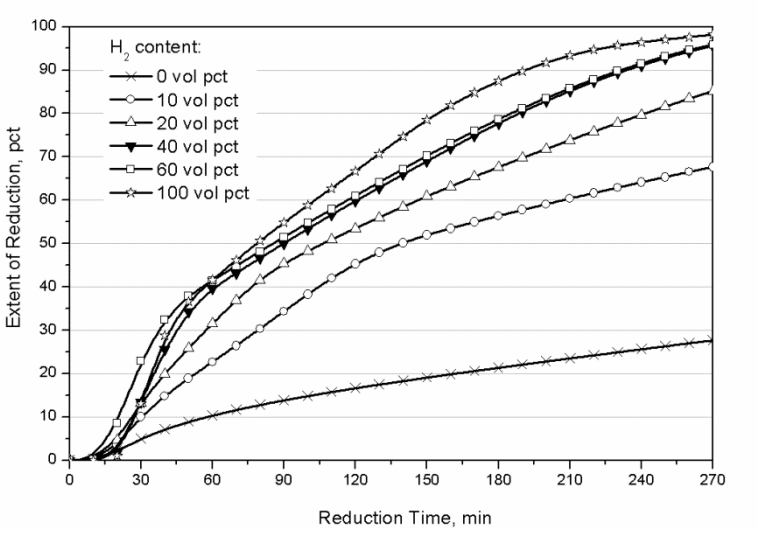

Fig. 10 Effect of hydrogen content in Ar–H_2 gas mixtures on the extent of reduction at 1673 K (1400 °C).

IV. Discussion

Gas atmosphere had a pronounced effect on the carbothermal reduction of quartz. Figure 11 compares the rate of generation of CO in the temperature programmed reduction experiments in different gas atmospheres. In general, the reduction curves in hydrogen containing gases include two peaks. With the increase of hydrogen content in the inlet gas, both CO peaks shifted towards lower temperatures. When the hydrogen content was increased to 100 vol pct, the two CO peaks appeared at 1594 K (1321 °C) and 1781 K (1508 °C), respectively. In the reduction in argon, only one peak was observed on the reduction curve which did not reach maximum in the studied temperature range (up to 1873 K (1600 °C)). The CO peak positions in reduction in different gas atmospheres are summarized in Table 1.

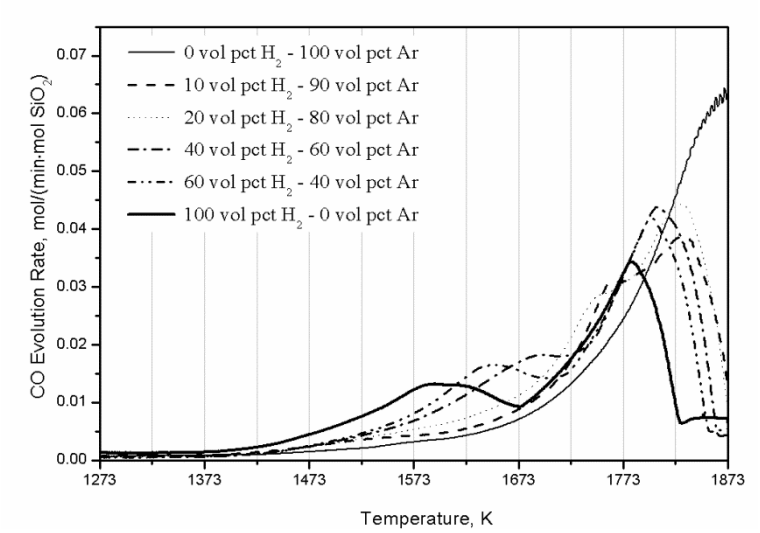

Fig. 11 CO evolution rates in the temperature programmed reduction of quartz in different gas atmospheres. The ramping rate was 3 K/min.

Table 1. The change of temperatures of CO peaks in temperature programmed reduction with hydrogen content in H_2–Ar mixture

H_2 content, vol pct	Peak 1, K	Peak 2, K
0	> 1873	N/A
10	1834	1767
20	1824	1756
40	1805	1697
60	1795	1639
100	1781	1594

It is well recognised that the carbothermal reduction of silica involves gaseous intermediate SiO. When the reduction of quartz is carried out in argon, SiO is initially formed at the contact points of graphite and quartz particles following the solid-solid Reaction (2), and then SiO is further reacted with carbon to form SiC following Reaction (3). SiO can also be generated by Reaction (6) which, with the decrease in the contact area between quartz and graphite, becomes a major reaction for the SiO formation. CO_2 formed in Reaction (6) is converted back to CO by Boudouard Reaction

(7) which is highly favoured thermodynamically within the temperature range of isothermal reduction experiments of this investigation.

$$SiO_2\ (s) + CO\ (g) = SiO\ (g) + CO_2\ (g) \quad (6)$$

$$\Delta G^\circ = 505.76 - 0.1598\ T\ (kJ)$$

$$C\ (s) + CO_2\ (g) = 2CO\ (g) \quad (7)$$

$$\Delta G^\circ = 162.31 - 0.1690\ T\ (kJ)$$

When the reduction is carried out in the H_2–Ar gas mixture, hydrogen reacts with carbon forming methane (Reaction (8)), which reacts with SiO_2 forming SiO (Reaction (9)).

$$C\ (s) + 2H_2\ (g) = CH_4\ (g) \quad (8)$$

$$\Delta G^\circ = -89.00 + 0.1085\ T\ (kJ)$$

$$SiO_2\ (s) + CH_4\ (g) = SiO\ (g) + CO\ (g) + 2H_2\ (g) \quad (9)$$

$$\Delta G^\circ = 757.07 - 0.4373\ T\ (kJ)$$

In the presence of carbon, hydrogen can also directly reduce silica [26] (Reactions (10) and (11)).

$$SiO_2\ (s) + H_2\ (g) = SiO\ (g) + H_2O\ (g) \quad (10)$$

$$\Delta G^\circ = 534.35 - 0.1869\ T\ (kJ)$$

$$H_2O\ (g) + C\ (s) = H_2\ (g) + CO\ (g) \quad (11)$$

$$\Delta G^\circ = 133.72 - 0.1419\ T\ (kJ)$$

Formation of the reaction intermediates CO_2, CH_4 or H_2O in the carbothermal reduction does not change the thermodynamics of Reactions (2) and (3) or the overall Reaction (1), but affects the reaction mechanism and kinetics. Assuming CO partial pressure of 1 KPa, H_2 partial pressure of 100 kPa and CH_4 partial pressure of 0.05 KPa, the equilibrium

partial pressures of SiO in Reactions (2), (6), (9) and (10) are calculated and plotted in Figure 12. For Reactions (6) and (10), it is also assumed that the equilibrium partial pressure of CO_2 or H_2O on the quartz particle is the same as that of SiO. The assumption is made based on the understanding that SiO and CO_2 or SiO and H_2O were formed simultaneously on the quartz particles by Reactions (6) or (10), then diffused to the graphite particles where SiO formed SiC (Reaction (3)), while CO_2 and H_2O were converted to CO (Reaction (7)), and H_2 and CO (Reaction (11)) respectively. Although differences exist between the diffusivities of SiO and CO_2 or H_2O, it is expected that the partial pressures of SiO and CO_2 or H_2O on the quartz surface were of the same order. This figure also presents the partial pressure of intermediate CH_4 formed by Reaction (8) and partial pressures of CO_2 and H_2O on the graphite particle following Reactions (7) and (11) with the same assumptions.

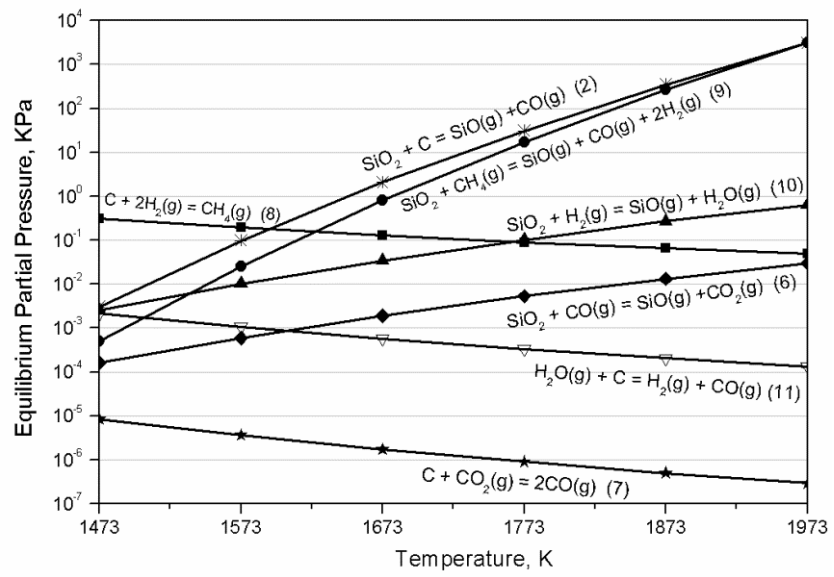

Fig. 12 Equilibrium partial pressure of SiO for Reactions (2), (6), (9) and (10) calculated with P_{CO} = 1 KPa, P_{H2} = 100 KPa and P_{CH4} = 0.05 KPa; equilibrium partial pressure of CO_2 for Reaction (7) calculated with P_{CO} = 1 KPa; equilibrium partial pressure of CH_4 for Reaction (8) calculated with P_{H2} = 100 KPa; equilibrium partial pressure of H_2O for Reaction (11) calculated with P_{H2} = 100 KPa and P_{CO} = 1 KPa. It is assumed that $P_{CO2} = P_{SiO}$ for Reaction (6) and $P_{H2O} = P_{SiO}$ for Reaction (10).

CO_2 had a very low partial pressure, being at least an order lower than the thermodynamic equilibrium value when solid carbon is present, meaning that the reduction kinetics was controlled by Reaction (6) in the temperature range of this study. Reaction (6) generates SiO and CO_2 at ppm level at 1473 K (1200 °C) according to Figure 12 (under assumption that CO concentration was 1 vol pct), which makes reduction of quartz in argon at 1473 K (1200 °C) negligible. With the increase in temperature, the partial pressures of SiO and CO_2 significantly increase, and reach 100s ppm level. This explains why carbothermal reduction of quartz in argon needs high temperatures.

According to Figure 12, the partial pressures of SiO and H_2O generated by Reaction (10) are always more than one order higher than those of SiO and CO_2 by Reaction (6), which explains the faster reduction of quartz in hydrogen. However, it should be noted that at temperatures lower than 1473 K (1200 °C), Reaction (10) is not feasible, as the equilibrium partial pressure of H_2O at the surface of graphite particle is higher than that at the quartz particle. Therefore the direct reduction by hydrogen at relatively low temperatures can be limited by the removal of H_2O by Reaction (11).

Similar to reduction of other stable metal oxides, CH_4 may play a significant role as an intermediate reductant in reduction in hydrogen containing atmosphere [27]. Formation of CH_4 in the reduction experiments in hydrogen was confirmed experimentally by analyzing the off-gas composition. The observed changes of CH_4 concentration in the temperature programmed reduction of quartz in hydrogen containing gas are presented in Figure 13. The CH_4 concentration was close to zero when hydrogen content was below 40 vol pct, due to the lower generation rate of CH_4 by Reaction (8) than consumption rate by Reaction (9). When the H_2–Ar gas mixture contained more than 40 vol pct hydrogen, generation of CH_4 was faster than its consumption; CH_4 in the off-gas was detected at the level of hundreds ppm, as shown in Figure 13. Increasing the partial

pressure of hydrogen increased the equilibrium partial pressure of CH_4 and enhanced the reduction rate of SiO_2. CH_4 stability decreases with increasing temperature (Figure 12); its concentration in reduction experiments at temperatures > 1673 K (1400 °C) was very low (Figure 13).

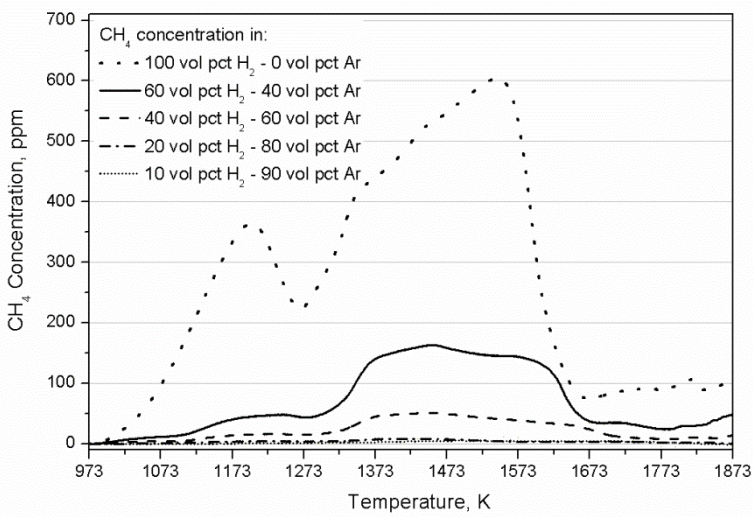

Fig. 13 Concentration of CH_4 in the progress of temperature programmed reduction in the Ar–H_2 gas mixtures with different hydrogen contents.

SiC can be generated by Reaction (7), or by Reaction (12):

$$SiO\ (g) + 2\ CH_4\ (g) = SiC\ (s) + CO\ (g) + 4\ H_2\ (g) \qquad (12)$$

$$\Delta G^\circ = 99.113 - 0.2160\ T \quad (kJ)$$

Thermodynamic calculation with HSC Chemistry 6.1 shows that Reaction (12) is thermodynamically irreversible with equilibrium constant in the order of 10^7 to 10^8 in the considered temperature range. Reaction (12) is used for synthesis of SiC whiskers, which can be implemented with or without a catalyst [28–30].

The morphologies of samples reduced in pure argon and hydrogen were examined by SEM. Figure 14 compares the morphologies of samples before and after temperature

programmed reduction in argon. Most of quartz was reduced to SiC; some unreacted SiO_2 was observed in the form of cristobalite.

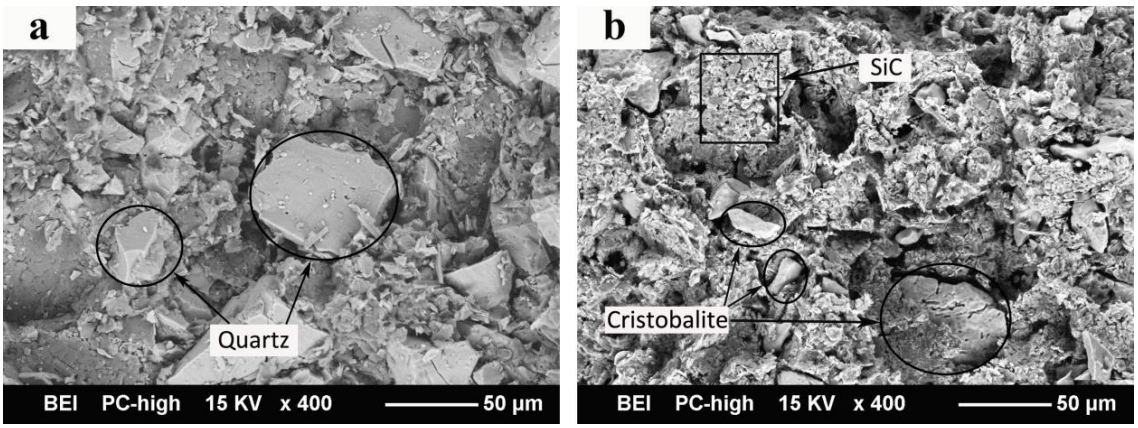

Fig. 14 (a) SEM image of an unreduced pellet, cross section; (b) SEM image of a sample after temperature programmed reduction in pure argon. The furnace temperature was ramped from 573 K (300 °C) to 1873 K (1600 °C) at 3 K/min.

Figure 15 presents the morphologies of samples in the process of temperature programmed reduction in pure hydrogen. When the reduction was stopped at 1573 K (1300 °C) (Figure 15(a)), the sample's morphology resembles that of the original pellet. With increasing temperature to 1673 K (1400 °C), whiskers with diameter 0.4–0.8 μm were observed in the cross section of the pellet (Figure 15(b) and (c)). Most whiskers had a globule at the growing end, and grew to less than 4 μm. Meanwhile, more whiskers were observed at the surface of the pellet (Figure 15(d)). When the temperature was increased to 1773 K (1500 °C), the whiskers on the cross section of pellet grew to 5–8 μm (Figure 15(e)), and the surface whiskers were longer, even more than 20 μm (Figure 15(f)). Higher temperature promoted the growth of whiskers, which totally covered the surface of the pellet at 1873 K (1600 °C) (Figure 15(g)). Figure 15(h) presents an image of a whisker at high magnification, which shows that the whisker grew in the form of hexagonal prisms. According to the EDS analysis, the whisker consisted of SiC, while the globule contained 20~30 at pct Fe, 10~20 at pct Al and < 2 at pct Cr, with C and Si the rest. It can be suggested that SiC whiskers were formed by

Reaction (12) through the vapor-liquid-solid (VLS) mechanism with iron as a catalyst [31]. Iron and chromium in the samples originated from contamination of a pellet in the process of pressing with stainless steel die because the die was the only possible source of chromium. The presence of aluminum can be attributed to the reduction of alumina tubes under hydrogen containing atmosphere at high temperatures, generating Al_2O vapor deposited on the sample pellets [24]. Aluminum and iron were also present as impurities in quartz, as shown in Table 2.

Table 2. Impurity contents in quartz lumps, mg/kg

B	P	Fe	Al	Ca	Ti	Mn	Mg
0.5	1.0	33.0	219.0	26.0	7.9	1.9	27.0

Based on the discussion above, it can be concluded that synthesis of SiC from quartz and graphite in pure argon was initiated by Reactions (2) and (3) and then proceeded by the SiO–CO–CO_2 path through Reactions (6), (7) and (3). In synthesis of SiC in the hydrogen containing gas atmosphere, this path plays a less significant role. Instead, it can proceed by the SiO–H_2–CH_4 path through Reactions (8), (9) and (3) and/or SiO–H_2–H_2O path through Reactions (10), (11) and (3). SiC whiskers were formed through Reactions (8), (9) and (12). The measured partial pressure of CH_4 was very low at temperatures above 1673 K (1400 °C); it can be expected that the SiO–H_2–CH_4 path dominates at low temperatures, while at high temperatures SiC synthesis occurs by the SiO–H_2–H_2O path. These reduction mechanisms also explain two peaks in the CO evolution curves observed in the reduction in H_2–Ar gas mixtures as shown in Figure 11. The low temperature peak can be attributed to the formation of SiC by the SiO–H_2–CH_4 path. The SiO–H_2–H_2O path is the major mechanism in the formation of SiC at high temperatures.

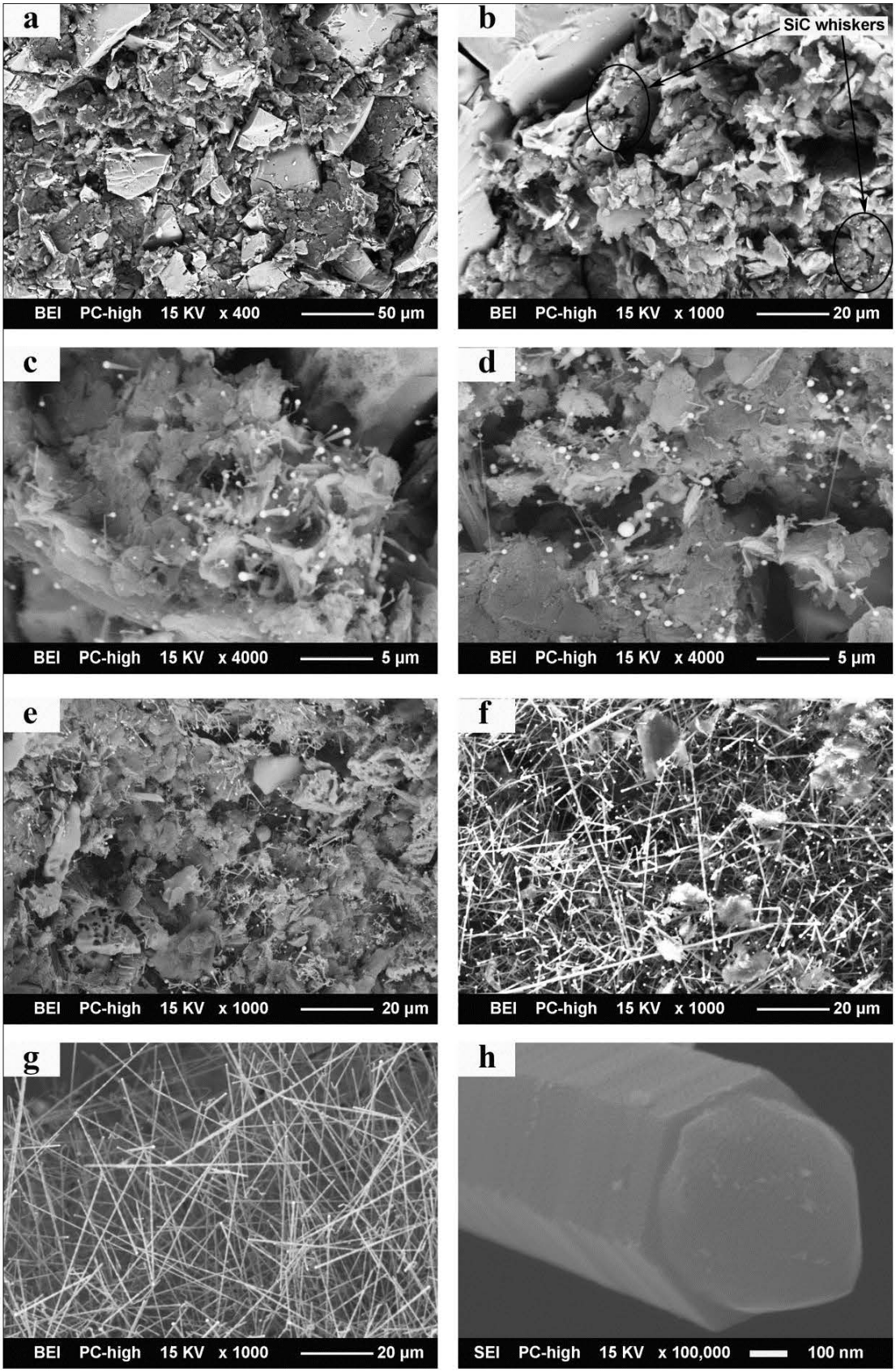

Fig. 15 SEM images of quartz in the progress of temperature programmed reduction in pure hydrogen. The furnace temperature was ramped from 573 K (300 °C) to

different temperatures at 3 K/min: (a) at 1573 K (1300 °C), cross section; (b) and (c) 1673 K (1400 °C), cross section; (d) 1673 K (1400 °C), surface; (e) 1773 K (1500 °C), cross section; (f) 1773 K (1500 °C), surface; (g) 1873 K (1600 °C), surface; (h) 1873 K (1600 °C), a SiC fibre at a high magnification.

V. Conclusions

Carbothermal reduction of quartz was strongly affected by the gas atmosphere and temperature. The reduction rate increased with increasing hydrogen partial pressure and temperature. SiC began to form at 1473 K (1200 °C) in hydrogen. The conversion of quartz to SiC at 1673 K (1400 °C) was completed in 270 minutes. This period was reduced to 140 minutes at 1773 K (1500 °C) and 70 minutes at 1873 K (1600 °C). In the carbothermal reduction of SiO_2 in argon, the conversion of quartz to SiC started at 1573 K (1300 °C), and was incomplete after 270 minutes at 1773 K (1500 °C).

The faster reduction rate in hydrogen containing gas was attributed to the involvement of hydrogen in the reactions. Quartz was directly reduced by hydrogen to SiO; CH_4 formed by reacting hydrogen with graphite also accelerated reduction of quartz to SiC. The reaction between CH_4 and SiO resulted in growth of SiC whiskers under catalytic effect of iron.

Acknowledgments

This research was supported under the Australian Research Council's Linkage Projects funding scheme (Project No. LP100100866) and the Norwegian Research Council under the project Kiselrox (Project No. 228722/O30). Xiang Li is a recipient of University of Wollongong Deputy Vice Chancellor's Special Scholarship. The authors would also like to thank the Mark Wainwright Analytical Centre at the University of New South Wales for LECO analysis, and the Electron Microscopy Centre (EMC) at the

University of Wollongong for the electron microscopy characterization.

References

1. K. Järrendahl and R. Davis: *Semiconductors & Semimetals*, 1998, vol. 52, pp. 1–20.
2. Y.L. Chiew and K.Y. Cheong: *Mater. Sci. Eng. B*, 2011, vol. 176, pp. 951–964.
3. G.S. Gupta, P. Vasanth Kumar, V.R. Rudolph, and M. Gupta: *Metall. Mater. Trans. A*, 2001, vol. 32, pp. 1301–1308.
4. C. Zollfrank: *J. Eur. Ceram. Soc.*, 2004, vol. 24, pp. 495–506.
5. Z.S. Ermekova, Z.A. Mansurov, and A.S. Mukasyan: *Ceram. Int.*, 2010, vol. 36, pp. 2297–2305.
6. M. Suzuki, Y. Maniette, Y. Nakata, and T. Okutani: *Ceram. Int.*, 1993, vol. 19, pp. 407–413.
7. M. Narisawa, Y. Okabe, M. Iguchi, and K. Okamura: *J. Sol-Gel Sci. Techn.*, 1998, vol. **12,** pp. 143–152.
8. HSC Chemistry 6.1: Chemical Reaction and Equilibrium Software with extensive thermochemical database, Outokumpu, 2007.
9. Y. Duan, B. Zhang, D.C. Sorescu, and J.K. Johnson: *J. Solid. State. Chem.*, 2011, vol. 184, pp. 304–311.
10. J.G. Lee, P.D. Miller, and I.B. Cutler: *Reactiviity of solids*, Plenum Press, New York, 1976, pp. 707–712.
11. Y. Zhong, L.L. Shaw, M. Manjarres, and M.F. Zawrah: *J. Am. Ceram. Soc.*, 2010. vol. 93, pp. 3159–3167.
12. B.M. Moshtaghioun, R. Poyato, F.L. Cumbrera, S. de Bernardi-Martin, A. Monshi, M. H. Abbasi, F. Karimzadeh, and A. Dominguez-Rodriguez: *J. Eur. Ceram. Soc.*, 2012, vol. 32, pp. 1787–1794.
13. A. Agarwal and U. Pal: *Metall. Mater. Trans. B*, 1999, vol. 30, pp. 295–306.
14. B.M. Moshtaghioun, A. Monshi, M.H. Abbasi, and F. Karimzadeh: *Int. J. Refract. Met. H.*, 2011, vol. 29, pp. 645–650.
15. E. Dal Martello, G. Tranell, S. Gaal, O.S. Raaness, K. Tang, and L. Arnberg: *Metall.*

Mater. Trans. B, 2011, vol. 42B, pp. 939–950.

16. J. Yao, H. Wang, X. Zhang, W. Zhu, J. Wei, and Y.B. Cheng: *J. Phys. Chem. C*, 2007, vol. 111, pp. 636–641.
17. R. Kononov, O. Ostrovski, and S. Ganguly: *11th International Conference on Innovations in the Ferro Alloy Industry,* New Delhi, 2007, pp. 258–267.
18. R. Kononov, O. Ostrovski, and S. Ganguly: *Metall. Mater. Trans. B*, 2008, vol. 39, pp. 662–668.
19. M. Yastreboff, O. Ostrovski, and S. Ganguly: *ISIJ Int.*, 2003, vol. 43, pp. 161–165.
20. K. Terayama and M. Ikeda: *T. Jan. I. Met*., 1985, vol. 26, pp. 108–114.
21. M.A.R. Dewan, G. Zhang, and O. Ostrovski: *Miner. Process. Extr. M. C*, 2011, vol. 120, pp. 111–117.
22. M.A.R. Dewan, G. Zhang, and O. Ostrovski: *Metall. Mater. Trans. B*, 2009, vol. 40, pp. 62–69.
23. R.J. Fruehan and G. Carkin: *Metall. Mater. Trans. B*, 2004, vol. 35, pp. 617–623.
24. O. Ostrovski, G. Zhang, R. Kononov, M.A.R. Dewan, and J. Li: *Steel Res. Int.*, 2010, vol. **81,** pp. 841–846.
25. A.C.D. Chaklader and A.L. Roberts: *J. Am. Ceram. Soc.*, 1961, vol. 44, pp. 35–41.
26. B. Ozturk and R.J. Fruehan: *Metall. Trans. B*, 1985, vol. 16B, pp. 801–806.
27. O. Ostrovski, and G. Zhang: *AIChE J.*, 2006, vol. 52, pp. 300–310.
28. G. Urretavizcaya and J.M. Petro Lopez: *J. Mater. Res.*, 1994, vol. **9**, pp. 2981–86.
29. H.J. Choi and J.G. Lee: *J. Mater. Sci.*, 1995, vol. 30. pp. 1982–1986.
30. U. Setiowati and S. Kimura: *J. Am. Ceram. Soc.*, 1997, vol. 80, pp. 757–760.
31. G.A. Bootsma, W.F. Knippenberg, and G. Verspui: *J. Cryst. Growth*, 1971, vol. 11, pp. 297–309.

CHAPTER 3

CARBOTHERMAL REDUCTION OF QUARTZ IN METHANE-HYDROGEN–ARGON GAS MIXTURE

Carbothermal Reduction of Quartz in Methane–Hydrogen–Argon Gas Mixture

Xiang Li[1], Guangqing Zhang[1], Kai Tang[2], Oleg Ostrovski[3], Ragnar Tronstad[4]

[1]School of Mechanical, Materials and Mechatronic Engineering, University of Wollongong, Wollongong, NSW 2522, Australia

[2]SINTEF Materials and Chemistry, N-7465 Trondheim, Norway

[3]School of Materials Science and Engineering, University of New South Wales, Sydney, NSW 2052, Australia

[4]Elkem AS, Drammensveien 169, P.O Box 334 Skøyen, 0213 Oslo, Norway

Abstract

Synthesis of silicon carbide (SiC) by carbothermal reduction of quartz in a CH_4–H_2–Ar gas mixture was investigated in a laboratory fixed-bed reactor in the temperature range of 1573 to 1823 K (1300 to 1550 °C). The reduction process was monitored by an infrared gas analyser, and the reduction products were characterised by LECO, XRD and SEM. A mixture of quartz-graphite powders with C/SiO_2 molar ratio of 2 was pressed into pellets and used for reduction experiments. The reduction was completed within 2 hours under the conditions of temperature at or above 1773 K (1500 °C), methane content 0.5 to 2 vol pct and hydrogen content ≥ 70 vol pct. Methane partially substituted carbon as a reductant in the SiC synthesis and enhanced the reduction kinetics significantly. An increase in the methane content above 2 vol pct caused excessive carbon deposition which had a detrimental effect on the reaction rate. Hydrogen content in the gas mixture above 70 vol pct effectively suppressed the cracking of methane.

I. Introduction

Silicon carbide (SiC) has a long history as a cutting material, refractory material, high-temperature semiconductor and in other advanced applications [1]. SiC is distinguished by a combination of high thermal conductivity (higher than that of copper), hardness second to diamond, high thermal stability, and chemical inertness. It is also a wide bandgap semiconductor material with high breakdown electric field strength and high saturated drift velocity of electrons [2].

The overall reaction for the formation of SiC through carbothermal reduction of silica can be represented as:

$$SiO_2\ (s) + 3\ C\ (s) = SiC\ (s) + 2\ CO\ (g) \qquad (1)$$

$$\Delta G^\circ = 598.18 - 0.3278\ T \quad (kJ)$$

This reaction is strongly endothermic with $\Delta H^o_{298} = 618.5$ kJ [3]. The basic building block of a SiC crystal is the tetrahedron of four carbon atoms with a silicon atom in the center. Synthesis of SiC materials requires high temperatures (> 1273 K (1000 °C)) [4, 5]. The commercial production of SiC was established as early as in 1892 using a process known as the Acheson method. In this process, SiC was produced by reaction between silica sand and petroleum coke at very high temperature (above 2773 K (2500 °C)) [6, 7]. However, this reaction proceeds slowly due to inadequate contact between the solid particles. A much faster process involves a direct carburization of metallic silicon by combustion synthesis (self-propagating) [8, 9]. However, this method is expensive because of the cost of elemental silicon. SiC can also be produced by gaseous pyrolysis of silane (SiH_4) [10, 11] or methylchlorosilane (CH_3SiCl_3) [12] in a carbon-containing atmosphere (chemical vapour deposition technique). This process is not only expensive, but also very corrosive. Therefore, development of a new, efficient process for synthesis of SiC is of high importance.

A carbothermal reduction process requires intimate contact between a solid oxide and a carbonaceous material. Intensive researches have been conducted in the production of various metal carbides using methane. Ostrovski and Zhang [13–18] investigated the reduction and carburization of the oxides of iron, manganese, chromium, and titanium by CH_4–H_2–Ar gas mixtures. Methane containing gas with high carbon activity (above unity relative to graphite) provided strongly reducing conditions, in which metal oxides were reduced and carburized to metal carbides. Iron oxide was first reduced to metallic iron by hydrogen, and then carburized to cementite Fe_3C [17, 18]. Manganese oxide was reduced to carbide Mn_7C_3 through the sequence: $MnO_2 \rightarrow Mn_2O_3 \rightarrow Mn_3O_4 \rightarrow MnO \rightarrow Mn_7C_3$ [15]; and Rutile was reduced to titanium oxycarbide in the following sequence:$TiO_2 \rightarrow Ti_5O_9 \rightarrow Ti_4O_7 \rightarrow Ti_3O_5 \rightarrow Ti_2O_3 \rightarrow TiO_xC_y$ [14].

Lee et al. [19] implemented a thermodynamic analysis of carbothermal formation of SiC and elemental Si. They demonstrated that methane decomposes completely at temperatures above 1250 °C. In a practical process, a thermodynamic equilibrium state is not immediately reached, so inclusion of highly reactive methane in a high temperature reaction system can improve the reaction kinetics as demonstrated by reduction of other metal oxides. However, no experimental investigations have been reported in literature on the direct reduction of SiO_2 to SiC by methane containing gas. Our experimental study of direct reduction of quartz or amorphous silica powder by methane demonstrated that intermediate product SiO vapour escaped from the reaction zone as fume during reaction without conversion to SiC. This problem is not encountered in reduction of other metal oxides by methane as their intermediates are in the form of metals (Fe [17, 18]) or solid suboxides (Mn_xO_y [15] and Ti_xO_y [14]) which are further converted to metal carbides by reacting with methane or deposited carbon. The gaseous SiO can be “caught” providing an intimate contact of quartz with solid carbon either by chemical vapour deposition from methane in silica particles before reduction [20], or by mechanical mixing of carbon and silica [21–23].

This work presents an investigation of synthesis of SiC by the carbothermal reduction of quartz in CH_4–H_2–Ar gas mixtures. The reactant pellet is a quartz-graphite mixture with C/SiO_2 molar ratio of 2 which is less than the stoichiometric ratio for SiC production ($C/SiO_2 = 3$). Methane is expected to substitute partial reductant graphite and enhance the reduction rate. The main objective of this study was to establish the mechanism of carbothermal reduction of quartz in the CH_4–H_2–Ar gas mixture under strongly irreversible conditions.

II. Experimental

Quartz powder (particle size < 70 μm) was obtained by crushing quartz lumps in a 6 inch agate pulveriser in a Rocklabs ring mill. The agate was made of grey silica so that contamination to the quartz sample was minimized. The contents of impurities in quartz lumps were presented elsewhere [24]. Quartz powder and synthetic graphite (≥ 99.99 pct, < 45 μm, Sigma-Aldrich Co. Ltd, Germany) were mixed with distilled water (80 wt pct of solid mixture) in a plastic jar with zirconia balls for 8 hours. The quartz–graphite mixture had a C/SiO_2 molar ratio of 2.0. This ratio was below the stoichiometric ratio 3:1 needed for complete conversion of quartz to SiC. Carbon deficit was covered by methane. Reduction of quartz with $C/SiO_2 = 3$ was also examined for comparison. Water was removed by heating the mixture at 393 K (120 °C) for 48 hours. Then the mixture was pressed into pellets in a uniaxial hydraulic press by applying 20 KN of load for 2 minutes. The pellets with a mass of approximately 1 g were 8 mm in diameter and about 12 mm in height.

Reduction experiments were carried out in a laboratory fixed bed reactor heated in a vertical tube electric furnace. The reactor setup was presented previously [24]. A weighed pellet was loaded at the bottom of the reactor, and then heated to the desired temperature by inserting the reactor into the furnace so that the sample was located in the furnace hot zone. Reduction was studied in CH_4–H_2–Ar gas mixtures of different compositions which were formed by mixing individual gases of 99.999 wt pct purity.

The gas flow rates were controlled by mass flow controllers. The total gas flow rate was maintained at 1.00 NL/min. The outlet gas composition was continuously monitored by an infrared $CO/CO_2/CH_4$ analyzer (Advanced optima AO2020, ABB Ltd., Ladenburg, Germany) connected with a computer. Data of gas concentrations were recorded every 5 seconds. Reaction was stopped after certain duration by raising the reactor above the furnace hot zone and cooling down. After that, the reduced pellet was weighed and subjected to characterisation.

The original mixture and reduced samples were analyzed by X-ray diffraction (XRD, MMA, GBC Scientific Equipment, Braeside, Australia). The fine powder of a sample after grinding was scanned at a speed of 0.02° s^{-1} and step size 0.02° with CuK radiation generated at 35 kV and 28.6 mA.

The morphology of the samples was investigated by field-emission scanning electron microscopy (FESEM, JSM-6000, JEOL, Tokyo, Japan) operated at 15 KV.

The oxygen content of the reduced samples was determined by LECO Nitrogen/Oxygen Determinator (TC-436 DR, St. Joseph, USA). A weighed sample was loaded into a tin crucible and then a nickel basket. A graphite crucible was placed between two electrodes. High current passed through this crucible heating it up to temperatures above 3100 °C. After an outgassing procedure the nickel basket containing a sample was dropped into the graphite crucible from a loading head purged by helium. At the high temperature, oxygen from the sample combined with the carbon of the crucible to form carbon monoxide (CO) and carbon dioxide (CO_2) which were detected by infrared detectors. The instrument was calibrated using standard samples with appropriate oxygen contents.

The contents of free carbon in samples were determined by Carbon/Sulfur Determinator (CS-2000, ELTRA Elemental Analyzers, Haan, Germany). A weighed sample was

placed into a ceramic crucible. The system was closed and purged with oxygen. The crucible was heated in a resistance furnace with fixed temperature 940°C in oxygen atmosphere. Free carbon from the sample reacts with oxygen to form CO and CO_2 which were analysed by infrared detectors. The instrument was calibrated using standard samples with appropriate carbon contents.

The equilibrium phases in the system of carbothermal reduction of quartz were calculated using Outokumpu HSC Chemistry software (Version 6.1, Outokumpu Research Oy, Pori, Finland).

The extent of reduction was defined as a fraction of oxygen in quartz removed in the course of reduction. Oxygen was removed in the form of CO, CO_2 and SiO. The main oxygen-containing compound in gas phase was CO, as CO_2 was converted to CO by the Boudouard reaction, and SiO reacted with graphite forming SiC. Using the CO and CO_2 concentrations in the off gas, the extent of reduction was calculated using Eq. (2).

$$X' = \frac{1}{n_{O-i}} \int_0^t \frac{F}{22.4} \left(C_{V-CO} + 2 \times C_{V-CO_2}\right) dt \quad (2)$$

where X' is the conversion of silica based on CO and CO_2 concentrations, pct at time t; C_{V-CO} is the concentration of CO and C_{V-CO_2} the concentration of CO_2, vol pct; F is the gas flow rate, NL/min; n_{O-i} is the initial content of oxygen in quartz, mol; and t is the reaction time, min.

More accurate value of X was obtained using a residual oxygen content in the reacted sample derived from the LECO oxygen analysis. In this case, the conversion of SiO_2 can be simply presented as

$$X = \frac{1}{n_{O-i}} \left(n_{O-i} - n_{O-LECO}\right) \times 100 \quad (3)$$

where X is the conversion of silica at the end of reduction, pct; n_{O-LECO} is the content of oxygen in the reacted sample, mol.

Plots of the extent of reduction X versus the reaction time t were obtained by normalizing the final extent of reduction from on-line gas analysis (X′ from Eq. (2)) to the values determined using LECO analyzer. The error of measured oxygen content by LECO analysis depends on the residual oxygen content in the reduced sample. For a sample with the extent of reduction 90 pct, the error of oxygen analysis was about 0.1 pct, which gives an error in the extent of reduction 0.3 pct. Including other errors such as in weighing and gas flow rate, the overall error of the final extent of reduction is estimated to be less than 1 pct.

Assuming that reduced samples consisted of SiC, SiO_2 and free carbon, the yield of SiC (percentage of silicon in an original sample converted to SiC) was calculated using the following equation:

$$Y_{SiC} = \frac{100}{40 \times n_{Si}} \times m \times (1 - C_{C-LECO} - C_{O-LECO} \times 60/32) \quad (4)$$

where n_{Si} is the initial amount of SiO_2 in pellet before reduction, mol; m is the weight of pellet after reduction, g; C_{C-LECO} and C_{O-LECO} are the mass contents of free carbon and oxygen in the reduced sample, pct.

During reduction, the part of generated SiO blown out from the pellet was defined as loss of silicon as SiO and calculated by Eq. (5).

$$Y_{SiO} = \frac{1}{n_{Si}} \times [n_{Si} \times (100 - Y_{SiC}) - m \times C_{O-LECO}/32] \quad (5)$$

III. Results

3.1 Effect of Temperature

The effect of temperature on the reduction of quartz was studied in the temperature range of 1573 K (1300 °C) to 1823 K (1550 °C). The inlet gas mixture contained 1 vol pct of methane, 70 vol pct of hydrogen and 29 vol pct of argon. The extent of reduction *vs* time at different temperatures is shown in Figure 1. Figure 2 presents the XRD spectra of samples reduced for 150 minutes. Table 1 lists the final extent of reduction and yield of SiC after 150 minutes reduction.

At 1573 K (1300 °C), carbothermal reduction of quartz was slow, reaching an extent of reduction of 48.8 pct after 150 minutes. A small amount of β-SiC was identified in the reduction product, corresponding to the weak peaks at 2θ = 35.66 (d = 2.5161 **Å**), 2θ = 41.40 (d = 2.1790 **Å**) and 2θ = 59.99 (d = 1.5408 **Å**). The yield of SiC was 38.5 pct as shown in Table 1. With the increase of temperature, the rate of reduction and the composition of reduced samples changed consistently. In reduction at 1773 K (1500 °C), the oxygen content decreased to 0.49 wt pct, and free carbon content was 3.67 wt pct. Corresponding extent of reduction was 99.5 pct which did not increase further with extension of reduction time. The yield of SiC was 72.4 pct; a significant fraction of silicon in the raw material was lost as SiO which will be discussed in Section IV. Further increase in temperature to 1773 K (1500 °C) and 1823 K (1550 °C) accelerated the reduction but no effect on the extent of reduction, which was close to completion at these temperatures.

In addition to quartz, cristobalite peaks were detected in the samples reduced at 1623 K (1350 °C), 1673 K (1400 °C) and 1723 K (1450 °C), as a result of the transformation of quartz to cristobalite in high temperatures [25]. Neither quartz nor cristobalite were detected in the samples reduced at 1773 K (1500 °C) and 1823 K (1550 °C).

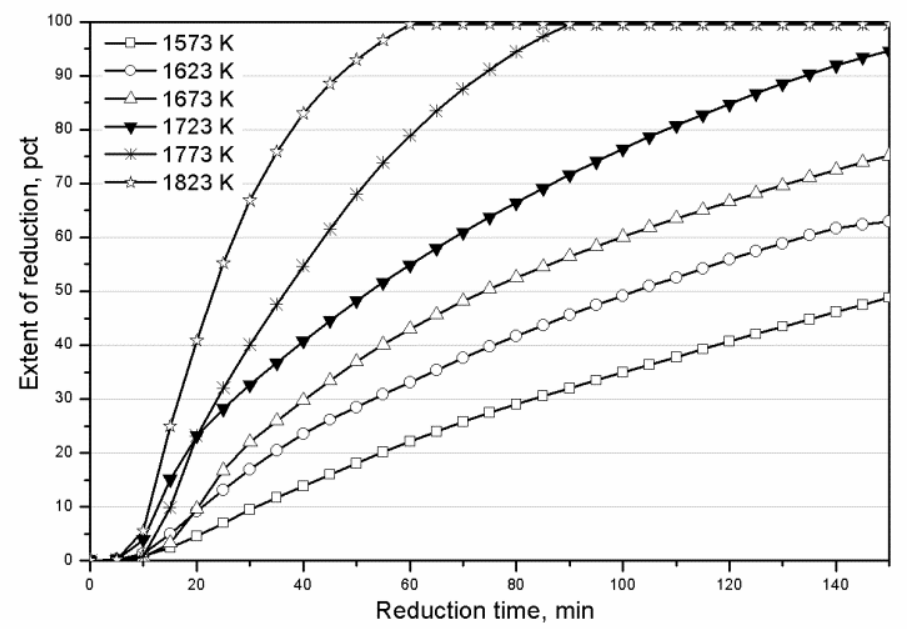

Fig. 1 Effect of temperature on the extent of reduction in 1 vol pct CH_4–70 vol pct H_2–29 vol pct Ar gas mixture.

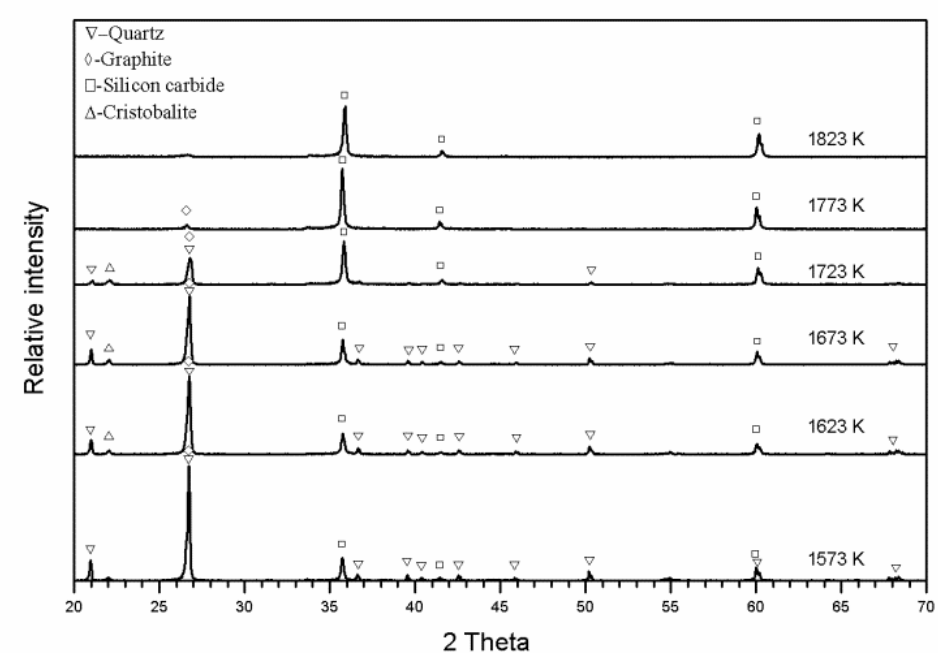

Fig. 2 XRD patterns of samples reduced in 1 vol pct CH_4–70 vol pct H_2–29 vol pct Ar gas mixture at different temperatures for 150 min.

Table 1. Extent of reduction and yield of SiC after carbothermal reduction in CH_4–H_2–Ar gas mixture at different temperatures for 150 minutes.

Temperature, K	1573	1623	1673	1723	1773	1823
Free carbon content, wt pct	26.5	23.2	18.3	11.4	3.67	4.25
Oxygen content, wt pct	26.9	22.9	20.0	11.5	0.49	0.50
Weight loss, pct	20.4	24.5	33.0	51.6	63.9	62.9
Loss of Si as SiO, mol pct	5.27	0.93	2.69	17.2	27.2	26.6
Extent of reduction, pct	48.8	62.9	75.1	94.6	99.5	99.6
Yield of SiC, pct	38.5	53.8	62.1	68.2	72.4	73.0

3.2 Effect of Methane Content in the Gas Mixture

The effect of methane content in the gas mixture on the carbothermal reduction of quartz was examined in the range of 0 to 6 vol pct, keeping hydrogen content at 70 vol pct and temperature at 1773 K (1500 °C). The extent of reduction *vs* time for different methane contents is shown in Figure 3. The XRD spectra of samples after reduction are presented in Figure 4. Table 2 presents the characterization of the samples after 150 min reduction. During reduction without addition of methane, the weight loss was 79.4 pct, while the extent of reduction was 85.0 pct. Graphite in the original mixture was almost consumed completely by the carbothermal reduction; graphite peaks were not detected by the XRD analysis of the reduced sample. The SiC yield was only 42.6 pct. Addition of 0.5 pct methane in the gas mixture remarkably increased reduction rate, resulting in the decrease in weight loss to 69.0 pct, and the increase in the extent of reduction and SiC yield to 99.3 and 62.8 pct, correspondingly. Further increasing methane content to 1 vol pct resulted in a slight further increase in the reduction rate, however the SiC yield increased by approximately 10 pct. There was an insignificant increase in the content of

free carbon in the reduced samples. When the methane content further increased to 2 vol pct, the reduction rate was barely changed. The extent of reduction was slightly decreased while the yield of SiC marginally increased. A marked change was the free carbon content in the reduced sample which increased to 10.1 pct. This is an indication of thermal cracking of methane. Further increasing the concentration of methane in the gas mixture, although had a small effect on the initial rate of reduction, resulted in significant suppression of the reduction at the later stage, resulting in a sharp decrease in the weight loss, extent of reduction and the yield of SiC. The content of free carbon in the samples reduced in the gas mixture containing 6 pct methane increased to 32.0 pct reflecting the strong effect of the methane cracking on the reduction of silica.

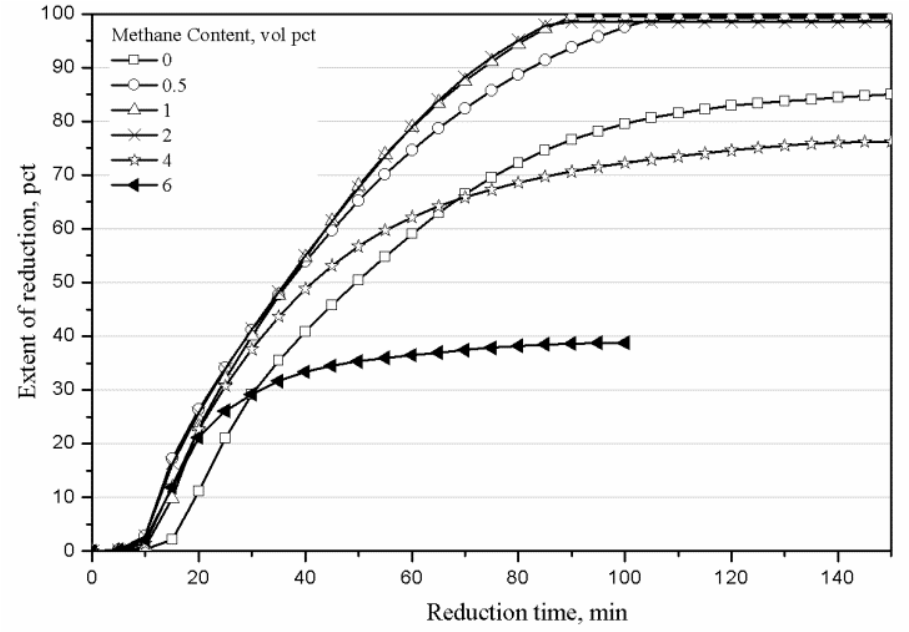

Fig. 3 Effect of methane content in CH_4–H_2–Ar gas mixtures on extent of reduction at 1773 K (1500 °C).

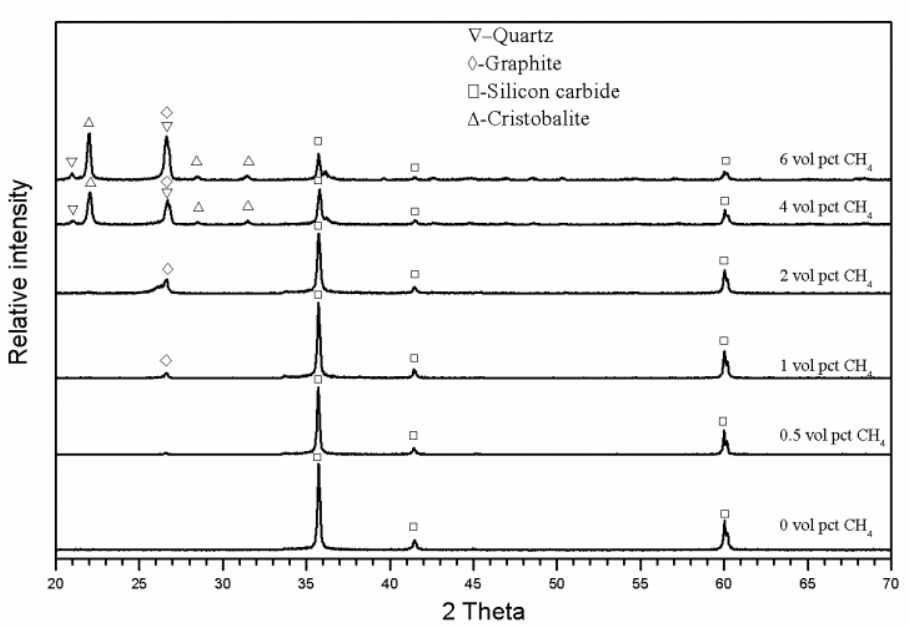

Fig. 4 XRD patterns of samples reduced in CH_4–H_2–Ar gas mixtures with different methane content at 1773 K (1500 °C) for 150 min.

Table 2. Extent of reduction and yield of SiC after carbothermal reduction at 1773 K (1500 °C) in the CH_4–H_2–Ar gas mixtures with different methane contents for 150 minutes.

Methane content, vol pct	0	0.5	1.0	2.0	4.0	6.0*
Free carbon content, wt pct	0.12	1.68	3.67	10.1	28.2	32.0
Oxygen content, wt pct	0.94	0.91	0.49	1.64	19.5	27.3
Weight loss, pct	79.4	69.0	63.9	58.1	28.1	13.2
Loss of Si as SiO, mol pct	56.9	36.4	27.2	25.0	10.0	7.22
Extent of reduction, pct	85.0	99.3	99.5	98.5	76.2	38.8
Yield of SiC, pct	42.6	62.8	72.4	73.3	53.1	30.5

* The reduction was proceeded for 100 minutes.

3.3 Effect of Hydrogen Content in the Gas Mixture

The effect of hydrogen content in the gas mixture on the carbothermal reduction of quartz was examined at 1773 K (1500 °C) with a constant methane concentration of 1 vol pct. The hydrogen content in the gas mixture was varied from 0 to 99 vol pct. Figure 5 depicts the progress of reduction *vs* time for different hydrogen contents, and Figure 6 presents the XRD patterns of samples after reduction for 150 minutes. Table 3 presents the final extent of reduction and yield of SiC after 150 minutes reduction. Increase in the hydrogen concentration in the reducing gas in the range of 0 to 70 vol pct strongly increased the extent of reduction and yield of SiC, and did not show further visible enhancing effect on the reduction in the range of 70 to 99 vol pct. The content of free carbon decreased from 27.3 wt pct when the gas mixture contained no hydrogen to 3.67 wt pct when hydrogen content was 70 vol pct.

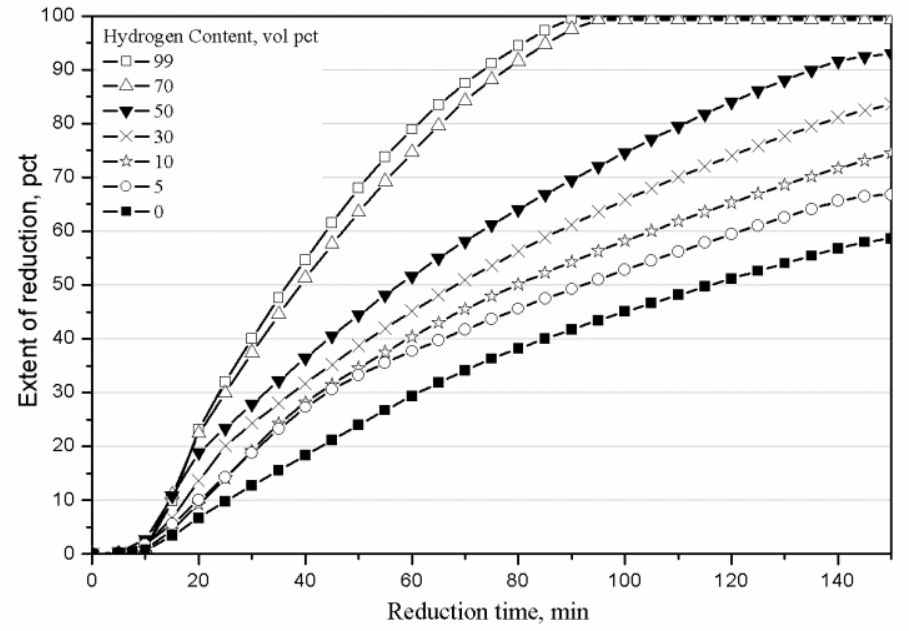

Fig. 5 Effect of hydrogen content in CH_4–H_2–Ar gas mixtures on extent of reduction at 1773 K (1500 °C).

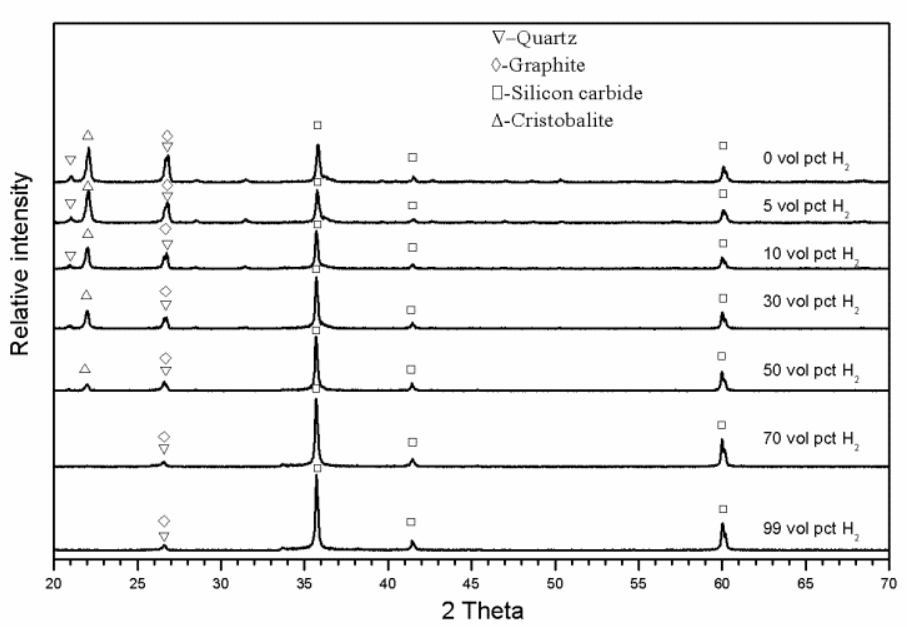

Fig. 6 XRD patterns of samples reduced in CH_4–H_2–Ar gas mixtures with different hydrogen content at 1773 K (1500 °C) for 150 min.

Table 3. Extent of reduction and yield of SiC after carbothermal reduction at 1773 K (1500 °C) in the CH_4–H_2–Ar gas mixtures with different hydrogen contents for 150 minutes.

Hydrogen content, vol pct	0	5	10	30	50	70	99
Free carbon content, wt pct	27.3	24.1	17.7	11.4	8.67	3.67	3.05
Oxygen content, wt pct	21.0	18.0	15.0	11.0	3.26	0.49	0.23
Weight loss, pct	35.2	41.2	48.3	55.5	60.5	63.9	64.3
Loss of Si as SiO, mol pct	18.9	20.1	20.7	23.7	25.9	27.2	27.3
Extent of reduction, pct	58.6	66.8	74.5	83.5	93.0	99.5	99.6
Yield of SiC, pct	45.5	52.1	58.9	63.5	70.7	72.4	72.5

IV. Discussion

Reduction of quartz by carbon described by Reaction (1) is a combination of Reactions (6) and (7):

$$SiO_2\ (s) + C\ (s) = SiO\ (g) + CO\ (g) \quad (6)$$

$$\Delta G^\circ = 668.07 - 0.3288\ T \quad (kJ)$$

$$SiO\ (g) + 2\ C\ (s) = SiC\ (s) + CO\ (g) \quad (7)$$

$$\Delta G^\circ = -78.891 + 0.001\ T \quad (kJ)$$

The reactions generate both SiC and SiO of which amounts depend on the carbon to quartz ratio *x*. When $1<x<3$:

$$SiO_2\ (s) + x\ C\ (s) = (x-1)/2\ SiC\ (s) + (3-x)/2\ SiO\ (g) + (1+x)/2\ CO\ (g) \quad (8)$$

Schei and Halvorsen [26] defined *x* in Reaction (8) as carbon coverage. Reaction (8) indicates that when C/SiO_2 molar ratio is less than a stoichiometric ratio of 3 silicon can be lost in the form of SiO(g) which is blown out of the reactor. The SiC recovery depends on the carbon coverage. Introduction of methane to the reaction system with $C/SiO_2 = 2$ enhances formation of SiC:

$$SiO_2(s) + 2\ C(s) + y\ CH_4\ (g) = (0.5 + 0.5y)\ SiC\ (s) +$$
$$(0.5 - 0.5y)\ SiO\ (g) + (1.5 + 0.5y)\ CO\ (g) + 2y\ H_2\ (g) \quad (9)$$

Along with increasing y ($y \leq 1$), the yield of SiC increases. Complete conversion of silica to SiC theoretically can be reached at $y = 1$.

Figure 7 presents the calculated equilibrium compositions in the carbothermal reduction of quartz with and without methane addition. To reduce the CO partial pressure, 1 mol

of argon was added to the reaction systems. In the system containing 1 mol SiO_2, 2 mol C and 1 mol argon (Figure 7(a)), reduction of SiO_2 starts at 1373 K (1100 °C); carbothermal reduction of SiO_2 proceeds until 1773 K (1500 °C) at which all carbon is used up. Further increasing temperature results in reduction of SiO_2 by SiC with evolution of SiO vapour by Reaction (10). SiO_2 is fully reacted when the temperature is increased to 2223 K (1950 °C).

$$2\ SiO_2\ (s) + SiC\ (s) = 3\ SiO\ (g) + CO\ (g) \qquad (10)$$

$$\Delta G° = 1444.3 - 0.6700\ T \quad (kJ)$$

When 1 mol of methane is added to the system (Figure 7(b)), decomposition of methane takes place before the reduction of SiO_2 starts at 1293 K (1020 °C); conversion of SiO_2 is completed at 1893 K (1620 °C). Quartz is predominantly reduced to SiC; evolution of SiO is negligible in the course of reduction which means there is no significant loss of silicon. The same effect can be achieved by increasing the amount of carbon in the system to $C/SiO_2 = 3$ (Figure 7(c)).

However, the experimental data were quite different from results of thermodynamic calculations. The studied reaction system with continuously flowing gas was not in the batch operation as in the thermodynamic modelling. CO formed by reduction was continuously removed from the reactor, what greatly enhanced the reduction process. On the other hand, SiO diffused out of the pellets and was flushed out of the reactor with a significant loss of silicon as SiO and decrease in the SiC yield.

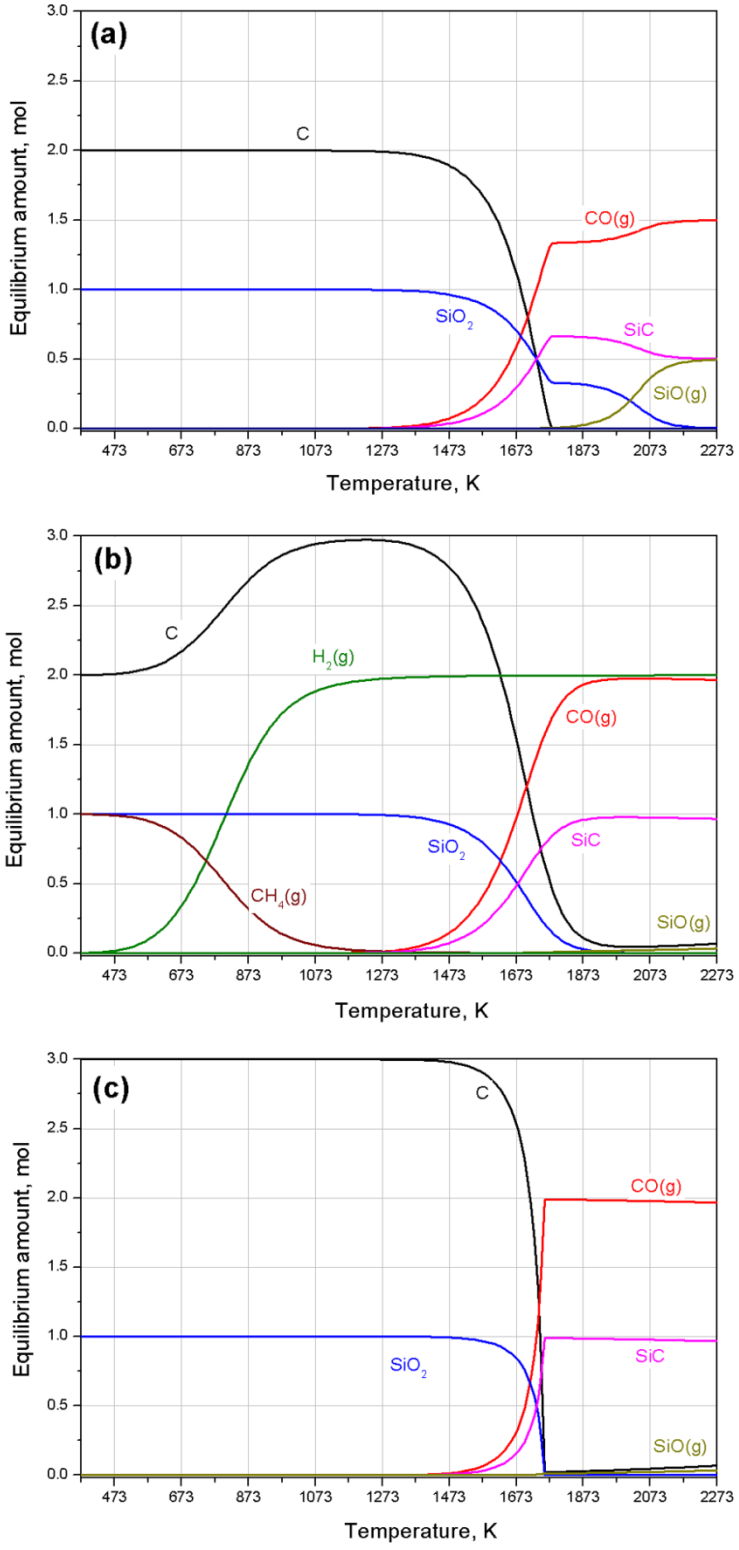

Fig. 7 Equilibrium compositions of the systems (a) 1 mol SiO_2 + 2 mol C + 1 mol Ar; (b) 1 mol SiO_2 + 2 mol C + 1 mol CH_4 + 1 mol Ar; (c) 1 mol SiO_2 + 3 mol C + 1 mol Ar calculated using HSC Chemistry 6.1.

Figure 8 presents the rate of generation of CO in carbothermal reduction of quartz with molar $C/SiO_2 = 2$ in argon and CH_4–H_2–Ar gas mixture, and molar $C/SiO_2 = 3$ in argon and hydrogen at 1500 °C. Reduction of quartz with $C/SiO_2 = 3$ was faster than that with $C/SiO_2 = 2$ in argon, but it was not completed at 150 minutes. Reduction of quartz in the CH_4–H_2–Ar gas mixture was much faster than those in argon, and was completed at 116 minutes. In the main period of reduction time, reduction of quartz with $C/SiO_2 = 2$ in CH_4–H_2–Ar gas mixture was faster than with $C/SiO_2 = 3$ in hydrogen, which is attributed to high carbon activity in the CH_4–H_2–Ar gas mixture.

Table 4 compares the composition of four samples reduced at 1773 K (1500 °C) for 150 minutes. Increasing carbon content in the C–SiO_2 mixture decreased the loss of Si as SiO during reduction in argon. Reduction of quartz with $C/SiO_2 = 3$ in hydrogen enhanced the extent of reduction of quartz and the yield of SiC, but the loss of Si as SiO was pretty high, 33.8 pct. Partial replacement of carbon by methane in the gas phase made the reduction close to completion, decreased the loss of SiO and increased the SiC yield in the carbothermal reduction of silica.

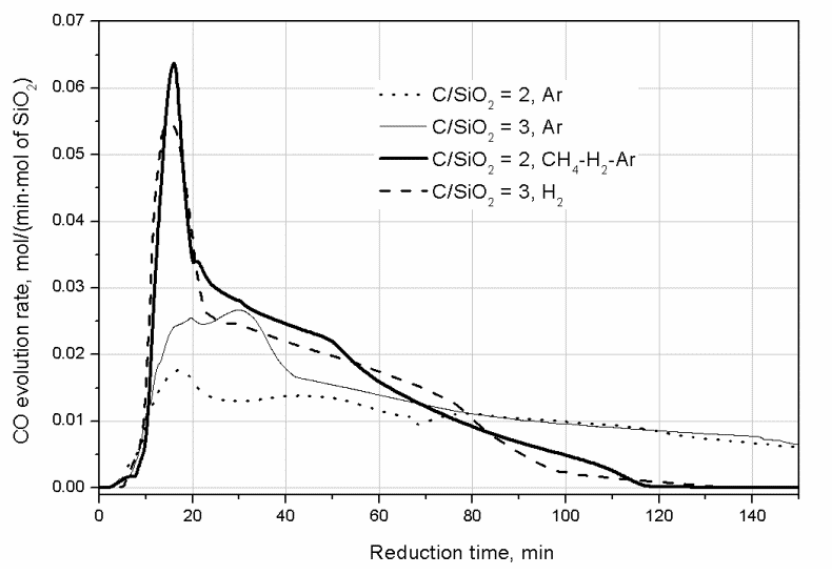

Fig. 8 CO evolution rate in carbothermal reduction at 1500 °C with changing C/SiO_2 ratios and gas composition. The gas mixture contained 1 vol pct methane, 70 vol pct hydrogen and 29 vol pct argon.

Table 4. Extent of carbothermal reduction of quartz and yield of SiC at 1773 K (1500 °C) with changing C/SiO_2 ratios and gas composition after 150 minutes reaction.

C/SiO_2 molar ratio	2	3	2	3
Reduction gas atmosphere	Ar	Ar	CH_4–H_2–Ar*	H_2
Free carbon content, wt pct	0.63	10.23	3.67	0.11
Oxygen content, wt pct	20.8	16.4	0.49	0.60
Weight loss, pct	65.2	58.0	63.9	72.04
Loss of Si as SiO, mol pct	36.9	29.9	27.2	33.8
Extent of reduction, pct	73.5	82.0	99.5	94.6
Yield of SiC, pct	44.1	52.1	72.4	65.7

*Gas composition was 1 vol pct methane, 70 vol pct hydrogen and 29 vol pct argon.

When carbothermal reduction of quartz occurred in the gas mixture with low concentration methane (0.5~2 vol pct), reaction rate increased significantly. The yield of SiC also increased due to the high reduction rate. Reduction of SiO_2 to SiC by methane can be described by Reactions (11) and (12).

$$SiO_2\,(s) + CH_4\,(g) = SiO\,(g) + CO\,(g) + 2\,H_2\,(g) \quad (11)$$

$$\Delta G^\circ = 757.07 - 0.4373\,T \quad (kJ)$$

$$SiO\,(g) + 2\,CH_4\,(g) = SiC\,(s) + CO\,(g) + 4\,H_2\,(g) \quad (12)$$

$$\Delta G^\circ = 99.113 - 0.2160\,T \quad (kJ)$$

In the reduction by methane, it decomposed into reactive carbon species and hydrogen via a series of steps [13]:

$$CH_4\,(g) \rightarrow \ldots\rightarrow C_{ad} + 2\,H_2\,(g) \quad (13)$$

in which C_{ad} represents active carbon species adsorbed on solid surface; this active carbon is substantially different from deposited solid carbon. The carbon activity in the gas phase can be defined as follows:

$$\alpha_C = \mathrm{K}(P_{CH_4} / P_{H_2}^2) \tag{14}$$

where K is the equilibrium constant of Reaction (14) of methane cracking:

$$CH_4\ (g) = C_{gr} + 2\ H_2\ (g) \tag{15}$$

$$\Delta G^\circ = 89.003 - 0.1085\ T \quad (kJ)$$

In a non-equilibrium system with a tendency of methane cracking, the carbon activity in the gas phase is greater than unity. In the reduction experiments, the CH_4–H_2–Ar gas mixture is maintained under non-equilibrium conditions with high carbon activity (relative to graphite), as shown in Figure 9. High carbon activity provides a strong thermodynamic driving force for the reduction reaction to proceed.

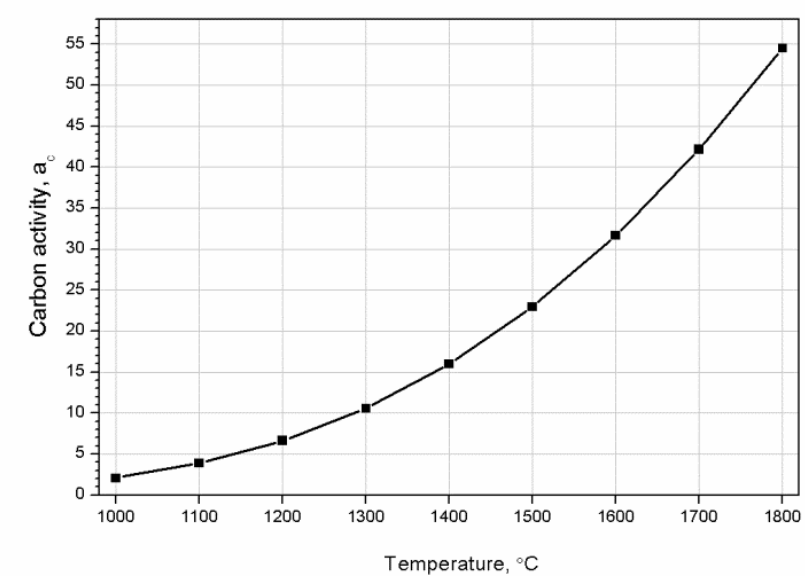

Fig. 9 Calculated carbon activity (relative to graphite) in 1 vol pct CH_4–70 vol pct H_2–29 vol pct Ar gas mixture.

However methane cracking and solid carbon deposition rate also increased with increasing methane concentration. Solid carbon deposited on the sample surface by Reaction (21), hindering the further progress of reduction by blocking the particles surface, preventing carbon supply for further reduction to the pellet's interior.

Therefore, the effect of methane on the carbothermal reduction of quartz was twofold. On one hand, increasing methane content in the gas mixture accelerated reduction and increased the yield of SiC; on the other hand, excess methane content (>2 vol pct) in the gas mixture resulted in accumulation of solid carbon on the surface of samples and retarded the reactions.

Hydrogen also played an important role in the carbothermal reduction of quartz. Increasing hydrogen content in the gas mixture from 0 to 70 vol pct significantly enhanced the rate and extent of reduction (Figure 5). Hydrogen directly reduced SiO_2 to SiO in the presence of carbon by Reaction (16) and (17) [27].

$$SiO_2\,(s) + H_2\,(g) = SiO\,(g) + H_2O\,(g) \quad (16)$$

$$\Delta G^\circ = 534.35 - 0.1869\,T \quad (kJ)$$

$$H_2O\,(g) + C\,(s) = H_2\,(g) + CO\,(g) \quad (17)$$

$$\Delta G^\circ = 133.72 - 0.1419\,T \quad (kJ)$$

Increasing hydrogen content suppressed methane cracking and solid carbon deposition by Reaction (15). Figure 10 presents the relationship between the extent of methane decomposition and the initial hydrogen content in the inlet gas at 1773 K (1500 °C). The extent of methane decomposition was calculated from the methane content in inlet gas controlled by the gas flowmeter and off gas, measured by the IR gas analyzer. Methane was almost completely decomposed when hydrogen content was less than 10 vol pct. About 91 pct of methane was decomposed with 50 vol pct of hydrogen. The suppression effect of hydrogen content on the rate of methane cracking became particularly strong

when it was above 50 vol pct: only 75 pct of methane was decomposed with 70 vol pct of hydrogen, which further decreased to 65% in pure hydrogen.

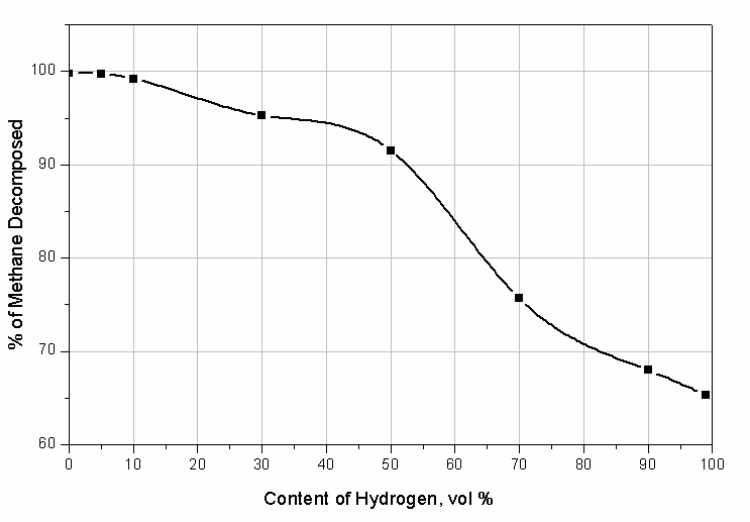

Fig. 10 Decomposition of methane *vs* hydrogen content in inlet gas. Methane content in inlet gas: 1 vol pct; temperature: 1773 K (1500 °C).

Figure 11 presents the SEM images of pellets before and after reduction at 1873 K (1600 °C) in different gas atmosphere. Original pellet presented an agglomeration of mixed quartz and graphite particles (Figure 11(a)). For the reduction in pure argon (Figure 11(b)), most of quartz was transformed to SiC particles, with some unreduced SiO_2 observed in the form of cristobalite which was identified by XRD analysis. The morphologies of pellets reduced in the CH_4–H_2–Ar gas mixture were quite different. The image of cross section near the pellet's surface (Figure 11(c)) shows that a layer of SiC fluff on the surface of the pellet, with a thickness from 200 to 500 μm. SiC whiskers with diameter of 300~800 nm and length of 3~10 μm were observed in the cross section centre, shown in Figure 11(d). These whiskers were thick and straight, grown on the iron-rich globule, suggesting that they were formed through Reaction (17) by a vapour-liquid-solid (VLS) mechanism [24,28–30]. The iron was originated from impurities in quartz and contamination of a pellet in the process of pressing with stainless steel die [24]. The rest SiC was in the form of irregular particles and flakes,

similar to the structure in Figure 11(b).

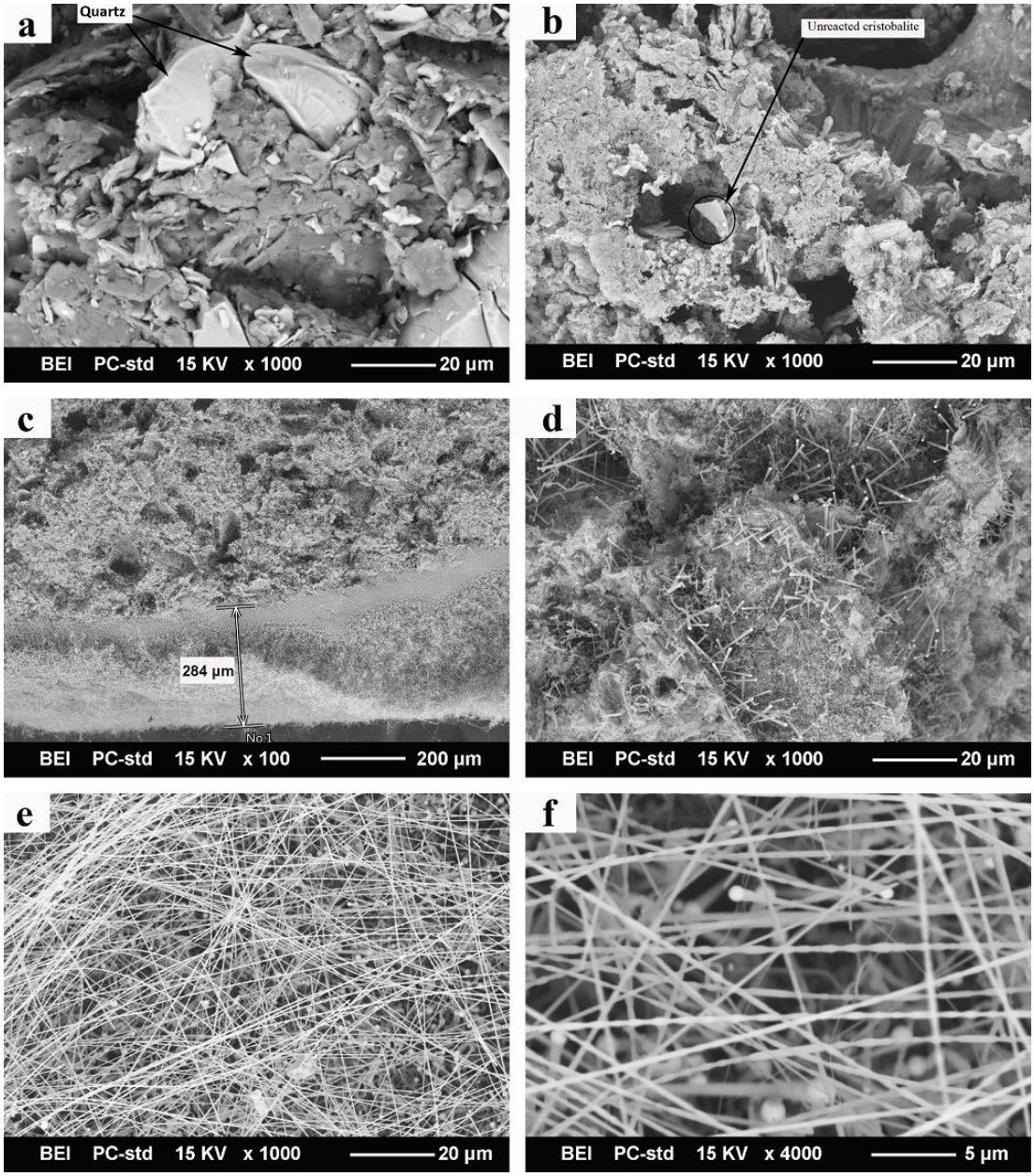

Fig. 11 SEM images of samples. (a) unreduced pellet, surface section; (b) after reduction at 1873 K (1600 °C) in pure argon, cross section; (c) and (d) after reduction at 1873 K (1600 °C) in gas mixture of 1 vol pct CH_4–70 vol pct H_2–29 vol pct Ar, cross section; (e) and (f) after reduction at 1873 K (1600 °C) in gas mixture of 1 vol pct CH_4–70 vol pct H_2–29 vol pct Ar, surface section.

SEM images obtained in further examination of the surface layer (fluff) shown in Figure 11(c) are presented in Figures 11(e) and 11(f). A large amount of long fibres were knit together on the surface (Figure 11(e)). These fibres grew to more than 100 μm long, with diameter of 300~400 nm, quite different from the whiskers in the internal of the pellet. Furthermore, iron-rich globules were not observed at the tips of fibres, what indicates that fibres were formed by Reaction (17) via the vapour-solid (VS) mechanism [19]. Whiskers with iron-rich globules were also observed under the fibres at the surface of pellet, as shown in Figure 11(f). Therefore, one-dimensional growth of SiC could take place through VLS or VS mechanism simultaneously at the surface of pellet.

V. Conclusions

The paper studied carbothermal reduction of quartz in the CH_4–H_2–Ar gas mixtures in the temperature range of 1573 to 1823 K (1300 °C to 1550 °C). The reduction of quartz mixed with graphite with C/SiO_2 ratio of 2 in the gas mixture containing 1 vol pct methane, 70 vol pct hydrogen and 29 vol pct argon was close to completion in 90 minutes at 1773 K (1500 °C) and in 60 minutes at 1823 K.

Methane supplied a part of carbon for SiC synthesis and revealed high reducing capacity compared to that of solid graphite in carbothermal reduction. The reduction rate and yield of SiC increased with increasing methane content in the CH_4–H_2–Ar gas mixture to 2 vol pct. Further increasing methane content caused excessive methane cracking with solid carbon deposition, which hindered access of reducing gas and decreased reduction rate. To suppress the deposition of solid carbon, the concentration of hydrogen in the gas mixture should be above 70 vol pct (at 1773 K (1500 °C) and 1 vol pct methane). Hydrogen was also directly involved in reduction of quartz to SiO.

Synthesis of SiC in the CH_4–H_2–Ar gas mixture resulted in three different morphologies, i.e. whiskers, fibres and irregular particles. One-dimensional growth of SiC in the form of whiskers and fibres was achieved by the gas-gas reaction, whereas SiC particles were

formed through the gas-solid reactions.

Acknowledgments

This research was supported under the Australian Research Council's Linkage Projects funding scheme (Project No. LP100100866) and the Norwegian Research Council under the project Kiselrox (Project No. 228722/O30). The authors would also like to thank the Mark Wainwright Analytical Centre at the University of New South Wales for LECO analysis, and the Electron Microscopy Centre (EMC) at the University of Wollongong for the electron microscopy characterization.

References

1. S.E. Saddow: *Silicon carbide biotechnology: a biocompatible semiconductor for advanced biomedical devices and applications*, Elsevier Science, Amsterdam, 2011, pp. 5–10.
2. S.E. Saddow and A. Agarwal: *Advances in Silicon Carbide Processing and Applications*, Artech House, Norwood, 2004, pp. 2–27.
3. H.P. Martin, R. Ecke, and E. Miiller: *J. Eur. Ceram. Soc.*, 1998. vol. 18, pp. 1737–42.
4. K. Järrendahl and R. Davis: *Semiconductors & Semimetals*, 1998, vol. 52, pp. 1–20.
5. Y.L. Chiew and K.Y. Cheong: *Mater. Sci. Eng. B*, 2011, vol. 176, pp. 951–64.
6. H.N. Baumann: *J. Electrochem. Soc.*, 1952, vol. 99, pp. 109–14.
7. G.S. Gupta, P. Vasanth Kumar, V.R. Rudolph, and M. Gupta: *Metall. Mater. Trans. A*, 2001, vol. 32, pp. 1301–8.
8. Y. Yang, K. Yang, Z.M. Lin, and J.T. Li: *Mat. Res. Bull*, 2007, vol. 42, pp. 1625–32.
9. Y. Yang, K. Yang, Z.M. Lin, and J.T. Li: J. Europ. Ceram. Soc., 2009, vol. 29, pp. 175–80.
10. O. Kordina, C. Hallin, A. Ellison, A.S. Bakin, I.G. Ivanov, A. Henry, R. Yakimova, M. Touminen, A. Vehanen, and E. Janzen: *Appl. Phys. Lett.*, 1996, vol. 69, pp. 1456–8.
11. A. Henry, I.G. Ivanov, T. Egilsson, C. Hallin, A. Ellison, O. Kordina, U. Lindefelt,

and E. Janzen: *Diam. Relat. Mater.*, 1997, vol. 6, 1289–92.

12. Q.G. Fu, H.J. Li, X.H. Shi, K.Z. Li, **J**. Wei, and Z.B. Hu: *Matetr. Chem. Phys.*, 2006, vol. 100, pp: 108–11.
13. O. Ostrovski and G. Zhang: *AIChE J.*, 2006, vol. 52, pp. 300–10.
14. G. Zhang and O. Ostrovski: *Metall. Mater. Trans. B*, 2000, vol. 31B, pp. 129–39.
15. N. Anacleto, O. Ostrovski, and S. Ganguly: *ISIJ Int.*, 2004, vol. 44, 1480–7.
16. N. Anacleto and O. Ostrovski: *Metall. Mater. Trans. B*, 2004, vol. 35B: 609–15.
17. J. Zhang and O. Ostrovski: *Ironmak. Steelmak.*, 2002, vol. 29, pp. 15–21.
18. J. Zhang and O. Ostrovski: *ISIJ Int.*, 2001, vol. 41, pp. 333–9.
19. H.C. Lee, S. Dhage, M.S. Akhtar, D.H. Kwak, W.J. Lee, C.Y. Kim and O.B. Yang: *Curr. Appl. Phys.*, 2010, vol. 10, pp. S218–21.
20. S. Cetinkaya and S. Eroglu: *Int. J. Refract. Met. H.*, 2011, vol. 29, pp. 566–72.
21. A. Agarwal and U. Pal: *Metall. Mater. Trans. B*, 1999, vol. 30, pp. 295–306.
22. B.M. Moshtaghioun, A. Monshi, M.H. Abbasi, and F. Karimzadeh: *Int. J. Refract. Met. H.*, 2011, vol. 29, pp. 645–50.
23. E. Dal Martello, G. Tranell, S. Gaal, O.S. Raaness, K. Tang and L. Arnberg: *Metall. Mater. Trans. B*, 2011, vol. 42B, pp. 939–50.
24. X. Li, G. Zhang, K. Tang, O. Ostrovski, and R. Tronstad: *Metall. Mater. Trans. B*, 2015. vol. 46, pp. 1343–52.
25. A. Schei and S.H. Halvorsen: *Proceedings from the Kjetil Motzfeldt Symposium*, Trondheim, Norway, 1991, pp. 41–6.
26. A.C.D. Chaklader and A.L. Roberts: *J. Am. Ceram. Soc.*, 1961, vol. 44, pp. 35–41.
27. X. Wan, G. Zhang, O. Ostrovski, and H. Aral: Proceedings of the Thirteenth International Ferroalloys Congress, Karaganda, Kazakhstan, pp. 739–48.
28. G.A. Bootsma, W.F. Knippenberg, and G. Verspui: *J. Cryst. Growth*, 1971, vol. 11, pp. 297–309.
29. H.J. Choi and J.G. Lee: *J. Mater. Sci.*, 1995, vol. 30. pp. 1982–6.
30. G. Urretavizcaya and J.M. Petro Lopez: *J. Mater. Res.*, 1994, vol. **9**, pp. 2981–6.

CHAPTER 4

SYNTHESIS OF SiC WHISKERS BY VLS AND VS PROCESS

Synthesis of SiC Whiskers by VLS and VS Process

Xiang Li[1*], Guangqing Zhang[1], Ragnar Tronstad[2], Oleg Ostrovski[3]

[1]School of Mechanical, Materials and Mechatronic Engineering, University of Wollongong, Wollongong, NSW 2522, Australia

[2]Elkem AS, Drammensveien 169, Skøyen, P.O Box 334, 0213 Oslo, Norway

[3]School of Materials Science and Engineering, University of New South Wales, Sydney, NSW 2052, Australia

Abstract

This study investigates the mechanisms of SiC whisker formation in the carbothermal reduction of quartz to SiC in different gas atmospheres. Reduction of quartz by graphite was studied in Ar, H_2, and CH_4–H_2–Ar gas mixture in a laboratory fixed bed reactor. The reduction products were characterised by XRD, SEM and TEM. Whiskers were not formed in the carbothermal reduction of quartz in argon. Two types of SiC whiskers were observed in the carbothermal reduction of quartz in H_2 and CH_4–H_2–Ar gas mixture. In the process of reduction at 1400–1600 ^oC in H_2 and at 1200–1600 °C in CH_4–H_2–Ar gas mixture, whiskers with hexagonal shape with diameter 100–800 nm and length up to tens of microns were formed by the VLS mechanism under catalytic effect of iron. The whiskers with the characteristics of cylindrical shape and high aspect ratio were synthesized in CH_4–H_2–Ar gas mixture at 1400–1600 °C by VS mechanism.

Keywords: Carbothermal reduction, SiC whiskers, quartz, atmosphere

*Author to whom correspondence should be addressed. e-mail: xl450@uowmail.edu.au; Tel.: +61 02 4211 5293; fax: +61 02 4221 3112.

1. Introduction

Silicon carbide (SiC) has excellent properties, such as high specific strength, specific stiffness, relatively low specific weight, high corrosion and erosion resistance. These qualities make SiC a perfect candidate for high power, high temperature electronic devices as well as abrasion and cutting applications [1, 2]. Silicon carbide has many polymorphs, such as 3C, 2H, 4H, and 6H. The 3C–SiC polytype has the zinc blende structure with a ⋯ABCABC⋯sequence, and the other three polytypes have the hexagonal structure with ⋯ABAB⋯ (2H), ⋯ABCBABCB⋯ (4H), and ⋯ABCACBABCACB⋯ (6H) sequences. 3C–SiC powder is commercially produced by Acheson process which involves carbothermal reduction of SiO_2 at temperatures above 2000 °C [3]. SiC bulk crystals used as semiconductor material are grown on substrates using chemical vapour deposition (CVD) or physical vapor transport (PVT) method [4, 5].

SiC whiskers are nearly single crystals and expected to have very high tensile strengths [6, 7], which makes them excellent candidates for reinforcement and toughening of ceramic and glass matrix composites [8–10]. Several methods and various starting raw materials have been used to grow SiC whiskers. In papers [6, 11–14], SiC whiskers were formed by the vapour–liquid–solid (VLS) process with transition metals (especially Fe, Co and Ni) as catalysts. This method involves vapour transport of the precursors to a liquid catalyst located at the tip of the whiskers, incorporation of the constituents into the liquid and precipitation of the solid crystal at the liquid–solid interface. The presence of liquid catalyst distinguishes this method from other whiskers growth techniques. SiC whiskers are generally of cubic SiC structure growing in the <1 1 1> direction. Bootsma *et al.* [6] found that whisker growth by the VLS mechanism, morphology and crystal structure were dependent on temperature, reactant concentration and distribution of catalyst. The whisker diameter was dependent on the dimension of molten catalyst droplets and its wettability of SiC. Milewski *et al.* [13] revealed that the

morphologies of whiskers formed in the VSL process were related to the degree of supersaturation and stoichiometry of the reactive gases. Choi *et al.* [11] developed a continuous process for synthesis of SiC whiskers. SiO vapour generated by the carbothermal reduction of silica reacted with carbon-carrying vapours (CO and CH_4), producing SiC whiskers on a substrate coated with iron powder.

Growth of SiC whiskers by a vapour phase chemical reaction method with deposition on a substrate (VS process) was reported in papers [15–19]. Carbothermal reduction of silica precursors is the most common VS process for the SiC production. Silica sources included various materials such as rice hulls [20–23], silica [24], silica gel [25], sea sand [26] and geothermal water [27]. The reductants reported in the literature were charcoal [28], carbon black [14] and CH_4 [11]. Other VS processes are based on the pyrolysis and crystallisation of preceramic precursors by chemical vapour deposition (CVD) [29, 30].

In the process known as a vapour phase formation and condensation, SiC is heated to high temperature (> 2220 °C) in a closed container to create a high vapour pressure of SiC gas and, upon cooling, the SiC condense out in the form of whiskers [31, 32].

The aim of the present paper was to study the growth of SiC whiskers by the carbothermal reduction of quartz in CH_4–H_2–Ar gas mixture. The paper discusses the effects of gas atmosphere and temperature on the structure and morphologies of SiC whiskers and whiskers' growth mechanisms.

2. Experimental

Quartz powder (particle size < 70 μm) was obtained by crushing quartz lumps using agate miller. Quartz powder and synthetic graphite (< 45 μm, Sigma-Aldrich Co. Ltd., Germany) were mixed with distilled water (80 wt% of solid mixture) by rolling in a plastic jar with zirconia balls for 8 h. Water was removed by heating the mixture at

120 °C for 48 h. Then the mixture was pressed into pellets in a uniaxial hydraulic press by applying 20 kN of load for 2 min. The pellets with a mass of approximately 1 g were 8 mm in diameter and about 14 mm in height.

Reduction of quartz by graphite in Ar, H_2, and CH_4–H_2–Ar gas mixture was studied in a laboratory fixed bed reactor heated in an electric vertical tube furnace. A pellet was loaded at the bottom of reactor at room temperature, and then heated to a desired temperature with control of heating rate. The gases used in the investigation were of 99.999 % purity. The total gas flow rate was maintained at 1.0 NL/min at 1 atm. The reduction experiment was stopped after certain duration by raising the reactor above the furnace hot zone and cooling down. After that, the reduced pellet was weighed and subjected to further analysis.

The outlet gas composition was continuously monitored by an infrared $CO/CO_2/CH_4$ analyzer (Advanced optima AO2020, ABB, Ladenburg, Germany) connected with a computer. Gas concentrations were recorded every 5 s.

The original mixture and reduced samples were analyzed by X-ray diffraction (XRD, MMA, GBC Scientific Equipment, Braeside, Australia). The fine powder of a sample after grinding was scanned at a speed of 0.02° s^{-1} and step size 0.02° with CuK radiation generated at 35 kV and 28.6 mA.

The morphology of the samples was observed by field-emission scanning electron microscopy (FESEM, JCM-6000 and JSM-7001F, JEOL, Tokyo, Japan) operated at 15 kV. The chemical composition of the samples was determined by the energy-dispersive X-ray spectrometer (EDS) equipped on the SEM. The samples for the SEM analysis were coated with gold.

Transmission electron microscope (TEM) images and selected area diffraction patterns

(SADE) were recorded on a JEM 2011 electron microscope (JEOL, Tokyo, Japan) operated at 200 kV. For this examination, the sample was dispersed in ethanol using an ultrasonic generator and then deposited on a copper grid.

3. Results and discussion

3.1 Carbothermal reduction in Ar atmosphere

Synthesis of SiC by carbothermal reduction of quartz in argon was examined by temperature programmed reduction experiment in which the temperature was ramped from 300 °C until 1600 °C at 3 °C/min. Fig. 1 presents the XRD patterns of SiO_2/C mixture before and after reduction. The patterns reveal that most of quartz was reduced to β-SiC when the temperature increased to 1600 °C. Meanwhile, the unreacted quartz was transformed to cristobalite. The SEM images of sample pellet before and after reduction are shown in Fig. 2. The pellet after reduction was cut to two parts for SEM observation on the cross section and surface of the pellet. Unreacted SiO_2 particles (cristobalite) were still seen in the cross section (Fig. 2(b)) and on the surface of the pellet (Fig. 2(c)) after reduction at 1600 °C. The synthesized SiC was in the form of particles.

The overall reaction of carbothermal production of SiC in Ar can be written as

$$SiO_2\ (s) + 3C\ (s) = SiC\ (s) + 2CO\ (g) \quad (1)$$

It is generally accepted that SiC is formed through intermediate SiO gas via the following reactions [19]:

$$C\ (s) + SiO_2\ (s) = SiO\ (g) + CO\ (g) \quad (2)$$

$$SiO_2\ (s) + CO\ (g) = SiO\ (g) + CO_2\ (g) \quad (3)$$

$$C\ (s) + CO_2\ (g) = 2CO\ (g) \quad (4)$$

$$SiO\ (g) + 2C\ (s) = SiC\ (s) + CO\ (g) \quad (5)$$

SiO is initially formed at the contact points of carbon and silica according to Reaction (2). Further SiO synthesis proceeds through the gas/solid Reactions (3) and (4). SiC is formed by Reaction (5). Works [11, 33, 34] reported that reaction of the generated SiO vapour with CO vapour produced SiC whiskers by the following reaction:

$$SiO\ (g) + 3\ CO\ (g) = SiC\ (s) + 2\ CO_2\ (g) \quad (6)$$

In this study, no SiC whisker was observed (Fig. 2). Probably, low vapour pressures of SiO and CO in the reduction of quartz in Ar atmosphere were not sufficient for the whiskers formation.

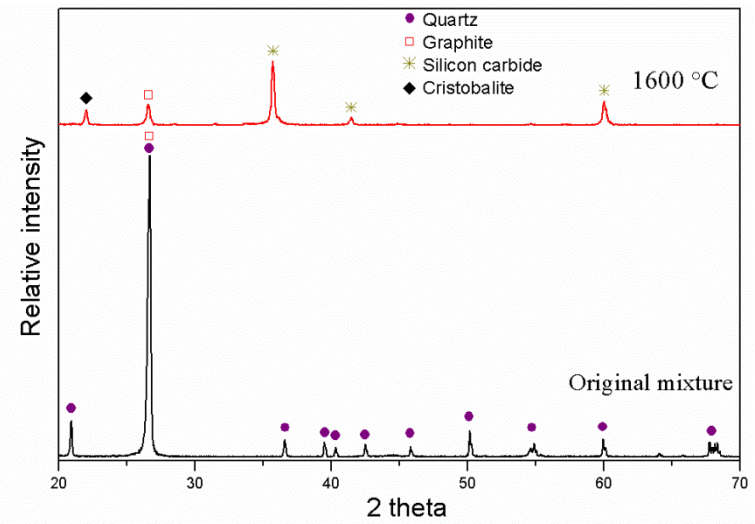

Fig. 1 XRD patterns of SiO_2–graphite sample before and after reduction in Ar. The sample was reduced at ramping temperature from 300 °C to 1600 °C at 3 °C/min.

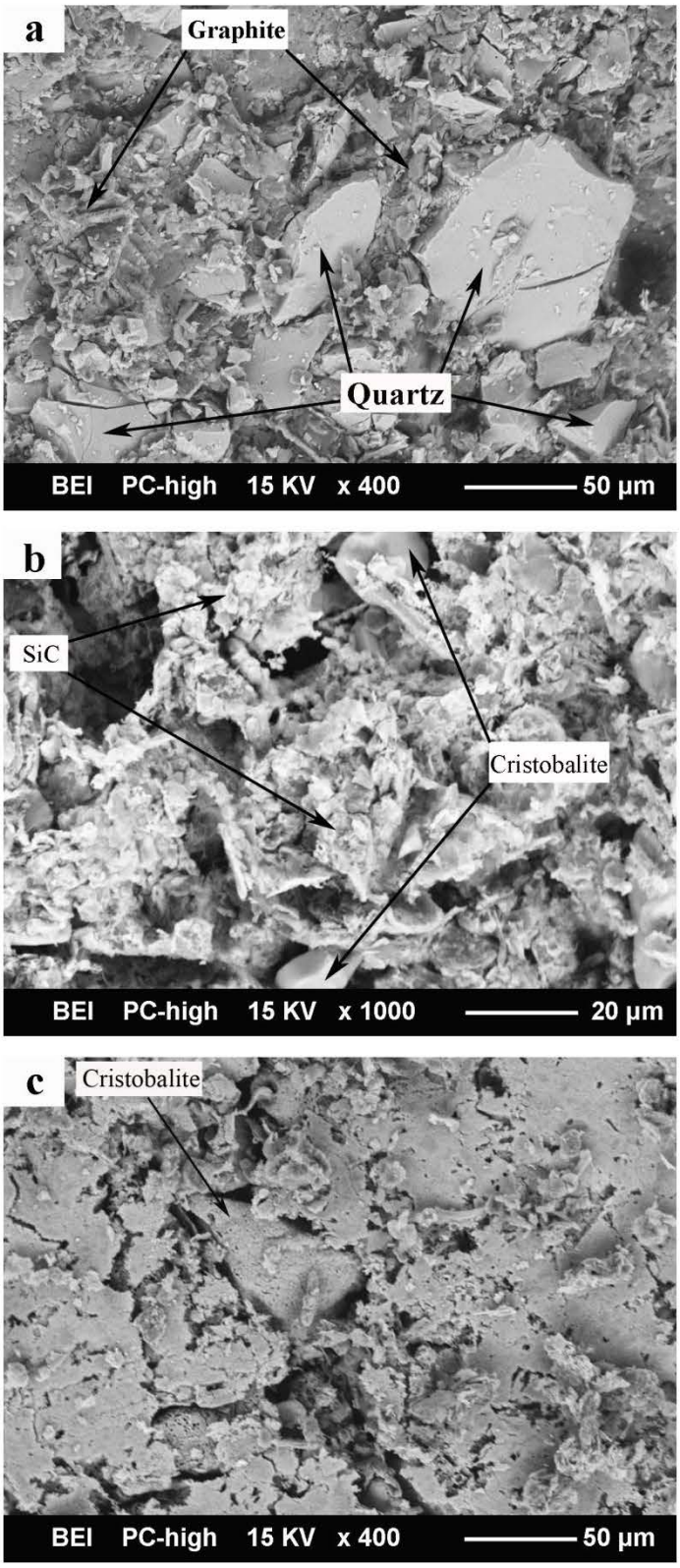

Fig. 2 SEM images of a sample: (a) original pellet, cross section; (b) after reduction in Ar, cross section; (c) after reduction in Ar, pellet surface. The temperature was ramped from 300 °C to 1600 °C at 3 °C/min.

3.2 Carbothermal reduction in H_2 atmosphere

The synthesis of SiC in hydrogen was carried out in temperature programmed reduction experiments. The reduction process was stopped at different temperatures, and the samples were analysed by XRD and SEM to identify the change in phase composition during the carbothermal reduction. Fig. 3 presents the XRD patterns of the samples reduced in the process of heating to 1200–1600 °C. No β-SiC was observed when the temperature was increased to 1200 °C. As the reduction temperature increased to 1300 °C, a weak peak of β-SiC was identified at $2\theta = 35.66^{o}$. With the increase of temperature, the amount of β-SiC increased significantly. It became the only crystalline phase after reduction at 1600 °C.

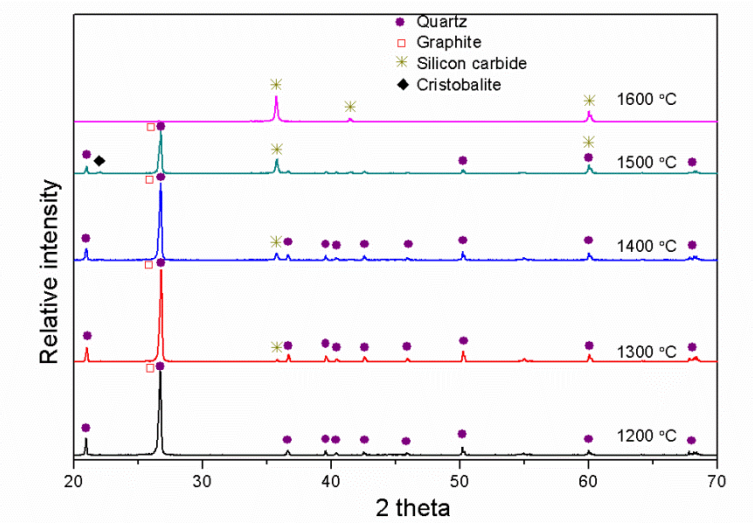

Fig. 3 XRD patterns of samples in the progress of reduction in H_2. The temperature was ramped from 300 °C to 1600 °C at 3 °C /min.

The microstructures of the cross section and surface of the pellet were quite different. The SEM images of samples reduced at 1400 °C, 1500 °C and 1600 °C are shown in Fig. 4–6, respectively. A small number of SiC whiskers with diameter from 100 nm to 800 nm were observed on the cross section of the sample after reduction at 1400 °C (Fig. 4(a)). Meanwhile, more whiskers were found on the surface of the pellet (Fig. 4(b)). The whiskers grew to less than 4 μm, and had a globule at the growing end.

An EDS analysis of a globule in Fig. 4(b) showed that it consisted of 9.1 at% of Fe, 3.9 at% of Al, 0.6 at% of Cr with a balance of Si, C, O, and Au. Fe and Cr in the samples originated from contamination of pellet in the process of pressing with stainless steel die. The presence of Al can be attributed to the reduction of alumina tube by H_2 at high temperatures, generating Al_2O vapour which deposited on the sample pellet. Fe and Al were also present as impurities in quartz.

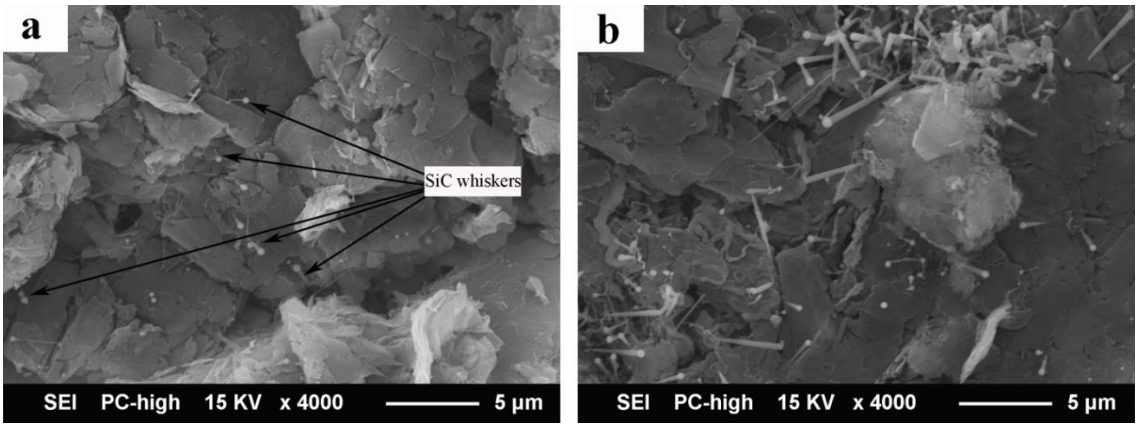

Fig. 4 SEM images of a sample after temperature programmed reduction in H_2 at 1400 °C: (a) cross section of the pellet; (b) surface of the pellet.

Increasing the reduction temperature to 1500 °C promoted the growth of SiC whiskers, as shown in Fig. 5. The whiskers on the cross section of the pellet grew to 5–8 μm (Fig. 5(a)), and those on the surface of the pellet were much longer (Fig. 5(b)). EDS analyses taken from the body of whisker proved that the composition of the whiskers was SiC.

After the reduction temperature increased to 1600 °C, the reduction of quartz was close to completion, as proved by the XRD analyses in Fig. 3. The growth of SiC ceased when no more SiO vapour was provided. A low magnification SEM image in Fig. 6(b) reveals a layer of flurry on the surface of the pellet. The whiskers on the cross section were very thick and straight (Fig. 6(a)), while the whiskers on the surface were characterized by the high aspect ratio (Fig. 6(c)). Figure 6(d) presents an image of a

whisker at a high magnification, which shows it grew in the form of a hexagonal column.

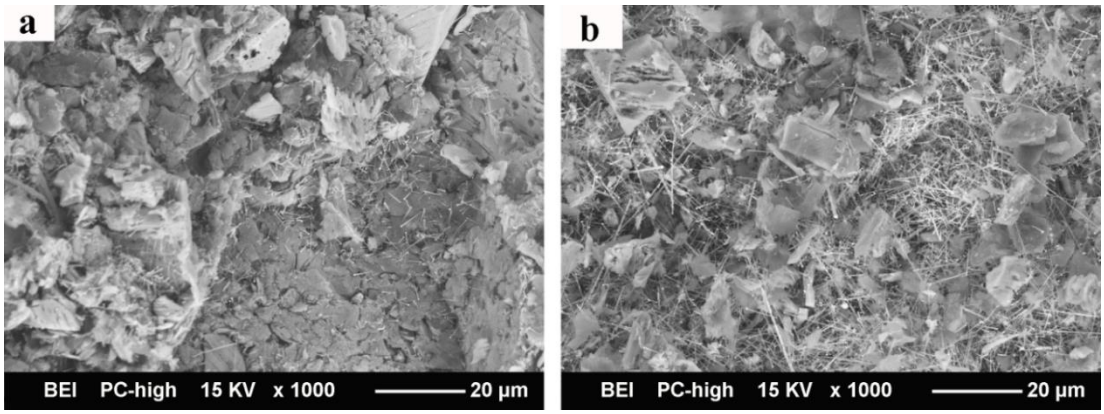

Fig. 5 SEM images of a sample after temperature programmed reduction in H_2 at 1500 °C: (a) cross section of the pellet; (b) surface of the pellet.

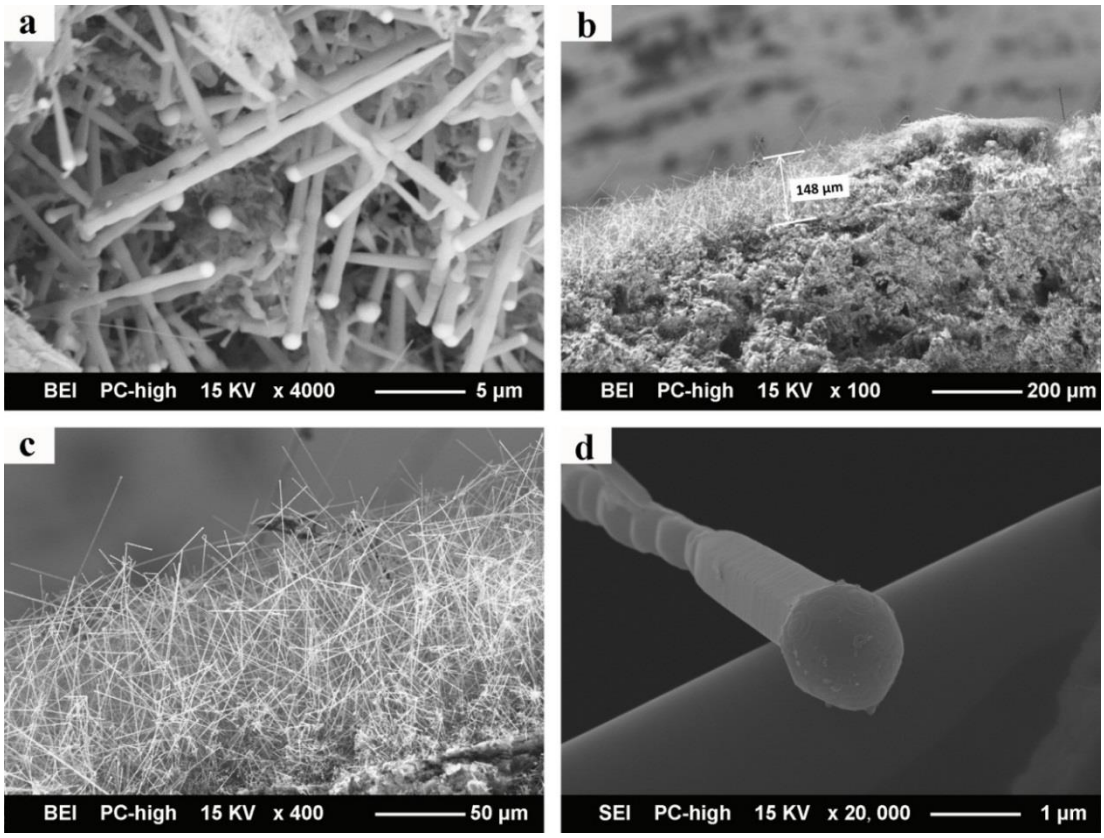

Fig. 6 SEM images of a sample after temperature programmed reduction in H_2 at 1600 °C: (a) and (b) cross section of the pellet; (c) surface of the pellet; (d) a SiC whisker at a high magnification.

Fig. 7(a) is the TEM image of a typical SiC whisker collected from the surface of the pellet heated to 1600 °C, which also displays the hexagonal structure of the whisker. Fig. 7(b) presents a globule at the end of a whisker, exhibiting lower transmission of electrons than SiC whiskers and particles.

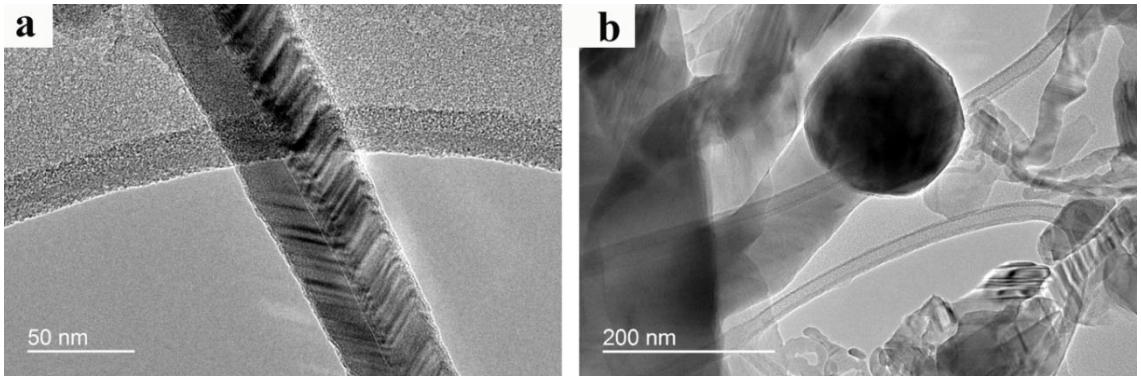

Fig. 7 TEM images of (a) SiC whisker body synthesized in H_2 at 1600 °C and (b) catalyst globule.

As stated previously, the globules on the top ends of the SiC whiskers included metallic iron which was in a molten state at the temperatures of whisker formation. These globules played a catalytic role in the formation process of SiC whiskers, as described below.

In the carbothermal reduction of quartz in hydrogen, H_2 reacted with carbon forming CH_4 (Reaction (7)), which reacted with SiO_2 forming SiO (Reaction (8)).

$$C\,(s) + 2H_2\,(g) = CH_4\,(g) \quad (7)$$

$$SiO_2\,(s) + CH_4\,(g) = SiO\,(g) + CO\,(g) + 2H_2\,(g) \quad (8)$$

In the presence of carbon, H_2 can also directly reduce silica [35] (Reactions (9) and (10)).

$$SiO_2\,(s) + H_2\,(g) = SiO\,(g) + H_2O\,(g) \quad (9)$$

$$H_2O\ (g) + C\ (s) = H_2\ (g) + CO\ (g) \quad (10)$$

The reaction between CH_4 and SiO (Reaction (11)) resulted in growth of SiC whiskers under catalytic effect of iron, followed the VLS mechanism.

$$SiO\ (g) + 2\ CH_4\ (g) = SiC\ (s) + CO\ (g) + 4\ H_2\ (g) \quad (11)$$

Practically, Reaction (11) can occur in multiple steps, involving dissolution of Si and C in the molten Fe globules and the deposition of SiC from the dissolved Si and C:

$$CH_4\ (g) = [C] + 2\ H_2\ (g) \quad (12)$$

$$SiO\ (g) + [C] = [Si] + CO\ (g) \quad (13)$$

$$[Si] + [C] = SiC \quad (14)$$

3.3 Carbothermal reduction in CH_4–H_2–Ar gas mixture

The synthesis of SiC by the carbothermal reduction in CH_4–H_2–Ar gas mixture was examined in temperature programmed experiments using a gas mixture containing 1 vol % of CH_4, 70 vol % of H_2 and 29 vol % of Ar. The XRD patterns of the samples heated to different temperatures are shown in Fig. 8. The phase changes of the sample in reduction in CH_4–H_2–Ar gas mixture were similar to those observed in reduction in H_2. A small amount of β-SiC was identified in a sample reduced at 1200 °C; the peaks of SiC at $2\theta = 35.66$ in samples reduced in CH_4–H_2–Ar gas mixture were stronger than the SiC peaks in the XRD spectra of the samples reduced in H_2 (Fig. 3) at the same temperature. This indicates that introducing 1 vol % of CH_4 accelerated the reduction of quartz to SiC. CH_4 has a higher reducing capacity compared to that of solid carbon in the carbothermal reduction processes [36]. After reduction at 1600 °C, there was significant amount carbon in the sample, because CH_4 was directly involved in the reduction reaction and also cracked to produce solid carbon depositing on the surface of the pellet.

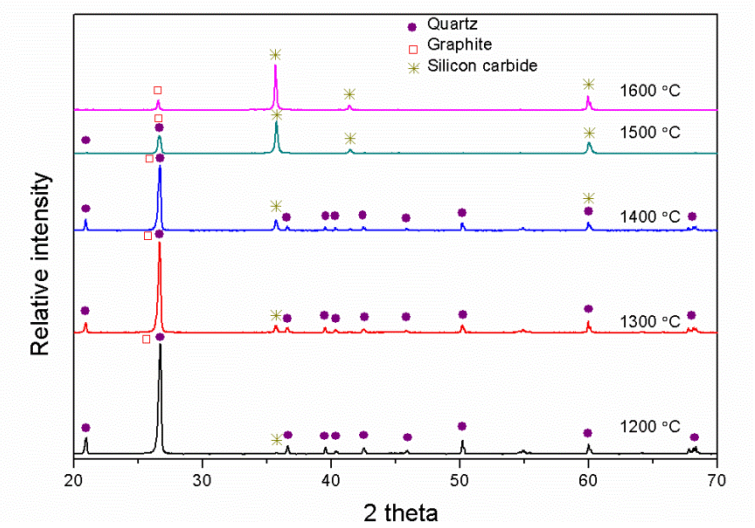

Fig. 8 XRD patterns of samples in the progress of reduction CH_4–H_2–Ar gas mixture. The temperature was ramped from 300 °C to 1600 °C at 3 °C /min.

Temperature also had a significant effect on the morphology of SiC whiskers. After reduction at 1200 °C and 1300 °C, only a few SiC whiskers were observed on the surface of pellets, as shown in Fig. 9(a) and 9(b). SiC of irregular form (marked by arrows) was also observed, due to the low SiO vapour pressure at the low temperatures [11]. Increasing reduction temperature to 1400 °C and 1500 °C resulted in generation of a large number of SiC whiskers, as shown in Fig. 9(c) and 9(d). Most of whiskers grew from the graphite substrate in pellets with a catalyst globule at the tip. A few thin and long whiskers marked with arrows in Fig. 9(c) and 9(d), were found to have no catalyst globules at the tips. Their growth directions were also different with whiskers with globules. They laid down on the surface of the pellet, rather than "stand" on the surface.

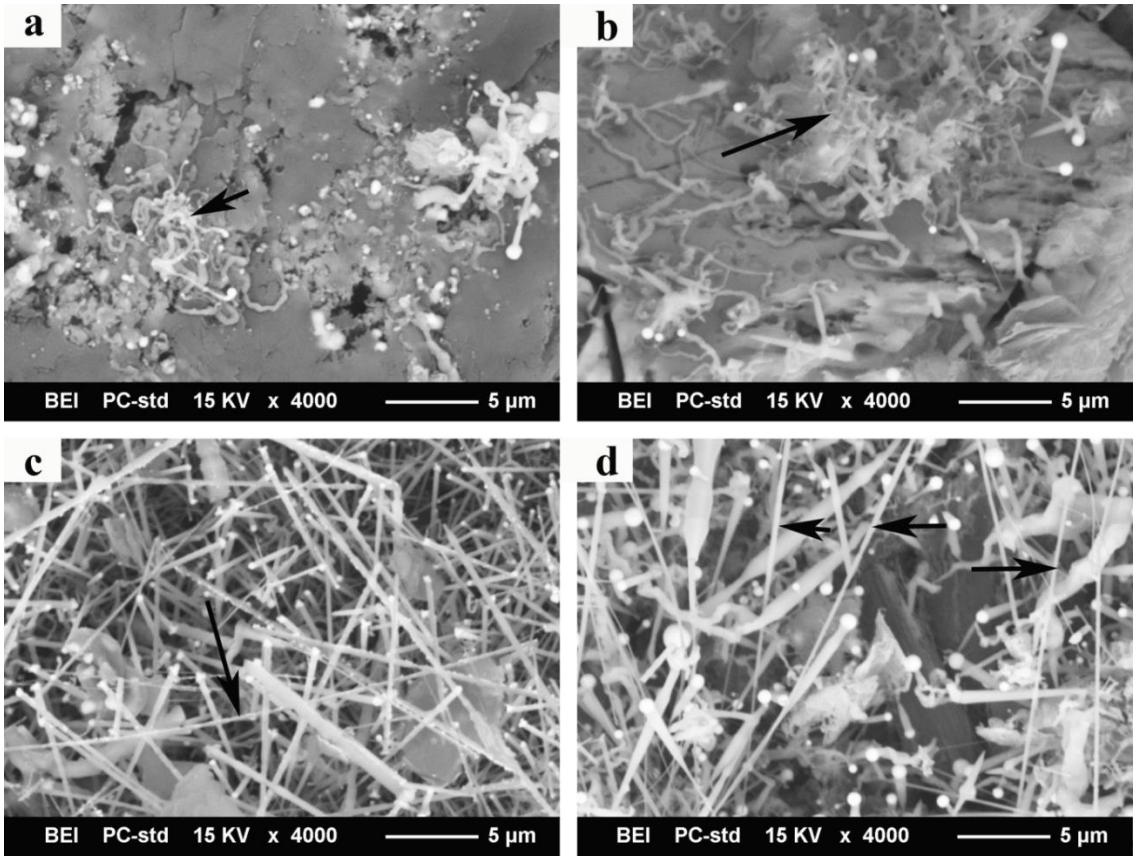

Fig. 9 SEM images of the surface of samples reduced in CH_4–H_2–Ar gas mixture in temperature programmed experiments upon heating to different temperatures: (a) 1200 °C; (b) 1300 °C; (c) 1400 °C; (d) 1500 °C. Arrows in (a) and (b) show SiC of irregular shape; arrows in (c) and (d) point at thin and long SiC whiskers.

The SEM images of the cross section of a pellet subjected to temperature programmed reduction in the CH_4–H_2–Ar gas mixture at 1600 °C (Fig. 10(a)), show that the layer of SiC fluff was much thicker than that formed in reduction in H_2, ranging from 250 to 500 µm. SiC whiskers with diameter of 300–800 nm and length of 3–10 µm were distributed in the center of the pellet's cross section, as shown in Fig. 10(b). However, the most of SiC was still in the form of irregular particles. Observed from the pellet surface, large amount of long whiskers without catalytic globules were knit together (Fig. 10(c)). These long whiskers grew to more than 100 µm long with uniform diameter of 350–450 nm. Whiskers with globules were also observed under the cover of long whiskers at the surface of pellet, as shown in Fig. 10(d).

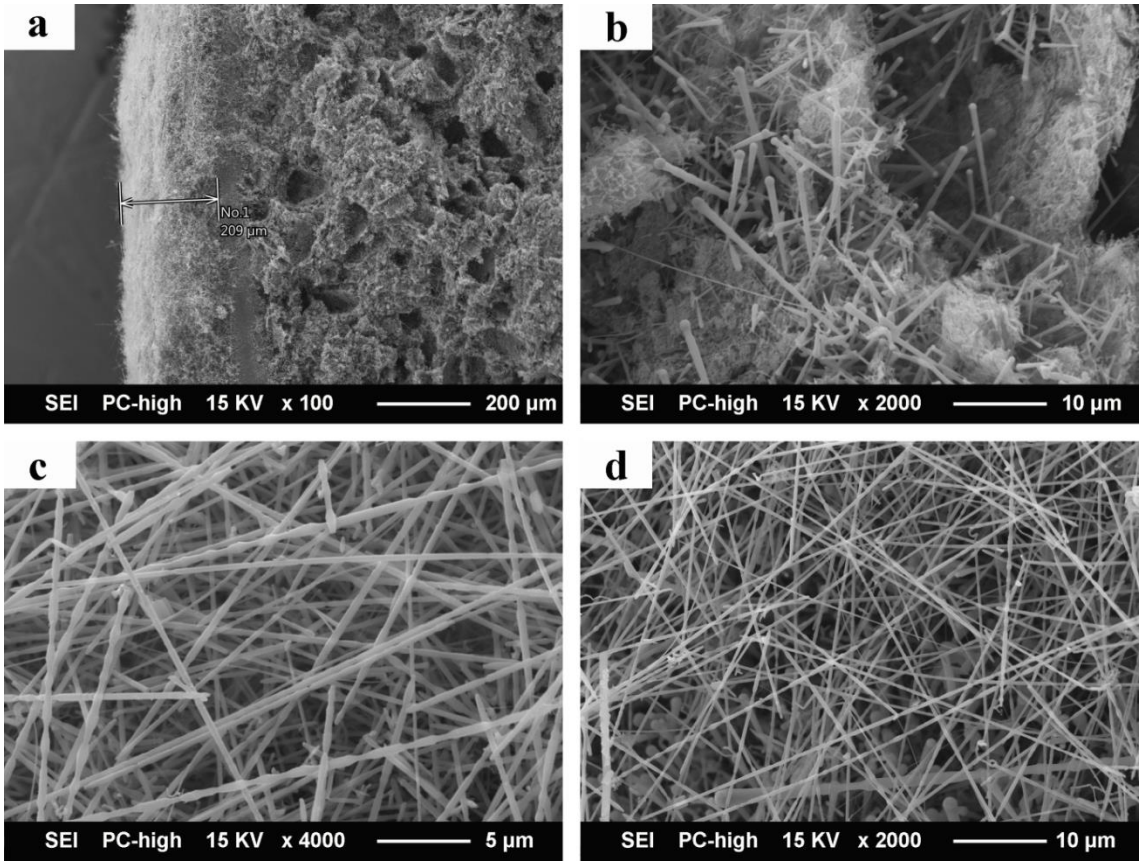

Fig. 10 SEM images of a sample after temperature programmed reduction in CH_4–H_2–Ar gas mixture at 1600 °C: (a) and (b) cross section; (c) and (d) surface of the pellet.

Fig. 11 presents the TEM images and the SAED patterns of two types of SiC whiskers from the sample reduced at 1600 °C. Fig. 11(a) represents the images of SiC whiskers with catalyst globules, which show hexagonal column structure, the same as the SiC whiskers synthesized in H_2 (Fig. 7(a)). The SAED patterns (Fig. 11(b)) of the whisker demonstrated that it was a single-crystal β-SiC, with <111> and <220> as the diffraction crystal surface. While the SiC whiskers without catalyst globules had a smooth cylindrical structure (Figure 11(c)), with <111> as the diffraction crystal surface (Fig. 11(d)).

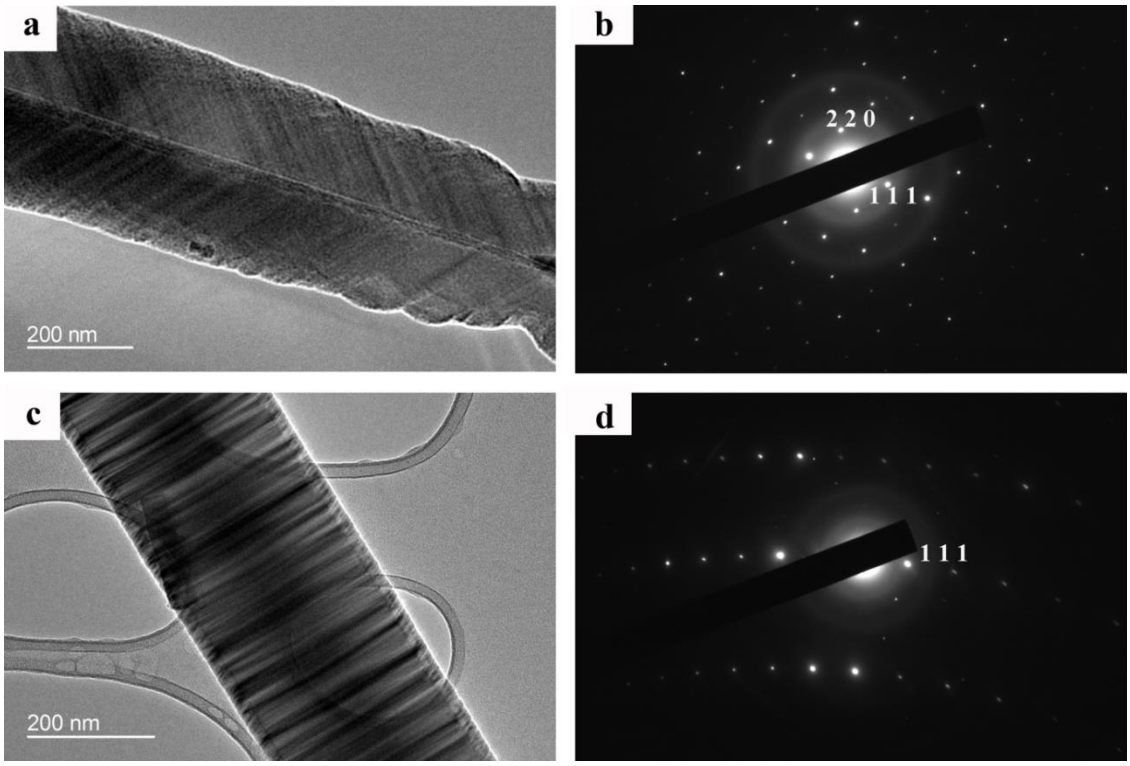

Fig. 11 (a) TEM image of SiC whisker synthesized by VLS mechanism; (b) SADE patterns of whisker shown in (a); (c) TEM image of SiC whisker synthesized by VS mechanism; (d) SADE patterns of whisker shown in (c).

The formation mechanism of SiC whiskers with catalyst globules is similar to that formed in reduction in H_2, which occurred at lower temperatures, probable due to higher SiO and CH_4 partial pressures in CH_4–H_2–Ar gas mixture. Based on the fact that Fe-rich globules were presented at the growing tips of SiC whiskers, its formation followed VLS mechanism. Initially, the Fe catalyst was in contact with substrate as the temperature was raised to the melting points of Fe [37]. The liquid globule absorbed Si and C from SiO and CH_4 vapour until it became supersaturated. Nucleation of SiC occurred at the interface with the substrate and continued solution of gas species into the liquid catalyst ball allowed the whiskers to grow as additional SiC precipitated.

The long whiskers shown in Fig. 11(c) were formed following a VS mechanism as no catalyst globule was observed at the tips. The formation of long whiskers cannot be

explained by gas–gas (SiO–CO) Reaction (6), as no SiC whisker was formed in Ar atmosphere. Therefore, growth of long SiC whiskers via VS mechanism occurred by gas–gas (SiO–CH_4) Reaction (11). Higher SiO and CH_4 vapour pressures were required for whiskers growth without catalyst via VS mechanism; therefore, long whiskers were formed at higher temperatures (>1400 °C). Non-catalytic formation of long whiskers in the reduction in H_2 by VS mechanism was not feasible because significantly lower CH_4 pressure, as detected by the infrared gas analyzer (Fig. 12).

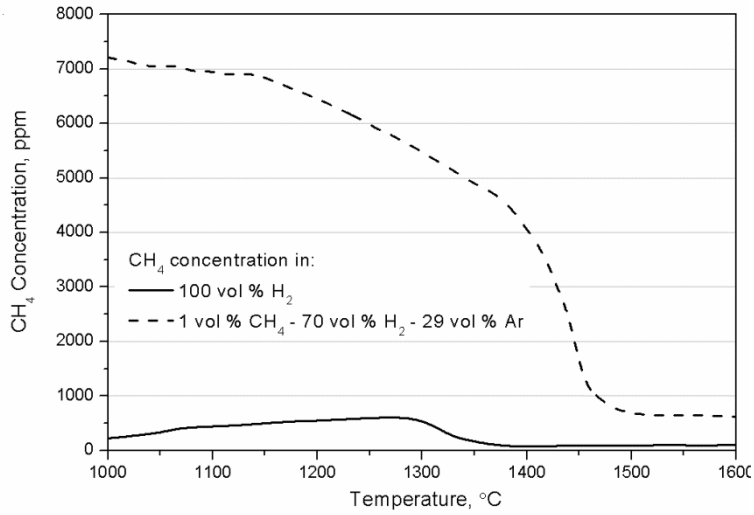

Fig. 12 Concentration of CH_4 in the gas phase in the progress of reduction in H_2 and CH_4–H_2–Ar gas mixture.

4. Conclusions

SiC whiskers were formed in the carbothermal reduction of quartz in H_2 and CH_4–H_2–Ar gas mixture. In reduction in H_2 atmosphere from 1400 to 1600 °C, SiC whiskers with diameter of 100–800 nm were formed following a VSL mechanism under catalytic effect of Fe. Whisker length increased with the increase of temperature. The amount of whiskers was higher on the surface than inside a pellet. Two different types of SiC whiskers were produced in reduction in a CH_4–H_2–Ar gas mixture; whiskers in the form of hexagonal columns were produced at 1200–1600 °C by VSL mechanism; whiskers in the form of long cylinders were synthesized at 1400–1600 °C by VS

mechanism. The morphology and mechanism of formation of SiC whiskers was affected by the partial pressures of SiO and CH_4 which change with reduction atmosphere and temperature.

Acknowledgments

This research was supported under the Australian Research Council Linkage Project funding scheme (Project no. LP100100866) in collaboration with Solar Elkem (Norway). The authors acknowledge use of facilities and the assistance of Mr Mitchell Nancarrow and Dr Gilberto Casillas-Garcia at the UOW Electron Microscopy Centre.

References

1. K. Järrendahl, R. Davis, Material properties and characterization of SiC, Semiconduct. Semimet. 52 (1998) 1–20.
2. Y.L. Chiew, K.Y. Cheong, A review on the synthesis of SiC from plant-based biomasses, Mater. Sci. Eng. B 176 (2011) 951–964.
3. G.S. Gupta, P. Vasanth Kumar, V.R. Rudolph, M. Gupta, Heat-transfer model for the acheson process, Metall. Mater. Trans. A 32 (2001) 1301–1308.
4. J.W. Sun, I.G. Ivanov, R. Liljedahl, R. Yakimova, M. Syväjärvi, Considerably long carrier lifetimes in high-quality 3C–SiC(111), Appl. Phys. Lett. 100 (2012), 252101.
5. R. Vasiliauskas, M. Marinova, M. Syväjärvi, E.K. Polychroniadis, R. Yakimova, Polytype transformation and structural characteristics of 3C–SiC on 6H–SiC substrates, J. Cryst. Growth. 395 (2014), 109–115.
6. G.A. Bootsma, W.F. Knippenberg, G. Verspui, Growth of SiC whiskers in the system SiO_2–C–H_2 nucleated by iron, J. Cryst. Growth. 11 (1971) 297–309.
7. A.W. Weimer, Carbide, Nitride and Boride Materials Synthesis and Processing, Chapman & Hall, London, 1997.
8. G.C. Wei, P.F. Becher, Development of SiC-whiskers-reinforced ceramics, Am. Ceram. Soc. Bull. 64 (1985) 298–304.
9. L. Silvestroni, D. Sciti, C. Melandri, S. Guicciardi, Toughened ZrB_2-based ceramics

through SiC whisker or SiC chopped fiber additions, J. Eur. Ceram. Soc. 30 (2010) 2155–2164.

10. F. Ye, J.M. Yang, L.T. Zhang, W.C. Zhou, Y. Zhou, T.C. Lei, Fracture behavior of SiC-whisker-reinforced barium aluminosilicate glass-ceramic matrix composites, J. Am. Ceram. Soc. 84 (2001) 881–883.
11. H.J. Choi, J.G. Lee, Continuous synthesis of silicon carbide whiskers, J. Mater. Sci. 30 (1995) 1982–1986.
12. G. Urretavizcaya, J.M. Petro Lopez, Growth of SiC whiskers by VLS process, J. Mater. Res. 9 (1994) 2981–2986. □
13. J.V. Milewski, F.D. Gac, J.J. Petrovic, S.R. Skaggs, Growth of beta-silicon carbide whiskers by the VLS process, J. Mater. Sci. 20 (1985) 1160–1166.
14. P.C. Silva, J.L. Figueiredo, Production of SiC and Si_3N_4 whiskers in $C+SiO_2$ solid mixtures, Mater. Chem. Phy. 72 (2001) 326–331.
15. T. Hayashi, F. Mochizuki, M. Ozawa, Process and continuous reaction furnace for production of β-type silicon carbide whiskers, UK Patent GB2162504A, 1985.
16. O.J.Jr. Horne, D.E. Ramesy, Production of SiC whiskers, US Patent 4283375, 1981.
17. S.K. Nadkarni, M.K. Jain, Method of preparing whiskers of silicon carbide and other materials, European Patent 88307432.0, 1988.
18. P.D. Shalek, Process for growing silicon carbide whiskers by undercooling. US Patent 4702901, 1987.
19. M. Tanaka, T. Kawabe, M. Kobune, Method of manufacturing crystalline silicon carbide employing acid pretreated rice husk, US Patent 4591492, 1986.
20. K. Janghorban, H.R. Tazesh, Effect of catalyst and process parameters on the production of silicon carbide from rice hulls, Ceram. Int. 25 (1999) 7–12.
21. B.V.R. Bhat, G.P. Sanghi, Increase in the yield of silicon carbide whiskers from rice husk, Bull. Mater. Sci. 9 (1987) 295–303.
22. R.V. Krishnarao, M.M. Godkhindi, M. Chakraborty, Maximisation of SiC whisker yield during the pyrolysis of burnt rice husks, J. Mater. Sci. 27 (1992) 1227–1230.
23. R.V. Krishnarao, Y.R. Mahajan, Preparation of silicon carbide fibres from cotton

fibre and silicon nitride, J. Mater. Sci. Lett. 15 (1996) 232–235.

24. S. Cetinkaya, S. Eroglu, Chemical vapor deposition of C on SiO_2 and subsequent carbothermal reduction for the synthesis of nanocrystalline SiC particles/whiskers, Int. J. Refract. Met. Hard Mater. 29 (2011) 566–572.
25. G.Q. Jin, X.Y. Guo, Synthesis and characterization of mesoporous silicon carbide, Microporous Mesoporous Mater. 60 (2003) 207–212.
26. W.W. Pultz, Method of making beta-silicon carbide fibers, US Patent 3161473, 1964.
27. J. Harada, Process for producing silicon carbide whisker, Canadian Patent 1253667A1, 1989.
28. T.L.Y. Cheung, D.H.L. Ng, Conversion of bamboo to biomorphic composites containing silica and silicon carbide nanowires, J. Am. Ceram. Soc. 90 (2007) 559–564.
29. H.F. Zhang, C.M. Wang, L.S. Wang, Helical crystalline SiC/SiO_2 core-Shell nanowires, Nano Lett. 2 (2002) 941–944.
30. G.Y. Li, X.D. Li, Z.D. Chen, J. Wang, H. Wang, R.C. Che, Large areas of centimeters-long SiC nanowires synthesized by pyrolysis of a polymer precursor by a CVD route, J. Phys. Chem. C 113 (2009) 17655–17660.
31. W.F. Kippenberg, G. Verspui, Whisker crystals. German Patent DE1910940, 1969.
32. S.K. Lilov, Study of the evaporation mechanism in silicon carbide crystal growth from vapor phase, Cryst. Res. Technol. 19 (1994) 513–516.
33. C. Vix-Guterl, B. McEnaney, P. Ehrburger, SiC Material produced by carbothermal reduction of a freeze gel silica–carbon artefact, J. Eur. Ceram. Soc. 19 (1999) 427–432.
34. L. Wang, H. Wada, L.F. Allard, Synthesis and characterization of SiC whiskers, J. Mater. Res. 7 (1992) 148–163.
35. B. Ozturk, R.J. Fruehan, The rate of formation of SiO by the reaction of CO or H_2 with silica and silicate slags, Metall. Trans. B 16 (1985) 801–806.
36. O. Ostrovski, G. Zhang, Reduction and carburization of metal oxides by

methane-containing gas, AIChE J. 52 (2006) 300–310.

37. D.P. Yu, Q.L. Hang, Y. Ding, H.Z. Zhang, Z.G. Bai, J.J. Wang, Y.H. Zou, W. Qian, G.C. Xiong, S.Q. Feng, Amorphous silica nanowires: intensive blue light emitters, Appl. Phys. Lett. 73 (1998) 3076–3078.

CHAPTER 5

REDUCTION OF QUARTZ TO SILICON MONOXIDE BY METHANE–HYDROGEN MIXTURES

Reduction of Quartz to Silicon Monoxide by Methane–hydrogen Mixtures

Xiang Li[1*], Guangqing Zhang[1], Ragnar Tronstad[2], Oleg Ostrovski[3]

[1]School of Mechanical, Materials and Mechatronic Engineering, University of Wollongong, Wollongong, NSW 2522, Australia

[2] Elkem AS, Drammensveien 169, Skøyen, P.O Box 334, 0213 Oslo, Norway

[3]School of Materials Science and Engineering, University of New South Wales, Sydney, NSW 2052, Australia

Abstract

The reduction of quartz was studied isothermally in a fluidized bed reactor with continuously flowing methane–hydrogen gas mixture in the temperature range 1623–1773 K (1350–1500 °C). The CO content in the off-gas was measured online using an infrared gas analyzer. The main phases of the reduced samples identified by XRD analysis were quartz and cristobalite. Significant weight loss in the reduction process indicated that the reduction products were SiO and CO. Reduction of SiO_2 to SiO by methane starts with adsorption and dissociation of CH_4 on the silica surface. The high carbon activity in the CH_4–H_2 gas mixture provided a strongly reducing condition. At 1623 K (1350 °C), the reduction was very slow. The rate and extent of reduction increased with increasing temperature to 1723 K (1450 °C). A further increase in temperature to 1773 K (1500 °C) resulted in a decrease in the rate and extent of reduction. An increase in the gas flow rate from 0.4 to 0.8 NL/min and increase in the methane content in the CH_4–H_2 gas mixture from 0 to 5 vol pct favored the reduction. Methane content in the gas mixture should be maintained below 5 vol pct in order to

* Author to whom correspondence should be addressed. e-mail: xl450@uowmail.edu.au; Tel.: +61 02 4211 5293; fax: +61 02 4221 3112.

suppress methane cracking.

I. Introduction

Metallurgical silicon and ferrosilicon alloys are produced in submerged electric arc furnaces by carbothermal reduction of silicon bearing oxides (typically quartz) with carbonaceous materials. Coal, coke, charcoal and woodchips are commonly used as reductants in these processes [1]. Carbothermal reduction requires high temperatures and is energy intensive. The contents of trace elements in both quartz and reductants determine the purity of the produced silicon [2]. SiC is also produced by the carbothermal reduction of quartz.

Silicon monoxide (SiO) vapor is one of the major intermediate species in the production of SiC and metallurgical silicon [3, 4]. SiO_2 is reduced by carbon to SiO by the following reaction:

$$SiO_2 + C = SiO\ (g) + CO\ (g) \quad [1]$$

SiO further reacts with carbon to form SiC:

$$SiO\ (g) + 2C = SiC + CO\ (g) \quad [2]$$

The primary reaction for production of Si is the following:

$$SiC + SiO\ (g) = 2Si\ (l) + CO\ (g) \quad [3]$$

Methane has the advantage of high purity over conventional carbonaceous reductants such as coal or coke which always contain impurities [5–7]. The gas-phase reaction between SiO and methane with or without a catalyst has been used for synthesis of SiC

whiskers [8–12]. However, no reports were found in the literature on the direct reduction of SiO_2 to SiO by the methane–containing gas. The purpose of the present study is to investigate the possibility of reduction of quartz to SiO via the gas–solid reaction by methane–hydrogen gas mixture, as described by Reaction [4]. Natural gas contains low harmful impurities of solar silicon, and provides high carbon activity for the reduction of quartz, which makes it an attractive reductant over conventional solid carbon.

$$SiO_2 + CH_4\,(g) = SiO\,(g) + CO\,(g) + 2H_2\,(g) \qquad [4]$$

Above 1729 K (1456 °C), Reaction [4] has a negative Gibbs free energy change under standard conditions (ΔG^o); at 1873 K (1600 °C), ΔG^o = -63.2 kJ (calculated using HSC Chemistry 6.1). However, methane is unstable at temperatures above 823 K (550 °C); it cracks with deposition of solid carbon (Reaction [5]) at temperatures above 1273 K (1000 °C) [13]. Solid carbon deposits on the sample surface, hindering further progress of the reduction by blocking the quartz particle surface.

$$CH_4\,(g) = C + 2\,H_2\,(g) \qquad [5]$$

Therefore, reduction of metal oxides by the methane-containing gas should be conducted under conditions at which cracking of methane is limited.

This study examines the effects of temperature, gas composition and gas flow rate on the reduction of quartz in the fluidized bed reactor by the CH_4–H_2 gas mixture with a low CH_4/H_2 ratio to suppress methane cracking. Reduction of quartz to SiO can be of commercial interest; however, scaling up and further study of this process are needed to find feasibility of the industrial reduction of quartz by the methane-containing gas.

II. Experimental

A fluidized bed reactor was adopted to mitigate the effect of carbon deposition on the surface of quartz particles. Quartz powder with a particle size of 100–140 μm was obtained by crushing and grinding quartz lumps (supplied by Elkem AS, Norway) by an agate mill and sieving to the size range. The impurity contents in quartz lumps were provided by the supplier, as shown in Table I. The gases (CH_4, Ar and H_2) used in the investigation were of 99.999 pct purity, supplied by Coregas Pty Ltd, Australia.

Table I. Impurity contents in the quartz lumps, mg/kg

B	P	Fe	Al	Ca	Ti	Mn	Mg
0.5	1.0	33.0	219.0	26.0	7.9	1.9	27.0

The fluidization of quartz particles was first verified using a cold model of the fluidization reactor made of Perspex material. It consisted of two zones, a fluidization zone (inner diameter 20 mm) in which a fluidized bed was formed, and a settling zone (inner diameter 40 mm). The settling zone had an enlarged intersection and therefore a lower gas flow rate, which allowed the quartz particles brought into the settling zone by ascending gas stream to settle and return to the fluidized bed. A connector with a filter was installed at the bottom of the fluidized bed which played a role of a gas distributor. Fluidisation of quartz powder with particle size in the ranges of 53–100 μm, 100–140 μm and 140–200 μm in the cold model was examined using nitrogen with different flow rates. The change of quartz bed was recorded by a video camera (D5100, Nikon Corporation, Tokyo, Japan).

The schematic of the fluidized bed high-temperature reactor for the reduction experiments is presented in Figure 1. The reactor was made from graphite; it was installed within an alumina tube of 50 mm ID. The inner diameter of the fluidization zone was 20 mm, and settling zone was 40 mm. A type B thermocouple protected by an

alumina sheath was inserted into the fluidization zone to measure the temperature before introducing quartz powder, then it was removed from the fluidization zone to avoid disturbing the fluidization of quartz powder during reaction. An alumina tube was inserted into the settling zone which was used to feed quartz samples into the reactor.

In an experiment, the reactor system was first assembled, purged with argon, and heated to the experimental temperature. Then the methane–hydrogen gas mixture was introduced, and 2 g of quartz was added into the fluidizing zone of the reactor via the feeding tube. After reduction for certain time, the furnace was cooled, the reactor was disassembled, and the sample taken for characterization. Argon was introduced between the graphite reactor and outside alumina tube to make sure that all of the gaseous reacting products were purged out of the reaction system. The total inlet gas flow rate (reducing and purging) was maintained at 1.00 NL/min.

The reaction between methane and quartz was also studied using a fused quartz sphere with diameter of 15.90 mm (99.99 pct SiO_2, provided by Guolun Quartz Products Co. Ltd, China) hung in the methane–hydrogen gas mixture. The reaction system was setup in a graphite tube furnace (Model 1000-2560-FP20, GT Advanced Technologies, Santa Rosa, U.S.A.). A quartz sphere was suspended by a tungsten wire with 0.5 mm diameter from the top into the hot zone of a reactor tube (high-purity graphite) with 26 mm internal diameter. A methane–hydrogen gas mixture flowed downward through the tube. The furnace was heated to the targeted temperature at 20 K/min under argon atmosphere. Then the gas was switched to a methane–hydrogen mixture. Reaction was stopped after certain time by lowering the temperature at 20 K/min. After reaction, the sphere was weighed and analyzed.

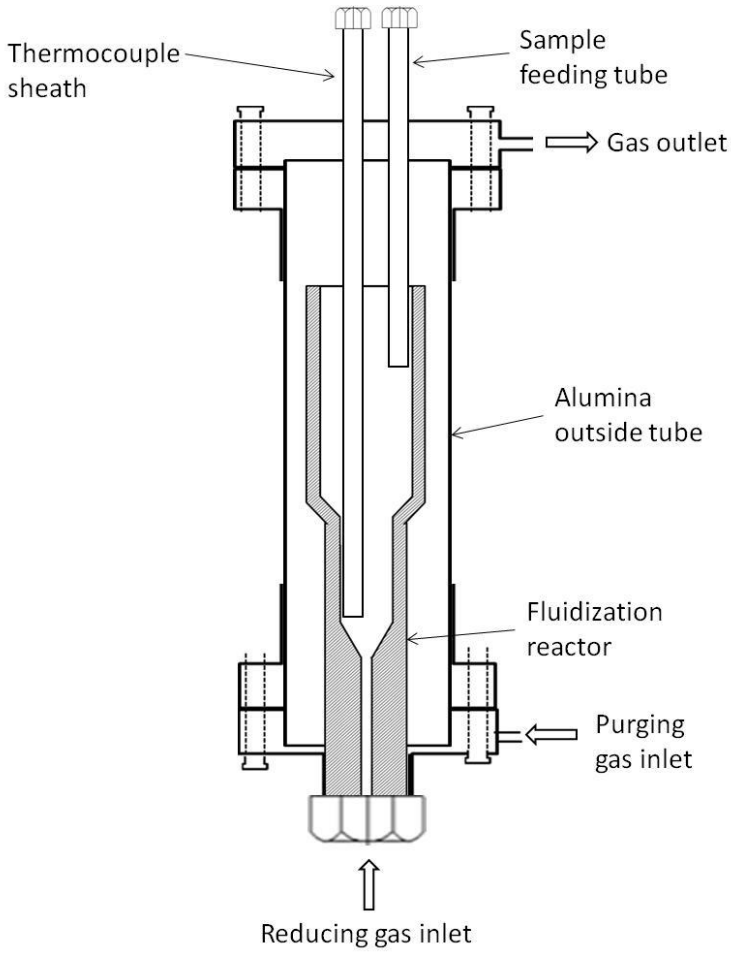

Fig. 1 Schematic of the fluidized bed reactor setup.

In both reduction experiments, the off gas composition was continuously monitored and recorded every 5 seconds by an infrared $CO/CO_2/CH_4$ analyzer (Advanced optima AO2020, ABB, Ladenburg, Germany) connected with a computer.

The original quartz particles and reduced samples were analyzed by X-ray diffraction (XRD, MMA, GBC Scientific Equipment, Braeside, Australia). The fine powder of a sample was scanned at a speed of 0.02 °/s and step size 0.02 ° with CuK radiation generated at 35 kV and 28.6 mA.

SEM images were recorded by field-emission scanning electron microscopy (FESEM, JSM-6000, JEOL, Tokyo, Japan) operated at 15 kV. The chemical composition of the

samples was analysed by an energy-dispersive X-ray spectrometer (EDS). The samples were coated with gold to enhance conductivity in SEM/EDS analyses.

The extent of reduction was defined as a fraction of oxygen in quartz removed in the course of reduction, in the form of CO and SiO according to Reaction [4]. Using the CO concentration in the off gas, the extent of reduction (X, pct) was calculated using Eq. [6].

$$X = \frac{2}{n_{O-i}} \int_0^t \frac{F}{22.4} C_{V-CO} dt \quad [6]$$

where C_{V-CO} is the concentration of CO, vol pct; n_{O-i} is the initial content of oxygen in quartz, mol, F is the inlet gas flow rate, NL/min, t is reaction time, min.

III. Experimental Results

A. Cold model of a fluidized bed reactor

The minimum fluidization velocity (U_{mf}, m/s) and terminal velocity (U_t, m/s) of particles were estimated using the following correlations [14]:

$$U_{mf} = \left[d_p^2 g(\rho_p - \rho_g)\right]/(1650\mu) \quad [7]$$

$$U_t = \left[d_p^2 g(\rho_p - \rho_g)\right]/(18\mu) \quad [8]$$

where d_p = diameter of quartz particles, cm;

ρ_p = density of quartz, g/cm^3;

ρ_g = density of fluidization gas, g/cm^3;

μ = dynamic viscosity of fluidization gas, g/(cm·s).

The fluidization of quartz particles of different particle size ranges was first verified using a cold model fluidization reactor. The N_2 flow rate was changed from 0.1–1.2

NL/min. Table II compares the measured U_{mf} values with calculated using Eq. [7] and gas properties at 293 K (25 °C). Calculated U_t using Eq. [8] is also listed in Table II.

Table II. Parameters of fluidization of quartz with different particle size ranges using pure nitrogen.

Particle size (μm)	Calculated U_{mf} (m/s)	Calculated U_t (m/s)	Measured gas flow rate at U_{mf} (NL/min)	Measured U_{mf} (m/s)
53–100	0.0090	0.239	Fluidization was not observed;	N/A
100–140	0.0180	0.956	0.32	0.0170
140–200	0.0361	1.667	0.41	0.0220

In the case of quartz particles in the size range 53–100 μm, fluidization by gas with tested flow rate 0.1–1.2 NL/min was not observed; channeling took place in the bed. The minimum fluidization velocity for particles 100–140 μm was close to that calculated by Eq. [7]. In the case of 140–200 μm quartz particles, the measured minimum fluidization velocity was significantly smaller than the calculated value. The terminal gas velocity was not reached in both cases in the tested range of gas flow rate.

The calculated parameters of fluidization of quartz particles with size 100–140 μm by pure hydrogen at temperatures 1623–1773 K (1350–1500 °C) are listed in Table III. Calculated data indicate that fluidization of quartz particles can be operated in a wide range of H_2 gas flow rate (0.036–1.494 NL/min).

Table III. Parameters of fluidization of 100–140 μm quartz particles by pure hydrogen at different temperatures.

Temperature (K)	Calculated U_{mf} (m/s)	Calculated gas flow rate at U_{mf} (NL/min)	Calculated U_t (m/s)	Calculated gas flow rate at U_t (NL/min)
1623	0.0113	0.036	0.545	1.728
1673	0.0111	0.034	0.534	1.644
1723	0.0109	0.033	0.524	1.566
1773	0.0107	0.031	0.515	1.494

B. Reduction of quartz to SiO in the fluidized bed reactor

Table IV summarises experimental conditions and weights of samples before and after reduction. The effect of temperature was studied in the temperature range of 1623–1773 K (1350–1500 °C) at constant fluidizing gas flow rate of 0.8 NL/min and gas composition of 5 vol pct CH_4–95 vol pct H_2. The reduction extent calculated from the off gas composition was always slightly higher that the extent of reduction found from the weight loss. This discrepancy can be attributed to the loss of some fine SiO_2 particles in the fluidized bed generated from the friction/collision among quartz particles. These fine particles were easily carried out of the fluidized bed by the gas stream. It was noticed that the deviation was greater with higher fluidizing gas flow rate and higher temperature. Therefore, the reduction extent calculated from the off gas composition was more reliable in this investigation.

The change of CO concentration in the off gas *vs* time at different temperatures is shown in Figure 2. Figure 3 presents the XRD spectra of the samples reduced at different temperatures for 120 min.

Table IV. Experimental conditions and extent of reduction of SiO_2 by CH_4-H_2 gas mixture after reaction for 120 min.

Sample	Temperature (K)	Fluidization flow rate (NL/min)	Methane content (vol pct)	Weight loss (pct)	Reduction Extent (pct)
1	1623	0.8	5	7.8	2.2
2	1673	0.8	5	29.0	12.5
3	1723	0.8	5	38.1	16.0
4	1723	0.4	5	20.0	9.1
5	1723	0.6	5	28.4	12.4
6	1723	0.8	2	21.9	9.3
7	1723	0.8	10	8.3	2.3
8	1773	0.8	5	31.2	13.1

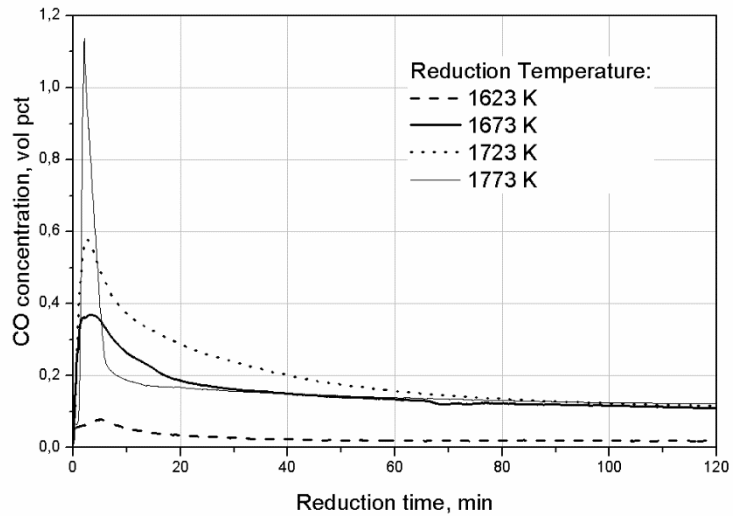

Fig. 2 Effect of temperature on the evolution of CO in the reduction of quartz by CH_4–H_2 gas mixture (5 vol pct CH_4) at gas flow rate 0.8 NL/min.

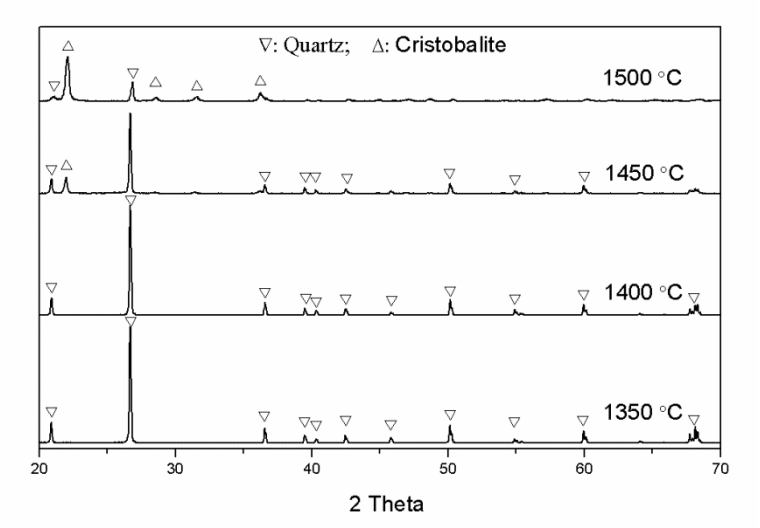

Fig. 3 XRD patterns of the samples reduced by CH_4–H_2 gas mixture (5 vol pct CH_4) at different temperatures after 120 min reaction.

At 1623 K (1350 °C), the CO concentration reached 0.078 vol pct in about 5 min after introducing quartz powder, then declined slowly to about 0.024 vol pct at 40 min. After 120 min of reaction, the extent of reduction calculated from the CO concentration in the off-gas was only 4.4 pct; XRD analysis of the sample after reaction detected only quartz. The reduction at this temperature was very slow. Increasing temperature to 1673 K (1400 °C) resulted in a significant increase of the reduction rate; the CO concentration in the off gas reached 0.37 vol pct after 3.2 min reaction. After 120 min reduction, the extent of reduction was 25.0 pct. Further increasing temperature to 1723 K (1450 °C) accelerated the reaction rate, brought about the extent of reduction to 32.0 pct in 120 min. In addition to the quartz peaks, cristobalite peaks were detected in the XRD spectrum of the reduced sample as a result of the transformation of quartz to cristobalite at high temperatures [15]. Stronger cristobalite peaks were observed in the XRD spectrum of the sample reduced at 1773 K (1500 °C). The CO concentration raised quickly to 1.14 vol pct after quartz powder was introduced to the reaction zone, however, it droped sharply to less than 0.19 vol pct after 10 min reaction.

No SiC was identified by the XRD analysis of the samples reduced at different

temperatures, although further reaction of SiO with CH4 via Reaction [9] is thermodynamically feasible. This means that either no SiC was formed on the surface of quartz particles or the SiC yield was too low to be detected by XRD. Thermodynamic calculation using HSC Chemistry 6.1 showed that Reaction [9] is practically irreversible with the equilibrium constant in the order of 107 to 108 in the considered temperature range. The fact that Reaction [9] did not occur in the fluidized bed is attributed to the kinetic barrier in the SiC nucleation in the bed.

$$SiO\,(g) + 2CH_4\,(g) = SiC + CO\,(g) + 4H_2\,(g) \qquad [9]$$

The effect of fluidizing gas flow rate on the reduction of quartz was examined at 1723 K (1450 °C) in the range 0.4 to 0.8 NL/min with a constant methane concentration of 5 vol pct. Total gas flow through the gas analyzer (fluidizing and purging) was kept constant at 1.0 NL/min. Figure 4 depicts the change of CO concentration in the off gas *vs* time for different gas flow rates. At a low gas flow rate of 0.4 NL/min, CO concentration reached 0.27 vol pct nearly instantly when the quartz powder was introduced into the reactor. The peak CO concentration increased nearly proportionally with increasing gas flow rate.

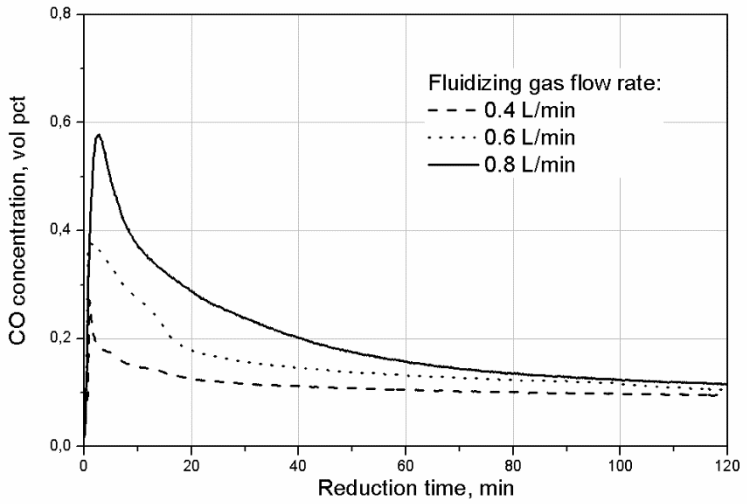

Fig. 4 Effect of gas flow rate on the reduction of quartz by CH_4–H_2 gas mixture (5 vol

pct CH_4) at 1723 K (1450 °C).

The effect of methane content in the gas mixture on the reduction of quartz was examined at 2, 5 and 10 vol pct, keeping fluidizing gas flow rate at 0.8 NL/min and temperature at 1723 K (1450 °C). The change of CO concentration *vs* time in experiments with different methane contents is shown in Figure 5. The CO peak concentration and extent of reduction increased with increasing methane content in the gas mixture from 2 to 5 vol pct. In the experiment with 10 vol pct of methane, the reduction rate was much faster at the beginning of the reaction, however it decreased dramatically, and the final extent of reduction was low (4.6 pct after 120 min). The sample after reduction became black, indicating deposition of solid carbon on the particle surface due to excessive methane decomposition (Reaction [5]) which retarded the reduction.

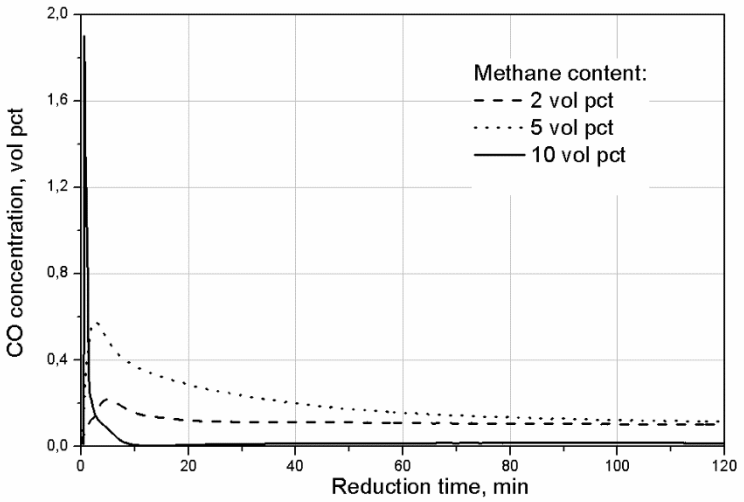

Fig. 5 Effect of methane content on the reduction of quartz by CH_4–H_2 gas mixture with flow rate 0.8 NL/min at 1723 K (1450 °C).

IV. Discussion

Reduction of solid silica by gaseous hydrogen–methane mixture is a typical gas-solid

reaction in which a gaseous reductant diffuses to the gas-solid phase boundary where reactions take place, and the gaseous products diffuse back into the bulk gas. The rate of the whole process is determined by the slowest step in a series of reactions and mass transfer steps.

Quartz reduction by CH_4–H_2 gas was strongly affected by the reduction temperature (Figure 2). Applying Arrhenius law to the peak rate of reduction at different temperatures, apparent activation energy of 408 kJ/mol was obtained, with a correlation coefficient of 0.94 between the CO peak concentration (which characterises the rate of reduction) and reciprocal of absolute temperature **(**Figure 6). Such high activation energy is expected for processes with intrinsic reaction kinetics. According to Figure 4, the reaction rate increased with gas flow rate. The increase of the reaction rate with flow rate is an indication of the effect of the external mass transfer. However, the gas flow rate also affected the thermal cracking of methane in the gas phase [16, 17]; the degree of methane cracking increased with increasing residence time which decreased with increasing gas flow rate. The actual methane concentration in the fluidized bed at the gas flow rates 0.4 and 0.6 NL/min was higher than that at 0.8 NL/min, at which the optimum methane content in the gas stream was established within the range of 5 vol pct (Figure 5). Therefore, increase in the gas flow rate decreased the actual methane content in the reactor with a positive effect on the reaction rate.

Reduction of SiO_2 to SiO by methane proceeds through Reaction (4). The reaction starts with adsorption and dissociation of CH_4 on the silica surface $CH_4 \rightarrow \ldots \rightarrow C_{ad} + 2H_2$. Carbon activity in the system is in the range of 15.2–27.1 [18]. Adsorbed highly active carbon forms strong bonds with oxygen atom and then forms CO which is released from the surface to the gas phase. The removal of an oxygen atom from the silica surface increases the energy states of nearby oxygen and silicon; a volatile SiO molecule is formed and released from the surface.

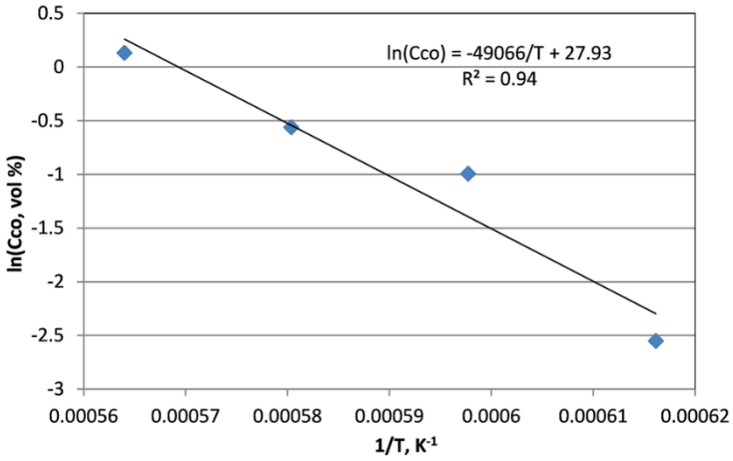

Fig. 6 Arrhenius plot calculated from peak rate of reduction at different temperatures.

However, the use of pure methane or CH_4–H_2 gas mixture with high methane concentration leads to cracking of methane and deposition of carbon black which blocks the reaction sites on the surface of quartz. Moreover, deposition of solid carbon decreases thermodynamic activity of carbon in the system. The major role of hydrogen in the CH_4–H_2 gas mixture is to control carbon activity in the system avoiding excessive methane cracking. Hydrogen can directly reduce silica to SiO by Reaction [10], which proceeds through adsorption of H atoms on the silica surface [19, 20]. Low partial pressure of H_2O needed for Reaction [10] to occur is maintained by Reaction [11]. A combination of these two reactions gives Reaction [4], therefore thermodynamics of the combination of Reactions [10] and [11] is equivalent to the thermodynamics of Reaction [4]. However, Reaction [4] proceeds under strongly non-equilibrium conditions; the use of active carbon secures reduction of SiO_2 to SiO.

$$SiO_2 + H_2\,(g) = H_2O\,(g) + SiO\,(g) \qquad [10]$$

$$CH_4\,(g) + H_2O\,(g) = CO\,(g) + 2H_2\,(g) \qquad [11]$$

Following Reaction [4], methane diffuses to the reaction interface while SiO, CO and H_2 diffuse away from the reaction interface. Mass transfer of SiO and CO in the gas phase can contribute to the reaction rate control. The concentration of hydrogen in the

gas phase is quite high; its diffusion is not expected to have an effect on the rate of reaction.

The low degree of conversion of SiO_2 to SiO can be explained by the low specific surface area of quartz sand (estimated value 0.008–0.011 m^2/g). Decrease in the rate of reduction with reaction time and relatively low extent of reduction was related to the deposition of carbon black as described above. Moreover, the change in the rate controlling mechanisms in the course of reduction cannot be excluded.

The reduction of quartz was studied further using quartz spheres, which were suspended by a tungsten wire in the CH_4–H_2 gas mixture. The methane content in the gas mixture was maintained at 0.5 vol pct to minimize the effect of the methane cracking. The change of CO concentration *vs* time in the off gas is presented in Figure 7. The CO concentration decreased rapidly in the first 40 min. With the increase of the reaction temperature, the reaction rate increased, and the CO concentration curve became more fluctuant.

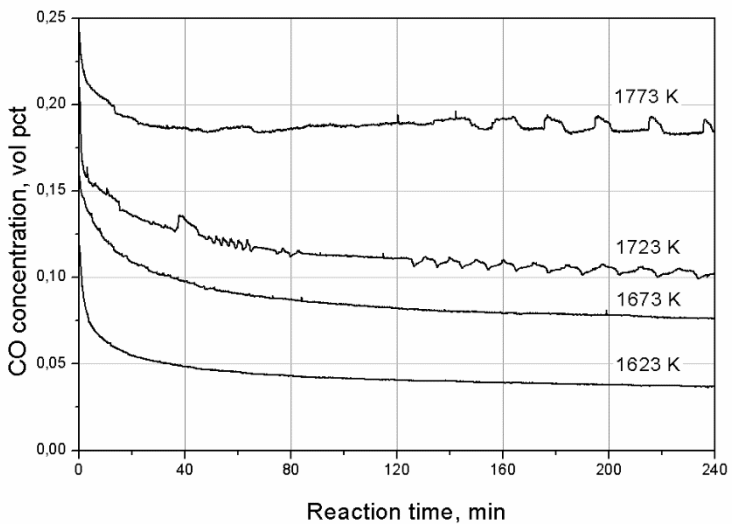

Fig. 7 CO concentration in the off gas in the reduction of quartz sphere by the CH_4–H_2 gas mixture with 0.5 vol pct CH_4 at different temperatures. The gas flow rate was 1.6 NL/min.

Applying Arrhenius law to the apparent reaction rate constant obtained from Figure 7, apparent activation energy was obtained to be 207 kJ/mol. This value is only about 50 pct of the value obtained from experimental data using the fluidized bed reactor, indicating that the reaction rate was affected by the external diffusion of gas species from the reaction interface. Continuous movement of the quartz particles in the fluidized bed reactor generated a stirring effect; the effect of external diffusion on the reaction rate in the fluidized bed reactor was relatively small.

The surfaces of quartz spheres after reduction at 1723 and 1773 K (1450 and 1500 °C) were examined by SEM. The SEM images of the quartz spheres presented in Figure 8 show cracks on the surfaces due to phase transformation of quartz into cristobalite which created stress within the spheres. Surface cracking exposed fresh surface of quartz to the reducing gas causing increase in the reduction rate, which explains fluctuations in the concentration of CO evolved in the reduction process.

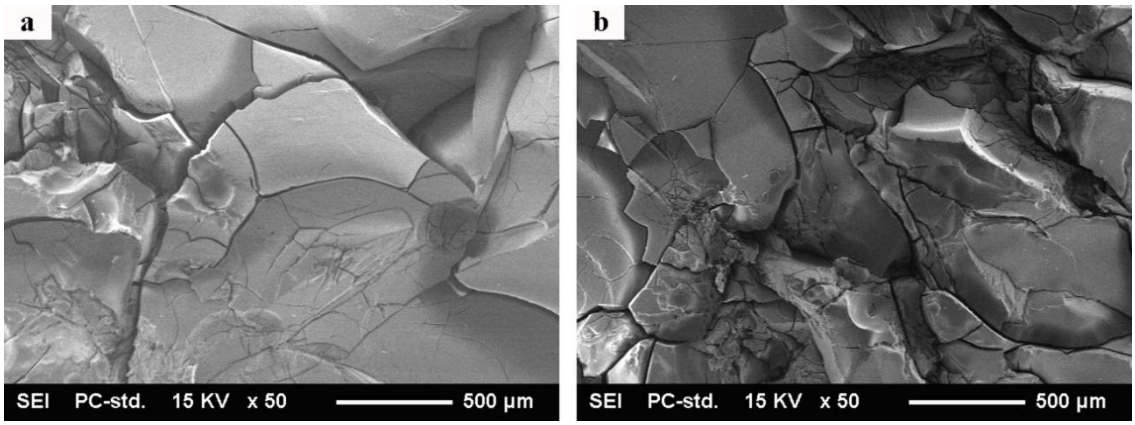

Fig. 8 SEM images of quartz spheres after reduction by the CH_4–H_2 gas mixture with 0.5 vol pct CH_4 at: (a) 1723 K (1450 °C); (b) 1773 K (1500 °C).

Figure 9 presents the surfaces of the quartz spheres after reaction at different temperatures at a higher magnification. The surface of quartz was smooth before reaction; it was eroded and became porous after reaction at 1623 K (1350 °C) (Figure 9a). Development of the porous structure increased surface area. In the reduction at

1723 and 1773 K (1450 and 1500 °C), a small amount of SiC particles was observed on the surfaces of quartz spheres (Figures 9b and 9c), which was confirmed by the EDS analysis. SiC was formed by the reaction of deposited carbon with SiO. Amount of observed SiC particles in the sphere reduced at 1723 K (1450 °C) was higher than in the sphere reacted at 1673 K (1400 °C).

The surface of the sphere after reaction at 1773 K (1500 °C) was covered by SiC whiskers (Figure 9d). As studied previously [8–11], SiC whiskers in the reduction of quartz containing iron impurities were formed by the reaction of CH_4 and SiO under catalytic effect of iron or other transition metal elements, *i.e.* VLS (vapor-liquid-solid) mechanism. However, no catalyst globules were observed at the tip of SiC whiskers in this study, indicating that they were formed via VS (vapor-solid) mechanism occurred by gas-gas (SiO–CH_4) Reaction [9]. SiC whiskers were not found in the samples reduced at lower temperatures due to low SiO vapor pressure [12].

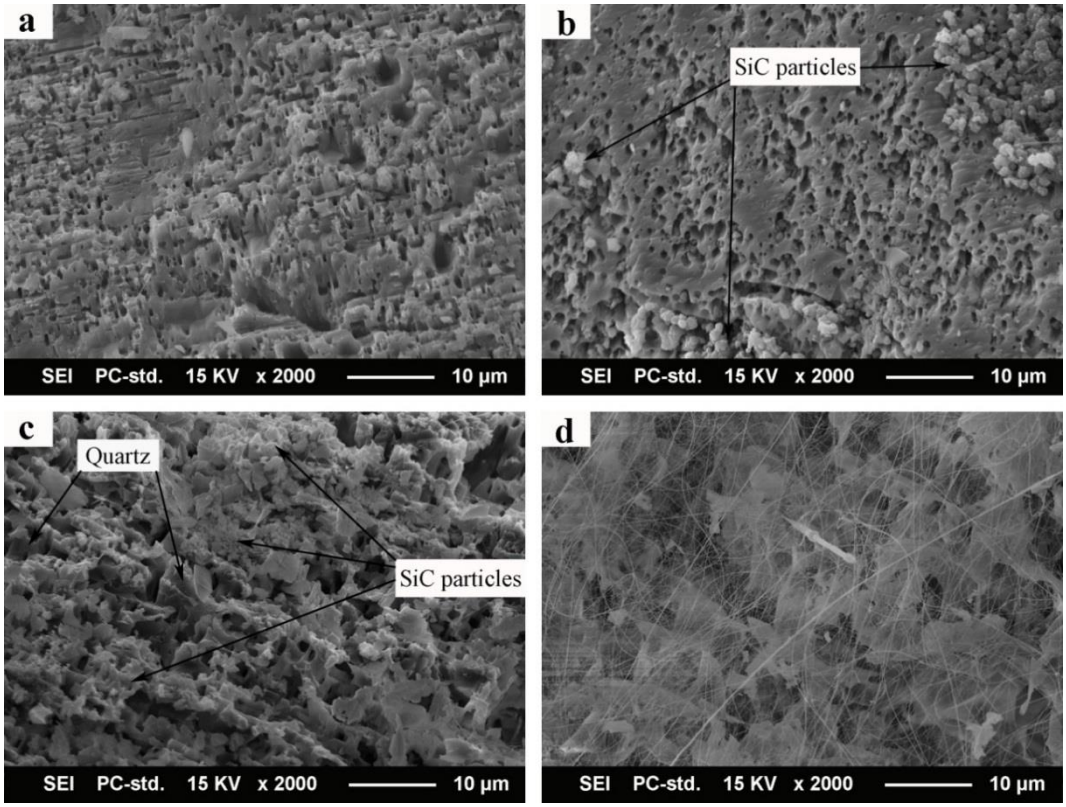

Fig. 9 SEM images of the surface of quartz sphere after reduction by the CH_4–H_2 gas mixture with 0.5 vol pct CH_4 at: (a) 1623 K (1350 °C); (b) 1673 K (1400 °C); (c) 1723 K (1450 °C); (d) 1773 K (1500 °C).

V. Conclusions

The reduction of quartz by methane-containing gas was studied in a laboratory fluidized bed reactor. A cold model was made which established the fluidization conditions of quartz powder. Direct reduction of quartz by CH_4–H_2 mixture is feasible, but in the temperature range of 1623 to 1773 K (1350 to 1500 °C) proceeded to gaseous SiO. The initial rate of reduction increased with increasing temperature, fluidization gas flow rate (0.4–0.8 NL/min) and methane content in the reducing gas (below 5 vol pct). However, temperature above 1723 K (1450 °C) and methane content above 5 vol pct caused significant methane cracking and carbon deposition on the surface of quartz particles, which hindered further reduction. In the reduction of quartz spheres at 1673–1773 K (1400–1500 °C), a small amount of SiC was observed in the form of particles (1673 and

1723 K (1400 and 1450 °C)) or whiskers (1773 K (1500 °C)).

Acknowledgements

This research was supported under the Australian Research Council Linkage Projects funding scheme (Project No. LP100100866). Commonwealth Scientific and Industrial Research Organization (CSIRO) provided quartz lumps crushing and grinding service. The electron microscopy characterization was carried out at the Electron Microscopy Centre (EMC) at the University of Wollongong.

References

1. A. Schei, J. Tuset, and H. Tveit: *Production of High Silicon Alloys*, Tapir Forlag, Trondheim, 1998.
2. S. Ranjan, S. Balaji, R.A. Panella, and B.E. Ydstie: *Comput. Chem. Eng.*, 2011, vol. 35 (8), pp. 1439–53.
3. D.H. Filsinger and D.B. Bourrie: *J. Am. Ceram. Soc.*, 1990, vol. 73 (6), pp. 1726–32.
4. J.G. Lee, P.D. Miller, and I.B. Cutler: *Reactivity of solids*, Plenum Press, New York, 1976.
5. N.S. Jacobson, K.N. Lee, and D.S. Fox: *J. Am. Ceram. Soc*., 1992, vol. 75 (6), pp. 1603–11.
6. F. Aratani, Y. Sakaguchi, N. Yuge, M. Ishizaki, and T. Kawahara: *Bull. Jpn. I. Met.*, 1991, vol. 30 (5), pp. 433–5.
7. E.H. Myrhaug and H. Tveit: *58th Electric Furnace Conference and 17th Process Technology Conference Proceedings*, Warrendale, 2000, pp. 591–604.
8. U. Setiowati and S. Kimura: *J. Am. Ceram. Soc.*, 1997, vol. 80 (3), pp. 757–60.
9. H.J. Choi and J.G. Lee: *J. Mater. Sci.*, 1995, vol. 30 (8), pp. 1982–6.
10. J.V. Milewski, F.D. Gac, J.J. Petrovic, and S.R. Skaggs: *J. Mater. Sci.*, 1985, vol. 20

(4), pp. 1160–6.

11. G. Urretavizcaya and J.M.P. Lopez: *J. Mater. Res.*, 1994, vol. 9 (11), pp. 2981–6.
12. X. Li, G. Zhang, R. Tronstad and O. Ostrovski: Ceram. Int., 2016, vol. 42(5), pp. 5668–76.
13. O. Ostrovski and G. Zhang: *AIChE J.*, 2006, vol. 52 (1), pp. 300–10.
14. T.C. Glayton: *Multiphase Flow Handbook*, CRC Press, Boca Raton, 2008.
15. A.C.D. Chaklader and A.L. Roberts: *J. Am. Ceram. Soc.*, 1961, vol. 44 (1), pp. 35–41.
16. G. Zhang and O. Ostrovski: *Metall. Mater. Trans. B*, 2000, vol. 31 (1), pp. 129–39.
17. X. Li, G. Zhang, K. Tang, O. Ostrovski and R. Tronstad: *Metall. Mater. Trans. B*, 2015, vol. 46 (5) 2384–93.
18. R.A. Gardner: *J. Solid. State. Chem.*, 1974, vol. 9 (4), pp. 336–44.
19. G. Han and H.Y. Sohn: *J. Am. Ceram. Soc.*, 2005, vol. 88 (4), pp. 882–8.
20. J. Szekely, J.W. Evans, and H.Y. Sohn: *Gas-solid Reactions*, Academic Press, New York, 1976.

CHAPTER 6

EFFECT OF GAS ATMOSPHERE ON THE FORMATION OF SILICON BY REACTION OF SiC AND SiO_2

Effect of Gas Atmosphere on the Formation of Silicon by Reaction of SiC and SiO_2

Xiang Li[1], Guangqing Zhang[1*], Oleg Ostrovski[2], Ragnar Tronstad[3]

[1]School of Mechanical, Materials and Mechatronic Engineering, University of Wollongong, Wollongong, NSW 2522, Australia

[2]School of Materials Science and Engineering, University of New South Wales, Sydney, NSW 2052, Australia

[3]Elkem AS, Drammensveien 169, Skøyen, P.O Box 334, 0213 Oslo, Norway

Abstract

The formation of silicon by reaction between quartz and SiC has been studied in the temperature range of 1600–1900 °C in argon and hydrogen atmospheres. The reaction process was monitored by an infrared gas analyser, and the reaction products were characterised by LECO, XRD and SEM. Quartz–SiC reactions with SiO_2/SiC molar ratio of 1:1 and 1:2 were studied in a fixed bed reactor in a graphite furnace. The production of silicon from quartz and SiC was strongly affected by temperature, SiO_2/SiC molar ratio and gas atmosphere. The yield of silicon in the reaction at 1900 °C in argon from samples with SiO_2/SiC molar ratios of 1:1 and 1:2 reached 32.7 and 44.5 % respectively. SiO_2–SiC reaction at 1900 °C in hydrogen with the SiO_2/SiC molar ratio of 1:2 resulted in the silicon yield of 66.7 %. Higher silicon yield in hydrogen was attributed for the involvement of hydrogen in the direct reduction of silica to SiO.

I. Introduction

Metallurgical grade silicon (MG-Si) and silicon alloys have been produced industrially

* Corresponding author; email: gzhang@uow.edu.au

since the end of the nineteenth century [1, 2]. Metallurgical silicon is produced in a submerged electric arc furnaces (SAF) by charging quartz or quartzite and a carbon source (coke, coal, charcoal and/or woodchips) from the top of the SAF; as the charge descends in the furnace, several reactions occur, yielding elemental silicon as the end product [3]. The overall reaction is given by Reaction (1).

$$SiO_2 + 2\,C = Si\,(l) + 2\,CO\,(g) \quad (1)$$
$$\Delta G^\circ = 711.77 - 0.3661T\ (kJ) \quad (1273\ K \leq T \leq 2273\ K)$$

However, the actual reaction process is much more complex and includes the formation of intermediate species SiO and SiC. SiO_2 is reduced to form SiO and CO:

$$SiO_2 + C = SiO\,(g) + CO\,(g) \quad (2)$$
$$\Delta G^\circ = 668.07 - 0.3288T\ (kJ) \quad (1273\ K \leq T \leq 2273\ K)$$

Gaseous SiO ascends in the reaction shaft and reacts with C to form SiC in the upper and cooler part of the furnace [4]. This process is described as follows:

$$SiO\,(g) + 2\,C = SiC + CO\,(g) \quad (3)$$
$$\Delta G^\circ = -78.89 + 0.0010T\ (kJ) \quad (1273\ K \leq T \leq 2273\ K)$$

The overall reaction of silicon formation from SiO_2 and SiC can be presented by the following equation:

$$SiO_2 + 2\,SiC = 3\,Si\,(l) + 2\,CO\,(g) \quad (4)$$
$$\Delta G^\circ = 887.76 - 0.4083T\ (kJ) \quad (1273\ K \leq T \leq 2273\ K)$$

The primary silicon production reactions in the inner zone of an electric arc furnace are Reactions (5)–(8):

$$2\ SiO_2 + SiC = 3\ SiO\ (g) + CO\ (g) \quad (5)$$

$$\Delta G^\circ = 1415 - 0.6586T\ (kJ) \quad (1273\ K \leq T \leq 2273\ K)$$

Reaction (5) proceeds through Reactions (6) and (7):

$$SiO_2 + CO(g) = SiO\ (g) + CO_2\ (g) \quad (6)$$

$$\Delta G^\circ = 1011.5 - 0.3196T\ (kJ) \quad (1273\ K \leq T \leq 2273\ K)$$

$$2\ CO_2\ (g) + SiC = SiO\ (g) + 3\ CO\ (g) \quad (7)$$

$$\Delta G^\circ = 403.51 - 0.3389T\ (kJ) \quad (1273\ K \leq T \leq 2273\ K)$$

Silicon is mainly formed by Reaction (8):

$$SiO\ (g) + SiC = 2\ Si\ (l) + CO\ (g) \quad (8)$$

$$\Delta G^\circ = 165.56 - 0.0751T\ (kJ) \quad (1673\ K \leq T \leq 2273\ K)$$

SiO_2 and SiC react with each other in the arc zone [5–7]. Then the SiO vapour can further react with SiC to form elementary silicon. When silicon is present with quartz, the following reaction can also take place:

$$Si\ (l) + SiO_2\ (l) = 2\ SiO\ (g) \quad (9)$$

$$\Delta G^\circ = 616.37 - 0.2875T\ (kJ) \quad (1673\ K \leq T \leq 2273\ K)$$

SiO vapour was also carried out of the hot zone of furnace and condensed at relatively low temperatures (below 1400 °C) by Reaction (10).

$$2\ SiO\ (g) = Si + SiO_2 \quad (10)$$

$$\Delta G^\circ = -683.75 + 0.3274T\ (kJ) \quad (1273\ K \leq T \leq 1673\ K)$$

Poch and Dietzel [8] investigated the reaction between SiO_2 and SiC in argon

atmosphere, in the range of 1480–2000 °C with SiO_2/SiC molar ratio of 2.5. The reaction rate was found to be rather slow at temperatures below 1550 °C but increased rapidly with increasing temperature. Below 1790 °C the final weight loss measured in the reaction agreed with the stoichiometry of Reaction (5). Above 1790 °C there was an additional weight loss of about 5 %. This was attributed to the silicon evaporation.

Tuset *et al.* [9, 10] investigated the reaction between SiO_2 and SiC by a thermogravimetric analysis (TGA). Below the melting point of silica, the rate of weight loss was found to be faster in Ar than in CO. It was rather insensitive to the quartz quality (quartz purity, thermal strength and softening properties), but increased by a factor of 10 when recrystallized SiC was replaced by an equivalent volume of SiC formed from charcoal. The molar ratio between consumed SiC and SiO_2 was found to be below 2. Dal Martello *et al.* [11] investigated silicon production from quartz and SiC using pellets of quartz-SiC powder and quartz lumps. More SiO was produced and almost no quartz was left when pellets of a SiO_2–SiC mixture were used as charge materials in the case of SiO_2/SiC molar ratio of 1:1. In comparison, a higher silicon yield was achieved with quartz lumps because of less loss of SiO.

Previous works [12–18] have demonstrated that gas atmosphere can change the reaction mechanisms of various reduction reactions and the reaction kinetics. Specifically, hydrogen as a reactive gas can be involved in the reactions and change the mechanisms of solid–solid reactions. This study explores the reaction of quartz and SiC for silicon production in argon and hydrogen atmospheres, to establish fundamental understanding of the reaction and provide evidence for improving silicon production technology.

II. Experimental

The investigation of the formation of silicon from silicon carbide and quartz was performed in a fixed bed reactor under argon and hydrogen gas atmospheres. The experimental details are as follows.

2.1 Materials

The quartz used in this investigation with particle size <70 μm was obtained by crushing quartz lumps in a 6 inch agate pulveriser in a Rocklabs ring mill. The agate was made of gray silica so that contamination to the quartz sample was minimized. The silicon carbide powder was synthetic α-SiC powder with a particle size range of 50–200 μm, which was supplied by Pacific Rundum Co., Ltd. (Toyama, Japan).

The quartz and α-SiC powders were mixed with distilled water (80 wt% of solid mixture) in a plastic jar with zirconia milling balls. Two mixtures were prepared with SiC/SiO_2 molar ratios of 1 and 2. The SiC/SiO_2 molar ratio of 2 is the stoichiometric ratio for silicon formation following Reaction (4); in the mixture with the SiC/SiO_2 molar ratio ratio of 1, SiO_2 was taken in excess relative to the stoichiometric ratio. The plastic jar containing a mixture and milling balls was rolled on a rolling machine for 8 h to ensure a homogeneous composition. Water was removed by heating the mixture at 120 °C for 48 h. Then, the dried mixture was rolled on the rolling machine for a few minutes to separate milling balls with loose powder. Argon and hydrogen with 99.999 % purity were supplied by Coregas Pty. Ltd. (Unanderra, Australia) in gas cylinders.

2.2 Experimental setup and procedure

Production of silicon in different gas atmospheres was studied in a laboratory graphite tube furnace (Model 1000-2560-FP20, GT Advanced Technologies, Santa Rosa, USA). The schematic of the fixed bed reactor is presented in Fig. 1. A sample of SiO_2–SiC mixture was contained in a silicon carbide crucible which was loaded inside a graphite tube to confine the reaction atmosphere. The crucible was supported by another graphite tube and located in the hot zone of furnace. The sample temperature during reaction was measured by a type C thermocouple which was protected against reaction gas atmosphere by a tungsten coated molybdenum thermocouple sheath. Argon or hydrogen gas was introduced into the reaction system from the top of graphite tube, and

withdrawn from the reactor from the bottom of the graphite tube.

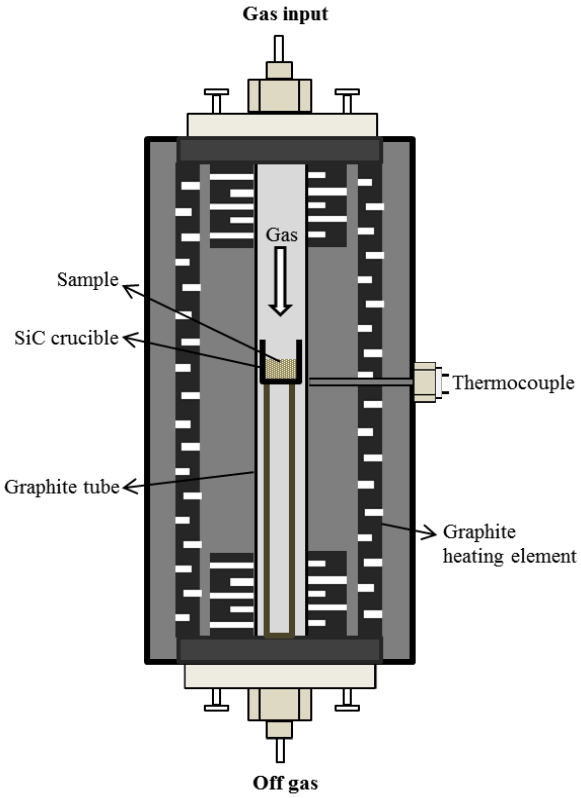

Fig. 1 Schematic of the reaction setup in a high-temperature graphite tube furnace.

In the experimental study of silicon formation, the furnace was first evacuated to pressure less than 1 kPa, and subsequently filled with argon at atmospheric pressure. Then, the furnace was heated to 400 °C at 10 °C/min and kept constant at this temperature for 20 min. Evacuation and argon refilling process was repeated twice at 400 °C, in order to remove any adsorbed moisture, CO_2, and O_2 from graphite parts of the furnace. Then, the mixture was heated in argon or hydrogen to the target temperature at 40 °C/min and kept constant (the heating rate was decreased to 10 °C/min in the range of 1800–1900 °C. The reaction was stopped after certain duration by lowering the temperature rapidly. After reaction, the sample was weighed and analyzed as described below.

During reaction experiments, the off gas composition was continuously monitored by an

infrared CO/CO_2 analyzer (ULTRAMAT 23, Siemens AG, Munich, Germany) connected with a computer. Concentrations of CO and CO_2 were recorded every 1 s.

2.3 Sample characterization and data analysis

The original mixture and reacted samples were analyzed by X-ray diffraction (XRD, MMA, GBC Scientific Equipment, Braeside, Australia). The fine powder of a sample after grinding was scanned at a speed of 0.02 °/s and step size 0.02 ° with CuK radiation generated at 35 kV and 28.6 mA.

The oxygen content in the reacted samples was determined by a LECO nitrogen/oxygen determinator (TC-436 DR, LECO Australia Pty. Ltd., Sydney, Australia). A graphite crucible containing a sample was placed between two electrodes. High current passing through this crucible heated the sample up to 3100 °C. After an outgassing procedure the sample was dropped into the crucible from a helium-purged loading head. The oxygen released from the sample combined with the carbon of the crucible to form CO and CO_2 of which the contents were measured by infrared detectors.

The content of total carbon in samples was determined by a LECO carbon/sulphur determinator (SC-444 DR, St. Joseph, U.S.A.). A sample mixed with a flux was placed into a ceramic crucible. The system was closed and purged with oxygen. The sample and the flux were heated in the high-frequency induction furnace. The pure oxygen atmosphere and the heat induced the combustion of the sample where all elements were oxidized. Carbon from the sample reacts with oxygen to form CO and CO_2 which were analyzed by infrared detectors.

SEM images were recorded by field-emission scanning electron microscopy (FESEM, JSM-7001F, JEOL, Tokyo, Japan) operated at 15 kV. Equipped with an energy-dispersive X-ray spectrometer (EDS), it was also used to characterize the chemical composition of the samples. The samples were mounted in Epoxy resin,

ground and polished carefully. Mounted-polished samples were coated with gold film to enhance conductivity during SEM/EDS observation.

The equilibrium phases in the reaction system were calculated using Outokumpu HSC Chemistry software (Version 6.1, Outokumpu Research Oy, Pori, Finland).

Assuming that reacted samples consisted of SiC, SiO_2, and elemental silicon, the yield of Si, (molar percentage of silicon in an original sample converted to elemental silicon, Y_{Si}), was calculated using the following equation:

$$Y_{Si} = \frac{1}{28 n_{Si}} m \left(100 - \frac{40}{12} C_{C-LECO} - \frac{60}{32} C_{O-LECO}\right) \quad (11)$$

where n_{Si} is the content of silicon in the mixture before reaction, mol; m is the weight of mixture after reaction, g; C_{C-LECO} and C_{O-LECO} are the mass concentrations of total carbon and oxygen in the reacted sample, %.

During reaction, the part of generated SiO blown out from the reacting sample was defined as loss of silicon as SiO, Y_{SiO}, and calculated by Eq. (12).

$$Y_{SiO} = \frac{100}{n_{Si}} \left[n_{Si} \left(1 - \frac{Y_{Si}}{100}\right) - m \frac{C_{O-LECO}}{32} - m \frac{C_{C-LECO}}{12} \right] \quad (12)$$

III. Results and discussion

3.1 Reaction between SiO_2 and SiC in argon atmosphere

A mixture of quartz and silicon carbide powders with a molar ratio SiO_2/SiC = 1:1 was heated in argon at different temperatures. The CO evolution rate versus time calculated from the CO concentration in the off gas is presented in Fig. 2 where the reaction time

was counted from the commencement of heating from 400 °C to the target temperature. Figure 3 shows the XRD spectra of the samples reacted at different temperatures. The conversion of SiO_2 and SiC and the yields of silicon and SiO calculated using LECO data are summarized in Table 1.

Table 1 SiO loss and yield of silicon after carbothermal reaction in argon at different temperatures.

Temperature (°C)	1600	1700	1800	1900	1600	1700	1800	1900
Initial SiO_2/SiC ratio	1:1	1:1	1:1	1:1	1:2	1:2	1:2	1:2
Reaction time (min)	150	94	56	66	150	94	56	66
Conversion of SiO_2 (%)[a]	67.7	99.4	99.6	99.6	87.3	98.4	99.3	99.3
Conversion of SiC (%)[b]	77.9	79.2	86.0	90.7	59.8	72.4	71.7	77.4
Weight loss (%)	63.4	73.8	73.2	77.7	55.8	58.3	55.2	60.1
SiO yield (%)	57.9	58.0	55.4	62.4	42.7	38.9	33.6	40.2
Silicon yield (%)	14.9	31.4	37.4	32.7	26.3	42.1	47.3	44.5

[a] Calculated from LECO oxygen content of reacted samples;

[b] Calculated from LECO carbon content of reacted samples.

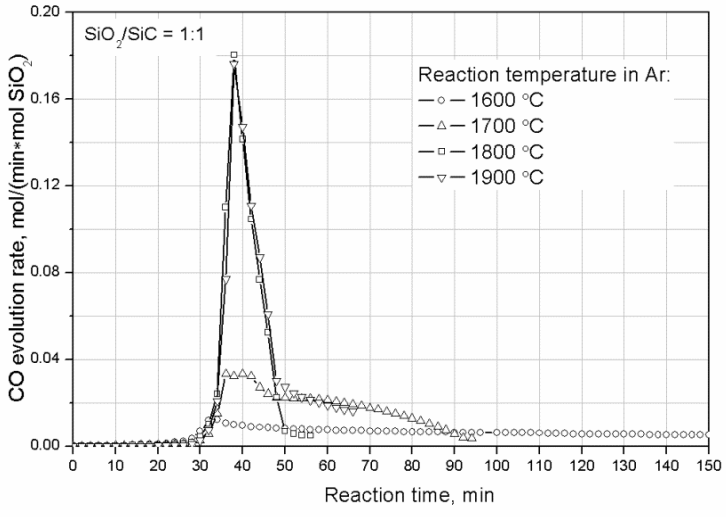

Fig. 2 CO evolution rate in the reactions at different temperatures in argon. Initial samples contained quartz and silicon carbide with a molar ratio SiO_2/SiC = 1:1.

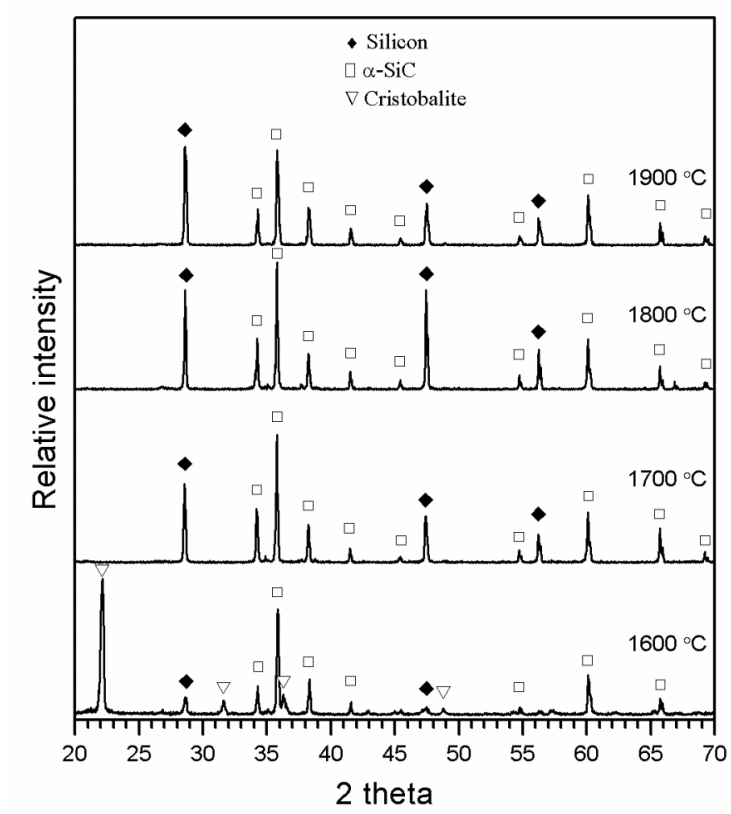

Fig. 3 XRD patterns of the samples reacted in argon at different temperatures. The initial samples had a molar ratio of SiO_2/SiC = 1:1. The reaction time including temperature ramping time was 150 min at 1600 °C, 94 min at 1700 °C, 56 min at 1800 °C, and 66 min at 1900 °C.

As shown in Fig. 2, no CO evolution was observed during the first 30 min of heating when the samples were heated from 400 to 1600 °C with a heating rate of 40 °C/min. The reaction rate at 1600 °C was quite slow, a peak of CO evolution rate of 0.012 mol/(min mol SiO_2) was reached for 34 min. The yield of silicon after 150 min was 14.9 %, as shown in Table 1. Phases in the reacted sample identified by XRD included silicon (weak peaks of 2θ at 28.59°, 47.57° and 56.40°), unreacted α-SiC and cristobalite. Cistobalite was formed from quartz at temperatures above 1470 °C [19]. The peak of CO evolution rate at 1700 °C increased to 0.033 mol/(min mol SiO_2), and silicon yield reached 31.4 % after reaction for 94 min. An increasing temperature to 1800 °C promoted the reaction significantly, and the CO evolution rate was raised to 0.180 mol/(min mol SiO_2) rapidly. A further increase in the temperature to 1900 °C did

not affect CO evolution rate but decreased the yield of silicon, which was attributed to a higher loss of silicon in the form of SiO, accounted to 62.4 %.

The CO evolution rate in the SiO_2–SiC reaction with SiO_2/SiC ratio 1:2 in argon *vs* time is presented in Fig. 4. Overall, the CO evolution rate followed a trend observed in the SiO_2-SiC reaction with SiO_2/SiC ratio 1:1 as presented in Fig. 2, but CO evolution peaks were visibly higher at all temperatures. The CO evolution rate increased with the increase of temperature from 1600 to 1800 °C. However, further increasing temperature to 1900 °C did not accelerate the reaction, probably due to the high reaction rate leading to the higher loss of SiO in comparison with reaction at 1800 °C (Table 1) and deficit of SiO_2. In general, increasing the SiC content in the SiO_2–SiC mixture increased the yield of Si, decreased the yield of SiO and overall weight loss of the reacted samples. SiC was not completely converted in reactions with both SiO_2/SiC ratios, although SiO_2 conversion was close to completion at high temperatures. These experimental results indicate that silica reacted not only with SiC but also with Si by Reaction (9).

Figure 5 presents the equilibrium partial pressure of CO calculated for Reaction (4), and partial pressure of SiO calculated for Reactions (5), (8), and (9) using HSC Chemistry 6.1 [20]. Equilibrium partial pressures of CO and SiO significantly increased with the increasing temperature. Therefore, increase in temperature favors the formation of silicon both thermodynamically and kinetically.

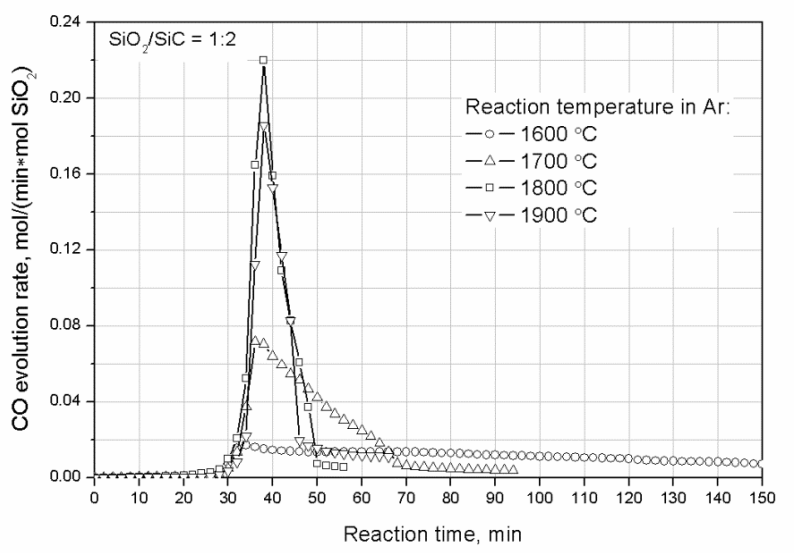

Fig. 4 CO evolution rate in the reactions at different temperatures in argon. Initial samples contained quartz and silicon carbide with a molar ratio $SiO_2/SiC = 1:2$.

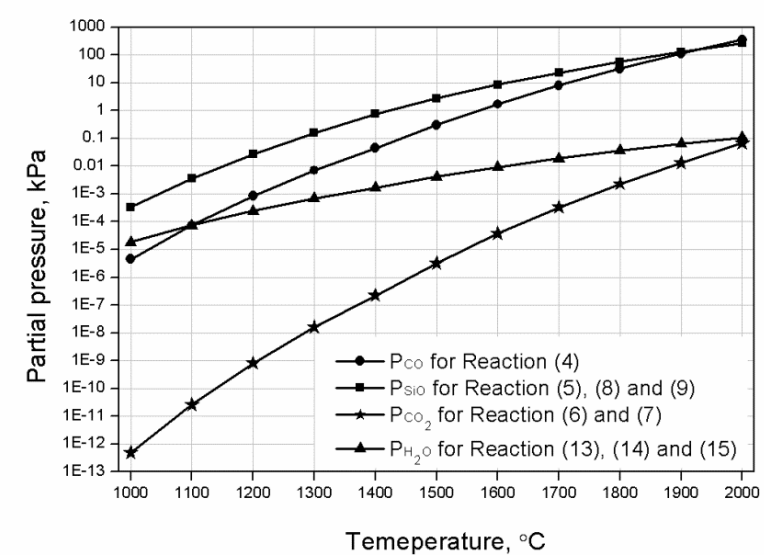

Fig. 5 Equilibrium CO partial pressure for Reaction (4); equilibrium SiO partial pressure for Reactions (5), (8), and (9), assuming CO partial pressure calculated for Reaction (4); equilibrium CO_2 partial pressure for Reactions (6) and (7), assuming CO partial pressure is the same as Reactions (4) and SiO partial pressure is the same as Reaction (5); equilibrium H_2O partial pressure for Reactions (13), (14) and (15), calculated with the SiO partial pressure in Reaction (5) and $P_{H2} = 100$ kPa.

Figure 6 presents the back-scattered electron (BSE) images of the samples with initial SiO_2/SiC ratio 1:2 reacted in argon at 1600 and 1800 °C. The sample reacted at 1600 °C mainly consisted of unreacted SiC, cristobalite, and a small amount of elemental silicon (Fig. 6a). A few bright spots of Fe–Si alloy were also observed; impurity iron originated from the commercial quartz raw materials as detected by an EDS analysis of the raw material powder. SEM/BSE analysis is consistent with Fig. 4 confirming that the reaction was not completed. The powder of the SiC–SiO_2 mixture contained in the SiC crucible was sintered and shrinked into a pellet which affected the diffusion of gas species. The distribution of elemental silicon in the sample was nonuniform. It was observed that the content of elemental silicon was higher in the external layer, showing that escape of CO from the pellet affected the kinetics of silicon formation. It was also noted that elemental silicon was always generated around SiC particles, but not SiO_2 particles. This phenomenon proved that the primary reaction for silicon production is Reaction (8).

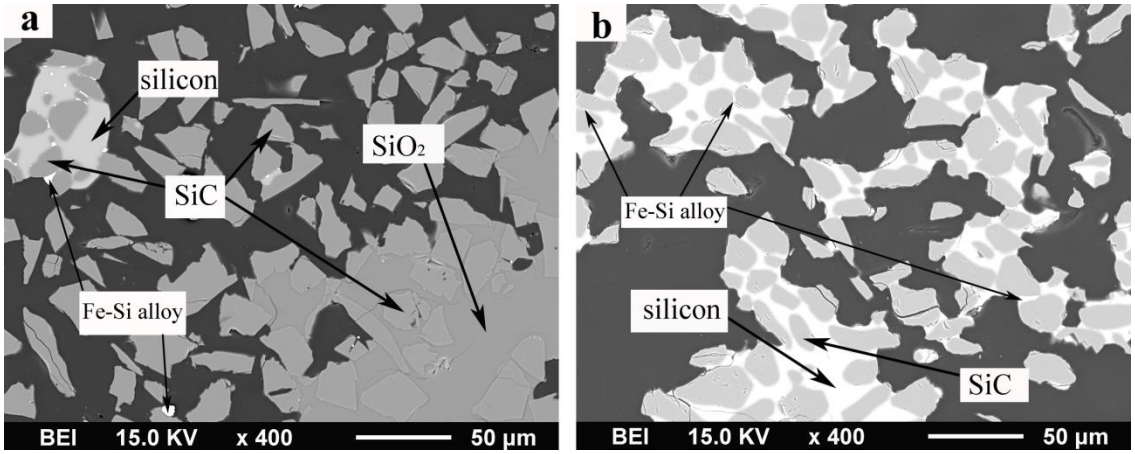

Fig. 6 SEM images of samples reacted in argon with initial molar SiO_2/SiC ratio = 1:2. **a** Reacted at 1600 °C; **b** reacted at 1800 °C.

SEM analysis of samples reacted in argon at 1800 °C (Fig. 6b) did not detect silica residue. The samples with SiO_2/SiC ratio 1:2 and 1:1 reacted at 1800 °C both consisted of SiC inclusions surrounded by elemental silicon. The fraction of silicon in the sample with SiO_2/SiC ratio 1:2 was higher than that with the SiO_2/SiC ratio 1:1, corresponding

to the silicon yields listed in Table 1. Some spots of Fe–Si alloy were also identified by the EDS analysis.

3.2 Reaction between SiO_2 and SiC in hydrogen atmosphere

Formation of silicon from quartz and SiC in hydrogen was examined with initial SiO_2/SiC molar ratios 1:1 and 1:2 in the temperature range of 1600–1900 °C. The CO evolution rate *vs* time in experiments with the samples with SiO_2/SiC molar ratio 1:1 is presented in Fig. 7. Figure 8 shows the XRD spectra of the reacted samples. The yield of silicon and loss of SiO calculated using LECO data are summarized in Table 2.

Table 2 SiO loss and yield of silicon after carbothermal reaction in hydrogen at different temperatures.

Temperature (°C)	1600	1700	1800	1900	1600	1700	1800	1900
Initial SiO_2/SiC ratio	1:1	1:1	1:1	1:1	1:2	1:2	1:2	1:2
Reaction time (min)	150	94	56	66	150	94	56	66
Conversion of SiO_2 (%)[a]	99.4	99.6	99.1	99.3	99.3	99.9	99.0	99.6
Conversion of SiC (%)[b]	77.2	92.6	65.3	83.2	77.4	84.3	78.7	93.4
Weight loss (%)	77.9	77.6	62.2	72.9	56.9	56.6	52.3	56.0
SiO yield (%)	65.8	61.8	40.4	55.3	34.8	32.5	26.9	28.7
Silicon yield (%)	22.5	34.3	41.8	36.1	49.9	56.8	58.6	66.7

[a] Calculated from LECO oxygen data of sample after reaction;

[b] Calculated from LECO total carbon data of sample after reaction.

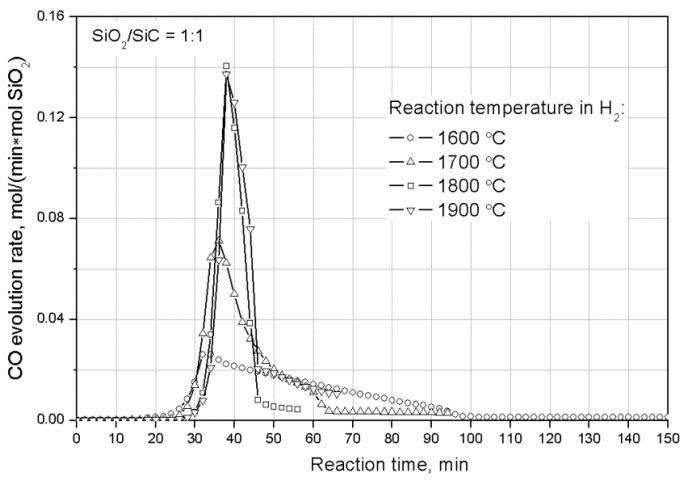

Fig. 7 CO evolution rate in the formation of silicon at different temperatures in hydrogen. The initial samples had a SiO_2/SiC molar ratio of 1:1.

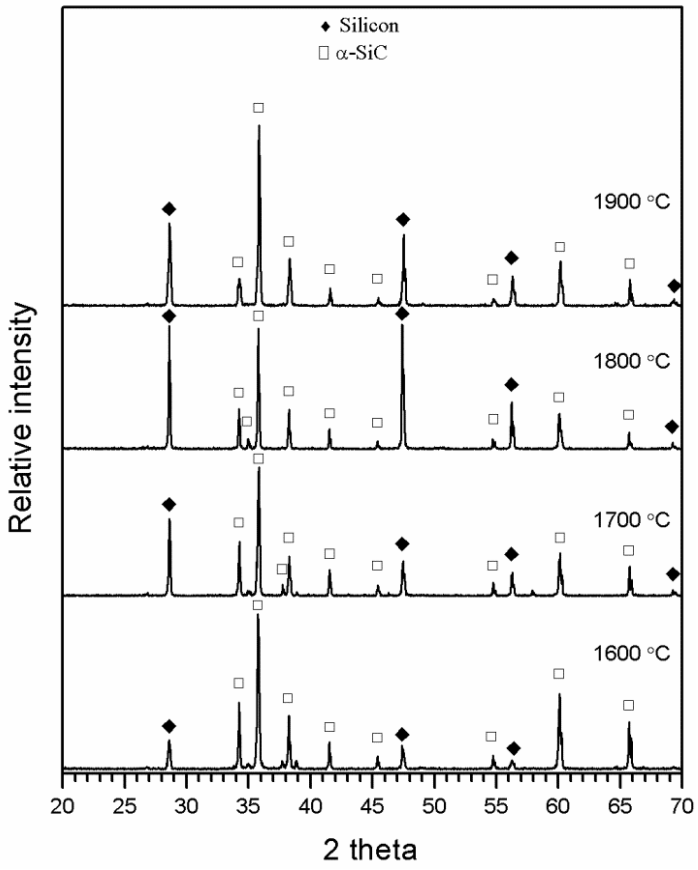

Fig. 8 XRD patterns of SiO_2-SiC samples reacted in hydrogen at different temperatures. The initial samples had a SiO_2/SiC molar ratio of 1:1. The reaction time was 150 min at 1600 °C, 94 min at 1700 °C, 56 min at 1800 °C, and 66 min at 1900 °C.

The CO evolution rate in the SiO_2–SiC reaction in hydrogen increased with increasing temperature with a similar trend as in the reaction in argon. At 1600 and 1700 °C, the CO evolution rate in hydrogen was much higher than in argon. However, the peaks of CO evolution rate at 1800 and 1900 °C were significantly lower than those reached in argon. It can also be noticed from the positions of the CO evolution peaks that the reactions commenced at a lower temperature (during heating of samples to the experimental temperature) and completed faster than in argon. As shown in Fig. 8, no residual silica was detected by the XRD analysis of the sample reacted at 1600 °C in hydrogen, and the conversion of silica was close to completion (Table 2), while the residual silica content was high in the sample reacted in argon (Fig. 3; Table 1). These data demonstrate that hydrogen atmosphere significantly promoted reactions of silicon formation.

Hydrogen was involved in the reactions of silicon formation. Quartz was partially directly reduced by hydrogen to SiO by Reaction (13) [16]:

$$SiO_2 + H_2\,(g) = SiO\,(g) + H_2O\,(g) \quad (13)$$

$$\Delta G^\circ = 534.35 - 0.1869\,T\,(kJ) \quad (1273\ K \leq T \leq 2273\ K)$$

H_2O vapor formed in Reaction (13) can be removed from the reaction system with the flowing gas or react with silicon carbide (Reaction (14)) and/or silicon (Reaction (15)):

$$2\,H_2O\,(g) + SiC = SiO\,(g) + 2\,H_2\,(g) + CO\,(g) \quad (14)$$

$$\Delta G^\circ = 256.30 - 0.1801\,T\,(kJ) \quad (1273\ K \leq T \leq 2273\ K)$$

$$H_2O\,(g) + Si\,(l) = SiO\,(g) + H_2\,(g) \quad (15)$$

$$\Delta G^\circ = 88.13 - 0.1037\,T\,(kJ) \quad (1773\ K \leq T \leq 2273\ K)$$

Both Reactions (14) and (15) have high equilibrium constants in the examined temperature range. The equilibrium partial pressure of H_2O in Reactions (14) and (15),

calculated with partial pressures of CO and SiO determined for Reactions (4) and (5) is plotted in Fig. 5. The equilibrium partial pressure of CO_2 in Reactions (6) and (7) is also calculated and presented in Figure 5. At temperatures below 1900 °C, partial pressure of H_2O is significantly higher than CO_2. Involvement of hydrogen in the reduction of silica does not change the thermodynamics of the overall reaction of silicon formation, but changes the reaction mechanism and enhances the reaction kinetics. Reaction (13) can provide the major path for reduction of SiO_2 to SiO because of the high concentration of hydrogen.

A hydrogen atmosphere also enhanced the mass transfer of gas species [12, 13, 15, 21, 22]. Except the experiment at 1600 °C which had a higher SiO yield due to increased quartz conversion, the loss of SiO in hydrogen was equivalent or lower than in argon at other temperatures. It can be attributed to the higher rate of utilization of SiO by Reaction (8) of silicon formation.

The CO evolution rates in the SiO_2–SiC reaction with SiO_2/SiC molar ratio 1:2 in hydrogen at different temperatures are presented in Fig. 9. The yields of silicon and SiO are summarized in Table 2. The peak of CO evolution rate increased by increasing the SiC content in the SiO_2–SiC mixture. The SiO yield and total weight loss decreased, while the silicon yield significantly increased as a result of increasing surface area of SiC in Reaction (8).

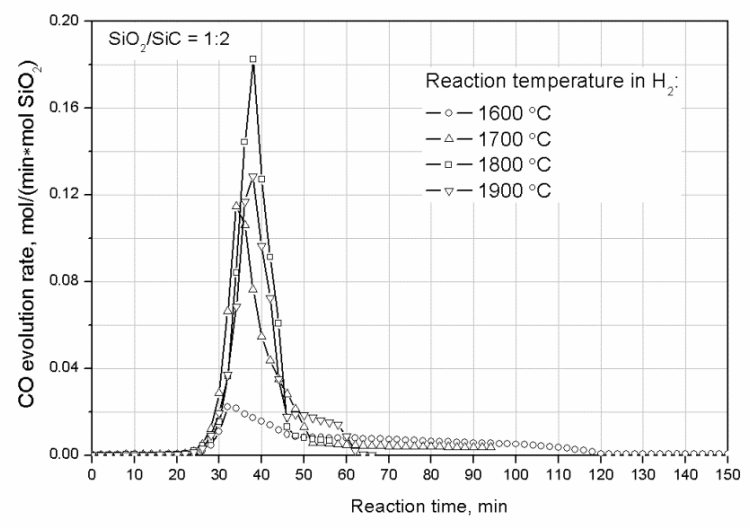

Fig. 9 CO evolution rate in formation of silicon at different temperatures in hydrogen. Initial samples contained quartz and silicon carbide with a molar ratio SiO_2/SiC = 1:2.

IV. Conclusions

The formation of silicon by reaction of quartz and SiC powders was studied in the temperature range of 1600–1900 °C. The yield of silicon was strongly affected by temperature, initial SiO_2/SiC molar ratio and reaction atmosphere. SiO_2–SiC reaction with SiO_2/SiC molar ratio 1:2 achieved a higher silicon yield and lower SiO loss. Reaction in hydrogen resulted in a higher silicon yield than in argon. Hydrogen enhanced the formation of silicon by direct reduction of quartz to SiO and increased SiO content in the gas phase which promoted reaction of SiO with SiC. This study may give useful information for the improvement of industrial carbothermal silicon process.

Acknowledgements

This research was supported under the Australian Research Council's Linkage Projects Funding scheme (Project No. LP100100868). The authors would also like to thank the Mark Wainwright Analytical Centre at the University of New South Wales for LECO analysis, and the Electron Microscopy Centre (EMC) at the University of Wollongong

for the electron microscopy characterization.

References

1. Schei A, Tuset J, Tveit H (1998) Production of high silicon alloys. Tapir forlag, Trondheim
2. Schei A, Halvorsen SH (1991) A stoichiometric model of the ferrosilicon process. In: Proceedings from the Kjetil Motzfeldt symposium, Institute of Inorganic Chemistry, NTH, Trondheim, pp 41–56
3. Filsinger DH, Bourrie DB (1990) Silica to silicon: key carbothermic reactions and kinetics. J Am Ceram Soc 73: 1726–1732
4. Hunt L (1990) Silicon precursors: their manufacture and properties., Handbook of semiconductor silicon technology. William Andrew Publishing, New York
5. Lee HC, Dhage S, Akhtar MS, Kwak DH, Lee WJ, Kim CY, Yang OB (2010) A simulation study on the direct carbothermal reduction of SiO_2 for Si metal. Curr Appl Phys 10: S218–S221
6. Hakamada M, Fukunaka Y, Oishi T, Nishiyama T, Kusuda H (2010) Carbothermic Reduction of Amorphous Silica Refined from Diatomaceous Earth. Metall Mater Trans B 41B: 350–358
7. Dal Martello E, Tranell G, Gaal S, Raaness O, Arnberg L (2011) Combined XRD and XRF technique for the quantification of the mass balance in a Si carbothermic production experiment. ISIJ Int 9: 1492–1496
8. Poch W, Dietzel A (1962) Bildung von Siliziumcarbid aus Siliziumoxid und Kohlenstoff. Ber. Deutsch. Ker Ges 39: 413–426
9. Müller MB, Olsen SE, Tuset JK (1972) Heat and mass transfer in the ferrosilicon process. Scand J Metall 1: 145–155
10. Rosenqvist T, Tuset JKr (1972) Discussion of “thermodynamics of the Si-C-O system for the production of silicon carbide and metallic silicon. Metall Trans B 18: 471–472
11. Dal Martello E, Tranell G, Gaal S, Raaness OS, Tang K, Arnberg L (2011) Study of

pellets and lumps as raw materials in silicon production from quartz and silicon carbide. Metall Mater Trans B 42B: 939–950

12. Kononov R, Ostrovski O, Ganguly S (2008) Carbothermal reduction of manganese oxide in different gas atmosphere. Metall Mater Trans B 39: 662–668
13. Dewan MAR, Zhang G, Ostrovski O (2011) Carbothermal reduction of ilmenite concentrates and synthetic rutile in different gas atmospheres. Miner Process Extr M 120: 111–117
14. Fruehan RJ, Carkin G (2004) Mechanism and rate of reaction of Al_2O, Al, and CO vapors with carbon. Metall Mater Trans B 35: 617–623
15. Ostrovski O, Zhang G, Kononov R, Dewan MAR, Li J (2010) Carbothermal solid state reduction of stable metal oxides. Steel Res Int 81: 841–846
16. Li X, Zhang G, Tang K, Ostrovski O, Tronstad R (2015) Carbothermal reduction of quartz in different gas atmospheres. Metall Mater Trans B 46B: 1343–1352
17. Wan X, Zhang G, Ostrovski O, Aral H (2013) Carbothermal reduction of silica in nitrogen and nitrogen-hydrogen mixture. In: Proceedings of the thirteenth international ferroalloys congress, Karaganda, Kazakhstan, pp 739–748
18. Li X, Zhang G, Tang K, Ostrovski O, Tronstad R (2015) Carbothermal reduction of quartz in methane-hydrogen-argon gas mixture. Metall Mater Trans B. doi: 10.1007/s11663-015-0407-x
19. Chaklader ACD, Roberts AL (1961) Transformation of quartz to cristobalite. J Am Ceram Soc 44: 35–41
20. HSC Chemistry 6.1 (2007) Chemical Reaction and Equilibrium Software with extensive thermochemical database. Outokumpu
21. Dewan MAR, Zhang G, Ostrovski O (2010) Carbothermal reduction of a primary ilmenite concentrate in different gas atmospheres. Metall Mater Trans B 41B: 182–192
22. Dewan MAR, Zhang G, Ostrovski O (2009) Carbothermal reduction of titania in different gas atmospheres. Metall Mater Trans B 40: 62–69

CHAPTER 7

CONCLUSIONS AND RECOMMENDATIONS FOR FURTHER WORK

7.1 Conclusions

The carbothermal reduction of quartz into SiC and its further conversion to high purity silicon is the aim to this project. The results and conclusions presents in this thesis is a result of different kinds of work. Chapter 2 and 3 presents mechamisms of the carbothermal reduction of quartz to SiC in hrdrogen and methane-containing gas, respectively. Most of synthesized SiC is in the form of particls, in spite of small amount of SiC wihiskers was found. Subsequently, the growth mechanisms of SiC whiskers are discussed in detail in Chapter 4. It is also proofed that direct reduction of quartz by methane-containing proceeds only to gaseous SiO. The reduction rate and kinetics of SiO generation was presented in Chapter 5. Finally, the silicon production by reaction of SiC with SiO_2 under different conditions is presented in Chapter 6.

The major findings in this project are summarized as follows.

(1) Carbothermal reduction of quartz by graphite was strongly affected by the gas atmosphere and temperature. The reduction rate increased with increasing hydrogen partial pressure and temperature. Formation of SiC started at 1300 °C in argon, and 1200 °C in hydrogen. Synthesis of SiC in hydrogen was close to completion in 270 minutes at 1400 °C, 140 minutes at 1500 °C, and 70 minutes at 1600 °C. Faster carbothermal reduction rate in hydrogen was attributed to the involvement of hydrogen in the reduction reactions by directly reducing silica and/or indirectly, by

reacting with graphite to form methane as an intermediate reductant.

(2) Carbothermal reduction of quartz to SiC in the methane-hydrogen-argon gas mixtures in the temperature range of 1300 °C to 1550 °C in comparison with reduction in argon. The reduction of quartz mixed with graphite with C/SiO_2 ratio of 2 in the gas mixture containing 1 vol % methane, 70 vol % hydrogen and 29 vol % argon was close to completion in 90 minutes at 1500 °C and in 60 minutes at 1600 °C. Methane supplied partially carbon for SiC synthesis and revealed high reducing capacity compared to that of solid graphite in carbothermal reduction. The reduction rate and yield of SiC increased with increasing methane content in the methane-hydrogen-argon gas mixture to 2 vol %. Further increasing methane content caused excessive methane cracking with solid carbon deposition, which hindered access of reducing gas and decreased reduction rate. To suppress the deposition of solid carbon, the concentration of hydrogen in the gas mixture should be above 70 vol % (at 1500 °C and 1 vol % methane). Hydrogen was also directly involved in reduction of quartz to SiO.

(3) SiC whiskers were synthesized by carbothermal reduction of quartz in hydrogen and methane-hydrogen-argon gas mixture. In hydrogen atmosphere, SiC whiskers with diameter of 100–800 μm started to grow from 1400 °C, followed VSL mechanism under catalytic effect of iron. Whisker length increased with the increase of temperature. The yield of whiskers was higher on the surface than inside the pellet. Two different types of SiC whiskers were synthesized in methane-hydrogen-argon gas mixture, one in the form of prism growing at 1200–1600 °C by VSL mechanism, the other in the form of long cylinders which were synthesized at 1400–1600 °C by VS mechanism. The morphology and production mechanism of SiC whiskers was affected by vapour pressure of SiO in different reduction atmospheres and temperatures.

(4) The reduction of quartz to SiO was studied in a fluidized bed reactor with continuously flowing methane-hydrogen gas mixture. A cold model has been made which takes into account the fluidization of quartz powder by stream of reducing gas. The reduction experimental results indicated that higher temperature, faster fluidization gas rate and higher methane content in the reducing gas accelerated the reduction rate. However, excessive temperature (> 1450 °C) and methane content (>5 vol %) brought serious methane cracking and carbon deposition on the surface of quartz particles, which inhibited the further reduction. The major reduction product of quartz in the fluidized bed was SiO. In the reduction of quartz spheres at 1400–1500 °C, a small amount of SiC was observed in the form of particles (1400 and 1450 °C) or whiskers (1500 °C).

(5) The reaction of quartz and SiC powders has been studied in detail using a graphite furnace in the temperature range of 1600–1900 °C. The yield of silicon was strongly affected by initial SiO_2/SiC mole ratio and reduction atmosphere. Sample with initial SiO_2/SiC = 2 was characterized by a higher silicon yield because of less SiO loss. Reduction in hydrogen resulted in higher silicon yield in comparison to reduction in argon, up to 66.7 % at 1900 °C for the sample with initial SiO_2/SiC = 2. This is attributed to direct reduction of quartz to SiO and enhanced the SiO content in the gas phase.

7.2 Recommendations for further work

The project has studied carbothermal reduction of quartz in hydrogen or methane containing gas atmosphere and established SiC formation conditions. Work on further reaction of SiC with quartz to form silicon was preliminary to demonstrate the feasibility of the process.

The following further study of reduction processes is recommended:

(1) Reduction behavior of carbothermal reduction using different silica and carbonaceous materials.

(2) Carbothermal reduction of quartz in hydrogen or methane containing gas with addition of CO, CO_2 and H_2O.

(3) Mathematical modelling of carbothermal processes.

(4) Kinetics and mechanism of production of silicon in different gas atmosphere.

(5) Effects of different gas atmospheres on impurity removal during reduction, especially for boron and phosphorus, and the kinetics and mechanisms of the impurity removal.

(6) Larger scale experiments in silicon production.